Mathematical Modelling of Salt Diffusion in Dry-Salted Cheese

A Thesis presented in partial fulfilment of the requirements for the degree of

Doctor of Philosophy

in

Food Engineering

at Massey University, Manawatu, New Zealand

Meghan Emily Keck

2019

Abstract

Control of salt uptake into cheese curds is vital to the production of safe, functional, and consistent cheese products. Development of mathematical models describing the mechanisms affecting salt uptake, namely the Fickian diffusion of salt into curds and osmotic pressure differential induced whey expulsion, are necessary to control curd properties, optimize salt uptake, and reduce final product inconsistency in commercial cheesemaking plants.

Novel image analysis techniques were developed to assess whey expulsion behaviour in individual model renneted skim milk gels under different brining conditions. Whey expulsion results were combined with salt uptake data to develop mechanistically-derived mathematical models of the simultaneous whey expulsion and salt uptake under brining conditions. Whey expulsion data was combined with gel meso-structural properties to estimate the pressure gradients driving the whey expulsion behaviour. Finally, the simultaneous salt uptake and whey expulsion models were used to model salt and whey transport in model renneted gels treated under different dry salting conditions and compared to samples collected from an industrial cheesemaking plant.

This work developed new techniques to evaluate whey expulsion in individual curds, demonstrated the importance of accounting for whey expulsion in the evaluation of salt uptake and modelling, and applied mathematical models describing simultaneous salt uptake and whey expulsion to milk gels exposed to brining and dry salting conditions.

Acknowledgements

Completing a PhD thesis takes significant direction and encouragement, and I would be remiss to not thank the many folks that have contributed to the success of this thesis. It has been a pleasure to work under the supervision of my primary supervisor, Tony Paterson, who has provided me excellent support and guidance throughout the whole PhD process. Thanks to my secondary supervisors John Bronlund, Jason Hindmarsh, and Jeremy McLeod for their ideas and contributions. All my supervisors were quick to challenge me to ask more "why?" questions, find ways to get around setbacks, and encouraged me to present my work beyond the cosy walls of Massey to far-flung spots around the world.

Thanks to the Hilmar Cheese Company for funding my PhD and giving me the incredible opportunity to study in the Land of the Long White Cloud and collaborate with the wonderful folks in Cheese R&D at Hilmar again.

I want to thank other supporters throughout the university staff, including Anne-Marie Jackson, John Sykes, John Edwards, Michelle Tamehana, Nicki Murray at MMIC, Ian Thomas, Morio Fukuoka, Anthony Wade, and Fliss Jackson for their assistance in making my experiments a success. Thanks to Glenda, Dilantha, and the rest of the team managing accounts and making sure all my orders and trips went smoothly.

Thanks to other folks around Massey and Palmy for making life better (which includes, but is not limited to): Sebastian, Siti, Florencia, Aimon, How, Esther, Kate, Sima, Nick, Sonja, Matt, and Eli. Special thanks to Caroline and Ty, and the Singaporean Captain's Ball crew. Thanks to my family for their constant love and support and frequent visits. Thanks to my cats for taking the care to reduce my blood pressure every evening.

Lastly, I would like to thank my husband, Spenser James. His constant patience, support, and willingness to "ride my coattails" to New Zealand were a vital part of "us" getting a PhD.

I can now confidently say I know more about salt and whey transport phenomena in renneted cheese curds than any regular person should know. I hope that this thesis proves as interesting to someone as transformative it was to me.

Table of Contents

List of Figures

List of Tables

List of Equations

Chapter 1 Research Premise and Justification

1.1 Research Premise

The landscape of the world dairy industry is rapidly changing to meet consumer demands for high-quality dairy products. This is true in Asia, where western style cuisines that use cheese have increased in popularity (Beghin, 2006; Dong, 2006). Cheeses are poised to fit into the new market needs of a growing Asian consumer population. Despite new opportunities for expansion, there remains significant volatility in dairy markets. In 2015, the price of cheddar cheese fell 26% to a final price of $3425 USD per tonne, with dry milk powders faring worse (Milk and Milk Products Price and Trade Update, 2015; OECD-FAO Agricultural Outlook 2015, 2015). Given the uncertainty in global dairy prices, improving production efficiency and consistency is a key part of maintaining viability and profitability for a cheese manufacturer (OECD-FAO Agricultural Outlook 2015, 2015).

Cheddar cheese represents one third of the world cheese production of 17.4 billion tonnes per annum (FAO, 2016). Dry salting is an essential step in the process of making Cheddar and other similar cheeses (Law, 2001; Ong et al., 2004). Knowledge of the mechanisms that control the uptake and transport of sodium and chloride ions throughout the salting and post-salting processes is important to optimizing the production of dry salted cheeses. Salt transport effects preservation, functionality, and flavour of the final cheese product. Despite an abundance of research conducted on cheese salting, current literature sources have not previously developed a mechanistically-derived mathematical model to describe the mechanisms that control salt ion uptake within individual curds or pressed cheese blocks.

1.2 Research Objectives

The purpose of this research was to create a comprehensive, functional mathematical model that may be used by the dairy industry to better understand and optimize the production of dry salted cheeses. A series of research objectives were developed to achieve this:

1) Investigate existing mathematical models used to describe salt uptake, their limitations, and variables of interest to the development of a mechanistically derived mathematical model.

2) Develop a method to assess syneresis and osmotic pressure differential induced whey expulsion, both due to salt and non-diffusing compounds, in single curd systems and model it as a function of time.

3) Evaluate the changing internal gel structure as a function of natural syneresis and osmotic pressured differential induced syneresis, both due to salt and non-diffusing compounds, and model this as a function of time.

4) Assess salt uptake relative to osmotically-induced whey expulsion in single curd systems and calculate an effective transport diffusion coefficient.

5) Assemble whey and salt transport data into a series of models to simultaneously describe salt and whey transport in a single curd system and apply it to theoretical curd beds and salting conditions.

6) Appraise the suitability for the models to describe gel contraction, moisture losses, and salt uptake observed in data collected from an industrial cheesemaking facility and provide suggestions for improved control of transport behaviours.

The research described in the following chapters examines the role of salt and free whey transport within single curd systems. It also explores the effect of induced osmotic pressure gradients and the presence of salt on the internal curd structure from salt-induced changes. This illustrates the complexity of the dynamic multi-boundary problem of salt transport into fresh cheese curd. This information is compiled into a mathematical model to describe salt and whey transport during the salting regime.

Chapter 2 Literature Review

2.1 Introduction

Sodium chloride, commonly referred to as salt, has had a far-reaching effect on the history of food production and preservation since antiquity. The addition of salt, usually in combination with fermentation and dehydration via air or sun-drying, was one of the earliest methods of food preservation for prehistoric people (Higman, 2012; Johnson & Law, 1999; Kindstedt, 2012). Salt was such a vital resource for food preservation from prehistory through the Middle Ages, that it often was used as a form of currency to be exchanged for goods or labour (T. P. Guinee & Fox, 2004; Higman, 2012). Indeed, the word salary originates from the Latin *salarium*, used to describe the money Roman soldiers were allowed to use for the purchase of salt (Dictionary, 1909). Salt became essential for food preservation through a series of chemical interactions with undesirable spoilage or pathogenic microorganisms, restricting microbial growth through dehydration and fermentation regulation.

The combination of decreased water content from the dehydration and salting, with the production of acids, carbon dioxide, ethanol, or antimicrobial compounds from fermentation prevented the rapid growth of undesirable spoilage and pathogenic microorganisms, thereby preserving the nutrition of fresh foods for longer periods of time (T. P. Guinee & Fox, 2004; Higman, 2012). Until the industrial adoption of temperature control methods of pasteurization and refrigeration in the nineteenth century to preserve foods, these three interdependent technologies were the primary means for the preservation of all manner of foods, including dairy products such as cheese (Bellwood, 2005; Higman, 2012; Salque et al., 2013). Modern cheese technology makes use of the traditional preservation technologies and temperature control to optimize the production of a variety of consistent, quality cheeses consumed throughout the world (T. P. Guinee & Fox, 2004).

Cheese, like salt, has its use and origins dating to prehistoric society, shortly after the first ruminants were domesticated and milked to feed infants (Greenfield, 2010; Johnson & Law, 1999; Kindstedt, 2012). Fresh milk was fermented by natural cultures and coagulated to form curds via exposure to chymosin enzymes found in the stomachs of young calves, lambs, or goat kids (Fox, Guinee, Cogan, & McSweeney, 2000c; Fox & McSweeney, 2004; Kindstedt, 2012). These curds were then cut, separated from the free whey expelled from the curd, and salted. The earliest successful forms of cheese making not only extended the effective "shelf-life" of fresh milk, but became a vital source of nutrition in various early communities

(Kindstedt, 2012). Early cheeses became extremely important to regional cuisines, and provided the foundation for the development of a variety of new cheeses throughout Europe and the Near East with unique properties (Phelan, Renaud, & Fox, 1993).

There are estimated to be over one-thousand varieties of cheese currently produced and consumed around the world (Fox, Guinee, Cogan, & McSweeney, 2000b; Fox & McSweeney, 2004; Sandine & Elliker, 1970). Cheese is a colloquial term used to describe a diverse collection of concentrated and fermented, dairy foods produced throughout the world in a variety of flavours, textures, and functionalities (Fox et al., 2000b, 2000c; Fox & McSweeney, 2004; Kindstedt, 2012). While the methods of production have changed since antiquity in scale, consistency, and safety, cheese production has maintained the same general processing steps to coagulate, ferment, and concentrate fresh milk into a form for extended future use. Salt continues to be a vital component to the efficient production of safe, functional, and appetizing cheeses. Understanding the mechanisms and modelling the movement of salt through fresh cheese curd, especially for dry salted cheese, is essential to optimizing the production of cheese and improving consistency.

2.2 Cheese Manufacturing Process

The mechanisms of fermentation were one of the first steps to be scientifically studied in the cheese making process with the discovery of lactic acid bacteria (Parente & Cogan, 2004). Advances in understanding the mechanisms that control the fermentation and biochemical processes of cheese making have continued since the early work of Pasteur, improving the safety and quality of cheese products (Caplice & Fitzgerald, 1999; McSweeney, Ottogalli, & Fox, 2004). Modern cheeses are produced with a variety of different milk types, starter cultures, and processing conditions to achieve a variety of final products with specific flavours, textures, functionalities, and stability for future consumption (Phelan et al., 1993).

Several factors are used to control the properties of the final product, including temperature control during the cheese making or in the aging process, ratio of fat-to-protein in the starting milk, the starter culture strains, and the addition of salt (Bennett & Johnston, 2004; Law, 2001). The processing steps prior to the addition of salt effect the rate of salt transport by controlling the growth of the culture, increasing moisture expulsion, and interacting with the curd matrix to improve quality (Chevanan & Muthukumarappan, 2007; T. Guinee, 2004; Moller, Rattray, Hoier, & Ardo, 2012; Turner & Thomas, 1980).

Figure 2-1 splits cheese making steps into the active manufacturing steps and the biochemically-driven ripening steps.

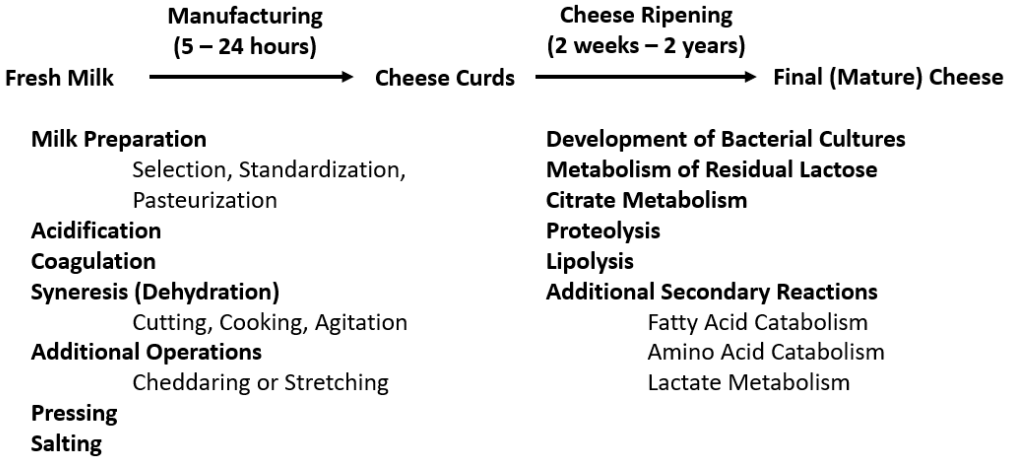

Figure 2-1: General outline of cheese manufacture adapted from Fox & McSweeney (2004).

Figure 2-2 provides a more in-depth depiction of the cheese making process for a Cheddar, a popular English-style, dry salted cheese.

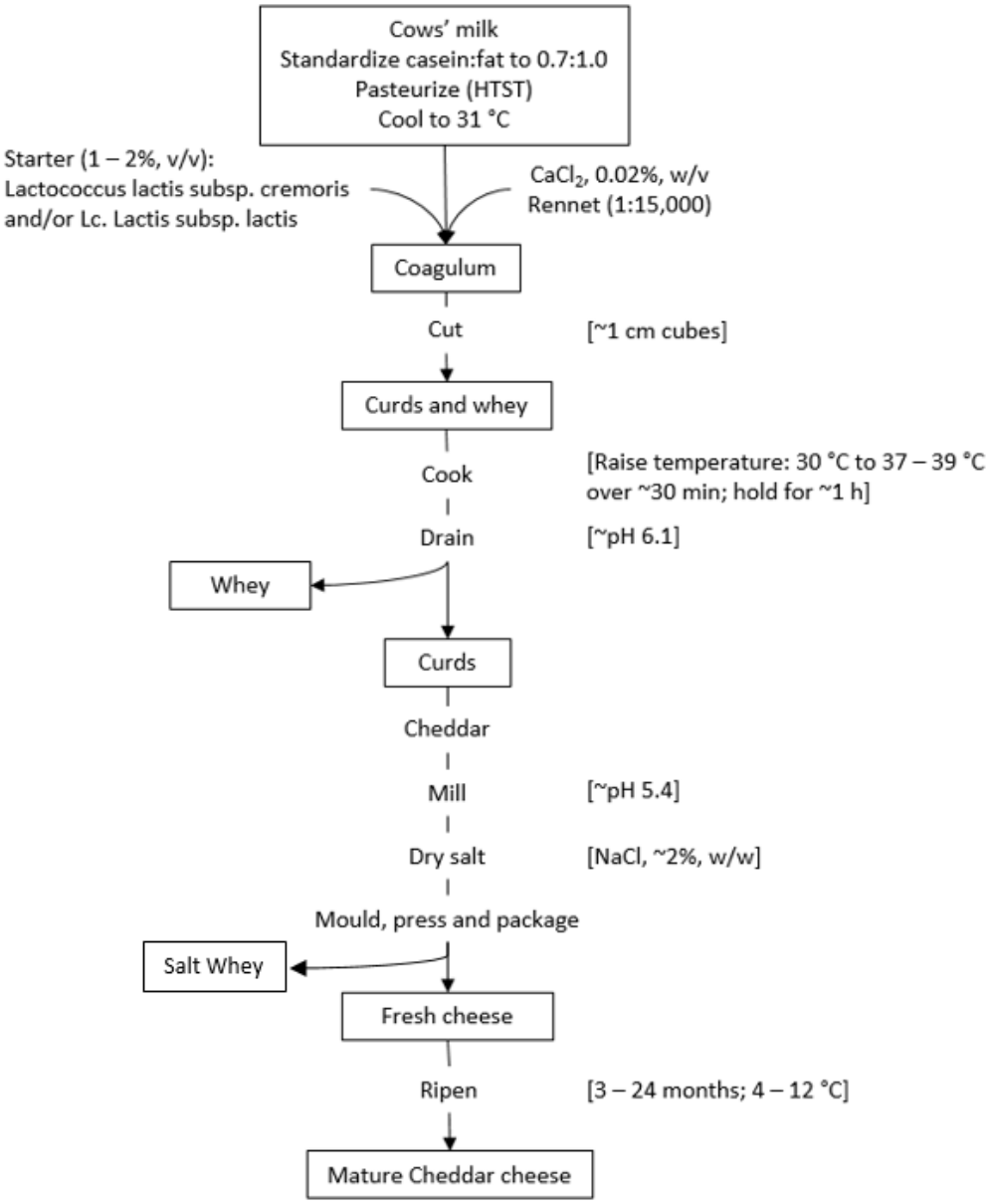

Figure 2-2: General flow diagram for the manufacture of traditional cheddar cheese adapted from Fox and McSweeney (2004).

2.2.1 Pre-Salting Steps

Cheese manufacturing provides a way to concentrate and preserve milk solids for extended storage times via fermentation, coagulation, and dehydration control (Fox et al., 2000c; Fox & McSweeney, 2004). Manipulating the conditions during the manufacturing and ripening steps converts fresh milk into a variety of different final cheese styles. The processing steps in modern cheese production generally include the standardization of fresh milk, a heating step (usually including pasteurization), fermentation, coagulation, curd and whey separation, salting, pressing, and ripening procedures (Bennett & Johnston, 2004; Johnson & Law,

1999). The first control step consists of the selection and standardization of clean, fresh milk to a desired protein-to-fat ratio, by mixing separated cream and non-fat milk or non-fat milk powder to the desired concentrations (Bennett & Johnston, 2004).

The next step usually includes the pasteurization or heating of the milk to a combined time-temperature combination that reduces the starting load of pathogenic and spoilage microorganisms in the raw milk (Bennett & Johnston, 2004). The most commonly used time-temperature combinations are High-Temperature-Short-Time (HTST), where milk is heated to 72 °C for fifteen seconds in a continuous process within a plate heat exchanger or Low-Temperature-Long-Time (LTLT), where the milk is heated to 63 °C for thirty minutes in a continuously-stirred batch process (Bennett & Johnston, 2004). The pasteurized milk is then cooled to the desirable fermentation temperatures for the starter cultures. The starter culture is selected and added into the warmed milk for a predetermined time to achieve a target pH reduction (Parente & Cogan, 2004). Following sufficient drop in pH, the curd is coagulated with rennet enzymes over a predetermined renneting time, usually ranging from twenty to forty minutes depending on the rennet source, enzyme activity, and desired starting curd gel strength (Cooper, Corredig, & Alexander, 2010; D. S. Horne & J. M. Banks, 2004; Logan et al., 2014; van den Bijgaart, 1989).

During the coagulation step, the chymosin enzymes in the rennet cleave the κ-caseins from the casein micelles, destabilizing the casein micelles and creating thermodynamically favourable conditions for the casein micelles to aggregate and interact to form three-dimensional networks (van den Bijgaart, 1988; Walstra, van Dijk, & Geurts, 1985). The first step in the dehydration process occurs after the new matrix is cut, leading to the expulsion of whey from the curd structure, in a process known as syneresis (McSweeney, 2007; van Dijk, 1982; van Dijk & Walstra, 1986; Walstra et al., 1985). Gentle agitation and increasing the temperature increases the rate of syneresis (van den Bijgaart, 1988; van Dijk & Walstra, 1986; Walstra et al., 1985). Curds are removed from the whey, allowed additional time for dehydration and cooling before being salted (Fox, Guinee, Cogan, & McSweeney, 2000d; Geurts, Walstra, & Mulder, 1980; T. Guinee, 2004).

2.2.2 Salting Methods

The traditional methods and level of salt incorporation into fresh cheeses are historically developed based on accessibility to salt and the available conditions for aging (Kindstedt, 2012). These restrictions served to develop unique, regional cheese types that varied in

flavour, texture, and overall preservative properties (McSweeney et al., 2004). Different styles of cheese used different types of salting procedures derived from two methods: brining and dry salting (Fox et al., 2000d; Geurts, 1978; Geurts, Walstra, & Mulder, 1974; T. Guinee, 2004). Table 2-1 lists the common salting techniques used for various cheese styles.

Table 2-1: Salting method descriptions and intended cheese styles (Bennett & Johnston, 2004; Fox et al., 2000c, 2000d; Fox & McSweeney, 2004).

Salting Method	Description	Cheese Types	Examples	Salt Concentrations	Salting Time	Final pH	Final Moisture Content
Brine Salting	Whole, pressed cheeses are immersed in a concentrated salt brine	Soft/semisoft & Hard/semihard	Camembert, Edam, Emmental, Feta, Gouda	Brine: 15-23 %, Final Product: 1-2.5% Total Mass	3-14 days	4.2-6.9	35.5-59.7% Total Mass
Dry Salting	Dry salt is mixed with small curd prior to moulding and pressing	Hard/semihard	Cheddar, Cheshire, English-Style Cheeses	Final Product: 1.5-2.5% Total Mass	10-40 minutes	5.3-5.5	37.0-39.0% Total Mass
Dry Salting (Whole Cheese)	Whole, pressed cheeses are rubbed on the surface with dry salt or a concentrated salt paste	Soft/semisoft	Some Blue Cheeses	Final Product: 3.0-4.5% Total Mass	1-2 days	5.2-6.5	38.3-42.0% Total Mass
Combination Method	Dry salt is mixed with small curd, moulded and pressed, and immersed in a concentrated salt brine	Soft/semisoft	Milled Mozzarella Curd	Final Product: 0.7-3.0 % Total Mass	2-3 hours	5.2	47.0-54.0% Total Mass

2.2.2.1 Brine Salting

Brine salted cheeses are usually moulded and pressed before being immersed in sodium chloride brines, generally for 3-14 days to allow for moisture within the cheese to gradually diffuse out, while salt diffuses into the cheese matrix (Baldwin & Wiles, 1996; Floury, Camier, et al., 2009; T. Guinee, 2007). Diffusing salt ions interact with the cheese matrix and microorganisms to slow the production of lactic acid, increase the firmness of the curd structure, and assist in the expulsion of free whey entrapped in the matrix. Brines are usually used for a variety of cheese styles, ranging from high pH, low salt alpine-style cheeses such as gruyere and other Swiss-styles to high salt, low pH styles such as Feta (McSweeney et al., 2004). The differences between feta and Gruyere are partly due to the differences in salting methods and degree of salting, which restrict the growth of natural starter cultures that would create lactic acid and flavour compounds (Lauverjat, Deleris, Trelea, Salles, & Souchon, 2009). The variation in brining conditions created cheeses with salt concentrations ranging from approximately 1% w/w sodium chloride in Alpine-style cheeses to 5.5% w/w sodium chloride in cheeses like Pecorino Romano (T. Guinee, 2007; T. P. Guinee & Fox, 2004).

Using a high concentration brine creates an osmotic pressure gradient on the surface of the pressed cheese, promoting moisture loss from the formed cheeses while maintaining a concentration gradient that provides a driving force for salt ions to slowly diffuse into the curd over a long period of time (Prasad & Alvarez, 1999). Higher salt concentrations in brines create a larger salt concentration gradient that leads to faster diffusion rates, making it appear ideal for increased brining efficiency (Prasad & Alvarez, 1999). However, under high concentration brines, “salting-out” of the proteins in the matrix can occur, causing a significant contraction of the matrix to form a surface layer which acts as a diffusion barrier (Melilli et al., 2003).

This gradual diffusion process decreases the activity of the surviving starter culture in the cheese, slowing the production of acid and limiting proteolysis that may otherwise produce unwanted flavour compounds (Dimos, Urbach, & Miller, 1996; Lauverjat et al., 2009; Vedamuthu, 1979). The slowing of the pH reduction also effects the amount of free moisture expelled as the protein network does not increase in strength. The rate of salt ion transport into brine-salted cheeses is limited primarily by the surface area to volume ratio of the moulded and pressed cheese, temperature of the brine, and the starting moisture content of the curd (Gencer & Turhan, 1988; Luna & Bressan, 1986; Melilli et al., 2003).

2.2.2.2 Dry Salting

Dry-salted cheeses, such as Cheddar, are salted by the addition of dry salt to a bed of curd chips that are quickly mixed, allowed to "mellow" over a specific period of time (thereby providing the time for moisture expulsion and salt ion uptake), and then knit together under the weight of accumulated cheese curd as a pressing measure before packaging (Ong et al., 2004). The application of dry salt to the surface of fresh cheese curd dissolves the salt in the free moisture to form a concentrated brine on the curd surface (Breene, Price, & Ernstrom, 1964; Sutherland, 1974). The brine creates an osmotic pressure gradient with the free moisture within the cheese curd, leading to an expulsion of whey from within the curd, similar to the processes from brine salting (Breene et al., 1964; Giroux, Bouchard, & Britten, 2014; Sutherland, 1974).

Dry salting tends to accelerate the uptake of salt into curd as the surface area to volume ratio and concentration gradients are larger than brined whole cheeses (Law, 2001; Ong et al., 2004). However, once the curds are moulded and pressed, the rate of salt transport through the cheese is extremely slow (Baldwin & Wiles, 1996; Floury, Camier, et al., 2009; Floury, Rouaud, Le Poullennec, & Famelart, 2009). Therefore, any poor mixing of the salted curd bed and an insufficient "mellowing" time may create conditions that are unideal for the even distribution of salt ions through the final, whole cheese matrix before consumption (Baldwin & Wiles, 1996).

2.2.3 Ripening Methods

Various control steps for ripening take place following the pressing and salting steps depending on the cheese style. These steps may include soaking or injecting cheeses with desirable mould slurries, drying or aging under controlled temperature and humidity conditions, bandaging or using wax to limit moisture loss during aging, or storing the cheeses in a brine until consumption (Bennett & Johnston, 2004; McSweeney, 2004). Control of the temperature, humidity, moisture content, and salt concentration are vital to the controlled regulation of the biochemical ripening processes that affect the final cheese flavour, texture, and functionality (McSweeney, 2004; O'Callaghan & Guinee, 2004). Salt transport within cheeses that are pressed and ripened is extremely slow as much of the moisture required for transport is entrapped within the gel network to the gel matrix (van Vliet & Walstra, 1994).

2.3 Role of Salt Addition during Cheesemaking

Salt serves three major functions in the production of cheese: (1) regulation of microbiological growth (pathogenic and non-pathogenic), (2) control of the structural and functional properties, and (3) development of desirable flavour and texture profiles unique to the cheese style and preparation methods. T. Guinee (2004) created a simplified demonstration of how salt impacts the properties of cheeses before consumption, shown in Figure 2-3.

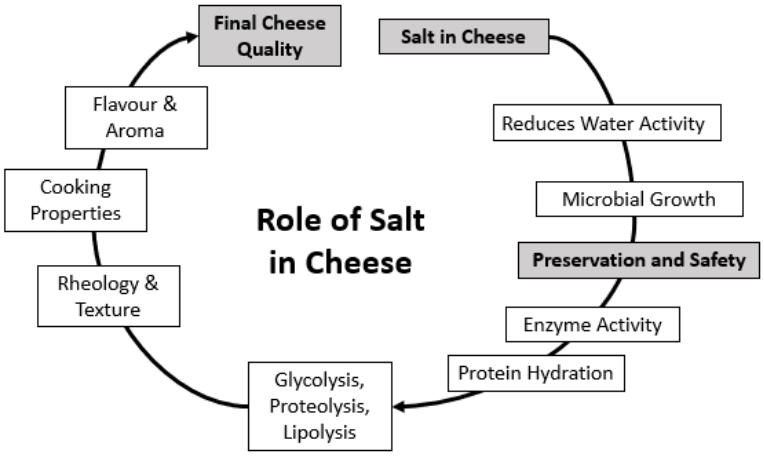

Figure 2-3: Roles of salt in cheese making, adapted from Guinee (2004).

This simplified view does not account for the factors that affect the rate of salt uptake and transport within cheese curds. Several factors that influence the rate of transport are interdependent, creating feedback loops that control the meso-structure of the curd matrix and the rate of microbiological growth and fermentation (T. Guinee, 2004). A slightly more nuanced view of the factors that affect the total salt uptake into curds and their roles in preservation and functionality is shown in Figure 2-4.

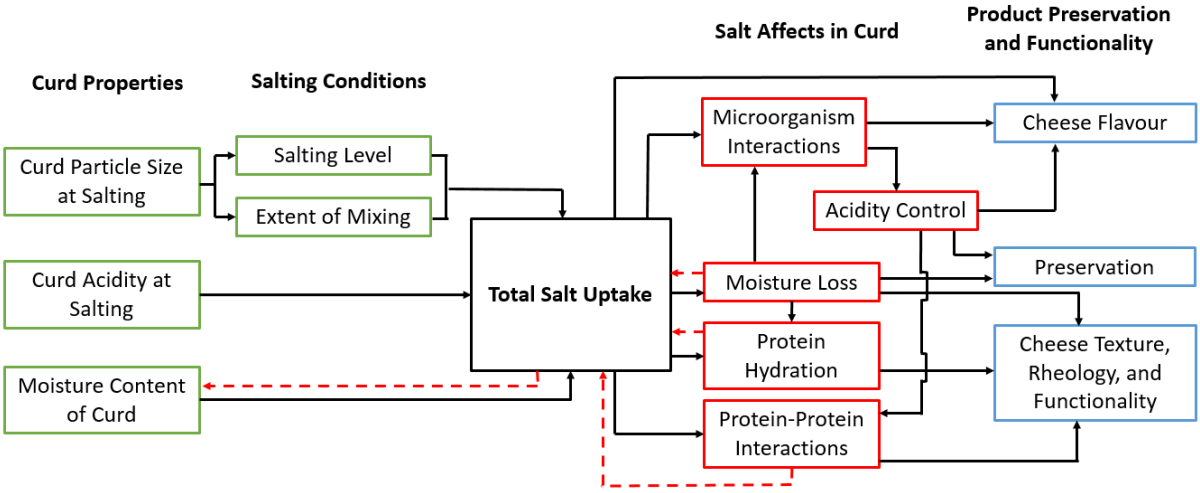

Figure 2-4: Diagram of critical salting variables for dry salted cheeses and the feedback loop associated with their effects on the curd and final cheese product.

This depiction of the interactions between salt uptake and its effect on the matrix and overall functionality properties is limited in expressing the role of each variable in controlling the uptake and transport of salt through cheese curds. The degree of interdependency between the curd and salting variables leads to the manufacture of cheese products with a variety of flavour, functionality, and preservation properties.

2.3.1 Improved Preservation

The most important role of salt in the manufacture of cheese is its role in increasing the preservation properties of the cheese. Salt interacts with both the cheese matrix and the microbiological cultures growing in the cheese to create conditions that prevent the growth of pathogens and limit the growth of unwanted spoilage microorganisms (Caplice & Fitzgerald, 1999; T. Guinee, 2004, 2007; McSweeney et al., 2004). Salt increases the preservation of cheeses by arresting the growth and activity of microorganisms, primarily through two different methods of dehydration: decreasing the water activity and promoting moisture expulsion (T. Guinee, 2004).

2.3.1.1 Decreased Water Activity

The addition of salt to cheese curds separation limits the growth of microorganisms in the curd system by decreasing the water activity of the system. Water activity relates the vapour pressure of the water within the cheese matrix to that of pure water, representing the degree of water binding within the system (T. P. Guinee & Fox, 2004). Dissolved salt ions reduce the mobility of water molecules due to stronger electrostatic water-ion bonds than water-water hydrogen bonds (Reid & Fennema, 2008; Roos, 1997). A reduction of moisture

mobility and increase of the osmotic pressure surrounding the microorganisms leads to rapid dehydration, slowing growth (T. P. Guinee & Fox, 2004).

Decreasing microbial growth also decreases the rate of fermentation, leading to slower production of lactic acid that would dissolve in the free water and decrease the pH of the surrounding space. Acids serve to preserve the safety of the product by restricting the growth of acid-intolerant pathogens. Starter cultures used in cheese making tend to have a higher resistance to the effects of low pH, and therefore survive for longer after metabolizing lactose into lactic acid (Gomes, Vieira, & Malcata, 1998; McSweeney et al., 2004).

2.3.1.2 Induced Osmotic Pressure Gradient Dehydration

The other method of preservation provided through salt addition to curd is the reduction of moisture content through osmotic pressure gradient driven whey expulsion (T. P. Guinee & Fox, 2004). Brines at the surface of curds or whole cheeses create an osmotic pressure gradient, providing a driving force to draw moisture from within the curd to help alleviate the high osmotic pressure differential (Breene et al., 1964; Giroux et al., 2014; Sutherland, 1974). The osmotic pressure gradient continues to provide a driving force for moisture expulsion until the osmotic pressure gradient is equivalent to the hydrostatic pressure gradient between the moisture within the curds to the curd surface. T. P. Guinee and Fox (2004) reported that the mass of moisture expulsion nearly doubled the mass of salt uptake, indicating that a limited amount of salt is required to prompt an accelerated expulsion of moisture, due to this osmotic gradient concept. The concept of dehydration as a function of osmotic pressure driven moisture expulsion is shown in Figure 2-5.

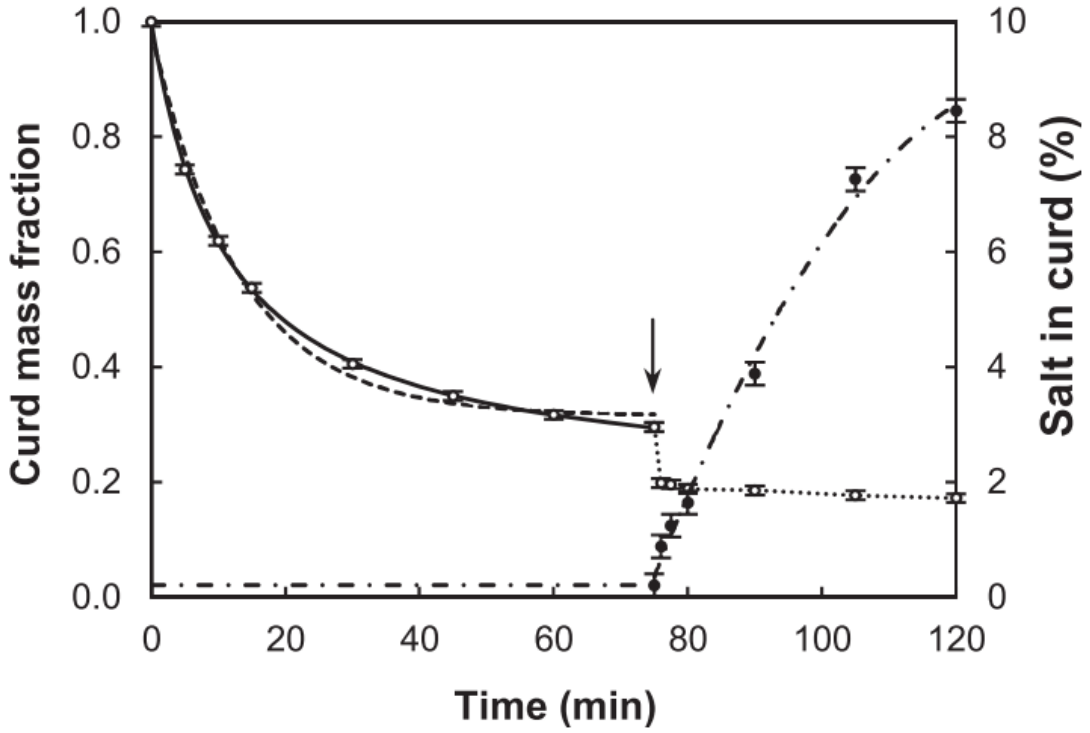

Figure 2-5: Curd mass fraction reduction as a function of salt addition and time, where salt is added after 75 minutes (Giroux et al., 2014).

Figure 2-5 illustrates the moisture loss due to syneresis from a fresh curd as a function of time in terms of curd mass fraction (solid line) and the increase in salt concentration (dash-dotted line) after the addition of salt to the curd surface. Syneresis due to the coagulation and development of the three-dimensional para-casein network dominated the reduction of the curd mass until the addition of salt to the curd surface (shown at 75 minutes with the arrow). The presence of salt created an osmotic pressure gradient that promoted the rapid expulsion of the last free whey within the curd, leading to the final curd mass fraction value (Giroux et al., 2014). Increasing the exposure time to the salt also increased the total salt uptake into the curd, as demonstrated in the figure. Salt-induced osmotic pressure gradients contribute to the expulsion of the remaining free whey within the curd, in addition to the dehydration effects from curd cooking and agitation (Baldwin & Wiles, 1996; Baroni, Menezes, Ardell, & Ribeiro, 2003; Fox et al., 2000d; Yanniotis & Anifantakis, 1983).

2.3.2 Functionality and Structure

The effect of salt on the functionality and structure of cheeses is interrelated to the dehydration and the regulation of fermentation previously discussed. Acid produced through fermentation directly impacts the structure of the proteins that form the bi-continuous para-casein gel matrix (Giroux et al., 2014; Lucey, Tamehana, Singh, & Munro, 2001; Ong,

Dagastine, Kentish, & Gras, 2012; van den Bijgaart, 1988). Slowing the rate of acid production also serves to create the target functionalities and textures. At pH levels that are very low, the amount of free calcium ions released is much higher from the colloidal casein micelles (Lucey, Johnson, & Horne, 2003; Ong et al., 2012). These ions interact with the proteins, thereby stabilizing existing bonds and increasing the strength of the gel network and overall firmness of the cheese curd (Fox, Guinee, Cogan, & McSweeney, 2000a; Lucey et al., 2003; O'Callaghan & Guinee, 2004; van Vliet, Lakemond, & Visschers, 2004).

Control of the acidification rate is also necessary to prevent acid levels from exceeding the buffering capacity of the cheese proteins and matrix, and causing salting-out of proteins which may affect the texture and functionality of the final product, such as the meltability or sliceability (Chevanan & Muthukumarappan, 2007; Henneberry, Wilkinson, Kilcawley, Kelly, & Guinee, 2015; Lucey et al., 2003; Melilli et al., 2003). Initial exposure of the surface of whole cheeses or individual curds to concentrated brines leads to a rapid expulsion of moisture from the curd due to differences in the osmotic pressures between the brine and cheese matrix (T. Guinee, 2004; T. P. Guinee & Fox, 2004). This in turn leads to a partial collapse of the curd structure and shrinkage as more water leaves the matrix. Shrinkage on the surface leads to an increase in the cheese surface area to volume ratio, thereby increasing the respective surface exposure to the surface brine. Dissolved salt ions diffuse into the curd matrix following the initial rapid expulsion of moisture.

Sodium ions interact with the protein matrix, affecting protein-protein interactions that continue the expulsion of free moisture from within the curd. The salt ions interacting with the proteins also interact with the water surrounding the proteins, preventing their expulsion and limiting the total moisture loss so that the hydration shells around the proteins are maintained (Geurts, 1978; Henneberry et al., 2015; McMahon, Paulson, & Oberg, 2005; Moller et al., 2012). Stronger protein-protein interactions promote strengthening of the cheese matrix, creating a firmer texture that is more reminiscent of the cheese upon consumption (Baldwin & Wiles, 1996; Halmos, Pollard, Sherkat, & Seuret, 2003; Lucey et al., 2003; O'Callaghan & Guinee, 2004).

The combination of strong protein-protein interactions and controlled pH and moisture content also affects the functionality of the final cheese products for the consumer. Cheeses with pH values lower than the isoelectric point of caseins (approximately pH 4.6) do not melt and flow upon heating. Likewise, cheeses with pH values ranging from 5.5 to 5.7 and lower

moisture content tend to have a crumbly consistency (Floury, Camier, et al., 2009; Lucey et al., 2003; O'Callaghan & Guinee, 2004; Ong et al., 2012).

2.3.3 Cheese Flavour

While the mathematical modelling of salt uptake and diffusion through cheeses is being investigated for improving production consistency, it is important to recognize the role of salt at the point of consumption to evaluate product desirability and consistency. The addition of salt and its transport throughout cheese is vital to the regulation of the flavours and texture of the final cheese product (Fox et al., 2000a; Lucey et al., 2003; Ong et al., 2012). The role of salt in cheese texture is demonstrated by the development of unique meso-structures produced through interactions with the para-casein matrix (El-Bakry & Sheehan, 2014; Everett & Auty, 2008). Salt also effects the flavour compounds produced through the regulation of enzymatic activity and flavour compounds from microbiological fermentation (Dimos et al., 1996; Lauverjat et al., 2009).

The flavour profiles of aged cheeses are attributed to the microbiological production of enzymes that produce specific flavour compounds that typify quality, aged Cheddars and similar aged cheeses. Salt serves to provide salty taste to young cheeses that may not have the high concentrations of other flavour compounds (Lauverjat et al., 2009; Lawrence & Gilles, 1969; McSweeney, 2004). Salt interacts with starter and non-starter cultures to limit their growth and fermentation rates, thereby limiting the production of metabolites that effect the structure of the cheese matrix or flavour compounds (Lucey et al., 2003; Parente & Cogan, 2004; St-Gelais, Lessard, Champagne, & Vuillemard, 2009).

Salt also affects the activity of enzymes by affecting the protein folding. This is especially important for the aging process where slow, controlled rates of proteolysis and lipolysis can produce distinct flavour compounds, long after the death of the starter cultures (Dimos et al., 1996). Arboatti et al. (2014) showed that cheeses that were only salted for five minutes had higher levels of aroma and bitterness that increased in intensity with respect to time, while cheeses that had undergone longer salting periods had higher values of saltiness, creaminess, and flavour. These findings are expected as the lower levels of salting time would limit the diffusion of salt into the curd to decrease the rate of fermentation and enzyme activity, making cheeses that tended to have higher levels of acidity from continued fermentation and bitterness from proteolysis (Arboatti et al., 2014; Lauverjat et al., 2009; Lawrence & Gilles, 1969; McSweeney, 2004). Salt serves to regulate the degradation of the protein matrix that

would otherwise occur due uncontrolled proteolysis. Moller et al. (2012) and Lawrence and Gilles (1969) specifically noted higher rates of casein degradation and lactose consumption in low-salt cheddar cheeses during aging.

Salt clearly plays a vital role in controlling the microbiological, functional, and flavour properties of cheeses. A mechanistically derived mathematical model to describe salt transport through cheese curd is necessary for optimizing and controlling those properties. Validation of the model must be completed under realistic cheese processing conditions with detection methods that use conventional destructive-type assessment of salt transport or real-time, non-invasive methods that track the concentration gradients with respect to diffusion time.

2.5 Methods for Assessing Salt Diffusion in Complex Matrices

Several analytical methods have been used to assess the movement of sodium and chloride ions within cheese curd systems, including destructive and non-destructive techniques. Destructive testing methods analyse the sodium or chloride ion content in small, distinct cheese samples of known dimensions, detecting the average concentrations over the dimensions of the sample. Typical destructive analysis equipment used to detect the average salt, chloride ion, or sodium ion concentration include inductively-coupled plasma mass spectroscopy (ICP-MS), ion-exchange chromatography, or stand-alone chloride analysis techniques (Floury, Jeanson, Aly, & Lortal, 2010; Floury, Madec, Waharte, Jeanson, & Lortal, 2012).

Non-destructive methods typically use magnetic resonance or fluorescence to track the diffusion of salt or salt ions throughout the cheese matrix as a function of time without requiring the sample separation and preparation at distinct times. These techniques allow for increased data collection from fewer salted curd samples. Typical tools used that provide a fast, real-time assessment of the diffusing salt ions include nuclear magnetic resonance (NMR), magnetic resonance imaging (MRI), and fluorescence spectroscopy such as fluorescence recovery after photobleaching (FRAP) (Boisard et al., 2013; Floury et al., 2010; Floury et al., 2012; Silva, Peixoto, Lortal, & Floury, 2013; Vogt et al., 2015). A combination of destructive and non-invasive techniques is usually employed to model the transport behaviour of salt ions in model or commercial cheese systems.

Although sources have endeavoured to model the movement of salt through various cheeses or cheese analogues, findings have been limited primarily to determining the effective

diffusion coefficient according to Fickian diffusion laws under limited, controlled curd properties and processing conditions (Floury et al., 2010). While this approach has proved adequate to estimate the diffusion behaviour for various cheese systems, there is a lack of work detailing the diffusion behaviour as a function of the curd properties and system itself, namely the changing matrix conditions that affect the transport of both moisture and salt ions out of and into the curd, respectively (Floury et al., 2010). Furthermore, while several sources have sought to analyse the transport behaviour through controlled cheese curd systems, there has been limited investigation to the mechanisms of the physical changes in the matrix structure at the meso-scale as a function of transport and processing conditions, which is vital to optimizing the textural and physical attributes of the cheeses experienced by the consumer (Aguilera, 2005; Floury et al., 2010; Silva et al., 2013).

2.6 Mathematical Models for Salt Diffusion in Complex Systems

Adolf Fick derived equations to model diffusion behaviours in 1855 that are frequently used as primary steps to describe diffusion behaviours in systems (Fick, 1995). The equations provide a framework to model the net movement of diffusing solutes as a function of the concentration gradients, diffusing time, and the diffusion coefficient between the solute and the solvent or solid matrix. Fick's Laws have been used by the majority of literature sources describing the transport of salt through cheese and other complex food matrices with varying degrees of success, usually using the unsteady-state transient semi-infinite system approach (Floury, Camier, et al., 2009; J. Luo, Pan, Guo, & Ren, 2013).

2.6.1 Fickian Diffusion

A common method for evaluating and modelling the transport of a soluble constituent through a complex system is under the simplest assumptions from Fick's Laws of Diffusion. Fick's laws of diffusion relate the rate of solute diffusion in a given matrix to the concentration differential across the system that provides the driving force for diffusion, and a constant diffusion coefficient for the diffusing solute in the stationary matrix describes the rate at which the solute is transported (Welty, Wicks, Wilson, & Rorrer, 2008). Fick's First Law relates the flux magnitude of a diffusing solute to the concentration gradient, where flux occurs from high concentration regimes to low concentrated regions. This relationship is shown in the following equation:

$$J_i = -D_i \frac{\partial C_i}{\partial x}$$

Equation 2-1: Fick's First Law (Welty et al., 2008).

where J_i [kg m^{-2} s^{-1}] is the mass flux rate for the solute *i*, D_i [m^2 s^{-1}] is the mass diffusion coefficient of solute *i* in the matrix, and dC_i/dx [kg m^{-4}] is the concentration gradient of solute *i* over a changing distance, *x*.

Fick's Second Law of Diffusion relates how the concentration changes with respect to time due to diffusion, using a partial differential equation. When evaluated from one dimension, the relationship reads as follows:

$$\frac{\partial C_i}{\partial t} = D_i \frac{\partial^2 C_i}{\partial x^2}$$

Equation 2-2: Fick's Second Law of Diffusion (Welty et al., 2008).

where $\partial C_i/\partial t$ [kg m^{-3} s^{-1}] is the concentration gradient of solute *i* over time and $\partial^2 C_i/\partial x^2$ [kg m^{-4}] is the second order concentration gradient of solute *i* over a changing distance. Both of Fick's Laws have been adapted for use in steady-state and unsteady-state conditions, dependent on the experimental designs.

2.6.1.1 Steady-State Diffusion

Fick's Laws can only be used if several different assumptions apply which may not be representative of the conditions encountered during the actual salting of cheese curd (Floury et al., 2010). Zorrilla and Rubiolo (1994b) used a diffusion cell design to assess the movement of salt through cheese curds under steady-state conditions. They assumed that the volume of solution in either vessel containing brine or water did not appreciably change throughout the course of the experiment, allowing for the following equation to be derived:

$$V_A \frac{dC_A}{dt} = -D_{eff}\, S\, \frac{C_A - C_B}{L}$$

Equation 2-3: Steady-state relationship between the solute concentration gradient and effective diffusion coefficient (Zorrilla & Rubiolo, 1994b).

where V_A [m^3] is the volume of liquid that is the source of the diffusing solute, *S* [m^2] is the cross-sectional area of the matrix where diffusion occurs, *L* [m] is the length of the matrix diffusion occurs through, and C_A and C_B [kg m^{-3}] are the solute concentrations in compartments *A* and *B*, respectively. The effective diffusion coefficient may be related to the

mass diffusion coefficient of the solute in the media, D_i, as a function of the pore qualities of tortuosity and porosity, which restrict or slow the transport of the solute through the media by decreasing the transport area or increasing the effective diffusion path length, respectively (Welti-Chanes, Mujica-Paz, Valdez-Fragoso, & Leon-Cruz, 2003). The following equation demonstrates the relationship between the effective diffusion coefficient and the mass diffusion coefficient of the solute in the media:

$$D_{eff} = \frac{\varepsilon}{\tau_D} D_i$$

Equation 2-4: Effective diffusion coefficient relationship with the diffusion coefficient of solute, *i*, through the matrix (Welti-Chanes et al., 2003).

where ε [dimensionless] is the porosity of the matrix, and τ_D [dimensionless] is the diffusive tortuosity of the pores in matrix. Given the challenges of determining the porosity and tortuosity of a system, most mathematical models that describe salt transport in cheeses and other complex systems describe the diffusion behaviour as a function of the effective diffusion coefficient (Floury et al., 2010).

2.6.1.2 Unsteady-State Diffusion

The most commonly used assessment of salt diffusion in cheese curd is the unsteady-state, transient diffusion in a semi-infinite medium. This approach determines the concentration profiles for solutes in a matrix with respect to time and location using Fick's Second Law of Diffusion. It is assumed that the matrix is infinitely long for the diffusion timeframe to not have accumulation effects, and that the solute source maintains the same solute concentration throughout the experiment. The use of the diffusion cell and key assumptions allows for the assessment of diffusion using the unsteady-state, semi-infinite calculation method according to Fick's second law that uses the boundary conditions to determine the effective diffusion coefficient for the target solute in the matrix.

$$t_D = 0, \quad C_i = C_0$$

$$x = 0, \quad C_i = C_s \; for \; t_D > 0$$

$$x \to \infty, \quad C_i = C_0 \; for \; t_D > 0$$

where t_D [s] is the solute diffusion time, x [m] is the distance of the concentration from the curd or cheese interface, C_s [kg m^{-3}] is the concentration of solute *i* at the interface between the curd or cheese and the solute source, and C_0 [kg m^{-3}] is the initial concentration of solute *i*

at start of diffusion time. Applying the initial conditions to Fick's Second Law of Diffusion yields the unsteady-state, semi-infinite method to determining the concentration values at specific distances from the concentrated surfaces with respect to time using the complementary error function, *erfc*, shown below:

$$\frac{C(x,t_D)-C_0}{C_s-C_0}=erfc\left(\frac{x}{2\sqrt{D_{eff}t_D}}\right)$$

Equation 2-5: Unsteady-state semi-infinite approach according to Fick's Law (Crank, 1975; Welty et al., 2008).

Assessing the concentration of solute *i* at different locations or at different times, provides the means to determine the effective diffusion coefficient. Likewise, if a reasonable estimation of the effective diffusion coefficient is known, the concentration of the solute *i* can be determined at different times and distances from the interface. This calculation is only assumed to be applicable for short enough experiment times such that the solute does not diffuse throughout the matrix. The unsteady-state, semi-infinite medium approach and boundary conditions are only appropriate for systems that meet the requirement of a Fourier number under 0.05, thereby restricting the mass transfer conditions to support slow diffusive transport that may be measured over long testing times. The Fourier number is defined as F_0 [dimensionless] in Equation 2-6.

$$F_0=\frac{D_{eff}t}{L^2}$$

Equation 2-6: Fourier number equation.

Figure 2-6 demonstrates a common experimental set-up for the unsteady-state, semi-infinite medium calculations using a uniform semi-infinite cylindrical matrix and a well-mixed solute source.

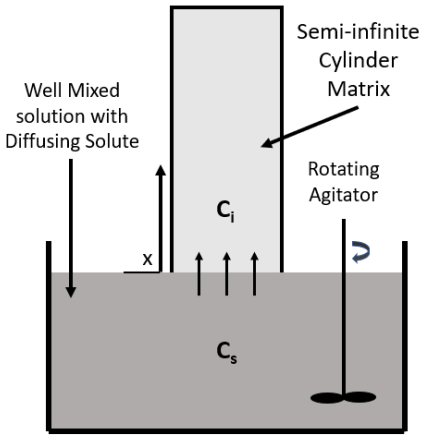

Figure 2-6: Semi-infinite cylinder experimental set up adapted from Floury et al. (2010).

The solute would diffuse into the semi-infinite matrix as a function of the effective diffusion coefficient of the diffusing solute in the matrix and the concentration gradient, according to Fick's Laws for diffusion. Part of the issue with modelling salt uptake and diffusion in the cases for dry salting is the issue of mixing. Salt brines may be agitated to promote mixing under laboratory and some commercial processing conditions, however creating good mixing conditions during dry-salting is difficult as there is limited moisture produced for agitation to occur. One method to improve mixing may be achieved through the agitation of the cheese curds themselves via ultrasound (Sanchez, Simal, Femenia, Benedito, & Rossello, 1999).

Application of Equation 2-6 to unsteady-state diffusion experimental conditions, such as those demonstrated in Figure 2-6 and careful sampling and destructive testing methods, allow the production of concentration curves that describe the diffusion of a solute with respect to time and distance from the interface. Figure 2-7 shows the actual concentration profiles of two cheeses brined under different temperatures as a function of time and distance from the cheese surface compared to the model predictions made with constant diffusion coefficient at two sampling times.

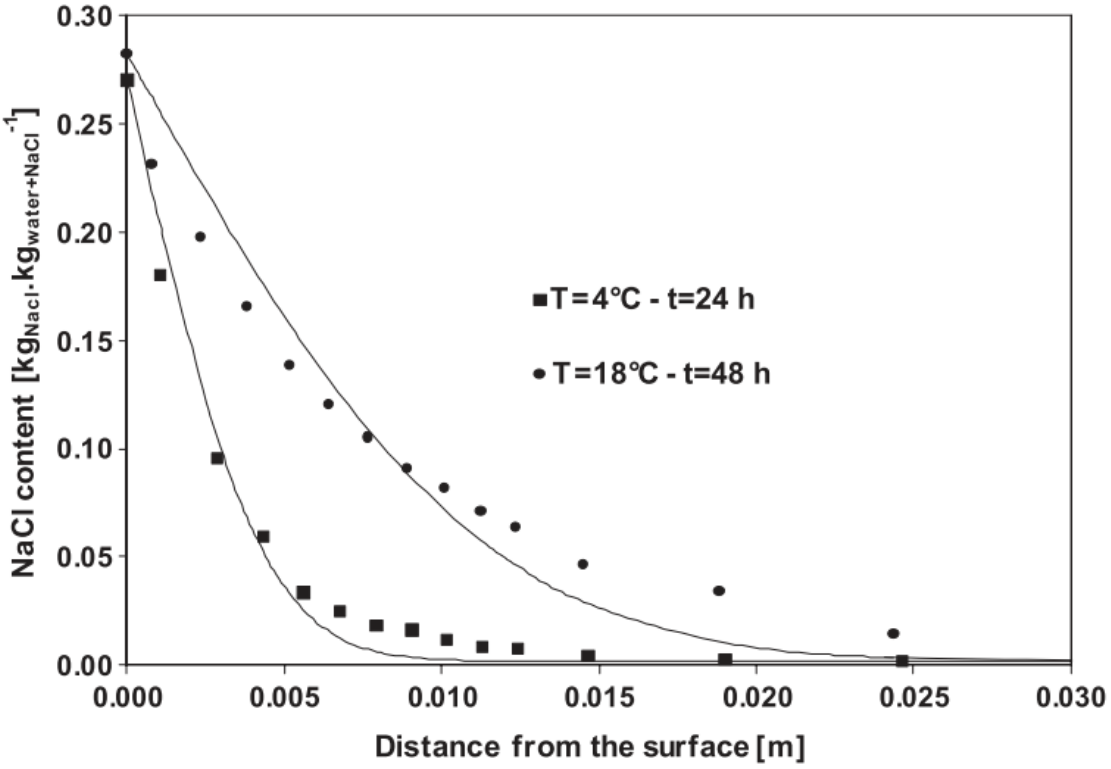

Figure 2-7: Difference between expected Fick diffusion and brining experiment results. Symbols are experimental and solid lines represent the salt distribution predicted by Fickian diffusion (Pajonk, Saurel, & Andrieu, 2003).

The salt concentration profiles from a brined cheese experiment over time (symbols) compared to the predicted model lines using constant diffusion coefficients demonstrate that although the diffusion curves are similar, the standard Fickian diffusion method does not exactly match the diffusion behaviour observed in salted cheeses (Pajonk et al., 2003). This indicates that a number of factors are likely to be affecting the diffusion behaviour and that standard Fickian diffusion modelling is not be sufficient for modelling the transport of salt ions through a changing curd matrix (Floury et al., 2010; T. P. Guinee & Fox, 2004).

2.6.1.3 Limitations to Fickian Diffusion Models

The derivations for Fick's Laws create simple mathematical functions to describe diffusion under controlled conditions. However, for the functions to be applied to a given system, several assumptions are made about the conditions of diffusing solute and solvent that may not be applicable for modelling diffusion in cheese matrices (Floury et al., 2010). The assumptions made using Fick's Laws to model diffusion fail to describe the physical conditions through which diffusion occurs. Doulia, Tzia, and Gekas (2000) note the problematic assumptions that are made when describing the diffusion of salt through cheese curd to determine the effective diffusion coefficient and they are reported below.

1. **The calculation of the effective diffusion coefficient, D_{eff}, assumes that diffusion is primarily a function of molecular diffusion.** Other mechanisms of diffusion, such as capillary or porous diffusion, may be involved in the transport behaviour of salt diffusion through cheese curd systems.
2. **The concentration gradient of the diffusing solute is the driving force for diffusion according to Fick's Law.** The chemical potential gradient is more likely to be the driving force for salt diffusion into the curd.
3. **The effect of temperature on the value of D_{eff} is assumed to be an Arrhenius relationship.** The truthfulness of this statement is uncertain, given that the curd structure is likely to change as a function of temperature.
4. **Any changes in the effective diffusion due to the matrix changes, such as swelling or contraction, are ignored and assumed to be accounted for in the calculation for D_{eff}.** This is a sweeping assumption that disregards the differences between curds that may be undergoing dynamic structural changes, making the model less applicable for real systems.

Welty et al. (2008) also report other general assumptions that have been made using Fickian diffusion to model the salt diffusion include:

1. **No reactions occur during diffusion.** The diffusing ions do not undergo reactions during the diffusion process, but the matrix may have reactions occurring that could affect the effective diffusion properties (i.e. changing pH due to lactose conversion to lactic acid).
2. **There are no interactions or adsorption between the diffusing solute and solvent or the para-casein matrix, making the concentration gradient the only driving force for solute diffusion.** This is not true for diffusing salt in cheese, where salt ions interact with the protein matrix. Furthermore, calcium salts and whey proteins expelled in the free whey may interact with the diffusing salt, affecting the overall diffusion behaviour.
3. **The physical properties of the whole system remain constant.** This premise is problematic as fresh cheese curd continue to expel moisture and the physical structure of the curd changes with respect to time, the moisture content, and the salt concentration.
4. **The source of the solute is well-mixed throughout the experiment.** This may not be true for dry-salted systems where the moisture content on the surface of the curds

may not provide perfect mixing conditions. Boundary layer conditions that limit the salt concentration available at the cheese surface may also exist for poorly mixed brining systems.

5. **Diffusion coefficients are constant at a given temperature.** Ideal Fickian diffusion coefficients are constant for specific solute-matrix or solvent conditions at a given temperature. The changing structure of the curd matrix and changing interactions between salt ions and the matrix inherently make the diffusion coefficient inconstant, regardless of changes in temperature.
6. **The solute concentration is constant at the domain boundaries of the interface between the concentrated solution and the matrix and at distances far from the interface, for unsteady-state diffusion conditions.** The concentration may not be constant at the interface because of expelled moisture (especially in dry-salted cases) and the changing matrix properties due to interactions with the salt that may change the domain boundary concentrations during the experiment.

Fickian diffusion provides the simplest approach to estimate the salt transport behaviour observed during the salting of cheese, especially via brining. It is the preferred modelling method for several cheese analogues and experimental conditions, evidenced by several literature sources investigated by Floury et al. (2010). Despite the limitations presented, Fickian diffusion models provide an essential first step to modelling salt uptake, especially since the mechanisms governing the movement of salt and whey into and out of cheese curds are not completely confirmed.

The differences between the predicted Fickian diffusion models and actual salt concentration profiles have led to a few groups applying the use of different diffusion modelling methods than the standard, single solute Fickian diffusion approach. These methods attempt to account for the effects of other diffusing solutes on the diffusion of salt and model, thereby alleviating some error associated with the assumptions from the one-dimensional, single solute Fickian diffusion approach. The next section discusses two other techniques to model salt uptake behaviour.

2.6.2 Other Mathematical Modelling Methods

The two other primary diffusion models used to describe the salt ion diffusion behaviour in curd matrices are multicomponent Fickian diffusion and Stefan-Maxwell diffusion. Both

methods account for salt diffusion behaviour that are affected by interactions between other diffusing solutes or interactions with the matrix.

2.6.2.1 Generalized Multicomponent Fickian Diffusion

One of the challenges with using Fickian diffusion to describe only the transport of salt through a curd matrix is that the mathematical assumptions required for Fickian diffusion do not match the behaviours observed during the salting of cheese, specifically the expulsion of whey from the curd matrix while salt is transported into the system (Geurts, 1978). The expulsion of whey automatically creates a counter-diffusion condition, where calcium salts, lactic acid, whey proteins, and other compounds are transported in the free whey with the added sodium chloride (Payne & Morison, 1999; Simal, Sanchez, Bon, Femenia, & Rossello, 2001). Generalized multicomponent Fickian diffusion is designed to account for any affects from interactions between other diffusing components in the free whey that may otherwise influence the diffusion rates.

Multicomponent diffusion modelling shares some similarities to standard single-solute Fickian diffusion in that concentration gradients provide the driving force for diffusion, but the role of interacting diffusing solutes on the diffusion is assessed through the use of diffusion coefficients that describe the diffusion behaviours between two different solutes (Bird, Stewart, & Lightfoot, 2007). The origin for this approach begins with the thermodynamic understanding of the driving forces for diffusion, where the influence of components on the entropy and internal energy of a system (Bird & Klingenberg, 2013; Crank, 1975).

Bird and Klingenberg (2013) carefully demonstrate the development of Fickian multicomponent diffusion from thermodynamic principles. Through careful use of the Gibbs-Duhem equation and several thermodynamic assumptions, the flux rate for a specific species in a curd matrix may be assessed as a function of the component's concentration gradient, the concentration gradients of other diffusing solutes, and the diffusion coefficients describing the interactions between the diffusing solutes (Bird & Klingenberg, 2013; Gerla & Rubiolo, 2003). A simplified demonstration of the multicomponent Fickian diffusion relationship for a system with *N* diffusing solutes at a constant temperature is shown in Equation 2-7.

$$J_i = -\sum_{j=1}^{N-1} D_{ij} \nabla x_j$$

Equation 2-7: Multicomponent Fickian diffusion equation (Gerla & Rubiolo, 2003).

In Equation 2-7, D_{ii} [$m^2\ s^{-1}$] and D_{ij} [$m^2\ s^{-1}$] are the independent main and cross diffusion coefficients of solutes *i* and *j*, ∇x_j [$kg\ m^{-4}$] is the concentration gradient of a single solute *j* over the system length. The main diffusion coefficients describe the diffusive flux contribution due to the specific solute gradient while the cross-diffusion coefficients represent the contribution of other solute concentration gradients to the flux of the solute. There are *0.5N(N-1)* independent diffusivities for a system with *N* components (Bird, 2004). Equation 2-7 simplifies to the standard Fickian diffusion equation for binary systems when the number of diffusing solutes reduces from *N* to two components, with one of the components assigned as the reference species for determining the flux behaviour in the system.

The simplest demonstration of multicomponent diffusion is the assessment of diffusion in a ternary system, where a matrix may be used to describe the flux relationships to the main and cross diffusion coefficients. Equations 2-8 and 2-9 show the multicomponent diffusion flux relationships for a ternary component system.

$$\begin{bmatrix} J_i \\ J_j \end{bmatrix} = \rho \begin{bmatrix} D_{ii} & D_{ij} \\ D_{ji} & D_{jj} \end{bmatrix} \begin{bmatrix} \nabla \omega_i \\ \nabla \omega_j \end{bmatrix}$$

Equation 2-8: Multicomponent Fickian diffusion equation for a ternary system.

$$J_k = J_i - J_j$$

Equation 2-9: Flux balance for multicomponent Fickian diffusion in a ternary system, where component *k* is a reference species.

Equations 2-8 and 2-9 show the multicomponent Fickian diffusion case for a ternary species system, where ρ [$kg\ m^{-3}$] is the density of the system, $\nabla \omega_i$ [m^{-1}] is the gradient of mass fraction of species *i* with respect to a diffusion distance, and the subscripts *i*, *j*, and *k* are the different species in the ternary system (Floury et al., 2010). Equation 2-9 relates the flux of the reference component, *k*, to the calculated fluxes of the other two components.

The calculations for ternary systems are simple, but the effect of several components make assessing the diffusion behaviours of a large number of chemical species difficult to calculate when the cross diffusion coefficients are unknown (Bird & Klingenberg, 2013; Gerla & Rubiolo, 2003). A more nuanced approach to modelling salt diffusion that is affected by the

diffusion of other compounds and the chemical potential gradient of the system is achieved using the Maxwell-Stefan diffusion model.

2.6.2.2 Stefan-Maxwell Diffusion

The Stefan-Maxwell diffusion model assesses the transport rate of solutes in a system with their interactions with other components in a system. The differences between the multicomponent Fickian diffusion model and Stefan-Maxwell model is the use of chemical potential gradients as driving forces for diffusion instead of concentration gradients and the lack of a required reference species for flux analysis (Bird & Klingenberg, 2013; Floury et al., 2010; Payne & Morison, 1999). The Stefan-Maxwell diffusion model is shown in the following equation:

$$\frac{x_i}{RT}\left(\frac{\partial \mu_i}{\partial x}\right) = \sum_{j \neq i}^{n} \frac{x_j \boldsymbol{J}_i - x_i \boldsymbol{J}_j}{c_{Tot} D_{ij}^{SM}} \; for \; i = 1, \ldots n$$

Equation 2-10: Stefan-Maxwell equation for a multicomponent system.

where R [m^3 Pa K^{-1} mol^{-1}] is the ideal gas constant, T [K] is the temperature, D_{ij}^{SM} [m^2 s^{-1}] is the binary Stefan-Maxwell diffusion coefficient between components i and j, c_{Tot} [kg m^{-3}] is the total mass concentration of all the components in the system, x_i and x_j [dimensionless] are the molar fraction of components i and j, respectively, and $d\mu_i/dx$ [J mol^{-1} m^{-1}] is molar chemical potential gradient of component i over a distance of dx. Payne and Morison (1999) further simplified the right side of the equation by making it a function of the velocity of the diffusing components as follows:

$$\frac{x_i}{RT}\left(\frac{\partial \mu_i}{\partial x}\right) = \sum_{i=1}^{n} \frac{x_i x_j}{D_{ij}^{SM}} \left(v_j - v_i\right)$$

Equation 2-11: Stefan-Maxwell model (Floury et al., 2010; Payne & Morison, 1999).

where v_i and v_j [m s^{-1}] are the velocity relative to stationary coordinates of component i and j, respectively. The chemical potential of the components in the system are determined as a function of the Gibbs free energy of the system in Equation 2-12:

$$\mu_i = \frac{\partial G}{\partial c_i}$$

Equation 2-12: Chemical potential equation for a species *i*.

where dG [J] is the differential of the Gibbs free energy and dc_i [mol m^{-3}] is the differential of the molar concentration of species i in the system. The chemical potential of a component is a function of the system conditions, such as pressure and temperature, and concentrations of all components within the system. For isobaric and isothermal cases, the chemical potential of a species may be determined from the species activity in the system, as shown in Equation 2-13.

$$\mu_i = \mu_i^0 + RT \ln a_i$$

Equation 2-13: Chemical potential equation under isobaric and isothermal conditions.

In Equation 2-13, a_i [dimensionless] is the activity of species i and μ_i^0 [J mol^{-1}] is the standard chemical potential under prescribed temperature and pressure conditions. The activity of a component is a function of the component's activity coefficient and the molar ratio of the species to the entire molar system. Given that the activity coefficients are only appropriate for ideal-like systems that are very dilute, the ability to determine the chemical potential for a system using the above equations becomes fraught with error in non-dilute systems (Bird & Klingenberg, 2013).

While the Stefan-Maxwell diffusion model allows for a more realistic reflection of the diffusion behaviours of multicomponent systems by accounting for interactions between components as functions of chemical potentials and not concentrations, it poses new challenges for implementation to complex food systems.

2.6.2.3 Limitations of Multicomponent Fickian Diffusion and Stefan-Maxwell Assessment

Multicomponent Fickian diffusion and Stefan-Maxwell diffusion models provide additional complexity to the standard Fickian diffusion method used to model salt transport in cheese, by accounting for the effects of interactions between the diffusing salt and other compounds in the curd system on the salt diffusion behaviour (Bird & Klingenberg, 2013; Floury et al., 2010; Payne & Morison, 1999). While the added complexity improves the understanding of the factors that affect salt diffusion, these methods are more cumbersome to employ and are limited in their application without meticulous assessment of all interacting components in the curd system.

Multicomponent Fickian diffusion requires the establishment of a reference component to determine the diffusion performance of other compounds relative to the reference (Bird & Klingenberg, 2013; Floury et al., 2010). This requirement is not ideal as it restricts the ability to compare diffusion performance in different curd systems without evaluating the exact

same compounds. It also requires significant investigation of every compound that may influence salt diffusion and the determination of their cross-diffusion coefficients. Furthermore, multicomponent Fickian diffusion uses several of the assumptions and simplifications of Fickian diffusion, which are not representative for the cheese curd system (Floury et al., 2010).

The Stefan-Maxwell model approach also poses problems in evaluating the diffusion behaviour in complicated food matrices. Evaluation of the chemical potential gradient for each component is challenging, especially for concentrated systems that do not demonstrate ideal solution behaviour. Solving the Stefan-Maxwell equation also requires knowledge of the Stefan-Maxwell diffusion coefficients for the interacting components, which are not likely to be available in current literature sources (Floury et al., 2010). Payne and Morison (1999) applied the Stefan-Maxwell approach to model salt diffusion in Gouda-type cheeses achieving an excellent fit to existing data regarding salt uptake and whey expulsion. The accuracy of the estimates was reliant on several assumptions concerning the activity coefficients governing salt and water transport with limited understanding of the mechanisms governing the interactions between the parameters modelled.

Both methods do not account for the effect of structural changes in the curd that occur throughout the salting process on the diffusion performance. Care must be taken to include the roles of changing curd porosity on the ability of moisture to be expelled from the curd matrix and salt to be transported through the matrix. Diffusion coefficients that account for the porous structure of the curd may improve model applicability to a variety of curd conditions.

2.6.3 Literature Diffusion Coefficients

Several groups have worked to assess the transport of salt and other cheese compounds through a variety of curd matrices. While the majority of the sources used the standard Fickian diffusion approach to estimate the diffusion coefficient for salt in a given curd system, a few literature sources utilized multicomponent Fickian diffusion and Stefan-Maxwell diffusion methods to evaluate the diffusion of salt and other components in the curd matrix (Floury et al., 2010; Floury, Rouaud, et al., 2009). Table 2-2 provides a summary of literature sources that evaluated the effective diffusion coefficient of salt in cheeses with a variety of different properties.

Table 2-2: Review of previous effective diffusion coefficients of sodium chloride in cheese systems (Juliane Floury et al., 2010; Luo, Pan, Guo, & Ren, 2013; Santapaola, Maldonado, & Medina, 2013).

Cheese Type	Composition			Brining and/or ripening conditions			Geometry	Model	Effective Diffusion Coefficient (D_{eff}) [x 10^{-10} m^2 s^{-1}]	Study
	Dry Matter (DM) [g kg^{-1}]	Fat/DM [g 100 g^{-1}]	pH	Process	Temperature [°C]	Brine Composition				
Camembert (soft-type cheese)	410	45	-	Brining and Ripening	14	300 g kg^{-1} NaCl, pH = 4.6	Slab	Fick (1D)	2.54	(Hardy, 1976)
Cuartirolo Argentino (soft-type cheese)	480	51.7	-	Brining and Ripening	7.5	205 g kg^{-1} NaCl, With or Without Agitation	Finite Rigid Slab	Fick (1D)	3.6	(Luna & Bressan, 1986, 1987)
Feta	440	43	-	Dry-Salted	13	-	Semi-finite geometry	Fick (1D)	2.3	(Yanniotis & Anifantakis, 1983)
White cheese (semi-hard, Turkey)	450	42	5.3	Brining	4, 12.5, and 20	150-200 g kg^{-1} NaCl	Finite Slab	Fick (1D)	2.1, 3.0, and 4.0 (no effect of brine concentration)	(Turhan, 1996)
White cheese (semi-hard, Turkey)	450	42	5.3	Brining	4-20	150-200 g kg^{-1} NaCl	Finite Slab	Fick (1D)	2.2-4.2	(Turhan & Gunasekaran, 1999)
Prato cheese (semi-hard, Brazil)	517	53	5.2	Brining	10	150, 200, and 250 g kg^{-1} NaCl	Parallelepiped	Fick (3D) and Neural Network	1.64, 4.25, and 3.0	(Baroni et al., 2003)
Romano (hard-type cheese)	535	38	-	Brining	20	160 g kg^{-1} NaCl	Slab	Fick (1D)	2.54-3.35	(T. Guinee & Fox, 1986)

Table 2-2 (continued)

Cheese Type	Composition			Brining and/or ripening conditions			Geometry	Model	Effective Diffusion Coefficient (D_{eff}) [x 10^{-10} m^2 s^{-1}]	Study
	Dry Matter (DM) [g kg^{-1}]	Fat/DM [g 100 g^{-1}]	pH	Process	Temperature [°C]	Brine Composition				
Sbrinz (hard-type cheese)	650	48	-	Brining and Ripening	7, 11, 15, and 20	200 g kg^{-1} NaCl	Touching semi-infinite cylinders	Fick (1D)	1.06 (± 0.15) to 1.88 (±0.27)	(Gros & Ruegg, 1987)
Cheddar (hard-type cheese)	650	-	-	Ripening	10	-	Slab	Fick (1D)	1.16	(Wiles & Baldwin, 1996)
Emmental (hard-type cheese)	600	48	5.4	Brining	4-18	250 g kg^{-1} NaCl, 0.3 g kg^{-1} $CaCl_2$	Infinite Cylinder	Fick (1D)	0.62-2.22	(Pajonk et al., 2003)
Model cheese (Gouda style)	580-630	~50	5.3	Ripening, Relative Humidity = 87%	13	-	Slab	Fick (1D)	2.3	(Gomes et al., 1998)
Model cheese (Gouda style)	533, 566, and 638	62, 50, and 12	4.9-5.6	Brining	12.6	130-310 g kg^{-1} NaCl, 15 g kg^{-1} $CaCl_2$	Flat cylindrical shape	Fick (1D)	~2.3 1.16-3.24	(Geurts & Oortwijn, 1975)
Model cheese	370 and 440 (with 0.5 and 1.5 g 100 g^{-1} NaCl)	20 and 40	6.2, 6.5	Release of NaCl into water	13	Water	Infinite Cylinder	Fick (1D)	2.74-5.1 (± 0.01)	(Lauverjat et al., 2009)
Model cheese	370 and 440 (with 0.5 and 1.5 g 100 g^{-1} NaCl)	20 and 40	6.2, 6.5	Release of NaCl into saliva	15	Artificial Saliva	Infinite Cylinder	Fick (1D)	2.81-3.43	(Floury, Rouaud, et al., 2009)

Table 2-2 (continued)

Cheese Type	Composition			Brining and/or ripening conditions			Geometry	Model	Effective Diffusion Coefficient (D_{eff}) [x 10^{-10} m^2 s^{-1}]	Study
	Dry Matter (DM) [g kg^{-1}]	Fat/DM [g 100 g^{-1}]	pH	Process	Temperature [°C]	Brine Composition				
Mozzarella	431	46.3	5.2	Brining	4	200 g kg^{-1} NaCl, 0, 0.1, 0.25% $CaCl_2$	Infinite Cylinder	Fick (1D)	0.59	(J. Luo et al., 2013)
Goat Cheese	-	-	-	Dry Salting	10	-	Infinite Slab	Fick (1D)	11.3	(Santapaola, Maldonado, & Medina, 2013)
Solutes: NaCl & KCl										
Prato cheese (semi-hard, Brazil)	563	52.8	5.5	Brining & Ripening	10	135.9 g kg^{-1} NaCl, 50.6 g kg^{-1} KCl	Short Cylinders	Fick (3D)	2.16 (NaCl), 1.82 (KCl)	(Bona, dos Santos Ferreira da Silva, Borsato, Monken e Silva, & de Souza Fidelis, 2010)
Prato cheese (semi-hard, Brazil)	540	52.8	5.5	Brining	10	146 g L^{-1}, 5 g L^{-1} $CaCl_2$ NaCl, 50.6 g L^{-1} KCl, 5 g L^{-1} $CaCl_2$	Parallelepiped	Fick (1D)	2.6 (NaCl), 2.77 (KCl)	(Bona, Borsato, Silva, & Silva, 2005)
Fynbo cheese (semi-hard, Turkey)	470	29.6-36.2	-	Brining	12	100 g L^{-1} NaCl, 100 g L^{-1} KCl, 15 g L^{-1} $CaCl_2$	Diffusion Cell	Fick (1D)	4.14 (NaCl), 3.91 (KCl)	(Zorrilla & Rubiolo, 1994a)
Solutes: NaCl & H_2O										
Fresh Cheese (Pasteurized Cow & Goat Milk)	-	-	-	Brining	5, 15, 20	280 g L^{-1} NaCl, 15 g L^{-1} $CaCl_2$	Cylinder & Parallelepiped	Fick (1D)	3.56, 8.26, 9.17 (NaCl), 5.71, 8.83, 9.99 (H_2O)	(Simal et al., 2001)

Table 2-2 (continued)

Cheese Type	Composition			Brining and/or ripening conditions			Geometry	Model	Effective Diffusion Coefficient (D_{eff}) [x 10^{-10} m^2 s^{-1}]	Study
	Dry Matter (DM) [g kg^{-1}]	Fat/DM [g 100 g^{-1}]	pH	Process	Temperature [°C]	Brine Composition				
Mahon cheese (soft-type, Spain)	244	-	-	Brining & Ripening (RH=85%)	12	280 g L^{-1} NaCl, 15 g L^{-1} $CaCl_2$	Parallelepiped	Fick (3D)	5.3 (NaCl), 0.078 (H_2O)	(Simal et al., 2001)
Gouda (semi-hard cheese)	565	53	-	Brining	20	170 g kg^{-1} NaCl	Slab	Maxwell-Stefan (1D)	$D_{salt\text{-}cheese}$=0.0027 – 0.014 from the core to the edge of the cheese	(Payne & Morison, 1999)
Solutes: NaCl & Lactic Acid										
Pategras	544 (13 g kg^{-1} Lactic Acid)	43	-	Brining & Ripening (RH=90%)	13	200 g L^{-1} NaCl, 5 g L^{-1} $CaCl_2$	Finite Slab	Fick (1D) multicomponent diffusion	3.2 (NaCl), ~1 (Lactic Acid)	(Gerla & Rubiolo, 2003)
Solute: H_2O										
White cheese (semi-hard, Turkey)	450	42	5.3	Brining	4, 12.5, 20	150 – 200 g kg^{-1} NaCl	Finite Slab	Fick (1D)	1.96-3.64 (15% brine), 1.69-3.09 (20% brine)	(Turhan & Kaletunc, 1992)
Mahon cheese (soft-type, Spain)	-	-	5.10-5.55	Brining	12	280 g L^{-1} NaCl, 15 g L^{-1} $CaCl_2$	Parallelepiped	Fick (3D)	0.404 (conventional brining), 0.357 (acoustically brined)	(Sanchez, Simal, Femenia, & Rossello, 2000)

Floury et al. (2010) modelled the relationship between the calculated effective diffusion coefficient for salt in cheese systems as a function of specific cheese properties and experimental conditions from a variety of literature sources. Multilinear regression was used to specifically model the salt diffusion coefficient as a function of salting temperature, dry matter content, and ratio of fat to dry matter in the cheese. The resulting best-fit equation had a coefficient of multiple determination (r^2) of 0.75. The equation developed is provided below as Equation 2-14.

$$D_{eff} = (3.39 - 1.25 \times DM + 0.24 \times \frac{Fat}{DM} - 0.14 \times T_{\circ C}) \times 10^{-10}$$

Equation 2-14: Effective diffusion coefficient of sodium chloride in cheese as a function of process variables (Floury et al., 2010).

In this equation, *DM* [g kg^{-1}] is the dry matter content and *Fat* [g kg^{-1}] is the fat content, and $T_{\circ C}$ [°C] is the temperature. Floury et al. (2010) found that the dry matter content was the only variable found to be statistically significant ($P < 0.001$) for predicting the effective diffusion coefficient for salt in various cheeses as a function of several curd and processing variables. They plotted the average salt diffusion coefficient data with respect to the dry matter content to demonstrate the negative effect of dry matter content on the estimated effective salt diffusion coefficient. Figure 2-8 presents their plot demonstrating the inverse relationship between dry matter content and the effective salt diffusion coefficient. Moisture content had previously been found to significantly affect the effective diffusion coefficient of salt in cheese systems (Geurts et al., 1974; T. P. Guinee & Fox, 2004; van den Bijgaart, 1988).

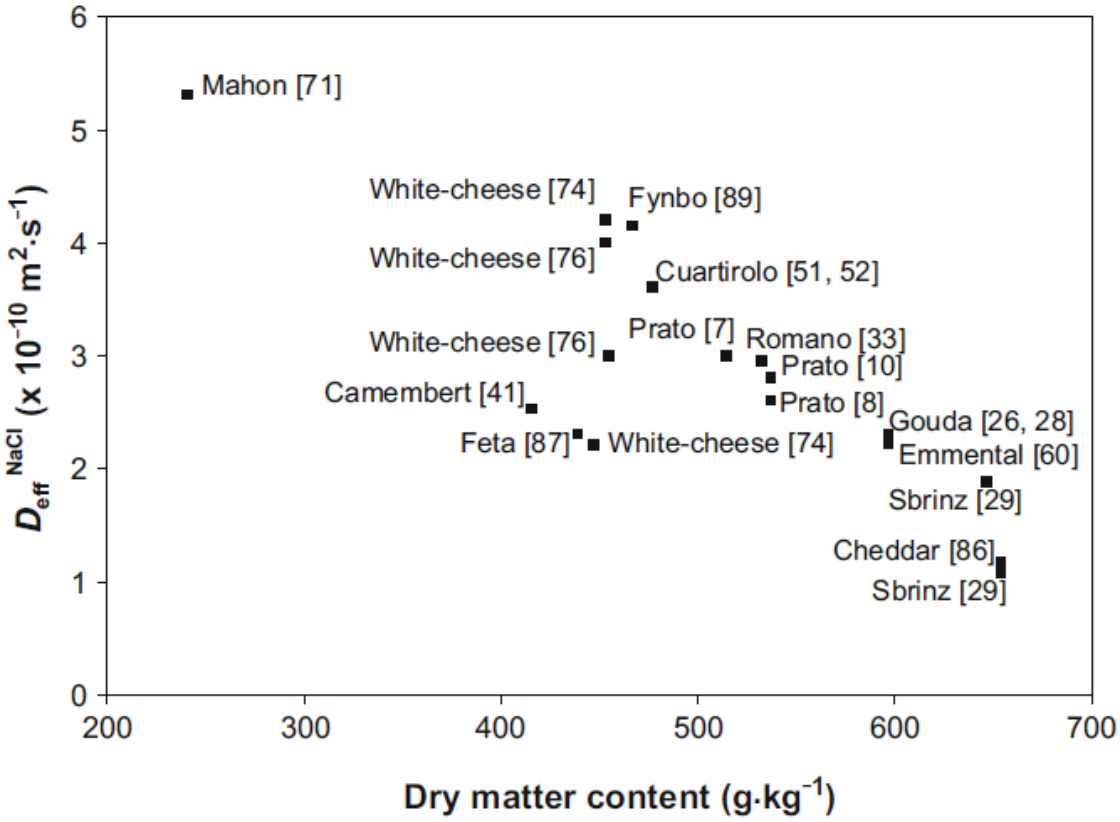

Figure 2-8: Relationship between effective diffusion coefficient for sodium chloride with the total dry matter content for cheese types tested (Juliane Floury et al., 2010).

A variety of literature sources have sought to identify the effective diffusion coefficient for salt through various cheese matrices and curd conditions. The effective diffusion coefficient, although valuable for estimating the approximate concentrations of diffused salt at various locations and salt exposure times, is only applicable for estimating the concentration of salt in the specific cheese and salting conditions of the experiment, which is not representative of the different types of cheese or the various salting conditions. Additional variables that account for changing curd structure and porosity and the effect of osmotic pressure differentials is necessary for the development of a mathematical model that mechanistically addresses the dynamic behaviour of the curd in its moisture expulsion, contraction, and changing porosity as a function of several variables.

2.7 Relevant Variables for Inclusion in a Mechanistically-Derived Mathematical Model

Previous approaches used to evaluate the effective diffusion coefficient for salt in cheese matrices have primarily relied on the concept of a concentration gradient driving force and an effective diffusion coefficient that describes the relationship between the diffusing solute and the surrounding matrix to model the diffusion of salt in complex cheese matrices. While the

previous work provides an initial point for the development of a representative model, other factors must be included to account for the changing curd properties, contraction of the matrix, and the expulsion of moisture from the matrix.

2.7.1 Moisture Expulsion

The work by Floury et al. (2010) and Geurts et al. (1974) demonstrated the importance of moisture content on the effective diffusion coefficient values for salt in various cheese curd matrices. Geurts et al. (1974) noted a relationship between the total amount of salt absorbed as a function of moisture content for curd systems. The moisture content association with salt absorption is shown in Equation 2-15.

$$-\Delta W_x \approx p\Delta S_x$$

Equation 2-15: Relationship of total salt uptake to moisture content in a cheese curd system (Geurts et al., 1974).

In Equation 2-15, W_x [g 100 g^{-1}] is the mass of water per 100 grams of solids-not-salt at a location x distance from the brined surface of the cheese, S_x [g 100 g^{-1}] is the mass of salt per 100 grams of solids-not-salt at a location x distance from the brined surface of the cheese, and p [dimensionless] is a proportionality factor for the salt and water flux behaviours. The value of p was estimated to be 2.3 to fit experimental results (Geurts et al., 1974; T. P. Guinee & Fox, 2004). Accounting for the initial moisture content value and any changes in the moisture content in the curd matrix is necessary for creating a mathematical model for the salt diffusion coefficient that reflects the actual process and curd properties for cheese systems. The role of moisture content is further complicated by the transport of moisture due to the induced osmotic pressure gradients from the salted curd surface or the mobility of the moisture due to interactions with the curd matrix.

2.7.1.1 Adaption of Darcy's Law for solvent transport

Darcy's Law describes fluid flow through porous matrices as a function of a pressure gradient across the porous system. Darcy's law could be used to model the whey expulsion behaviour observed during the salting of cheese (Horne & Lucey, 2017; Lodaite, Ostergren, Paulsson, & Dejmek, 2000). A one-dimensional adaption of Darcy's law for whey transport through a porous, curd system is shown in Equation 2-16.

$$J_W = \frac{\kappa}{\mu}\frac{dP}{dx}$$

Equation 2-16: Darcy's law flow equation adapted for a curd system.

In Equation 2-16, J_W [$m^3\ m^{-2}\ s^{-1}$] is the volume flux of whey across the cheese curd, κ [m^2] is the intrinsic permeability of the porous media, μ [Pa s] is the dynamic viscosity of the whey and dP/dx [$Pa\ m^{-1}$] is the pressure gradient across the cheese curd due to the osmotic and hydraulic pressure differentials. The intrinsic permeability may be used to estimate the whey transport properties of the porous media, under low flow conditions (where the Reynold's number is approximately one or less). This provides a starting point for modelling the whey expulsion from the curd interior during the early stages of salting. However, the diffusion of salt from the curd surface into the matrix also causes structural changes that will affect the matrix structure and overall permeability, therefore modelling the salt transport at the same time as the whey expulsion is necessary (Melilli et al., 2005; Tijskens & De Baerdemaeker, 2004).

2.7.1.2 Osmotic Pressure Effects

Application of dry salt or a salt brine to the surface of fresh cheese curds creates an osmotic pressure gradient between the brine and whey inside the cheese matrix. The osmotic pressure of a solution is defined as the amount of pressure required to prevent the solutes in solution from diffusing across a semipermeable membrane to a less concentrated solution (Kiil, 2003; Timkin & Lazarev, 2015). Osmotic pressure is a function of the number of particles within the solution, with larger numbers of distinct particles increasing the osmotic pressure, following the laws of thermodynamics (Timkin & Lazarev, 2015). The osmotic pressure of a dilute brine solution may be determined in the following equation:

$$\Pi = \sum_{j}^{\infty} i_j \mathrm{n}_j \mathrm{RT}$$

Equation 2-17: Osmotic pressure equation for dilute brine systems.

where Π [Pa] is the osmotic pressure n_j [$mol\ m^{-3}$] is the moles of solute dissolved per solution volume, and i_j [$mol\ mol^{-1}$] is the number of ions produced per dissolved solute molecule j (Alsvik & Hagg, 2013). The osmotic pressure is easily calculated for simple, dilute brine systems but is more difficult to evaluate for concentrated systems with a variety of different dissolved components. Timkin and Lazarev (2015) have investigated the osmotic pressure of

various curd and cheese whey as functions of dissolved mass concentration. Their results are shown in the Figure 2-9.

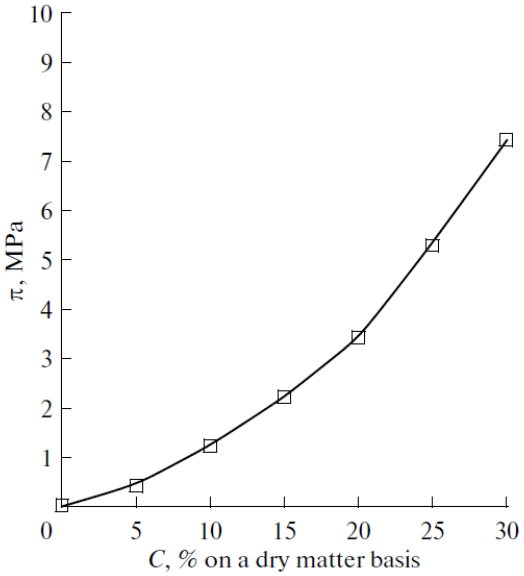

Figure 2-9: Osmotic pressure of whey as a function of concentration on a dry matter basis (Timkin & Lazarev, 2015).

Figure 2-9 demonstrates the nonlinear relationship between the solids content and the osmotic pressure in milk whey at high concentrations. Whey usually ranges between 6.3 and 6.7 percent solids by mass, so the especially nonlinear osmotic pressure behaviour observed at higher concentrations should have limited effects on the osmotic pressure value of whey in the curd matrix during the early salting stages (Fox, Guinee, Cogan, & McSweeney, 2000e). The osmotic pressure of a concentrated brine at the surface of the curd would exceed 30 MPa, creating a large osmotic pressure gradient across the curd surface (Y. Luo & Roux, 2010).

2.7.1.3 Moisture Mobility

Hinrichs, Bulca, and Kulozik (2007) investigated the mobility of water trapped in different milk gel types and determined that the renneted gel networks showed an increased level of water mobility trapped within the network pores, while acid-type gels showed even stronger moisture mobility. Gel pH and the presence of soluble calcium change the solvent quality of the moisture in the gel, thereby affecting aggregation and interactions between casein aggregates during gelation and syneresis (Lucey et al., 2003; Lucey, Tamehana, Singh, & Munro, 2000; Lucey et al., 2001; Lucey, van Vliet, Grolle, Geurts, & Walstra, 1997a). Although it would be thermodynamically favourable for highly mobile whey to be expelled as the whey becomes a lower quality solvent for the para-casein proteins, this may not be

easy if the protein structure is so tight that it limits transport out of the gel, entrapping the moisture.

The composition of the protein matrix, the pH of the system, and the strength of the matrix affect the mobility of free moisture available for expulsion from the matrix (Lucey, 2002; Lucey et al., 2000; Lucey, van Vliet, Grolle, Geurts, & Walstra, 1997b). Should the moisture be "bound" to the gel matrix due to thermodynamically favourable interactions between the matrix proteins and the whey, the rate of moisture expulsion expected from a large osmotic pressure gradient could be slower than expected.

2.7.2 Changing Porosity and Tortuosity of the Curd Matrix

Salt interactions with the curd matrix create protein hydration conditions and osmotic pressure gradients that promote additional expulsion of moisture, thereby changing the internal structure of the curd matrix (Fucà et al., 2012; Melilli et al., 2003; Melilli et al., 2005). In areas where the interactions induce a change in the structure of the matrix, porous regions may physically or chemically limit the transport of solutes (Anderson & Malone, 1974; Bhalla & Deen, 2007; Kapur, Charkoudian, & Anderson, 1997). The interactions between the ions and the pore walls make a charged concentration gradient, which may also affect the diffusion rate by restricting the cross-sectional area in the pores, whereby ions may diffuse freely to regimes with low concentrations of sodium and chloride ions (Anderson & Malone, 1974; Kapur et al., 1997; Shang, Tu, & Wang, 2009). Assessment of changing porosity and tortuosity conditions must be included in a mathematical model describing the transport of salt and whey as functions of changing curd structure.

2.8 Conclusions and Next Steps

The addition of salt to cheese is a vital step to preserving the nutritional integrity of milk for future consumption, and for the development of products that have desirable functional, textural, and flavour properties. Improving the consistency of dry-salted cheeses requires understanding of the mechanisms that control the salt diffusion process in fresh cheese curds, including the interactions with the para-casein matrix.

Salt diffusion models for cheese applications have been primarily limited to the application of traditional Fickian diffusion models for various cheese or cheese analogue systems (Floury et al., 2010). The Fickian approach does not investigate the relevant mechanisms involved in the diffusion process or account for the changing internal gel structure or expelled free whey. The following chapters will provide insight to the syneresis behaviours that occur prior to and

during the onset of salting. The role of the osmotic pressure gradient, moisture expulsion behaviour, and changing curd porosity will also be addressed with a variety of destructive and non-destructive techniques. Accounting for the various factors and driving forces controlling the changing curd structure and properties will allow for the development of a fundamentally-derived mathematical model to describe the transport processes that occur during the salting of fresh cheese curds that may be used in industrial cheese manufacture.

Chapter 3 Evaluation of Milk Gel Contraction

3.1 Introduction

Control of curd cutting and syneresis conditions are vital to the production of curds ready for salting and further processing. Previous practices used to evaluate syneresis behaviour commonly worked by measuring the changing free whey mass or volume of a given curd with respect to time (Walstra et al., 1985). These techniques provide a simple method to assess syneresis behaviour but may not be suitable for fundamentally describing syneresis under conditions of commercial cheesemaking plants. Furthermore, assessing syneresis as solely the change in whey or gel weight or volume neglects the role of gel surface area on the syneresis behaviour observed.

A mechanistic approach to assessing syneresis should simultaneously describe whey expulsion behaviour relative to the changing surface area of the curd, thereby describing a whey flux. Furthermore, evaluation of syneresis should occur under processing settings similar to industrial cheesemaking conditions, ideally without undue damage to the fragile gel and maintenance of a humid headspace if the curd is exposed to air. The following subsections provide a brief introduction to the relevant variables that effect syneresis, current methods used to evaluate syneresis behaviour, and the existing mathematical models.

3.1.1 Gelation and Syneresis Mechanisms

Milk is a stable oil-in-water colloidal system that contains high levels of calcium, phosphorus, and hydrophobic protein content due to the formation of stable casein micelles (Choi, Horne, Johnson, & Lucey, 2008; Horne, 2002; D. Horne & J. Banks, 2004; Horne & Lucey, 2017). Although the exact structure has yet to be ascertained, casein micelles may be described as a collection of hydrophobic caseins interspersed with small nanoclusters of colloidal calcium phosphate (CCP) and partially covered with hydrophilic κ-caseins that extend into the surrounding serum (Choi et al., 2008; Horne, 2002; D. Horne & J. Banks, 2004). Hydrophilic κ-casein "brushes" provide steric repulsion in tandem with the electrostatic repulsion between the negatively charged micelles to prevent the casein micelles from associating. This phenomenon creates a stable colloidal suspension and the conditions for light diffraction to create the white, "milky" colour observed in fluid milk (D. Horne & J. Banks, 2004).

Milk is converted from a stable emulsion to a soft gel during a coagulation process where chymosin enzymes hydrolyse the hydrophilic domain of the κ-caseins from the casein

micelles (Dalgleish, 2009; Fagan, O'Callaghan, Mateo, & Dejmek, 2017). Removal of the hydrophilic domain destabilizes the casein micelles, which creates thermodynamically favourable conditions for the hydrophobic casein micelles to aggregate and form clusters that increase in size (Fagan et al., 2017; Mellema, Heesakkers, van Opheusden, & van Vliet, 2000). Eventually, sufficient aggregation produces large clusters and chains that form a stable, three-dimensional para-casein network that gradually increases in structural rigidity over time (van den Bijgaart, 1988; Walstra et al., 1985). The solvent quality of the water surrounding the casein aggregates decreases, thereby creating a driving force for expulsion (van Dijk, 1982; Walstra & van Dijk, 1983; Walstra et al., 1985).

Syneresis commences once the gel is cut or otherwise disrupted and the entrapped whey can begin to escape from the gel (McSweeney, 2007; van Dijk, 1982; van Dijk & Walstra, 1986; Walstra et al., 1985). Loss of whey and increased protein-protein interactions lead to the rea-assembling of the gel structure, especially during the early stages of syneresis (Mellema et al., 2000). Reduction in gel moisture increases the rigidity of the gel, and gradually reassembly slows as gel approaches an equilibrium state (van Vliet & Walstra, 1994). Figure 3-1 shows the changes that occur on the meso and macro-scale during gelation and syneresis.

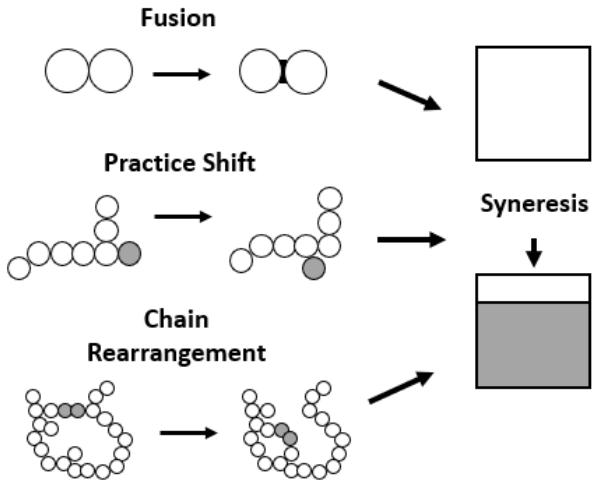

Figure 3-1: Demonstration of the meso and macro scale changes that occur during gelation and syneresis, where the white area represents the curd volume and grey area the whey volume after syneresis, adapted from Horne and Lucey (2017).

In Figure 3-1 the shaded circles represent protein sections that attach and form in different arrangements while whey is expelled at the macro-scale during syneresis and the curd volume contracts, as shown by the changed white box size. The rate of syneresis is increased during cheesemaking by controlling several different variables. Mixing, reduction of curd size,

temperature increase, and reduction of pH (thereby increasing the soluble calcium content which increases the electrostatic charge to induce casein aggregation) can all be used to increase the rate of syneresis (van den Bijgaart, 1988; van Dijk & Walstra, 1986; Walstra et al., 1985). The experiment described later in this chapter seeks to limit the effect of changing temperature, changing pH during syneresis, or the effect of gel damage from the assessment of syneresis.

3.1.2 Current Methodologies to Evaluate Syneresis

The most common methods of syneresis evaluation consist of (1) evaluation of the physical curd changes, (2) evaluation of whey changes, (3) assessment of dry matter content in the gel, and (4) examination of curd density changes (Walstra et al., 1985). Curd heights or weights would be assessed at specific timepoints during syneresis for the first case, but accurately measuring curd dimensions can be challenging while contracting. Total drained whey mass or volume or dilution via a tracer are the most common approaches in the second case evaluation type. (Dejmek & Walstra, 2004). Evaluation of curd moisture content to describe syneresis behaviour is a destructive measurement that usually over-calculates the amount of whey remaining inside the curd due to the presence of whey at the surface of the curd (Mateo, O'Callaghan, Gowen, & O'Donnell, 2010). The last approach listed is not commonly used as it requires immersion of the curd in varying solutions with different densities to ascertain the changing density of the curd (Walstra et al., 1985). Low resolution NMR has also been successfully used to evaluate the changing syneresis behaviour, but has not been frequently used since the early 1990's. (Tellier, Mariette, Guillement, & Marchal, 1993).

While some in-line syneresis assessment methods do incorporate the use of image analysis, little work has been done using image analysis techniques to evaluate syneresis in single curd systems (Fagan et al., 2007; Mateo et al., 2010; Mateo et al., 2009). Image analysis techniques provide advantages when evaluating syneresis behaviour as they are non-invasive, allow for evaluation within whey, and provide insight into the changing curd volume and surface area.

3.1.3 Current Methods of Modelling Syneresis

Syneresis has been historically modelled as a first-order rate equation, where a rate constant and a linear constant would describe the changing volume of the curd. Adjustments to a regular first-order rate decay equation have usually been included to account for the fact that the gels do not shrink to infinitely small sizes. Peri, Lucisano, and Donati (1985) described

syneresis as a function of both the rate constant, equilibrium curd volume, and initial curd volume. Equation 3-1 shows the solution to their rate equation.

$$V - V_{inf} = (V_0 - V_{inf})e^{-Kt}$$

Equation 3-1: Curd volume rate equation (Peri et al., 1985).

In Equation 3-1, V [mL] represents the curd volume, V_{inf} [mL] represents the curd volume at infinite time, V_0 [mL] represents the initial curd volume, and K [s^{-1}] represents the rate constant. Daviau et al. (2000) used a two-relaxation time model to describe syneresis, as shown in Equation 3-2.

$$R_{Total} = R_1 e^{-t/\tau_1} + R_2 e^{-t/\tau_2} + R_3$$

Equation 3-2: Syneresis modelled as water mass per casein mass (Daviau et al., 2000).

In Equation 3-2, R_{Total} [g H_2O g^{-1} casein] refers to the mass of water per mass of casein in the curd, R_1 and R_2 [g H_2O g^{-1} casein] are linear constants, R_3 [g H_2O g^{-1} casein] is the mass of water per mass of casein in the curd at equilibrium, and τ_1 and τ_2 [s] are relaxation constants. Although this equation does not specifically model the changing curd volume, it does include a second exponential decay term to describe non-ideal syneresis behaviour. The majority of the models proposed to describe syneresis usually model syneresis as an exponential or power-based rate equation for curd volume or some other volume proxy, such as yield or moisture content (Dejmek & Walstra, 2004). None of these models examined whey expulsion relative to changes in the curd surface area.

3.1.4 Summary of Current Methods and Limitations

The common methodologies used to evaluate syneresis either require the destruction of the curd (moisture content method) or rely on measurement of whey volume or mass as the curd undergoes syneresis. These methods may or may not be utilized under plant-like conditions, where humid airspaces limit the effects of local drying on the rate of syneresis. Furthermore, if the curds tested are removed from the whey, they could experience gravitational weight effects on the curd matrix, thereby affecting the curd integrity and the observed syneresis. An alternative approach would be to evaluate the changing curd volume in a whey solution in-situ, thereby limiting the effect of those variables on the natural syneresis. The current rate decay models used to describe syneresis are also limited due to the lack of surface area value inclusion.

The purpose of this chapter is to introduce a novel technique used for assessing renneted milk gel syneresis in-situ using image analysis and mathematical modelling techniques under

experimental conditions akin to cheesemaking processes within industry. The following sections provide the experimental design and results from non-destructive in-situ experiments evaluating gel contraction and whey expulsion as a function of syneresis time. They also introduce the reporting of syneresis behaviour as a flux value for a longer period of evaluation time.

3.2 Experimental Design

An experiment was designed to evaluate the contraction mechanics of renneted milk gels in-situ using image analysis techniques. Renneted milk gels were formed in clear dialysis tubing, exposed to temperature-controlled whey, and imaged throughout the spontaneous syneresis process. Analysis of the images was conducted using the MATLAB® Image Processing Toolbox to convert the pixel data of the gel outline to gel volume and surface areas for each image. Data from multiple gels undergoing syneresis was collected and fitted with a biexponential curve to describe total whey expulsion and gel surface area using MATLAB® software. Fitted equations were then used to describe the whey flux of the gel and its relationship to the syneresis time and estimated gel moisture content, as predicted from mass balances.

The techniques developed in this experiment provide a useful estimation of whey expulsion and changes to the gel surface area without the shortcomings of the usual methodologies employed to evaluate syneresis, involving destruction or damage of gel samples. These techniques also confer experimental environments similar to plant production conditions, whereby gels would not be exposed to dry air which could cause unwanted “skin” formation or be removed from the buoyant vat conditions that cause weight-derived strain on the fresh, weak gels. Evaluation of both gel surface area and the rate of whey expulsion allowed for a fundamental assessment of the syneresis behaviour in the form of a whey flux value. This served to remove the syneresis rate from any gel size or shape effects and allow for potential application to modelling syneresis in differently sized gels.

3.2.1 Milk and Rennet Preparation

The experiment required the use of milk powders to form gels, alleviating any composition variation expected in fresh milk to affect gelation or syneresis behaviours. Although most cheeses and cheese analogues incorporate the use of milkfat, whole milk powders require higher heat treatments to produce. The additional heat treatment deleteriously affects the state of both the fat globules and the casein micelles (Ye, Anema, & Singh, 2007).

Therefore, all gels were produced using low-heat skim milk powders to otherwise limit the effects of variation in fresh milk or component damage in whole milk powders.

Skim milk was prepared by rehydrating low-heat skim milk powder (NZMP, New Zealand) (10.94% w/w) with sodium azide (0.05% w/w) to prevent unwanted microbial growth, in Milli-Q water (89.01% w/w) overnight at room temperature (~22 °C). After achieving complete rehydration of milk, glucono-δ-lactone (Sigma-Aldrich Chemical Co., USA) was added at a known concentration to achieve the target equilibrium pH after twelve hours of mixing at room temperature. Glucono-δ-lactone has been successfully used to achieve similar pH reduction in dairy systems as bacterial cultures via slow hydrolysis to gluconic acid (Lucey et al., 2000; Lucey et al., 1997a, 1997b). The concentrations of glucono-δ-lactone used were 0.164%, 0.430%, and 0.790%, to create rehydrated skim milk with pH values of 6.25, 5.75, and 5.25, respectively. The rennet solution was prepared by producing a 10% v/v solution of ChyMax M® Rennet (Chr. Hansen, Denmark) in Milli-Q water.

3.2.2 Whey Preparation

Whey was prepared by weighing rehydrated and acidified milk and gradually heating in a water bath to 31 °C. Rennet solution was added at 0.05% w/w of the entire solution and the milk was quickly mixed for 15 seconds using a magnetic stir bar to achieve complete mixing and allowed to cool to room temperatures. The renneted milk underwent gelation on the benchtop for 30 ± 2 minutes to allow for adequate gel formation at 20 ± 2 °C. The gel was cut into one-inch cubes and gently agitated before undergoing a cook step of two hours at 40 °C in a water bath to promote syneresis. Whey was separated from the gel after the cook step and filtered twice with 40-micron gravitational filters to remove any particulates. The remaining gels were discarded, and the whey was stored for experimental use.

3.2.3 Dialysis Tubing Preparation

Clear, flexible dialysis tubing provided the ideal medium to set and observe renneted milk gels undergoing syneresis. The dialysis tubes selected allowed for free transport of moisture, whey proteins, and mineral content between the gels undergoing syneresis and the surrounding prepared whey but limited the transport of caseins. They also provided a soft structure from which to adhere during gelation and easily detach from during syneresis. Five sets of approximately 125 mm length of SnakeSkin® 10 kD, 16 mm I.D. dialysis tubing (Thermo Fisher Scientific, USA) were cut and rehydrated in Milli-Q water at room temperature for two hours prior to the experiment start. One end of each tube was tied into a

knot to hold the milk samples. The tubes were then placed in whey to acclimate for an additional hour at room temperature prior to the start of the experiment.

3.2.4 Imaging Apparatus

An imaging apparatus was prepared to standardize the image capture process for gel contraction evaluation. A matte black background was arranged behind a metal stand used to hold the imaging samples. A ring with an inner diameter of 40 mm was secured to the metal frame and positioned in front of the background approximately 0.3 m above the bench to provide a consistent imaging point. A tripod was placed approximately 0.3 m from the ring to achieve perpendicular alignment of the samples suspended from the ring. A Canon® EOS 1300D camera with EFS 18-55 mm lens was mounted on the tripod and manually focused at the sample location. A ruler was placed in the same subject position and imaged for calibration purposes. Figure 3-2 shows a simplified illustration of the imaging apparatus.

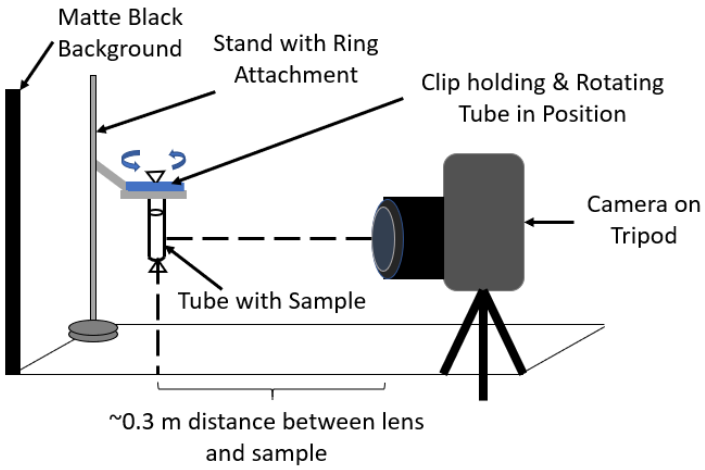

Figure 3-2: Simplified illustration of the image apparatus, not to scale.

3.2.5 Sample Gel Preparation and Evaluation

Prepared dialysis tubes were removed from the whey, patted dry, and weighed with numbered dialysis tubing clips. Prepared milk was weighed and warmed to 31 °C in a water bath for twenty minutes prior to the experiment. Rennet was added to the milk at 0.05% w/w using a dropper and quickly mixed into the sample for rapid incorporation. Ten millilitres of the renneted milk were rapidly pipetted into each of the prepared five dialysis tubes. Air was incorporated into the tube before the top of the tube was twisted and clasped shut using a dialysis clip to maintain even tension on the tube walls. Each filled tube was weighed once more before being suspended in the imaging apparatus ring. Six images were captured in total, with the tube being rotated approximately 60° for each image. The gels were then left

undisturbed and suspended upright within the dialysis tubes in empty 150 mL beakers on the benchtop for approximately 30 ± 2 minutes to prevent gel damage during the gelation process.

Prepared whey was warmed to 40 °C and gently poured into the beakers around the gel-filled dialysis tubes. Movement from the fluid and during the transfer was gentle enough to not damage the gel structure but provided enough disruption to commence syneresis. The beakers were then moved to a 40 °C water bath for the extent of the experiment and a timer was started. The gel contraction in the dialysis tubes were evaluated at distinct timepoints by removing the tubes from the whey and capturing six images of the tube rotated in the apparatus in approximately 60° increments, before returning the tube to the whey. Multiple images were captured to calculate the average gel volume and surface area. Images were captured in ten-minute intervals during the first two hours of syneresis, followed by fifteen-minute intervals for the next hour of syneresis, and thirty-minute intervals for the following hour of syneresis. Images were also captured at 24 and 48 hours after starting syneresis. Gels were removed from the tubes at the end of the experiment, blotted dry, and weighed before being discarded. The whole process was conducted with starting milk and whey pH values of 6.25, 5.75, and 5.25, reflecting a wide range of applicable cheesemaking pH values during syneresis.

3.3 Analysis Techniques

Evaluation of syneresis was completed using image analysis techniques with MATLAB® Image Processing Toolbox software. Images were converted to a binary and analysable state before assessing the diameter of the gel, pixel by pixel. Each pixel width diameter was converted into millimetre lengths using the images with the calibration ruler. The diameters were used to calculate the volumes and exposed surface area of each pixel-width cylinder of the gel, and then summed to determine the whole gel volume and surface area in each image. The average surface area and volume values from the six images were reported as the curd volume and surface area at each imaging time.

Gel volume and surface area data collected from the image analysis results were compiled and used to model the gel surface area and accumulated whey volume as a function of syneresis time. MATLAB® was once more used to fit two first-order exponential functions in series for both the changing accumulated whey volume and gel surface area using a MATLAB ® *lsqcurvefit* function to identify variable values that minimize the least-squares

error. These values were then used to describe the syneresis behaviour observed as a whey flux.

3.3.1 MATLAB® Image Analysis Methods

Image pre-processing consisted of cropping and converting the coloured image to grey-scale, *imcomplementing* the image, filling in holes, enhancing contrast of the pixels using histogram equalization, and converting the image to binary using a threshold value. A structured disk element was established and used to perform a morphological opening on the binary image consisting of an erosion followed by a dilation. This process was conducted to smooth the edges of the gel image and remove possible errors due to slight differences in thresholding and lighting effects, smoothing features on the order of 0.5 mm or less. All other objects were removed from the image and analysis commenced on the pre-processed outline of the gel.

Assessment of the gel started with the tracing of the gel outline and assessing the properties of the whole gel region using the *regionprops* function. The properties calculated with the *regionprops* function were converted from pixel-based units to millimetre-based units using the calibration image values, which were manually determined. The locations of each pixel on the boundary of the gel outline were sorted by location in the y-axis direction. Starting at the top of the gel, a local disk diameter was calculated from the difference between the x-axis coordinates for coordinates at the same y-axis coordinates. This disk diameter was converted into a millimetre-based length and used to calculate the volume and surface area of the local disk using Equations 3-3 and 3-4, respectively.

$$V_{Disk} = \left(\frac{\pi}{4}\right) {D_{Disk}}^2 H_{disk}$$

Equation 3-3: Local disk volume equation.

$$A_{Disk} = \pi D_{Disk} H_{disk}$$

Equation 3-4: Local disk surface area equation.

If the diameter of the local disk was found to be less than 2% of the bounding box width of the gel, it was assumed that the gel was at a local peak and the local surface area was calculated from Equation 3-5.

$$A_{Disk-Peak} = \frac{\pi}{4} {D_{Disk-Peak}}^2$$

Equation 3-5: Local disk surface area equation for localized gel peaks.

In Equations 3-3, 3-4, and 3-5, D_{Disk} [mm] is the diameter of the local disk, H_{disk} [mm] is the one-pixel length height of the local disk, V_{Disk} [mm^3] is the volume of the local disk, A_{Disk} [mm^2] is the outer edge surface area of the local disk, and $A_{Disk\text{-}Peak}$ [mm^2] is the surface area of the local disk at a peak. The process was performed in a loop for each pair of boundary coordinates until all had been assessed. The total gel volume and surface area for each image was calculated by summing all the local disk volumes and surface area values. The MATLAB® code developed for the evaluations is shown in Appendix A. The reported gel volume and surface area was calculated as an average of the gel volumes and surface areas from the six images captured at each timepoint per gel. Figure 3-3 provides a visual representation of the methods used to assess the curd volume and surface area.

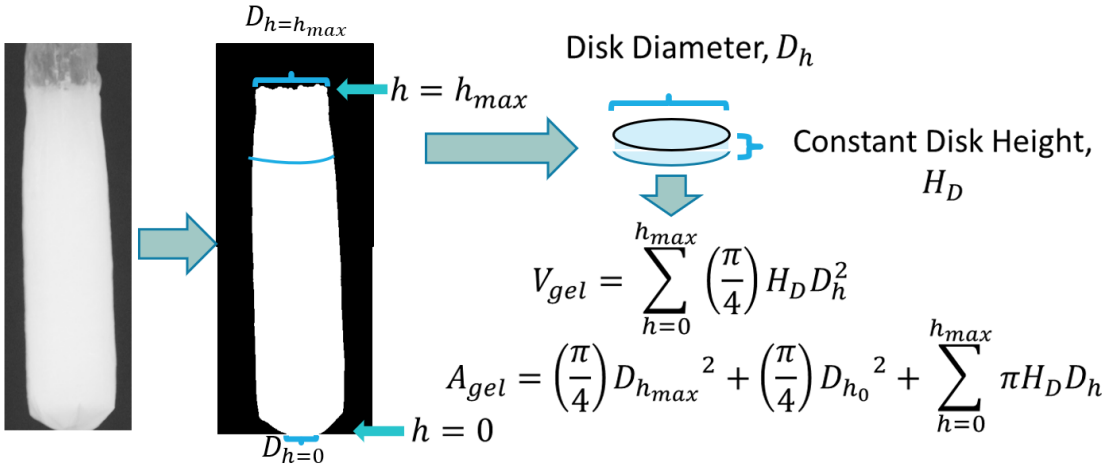

Figure 3-3: Process to calculate gel volume and surface area using images and MATLAB ® Image Processing Toolbox techniques.

3.3.2 Statistical Analysis of Gel Volume and Surface Area Results

Gel volume results for the initial time points prior to any syneresis were compared to the known starting renneted milk volumes pipetted into the dialysis tubes to determine the degree of error in the image analysis technique for assessing gel volume. The average gel volume and surface area for each gel at each time point was collected and assembled to form the complete results for each pH treatment tested. Results were then assessed using one-way analysis of variance (ANOVA) to determine if any of the treatments produced statistically significant differences, within 95% confidence.

3.3.3 Modelling of Gel Contraction and Whey Expulsion

The changing gel volumes were converted to accumulated whey volume by assuming that the difference between the volume values at sequential time points were equal and opposite to the amount of whey expelled in the same time difference, thereby maintaining a volume balance.

Accumulated whey volume expelled was calculated at each timepoint by summing all the previous whey volumes expelled, as shown in the equation below.

$$V_{W,i} = \sum_{i=1}^{n} (V_{gel,i-1} - V_{gel,i})$$

Equation 3-6: Accumulated whey volume at measurement *i* as a function of the changing gel volume.

In Equation 3-6, $V_{W,i}$ [mL] is the accumulated whey volume at measurement *i*, and $V_{gel,i-1}$ [mL] and $V_{gel,i}$ [mL] are the volume of the gel at measurement *i-1* and *i*, respectively. The curve produced for the accumulated whey volume expelled and the gel surface area were fitted with a biexponential curve with five unknown variables (including a constant) using the MATLAB® *lsqnonlin* function to determine values to minimize the sum of square errors. While single first-order models have proven sufficient for some previous modelling, the inclusion of a second first-order exponential component allows for modelling to account for changes in the dominating mechanisms as a function of syneresis time. The models fitted are shown in Equations 3-7 and 3-8 below.

$$V_w = A_W + B_W e^{-p_{W,1}t} + C_W e^{-p_{W,2}t}$$

Equation 3-7: Accumulated whey expulsion model fitted to gel syneresis data.

$$SA_{Gel} = A_{SA} + B_{SA} e^{-p_{SA,1}t} + C_{SA} e^{-p_{SA,2}t}$$

Equation 3-8: Gel surface area model fitted to gel syneresis data.

In Equations 3-7 and 3-8, SA_{Gel} [mm^2] represents the surface area of the gel, *A* [mL] or [mm^2] represents the best fit value at equilibrium, *B* and *C* [mL] or [mm^2] represent amplitude variables for the short and long-term dominating rate constants, and *p* [s^{-1}] represent the first-order rate constants. The subscripts *W* and *SA* refer to accumulated whey and gel surface area, respectively, and *1* and *2* refer to the first and second solved rate constants for the short term and long-term dominating mechanisms, respectively.

Fitting occurred using the least-squares method, whereby minimization of the sum of squared errors and the root mean squared errors were used to determine the quality in addition to the calculation of the coefficient of determination, r^2. The relevant statistical equations used to establish fit are shown below.

$$SST = \sum_{i=1}^{n} (y_i - \bar{y})^2$$

Equation 3-9: Sum of the total squares equation.

$$SSE = \sum_{i=1}^{n} (y_i - \hat{y}_i)^2$$

Equation 3-10: Sum of the squared errors equation.

$$RMSE = \sqrt{\frac{SSE}{n_t - p_n - 1}}$$

Equation 3-11: Root mean squared error equation.

$$r^2 = 1 - \frac{SSE}{SST}$$

Equation 3-12: Coefficient of determination equation.

In Equations 3-9 through 3-12, *SST* refers to the total sum of squares, *SSE* refers to the sum of the squared errors, *RMSE* refers to the root mean squared errors, r^2 refers to the coefficient of determination, n_t refers to the number of total observations, p_n refers to the number of parameters tested (four for the two first-order rate exponential functions in series), y_i refers to the data value of observation *i*, $\bar{y}$ refers to the average value of all data, and $\hat{y}_i$ refers to the predicted value of observation *i* using the model. Although the r^2 is not appropriate, statistically speaking, for assessing the quality of fit for a non-linear model, it was included as a general quality of fit consideration. The minimization of the root mean squared error is a superior statistic as it shows the average error of the residuals in the units of the data assessed, essentially showing the average distance between the data points and the model predictions.

Calculation of the best fit values of the variables was conducted by uploading the accumulated whey volume or gel surface area data with respect to evaluation time, evaluating the sum of the squared errors for a given starting estimate of the variable values, and using the *lsqcurvefit* function to determine the variable values to achieve the local minimum of the sum of squared errors. The model was split to first solve for the nonlinear exponential variables by transforming the data to eliminate the effects of the constant *A* and using a "dummy" initial guess for the linear variables and using *lsqncurvefit* to find the optimal nonlinear rate constants using a least squared approach. The new rate constants were then included in the next step for determining the linear and constant variable values that achieve best fit of the unadjusted data with a second run of *lsqcurvefit.* This method both determines the best variables for fitting using a least squares algorithm approach and minimizes the effect of poor initial variable value guesses on ascertaining the global minimum least squares error. The MATLAB ® code used for the fitting is shown in Appendix B.

3.3.4 Modelling Whey Flux and Changing Average Gel Moisture Content

Whey flux is calculated from the gel surface area and accumulated whey volume models as the rate of whey volume accumulation per surface area. The first derivative of the accumulated whey volume model is divided by the gel surface area model to produce the whey flux at any time, *t*. The equation describing the whey flux is shown below.

$$J_W = \frac{\frac{dV_W}{dt}}{SA_{Gel}} = \frac{-B_W p_{W,1} e^{-p_{W,1}t} - C_W p_{W,2} e^{-p_{W,2}t}}{A_{SA} + B_{SA} e^{-p_{SA,1}t} + C_{SA} e^{-p_{SA,2}t}}$$

Equation 3-13: Whey flux equation derived from the modelled gel surface area and accumulated whey volume.

The average internal gel moisture content may be estimated using the whey expulsion models combined with the known starting properties of each gel, such as starting milk moisture content, milk density, and the density of the whey produced. If it is assumed that the whey expelled maintains moisture content consistency, and the relevant whey and milk densities are the same, Equation 3-14 may be used to estimate the average internal gel moisture content.

$$MMF = \frac{\rho_{milk} V_{Gel,t=0} MMF_{milk} - \rho_{whey} MMF_{whey} V_W}{\rho_{milk} V_{Gel,t=0} - \rho_{whey} V_W}$$

Equation 3-14: Average internal gel moisture mass fraction, calculated from mass fractions.

In Equation 3-14, *MMF* [dimensionless] represents the moisture mass fraction of the gel, ρ_{milk} [kg m^{-3}] is the density of the milk used at the start of the experiment at the experimental temperature, $V_{Gel,t=0}$ [mL] is the volume of the gel at the before the onset of the syneresis, MMF_{milk} [dimensionless] is the moisture mass fraction of the starting milk gel before the onset of syneresis, ρ_{whey} [kg m^{-3}] is the density of the whey expelled from the gel at the experimental temperature, and MMF_{whey} [dimensionless] is the moisture mass fraction of the whey expelled. Equation 3-14 provides a simple estimate for the average overall internal moisture content but may not account for residual moisture at the surface of the gel which could affect the moisture content observed in a regular oven mass difference technique. Nevertheless, this approach could be useful for relating the average internal moisture content to the whey flux observed, as the gradient between the average internal moisture content and the moisture content at equilibrium would drive the whey expulsion.

3.4 Experimental Results and Discussion

3.4.1 Gel Volume

The initial volumes of each gel, prior to the onset of syneresis, were assessed and compared to the known renneted milk volumes deposited in the dialysis tubes. Results showed an average ± 4.45% (± 0.718% standard error) net difference random error between the known starting gel volume values and the image analysis value (equivalent to 0.445 ± 0.072 mL for the 10 mL gels assessed). While this finding indicates that there is some error associated with the image analysis techniques developed and shown here, the image analysis technique was deemed acceptable for the evaluation of changing gel volumes and surface areas for this experiment due to the high degree of sensitivity in detecting changes in the volume of individual gels.

A one-way ANOVA was conducted on the gel volume data within each pH treatment to determine if there was a significant difference between any of the gels evaluated within their respective treatments. Results indicated that there was no statistically significant difference between the individual gels evaluated in each pH treatment, within 95% confidence. However, one-way ANOVA assessment did show that the pH 6.25 treatment gel volumes were statistically significantly different from the pH 5.75 and 5.25 treatment gel volumes. This is reasonable as higher pH renneted gels tend to undergo syneresis at slower rates due to the lower free calcium ion content and higher insoluble colloidal calcium phosphate strengthening crosslinks within the para-casein matrix. Calcium ions decrease negative repulsive electrostatic forces and increase protein-protein interactions to enhance syneresis (Choi, Horne, & Lucey, 2015; Dejmek & Walstra, 2004; Grundelius, Lodaite, Ostergren, Paulsson, & Dejmek, 2000).

Results showed that the gel volumes gradually decreased with respect to syneresis time, following a general exponential rate decay function. This is indicative of a process that has a progressively decreasing driving force. Figures 3-4 through 3-6 show the changing gel volumes as a function of syneresis time under 40 °C whey conditions for the pH 6.25, 5.75, and 5.25 gel treatments, respectively.

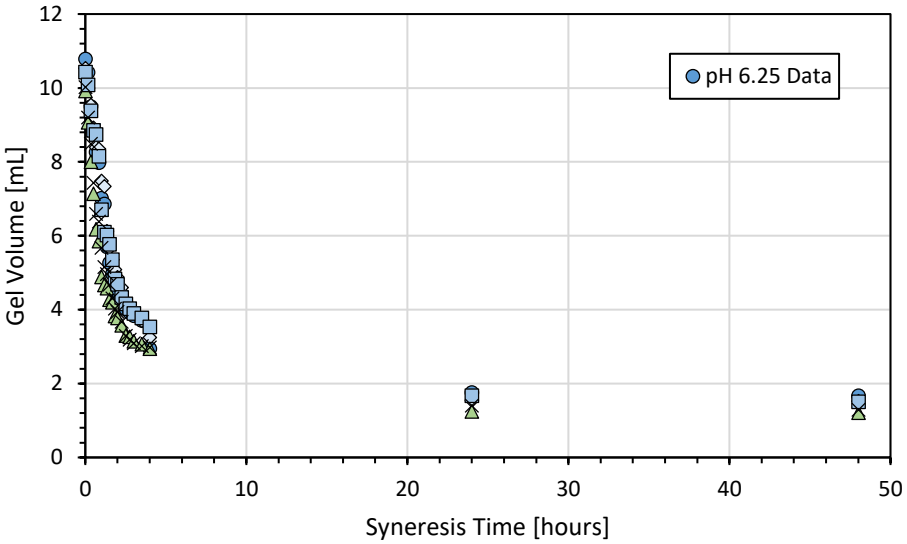

(a)

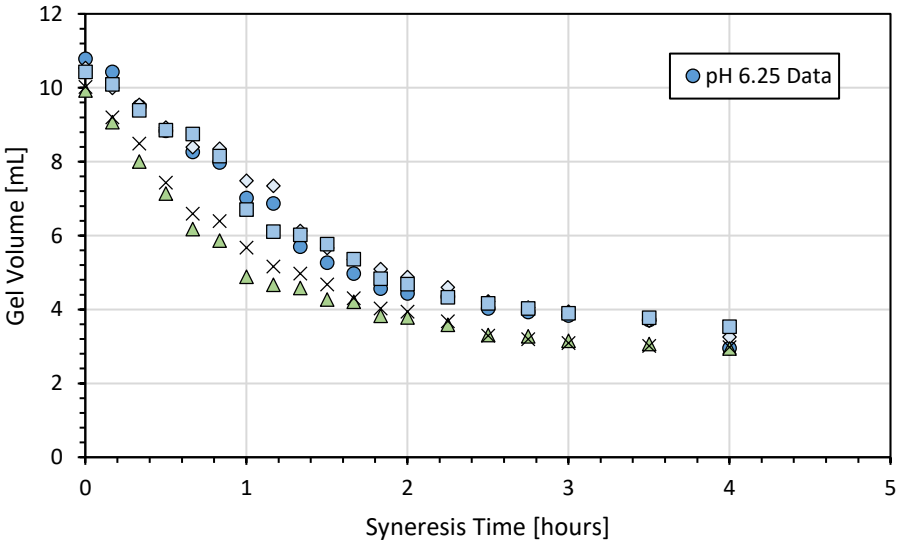

(b)

Figure 3-4: Gel volume contraction as a function of syneresis time for (a) the whole experiment and (b) the first five hours of the experiment for pH 6.25 gels held at 40 °C. Symbols represent the five replicates.

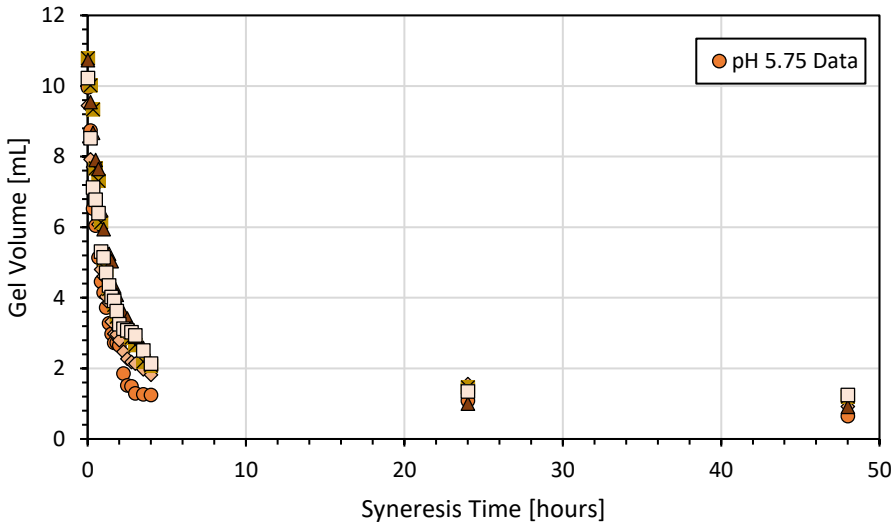

(a)

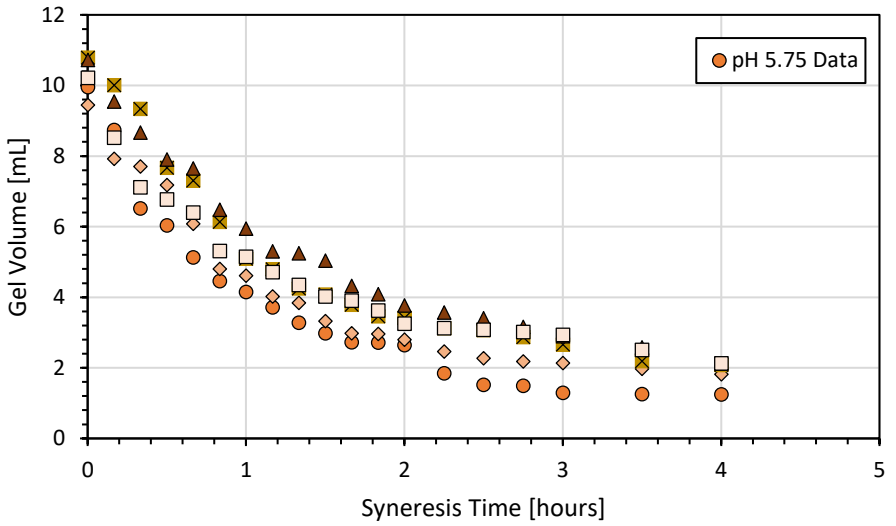

(b)

Figure 3-5: Gel volume contraction as a function of syneresis time for (a) the whole experiment and (b) the first five hours of the experiment for pH 5.75 gels held at 40 °C. Symbols represent the five replicates.

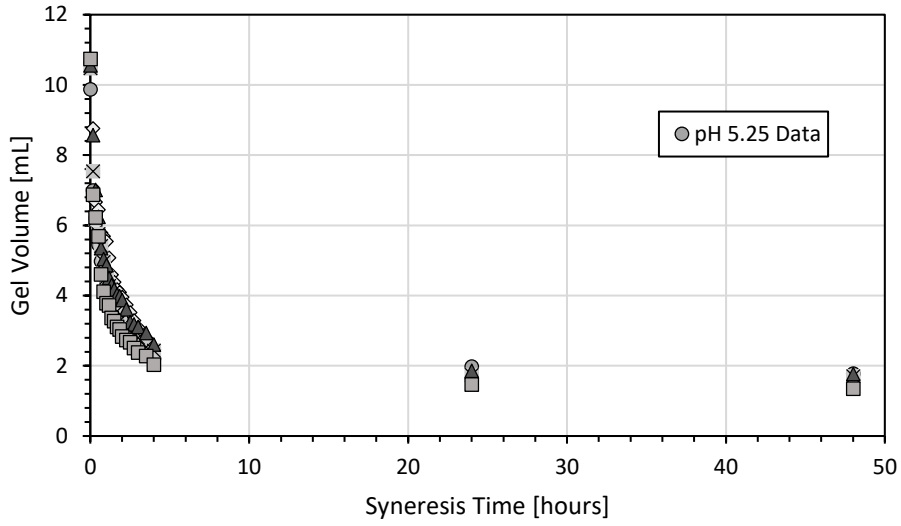

(a)

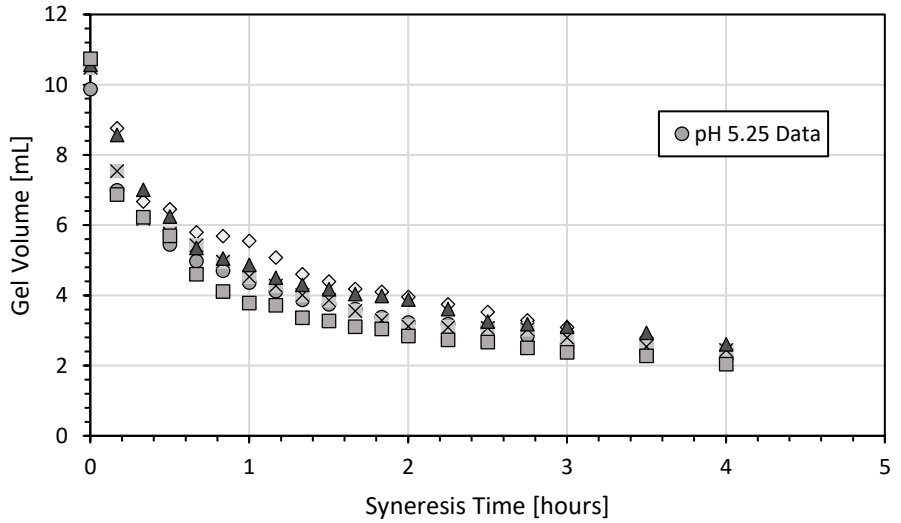

(b)

Figure 3-6: Gel volume contraction as a function of syneresis time for (a) the whole experiment and (b) the first five hours of the experiment for pH 5.25 gels held at 40 °C. Symbols represent the five replicates.

Lower gel pH appeared to increase the rate of syneresis early in the experiment, before gradually slowing to reach an equilibrium volume slightly larger than the higher pH gels. This may be explained as a function of the increased ionic calcium content and decreased negative repulsive electrostatic forces between the caseins in the lower pH gels. This promotes protein-protein interactions in the gel matrix and increase syneresis. However, the larger final volume of the lower pH gels follows the net lower total whey expulsion observed from low pH (almost acid-coagulated) gel experiments (Lucey et al., 1997b).

3.4.2 Accumulated Whey Volume

Equation 3-6 was used to successfully convert the changing gel volume data to the accumulated whey volume. This data was fitted with a five-parameter biexponential curve using the code listed in Appendix B to solve for the nonlinear and linear variables using a least squares approach. The biexponential fitting was used to describe two separate possible mechanisms that could affect the short and long-term kinetic whey expulsions behaviour. Figures 3-7 through 3-9 show the whey accumulation data, fitted model, and the contribution the exponential units and constant on the fit of the biexponential model to the data.

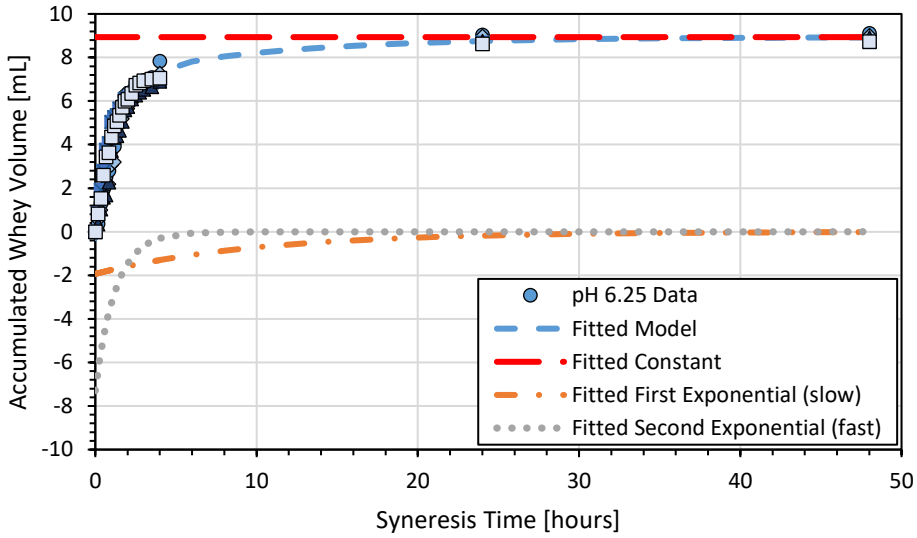

(a)

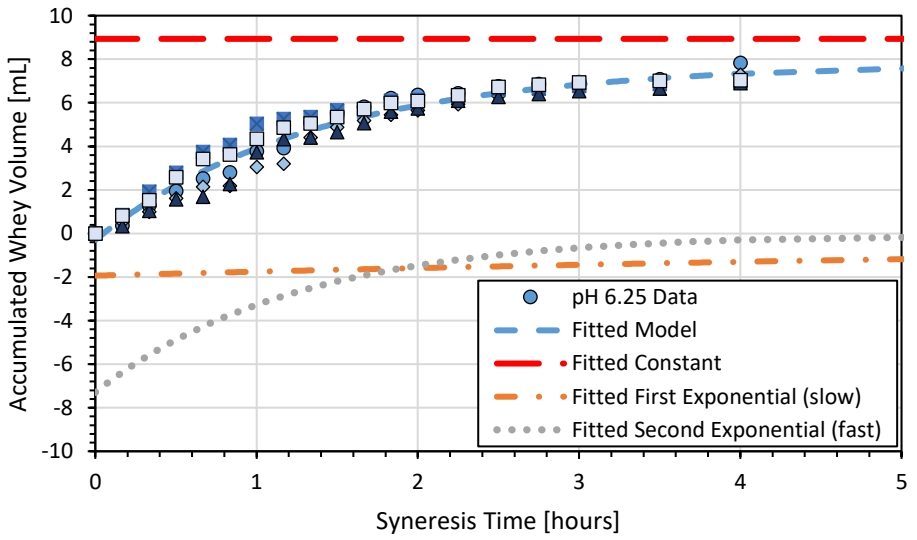

(b)

Figure 3-7: Accumulated whey volume data and fitted model as a function of syneresis time for (a) the whole experiment and (b) the first five hours of the experiment for pH 6.25 gels held at 40 °C. Symbols represent the five replicates.

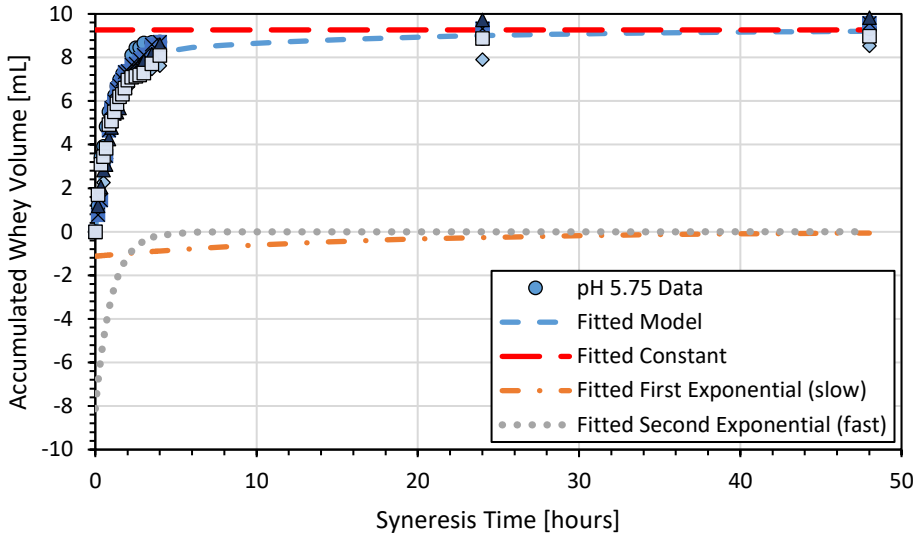

(a)

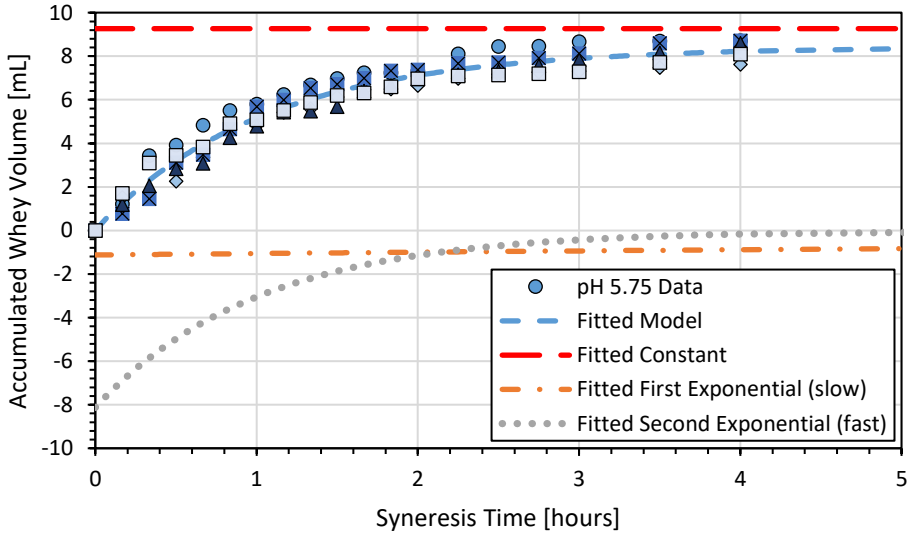

(b)

Figure 3-8: Accumulated whey volume data and fitted model as a function of syneresis time for (a) the whole experiment and (b) the first five hours of the experiment for pH 5.75 gels held at 40 °C. Symbols represent the five replicates.

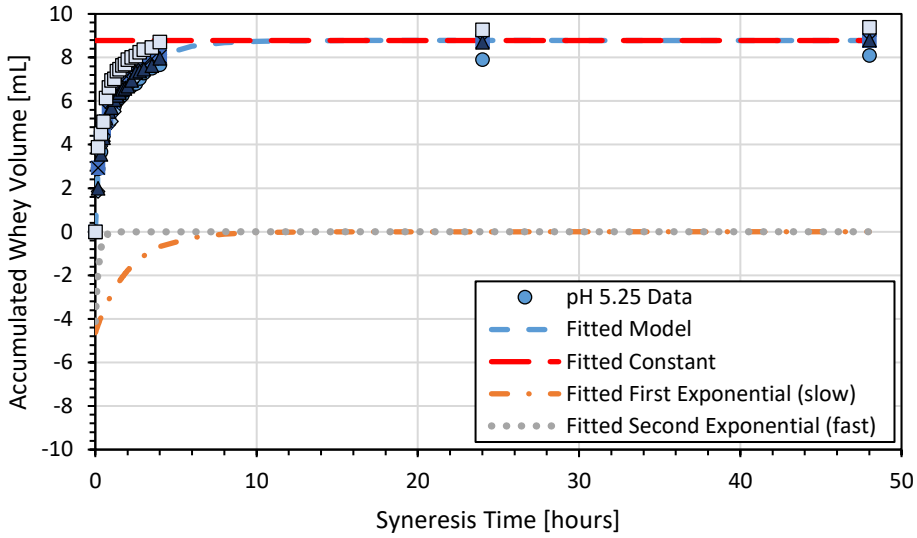

(a)

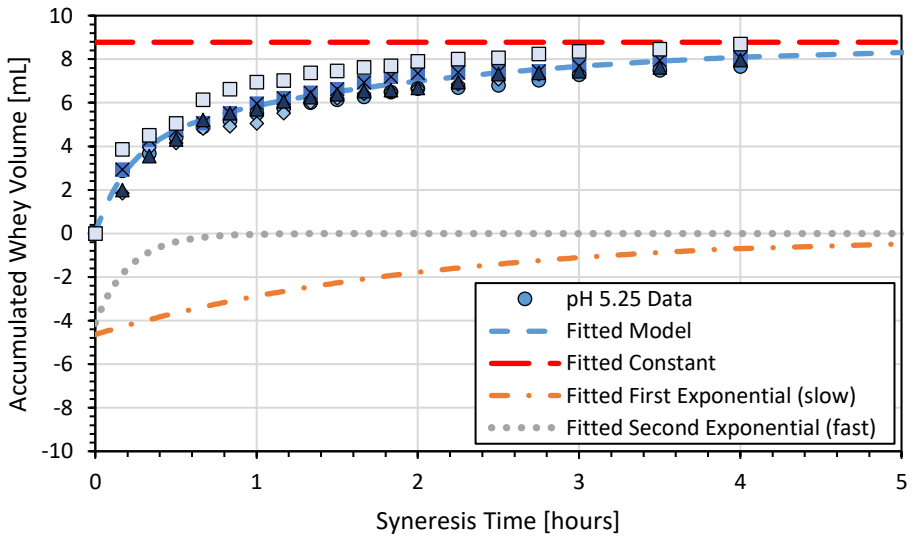

(b)

Figure 3-9: Accumulated whey volume data and fitted model as a function of syneresis time for (a) the whole experiment and (b) the first five hours of the experiment for pH 5.25 gels held at 40 °C. Symbols represent the five replicates.

Figures 3-7 through 3-9 show the contribution of the "slow" and "fast" exponential functions to the accumulated whey volume model. Fast exponentials show a faster rate of change at the beginning of syneresis, indicating that they may represent the dominant mechanism of syneresis observed shortly after its onset. The slow exponential component increases the accumulated whey volume at a slower rate, possibly representing a slower mechanism of syneresis after most of whey has been expelled. Differences between the exponential rates of change may be because of the gel pH on the rate of whey expulsion. Table 3-1 provides the

values of the fitted linear and nonlinear variables, in addition to the coefficient of determination (r^2) and the root mean squared error (RMSE).

Table 3-1: Fitted linear and nonlinear variables for the biexponential model for accumulated whey volume (Equation 3-7) with fitting statistics of root mean square error and coefficient of determination for each pH treatment.

Treatment	A_w [mL]	B_w (slow) [mL]	C_w (fast) [mL]	$p_{w,1}$ (slow) [s^{-1}]	$p_{w,2}$ (fast) [s^{-1}]	RMSE [mL]	r^2 [ ]
pH 6.25	8.93	-1.94	-7.29	2.76E-05	2.22E-04	0.443	0.970
pH 5.75	9.26	-1.12	-8.12	1.68E-05	2.72E-04	0.484	0.965
pH 5.25	8.78	-4.64	-4.12	1.33E-04	1.31E-03	0.480	0.950

Statistics presented in Table 3-1 show a high degree of fit between the fitted model and the data collected. The RMSE values also show the average error in the accumulated volume at any point to not exceed 0.5 mL for any of the models, which shows the high degree of fit. The variability in the accumulated whey expulsion is hypothesized to be related to the initial onset of syneresis, whereby slight variations in the attachment of the freshly renneted gel to the dialysis tubing affect the gel contraction behaviour and variation in gel volume and surface area.

3.4.3 Gel Surface Area

The surface area data was compiled and assessed with ANOVA to determine if there were any statistically significant differences between the gels within each pH treatment, with 95% confidence. Results indicated that there were no statistical differences within the gel surface areas for the pH 5.25 treatment, but that at least one gel showed statistically significant differences from the other gels in the pH 6.25 and 5.75 treatments, within 95% confidence. Although the gel volumes showed no difference between any of the gels within each treatment, the presence of differently shaped gels affected the assessed surface area. ANOVA was also performed to determine if there were statistically significant differences between the surface areas in each of the pH treatments. Results indicated that there was a statistically significant difference between the pH 6.25 treatment and the other two treatments, within 95% confidence. These results follow the same findings observed comparing the gel volumes for all three pH treatments.

The surface area data was successfully fitted with a five-parameter biexponential curve using the code listed in Appendix B to solve for the nonlinear and linear variables using a least

squares approach for all three pH treatments. Figures 3-10 through 3-12 show the surface area data and fitted biexponential models.

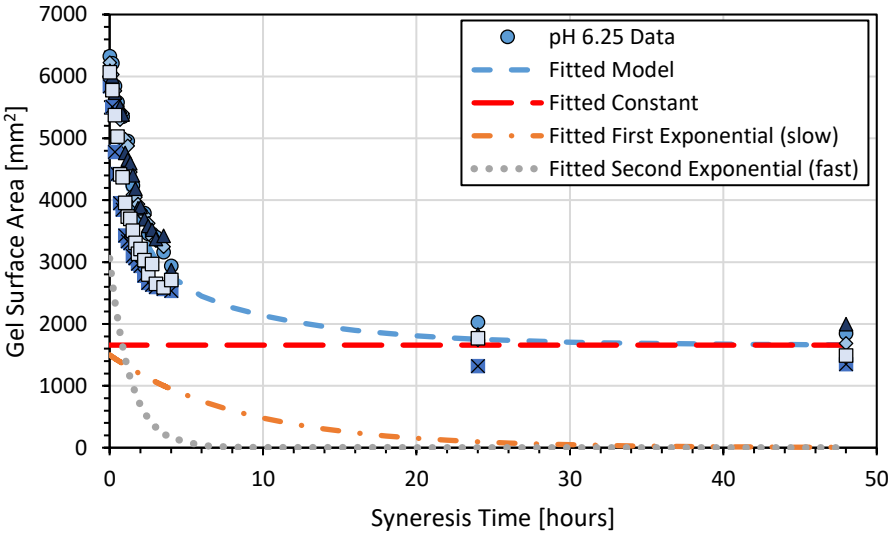

(a)

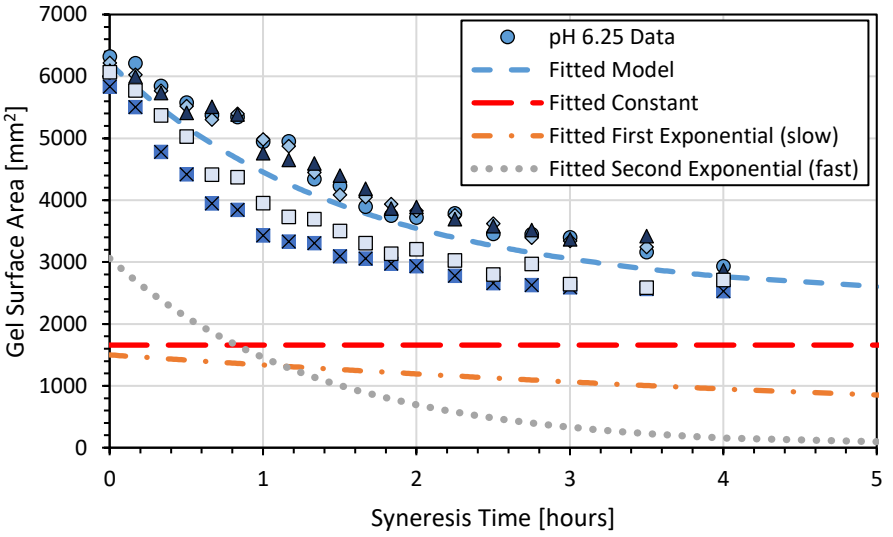

(b)

Figure 3-10: Gel surface area data and fitted model as a function of syneresis time for (a) the whole experiment and (b) the first five hours of the experiment for pH 6.25 gels held at 40 °C. Symbols represent the five replicates.

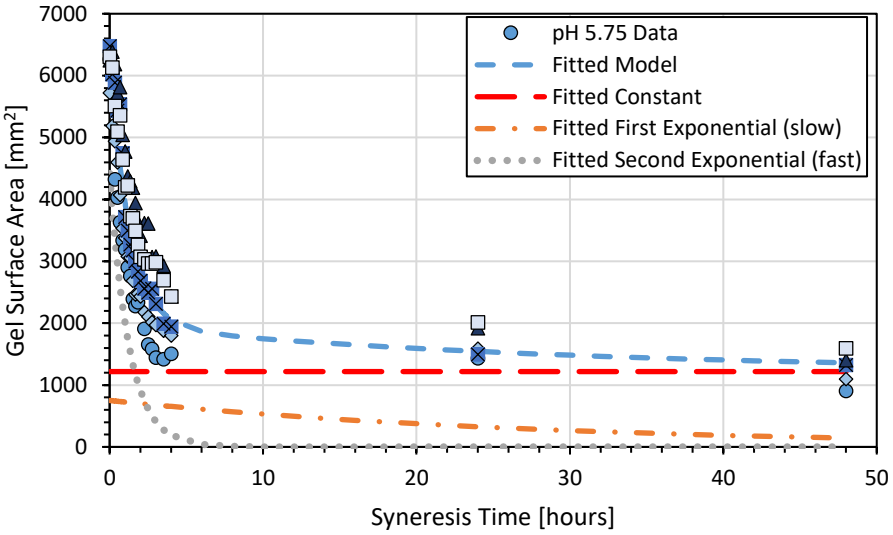

(a)

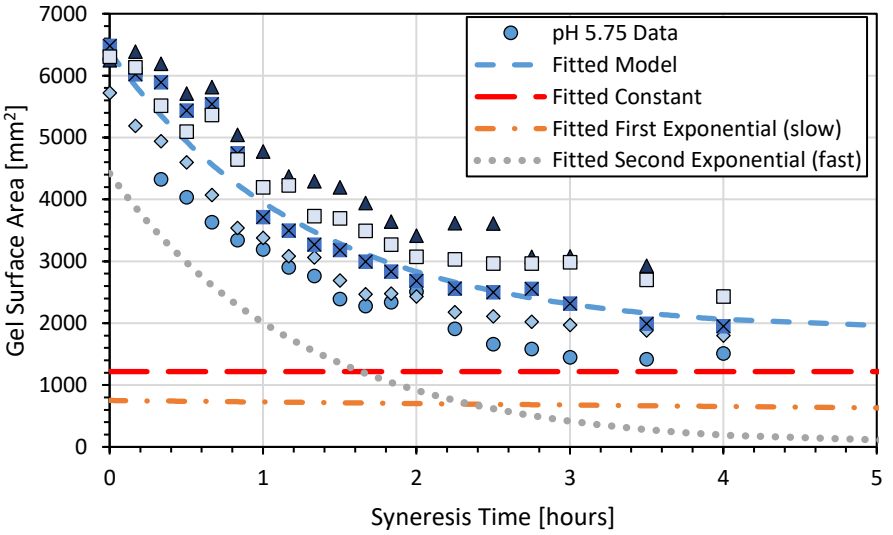

(b)

Figure 3-11: Gel surface area data and fitted model as a function of syneresis time for (a) the whole experiment and (b) the first five hours of the experiment for pH 5.75 gels held at 40 °C. Symbols represent the five replicates.

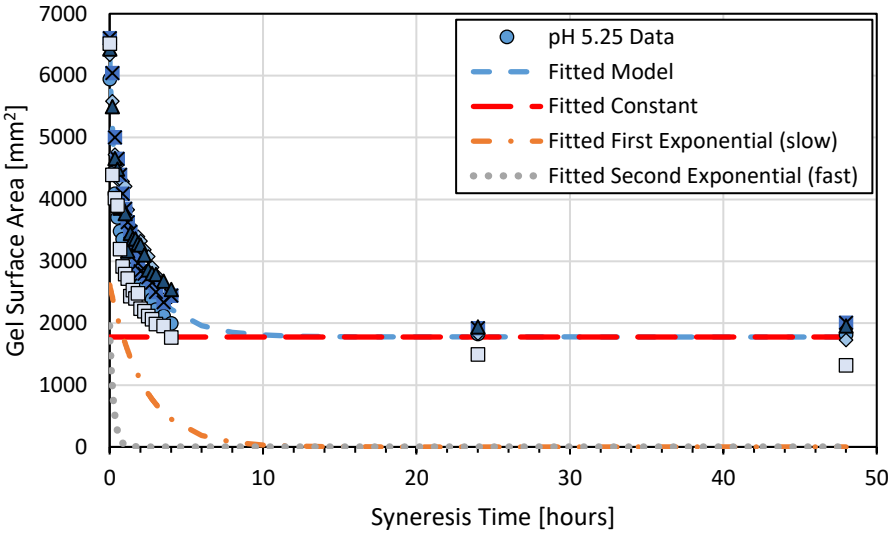

(a)

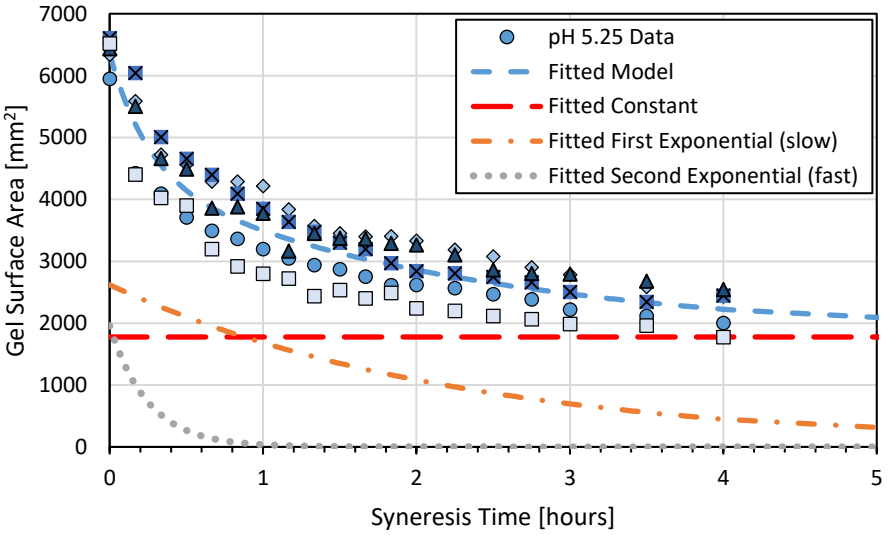

(b)

Figure 3-12: Gel surface area data and fitted model as a function of syneresis time for (a) the whole experiment and (b) the first five hours of the experiment for pH 5.25 gels held at 40 °C. Symbols represent the five replicates.

Figures 3-10 through 3-12 show the contribution of the "slow" and "fast" exponential functions to the gel surface area model. Fast exponentials show a faster rate of change at the beginning of syneresis, indicating that they may reflect the dominant mechanism of syneresis observed shortly after its onset. The slow exponential may relate to a slower mechanism of syneresis that dominates gel contraction after most of whey has been expelled. Table 3-2 provides the values of the for the fitted linear and nonlinear variables, in addition to the coefficient of determination (r^2) and the root mean squared error (RMSE).

Table 3-2: Fitted linear and nonlinear variables for the biexponential model for gel surface area (Equation 3-8) with fitting statistics of root mean square error and coefficient of determination for each pH treatment.

Treatment	A_{SA} [mm^2]	B_{SA} (slow) [mm^2]	C_{SA} (fast) [mm^2]	$p_{SA,1}$ (slow) [s^{-1}]	$p_{SA,2}$ (fast) [s^{-1}]	RMSE [mm^2]	r^2 [ ]
pH 6.25	1660	1500	3060	3.18E-05	2.06E-04	445	0.881
pH 5.75	1220	751	4420	9.63E-06	2.19E-04	579	0.852
pH 5.25	1780	2620	1960	1.23E-04	1.11E-03	396	0.888

Statistics presented in Table 3-2 show a high degree of fit between the fitted model and the data collected. The RMSE values also show the average error in the gel surface area at any point to not exceed 600 mm^2 for any of the models, which shows the high degree of fit.

3.4.4 Modelling Flux

The first derivative of the accumulated whey volume model and the gel surface area model were used to calculate the whey flux for each treatment, using Equation 3-13. The models show a high starting flux behaviour that quickly decreases as the gels shrink and less whey is available for expulsion. The pH of the gel clearly influences the initial whey expulsion, with lower pH gels having higher flux values at the onset of syneresis than higher pH gels. This finding is realistic, given that lower pH values lead to a decrease in electrostatic repulsion between caseins and an increase protein-protein interaction, thereby increasing the rate of syneresis.

High flux behaviour decreases at a faster rate for the low pH gels. Higher starting whey flux quickly reduces the total amount of remaining free whey entrapped in the gel, thereby decreasing the moisture content driving force for syneresis. As the gel approaches the equilibrium moisture content, the syneresis driving force continues to decrease and the whey flux decreases. Figure 3-13 shows the whey flux model as a function of syneresis time for all three pH treatments evaluated.

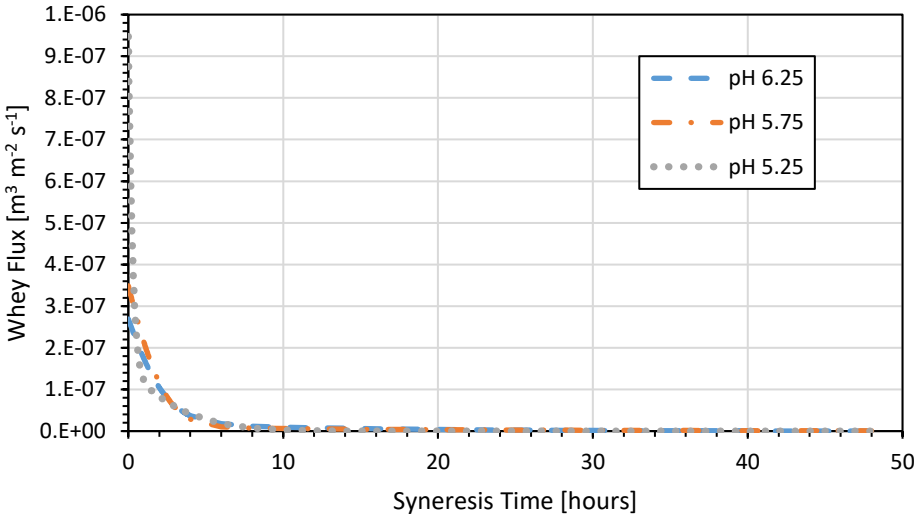

(a)

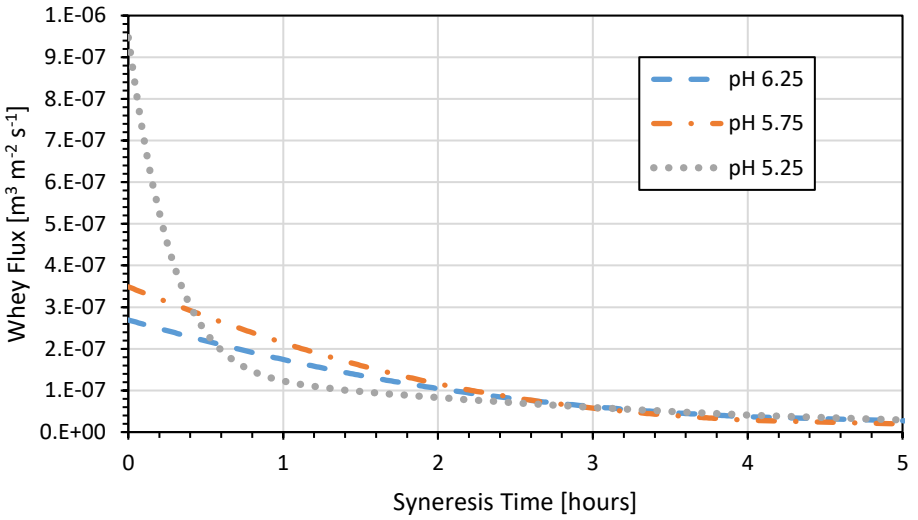

(b)

Figure 3-13: Whey flux models for all three pH treatments as a function of syneresis time for (a) the whole experiment and (b) the first five hours of the experiment for all gel pH treatments held at 40 °C.

The results shown in Figure 3-13 show that pH effects the syneresis behaviour of renneted skim milk gels, with the lower pH treatments producing the fastest whey expulsion. The findings are useful for understanding the net transport of moisture out of the gel prior to salting to create conditions optimal for salt uptake. The next section provides insight to the changing average internal gel moisture content with respect to syneresis time for the gels tested.

3.4.5 Average Internal Gel Moisture Content Estimation

The estimated average internal moisture mass fraction was calculated using Equation 3-14 for each pH treatment. The average internal gel moisture mass fraction was calculated assuming a starting milk density of 1.03 g mL^{-1}, a starting gel volume of 10 mL, and a starting moisture mass fraction of 0.89 in the milk. The whey was assumed to have a constant density of 1.04 g mL^{-1} and 0.94 moisture mass fraction. The results for all three pH treatments are shown as a function of syneresis time in Figure 3-14.

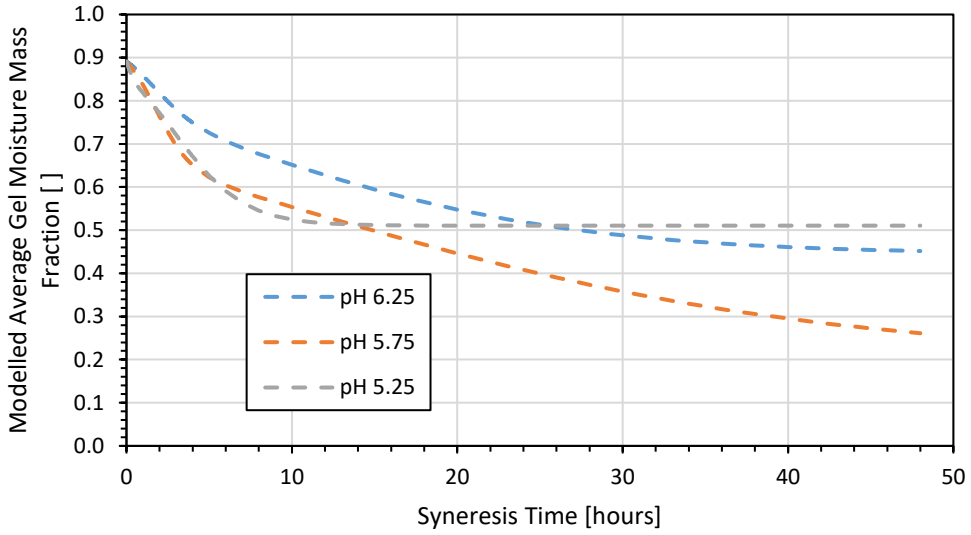

(a)

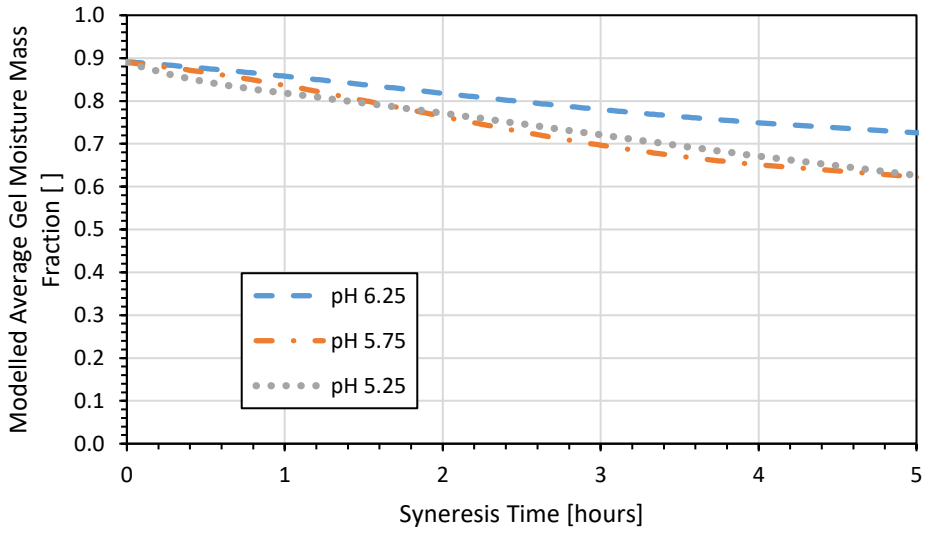

(b)

Figure 3-14: Modelled average gel internal moisture mass fraction as a function of syneresis time for (a) the whole experiment and (b) the first five hours of the experiment for all gel pH treatments held at 40 °C.

The modelled moisture mass fraction decreases quickly with respect to time during the early stages of syneresis, before gradually slowing the moisture mass fraction decline. Lower pH gels decrease in moisture mass fraction at a faster rate early during the syneresis process due to enhanced protein-protein interactions that promote whey expulsion. This finding is expected as it follows the same principles observed in the whey expulsion model. The pH 5.25 treatment differs from the other gel treatments due to its higher equilibrium moisture mass fraction. This is likely due to the differences in the internal structure of the low pH gels, which appear to have many acid-gel type qualities, which shall be discussed in greater detail in later chapters (Everett & Auty, 2017). This approach provides a useful step for estimating the average moisture mass fraction conditions that can be expected during syneresis, allowing for improved uptake of salt during the curd salting regime.

3.5 Conclusions

This chapter provided a brief introduction to typical methods used to describe and model syneresis and introduced a new approach to assess the changing gel volume and surface area using non-invasive image analysis techniques and the introduction of modelling techniques to mechanistically describe syneresis behaviour as a whey flux. The findings from the experiment discussed in this chapter have shown that (1) the new image analysis methods for assessing changing gel volume and surface area is consistent, (2) modelling of the results may be used to describe syneresis behaviour as a flux using biexponential curve fitting, and (3) syneresis behaviour differences may be observed in different pH treatments. These achievements provide the foundation to understand and model the effect of induced osmotic pressure effects on syneresis behaviour and changes in the internal microstructure of the gels. The following chapter applies the image analysis and modelling techniques introduced in this chapter to assess changes in syneresis behaviour under salt and non-salt derived induced osmotic pressure gradients.

Chapter 4 Osmotic Pressure Induced Syneresis Evaluation

4.1 Introduction

Understanding the transport of whey out of curds during syneresis is vital to the production of consistent curds ready for salting. The previous chapter provided a new approach to evaluate and model bulk whey loss during the syneresis step occurring right after cutting. However, syneresis continues after the onset of salting due to the induced osmotic pressure gradient between the surface brine and the free whey within the curd structure. Although this phenomenon has been observed in cheesemaking literature, limited research has been conducted to quantify the change in syneresis behaviour due to the presence of salt at the curd surface (Giroux et al., 2014; Lu & McMahon, 2015).

Most salt transport models in cheese literature have focused on the evaluation of salt transport through pressed cheese structures, such as in the case of brined Dutch-style or feta-like cheeses (Floury et al., 2010). These styles of cheese do not necessarily exhibit osmotically derived whey expulsion due to their pressed and moulded structure, which removes most of the free whey trapped in the individual curd structures. Furthermore, any free whey remaining in the pressed cheese would diffuse very slowly through the pressed matrix, thereby limiting the net amount of free whey that could be expelled (Melilli et al., 2005). The role of osmotic pressure induced syneresis on the total moisture loss and salt uptake is more significant for dry salted cheeses or brined individual curds as the net residual free whey in the curds is higher, and the average distance for the trapped whey to traverse out of the curd is shorter (T. Guinee & Fox, 2017).

The effects of osmotic pressure induced syneresis must be accounted for in the development of a mechanistic mathematical model to describe salt uptake and whey expulsion during cheesemaking. The following subsections provide a brief introduction to the concept and application of osmotic pressure in food processing and current methods used to evaluate and model osmotic pressure induced moisture expulsion.

4.1.1 Osmotic Pressure Overview

Osmotic pressure is defined as the amount of applied pressure required to prevent the transport of pure solvent across a semipermeable membrane into a solution. It relates to the tendency of a solution to undergo osmosis, whereby water is transported from a region of high water chemical potential to a region of low water chemical potential (Cath, Childress, & Elimelech, 2006). The osmotic pressure of a solution is a function of the amount and type of

compounds dissolved in solution, and any deviations from ideal behaviour they exhibit. Equation 4-1 shows how osmolarity, the concentration of particles that would induce osmosis in a solution, is determined using an adaption of the v'ant Hoff equation. Equation 4-2 adapts Equation 4-1 for a dilute binary system where the osmotic pressure is directly proportional to the concentration of the dissolved solute.

$$M_{osm} = \sum_{j=1}^{\infty} \varphi_j i_j C_j$$

Equation 4-1: Osmolarity equation.

$$\Pi = M_{osm} RT = i_j C_j RT$$

Equation 4-2: Equation for assessing osmotic pressure of a binary system at low concentrations.

In Equations 4-1 and 4-2, M_{osm} [osmoles m^{-3}] represents osmolarity, φ_j [dimensionless] represents the osmotic coefficient which accounts for the non-ideal solute *j* behaviour, and Π [Pa] is the osmotic pressure of the solution. Under ideal conditions, the osmotic coefficient would be equivalent to unity and the number of particles produced by a single solute would be equivalent to the number of particles predicted via dissolution assumptions. However, solutes do not behave ideally at high concentrations, where ion pairing and other interactions between particles affect the number of particles produced by a dissolved solute (Yousef, Datta, & Rodgers, 1998). Regardless of possible non-ideality, induced osmotic pressure differentials play a vital role to understanding moisture expulsion phenomena in tandem with salt uptake in food systems.

4.1.2 Osmotic Pressure Application in Other Foods

The concept of osmotically induced moisture expulsion has already been applied to other complex systems to assist in the preservation of various food items, particularly fruit and fish, in a process called osmotic dehydration (Casales, Capaccioni, & Yeannes, 2009; Ochoa-Martinez, Ramaswamy, & Ayala-Aponte, 2007). Osmotic dehydration uses the osmotic pressure differential to induce moisture expulsion from the food matrix, leading to product dehydration and an increased shelf life (Casales et al., 2009; Ochoa-Martinez et al., 2007). Brines and sugar solutions are used to induce the osmotic pressure gradient that reduce moisture content within the product and allow for salt or sugar to diffuse into the food matrix.

Fish salting studies frequently denote a relationship between the moisture expulsion and total absorbed salt, but limited work has been completed to mechanistically describe changes in fish matrix that contribute to the uptake and expulsion of moisture (Casales et al., 2009;

Sobukola & Olatunde, 2011). Fish salting experiments usually use kinetic-based equations to model uptake of salt and expulsion of moisture, without regard to the fish system composition (Bellagha, Sahli, Farhat, Kechaou, & Glenza, 2007; Boudhrioua, Djendoubi, Bellagha, & Kechaou, 2009; Casales et al., 2009; Sobukola & Olatunde, 2011). The development of empirical models to describe moisture and salt transport in fish does not provide any additional insight to the best methods to evaluate the role of the complicated matrix changes in modelling the transport behaviours of salted cheese curds.

Experimental work assessing the osmotic dehydration of fruit shows many of the same approaches used in the fish salting models to evaluate moisture expulsion and sugar uptake (Emam-Djomeh, Djelveh, & Gros, 2001; Ochoa-Martinez et al., 2007). The majority of experiments evaluated moisture expulsion and sugar uptake by fitting diffusion data with different kinetic-based models, with no regard to the changing structure of the fruit (Borsato et al., 2010; Emam-Djomeh et al., 2001; Ochoa-Martinez et al., 2007; Rodriguez, Rodriguez, & Mascheroni, 2015; Sereno, Moreira, & Martinez, 2001). Few studies evaluated the contraction of fruit samples due to moisture expulsion or the function of the changing matrix on the overall transport behaviours. Studies that did assess the contraction or structural properties of fruit during osmotic dehydration developed non-fundamental kinetic models to describe changes, with little investigation of the effect on moisture expulsion or sugar uptake (Mavroudis, Gekas, & Sjöholm, 1998; Moreira & Sereno, 2003). Like the fish studies, these literature sources do not provide any new insight for modelling the relationship between moisture expulsion, curd contraction, and salt uptake. These findings indicate that there may be an avenue for future mechanistically-derived model development for evaluating the transport behaviours in complex food systems.

4.1.3 Methods of Osmotic Pressure Evaluation

Osmotic pressure is directly related to the number of particles in solution, making it a colligative property. As such, it may be determined experimentally through assessment of the solution boiling point elevation, vapour point depression, or freezing point depression compared to pure water solvent (Parsegian, Rand, Fuller, & Rau, 1986; Timkin & Lazarev, 2015). Osmotic pressure may also be assessed by separating the solution of interest from pure solvent with a semipermeable membrane in a U-bend vessel open to the atmosphere. The net fluid height changes between the solution at the start of the experiment and at equilibrium may be used to calculate the osmotic pressure. Likewise, the required external

pressure to prevent the transport of solvent across the semipermeable membrane would be the osmotic pressure (Garcia-Castello, McCutcheon, & Elimelech, 2009; Y. Luo & Roux, 2010).

The purpose of this chapter is two-fold: (1) to evaluate and model the syneresis behaviours of renneted milk gels exposed to osmotic pressure differential inducing solutions, and (2) evaluate the role of the type of osmotic stressing component on the syneresis behaviours at the same osmotic pressure gradient. The objectives of this chapter were achieved using the image analysis and mathematical modelling techniques introduced in Chapter 3 to assess and model renneted milk gel syneresis under three different induced osmotic pressure gradient conditions. The following sections provide the experimental design and results from non-destructive in-situ experiments evaluating gel contraction and whey expulsion for three different osmotic pressure differential inducing conditions as a function of brining or exposure time.

4.2 Experimental Design

An experiment was designed to evaluate the syneresis behaviours of renneted milk gels exposed to osmotic pressure differential induced syneresis conditions using the in-situ using image analysis techniques described in Chapter 3. Briefly, renneted milk gels were set in clear dialysis tubing, exposed to temperature-controlled whey, and imaged throughout the regular syneresis process for two hours at 40 °C. After two hours of regular syneresis, the gels were removed from the regular whey, drained of any free whey in their respective tubes, and exposed to prewarmed osmotic stress inducing solution for 48 hours. Two hours of total regular bulk syneresis time prior to the onset of exposure to the osmotic solutions were chosen to standardize the evaluation procedure to a time-based frame, akin to industrial cheese plants where curds are transferred through unit operations in fixed times, regardless of variation in curd moisture content or pH in the curd bed.

Imaging continued for the first two hours of exposure and twice more during the following 46 hours. Analysis of the images was conducted using the procedure given in section 3.3.1. Data from multiple gels undergoing syneresis were collected and fitted with a biexponential curve to describe total osmotically induced whey expulsion and gel surface area using MATLAB ® software. A biexponential model was used to model the osmotic pressure differential induced syneresis to account for two different mechanisms possibly affecting whey expulsion behaviour, namely the rapid expulsion of whey near the gel surface and the slow sustained expulsion from the gel interior after longer exposure times. Fitted equations

were then used to describe the whey flux of the gel and its relationship to the osmotic pressure differential induced syneresis time and estimated gel moisture content, as predicted from mass balances.

Three different treatments were developed to evaluate the osmotic pressure induced syneresis behaviour for the three milk pH treatments: low salt, high salt, and non-salt low osmotic pressure differential conditions. The premise for testing three different osmotic pressure conditions were two-fold: (1) that higher salt concentrations (and therefore higher osmotic pressure) would induce higher rates of whey expulsion, and (2) that the choice of solute inducing the osmotic pressure differential would affect the whey expulsion behaviour due to possible interactions between the gel matrix and the solute. The following section details the experiment designed to investigate the role of different osmotic pressure gradients on the syneresis behaviours of renneted milk gels.

4.2.1 Experimental Material Preparation

Milk, rennet, and whey were prepared using the procedures detailed in sections 3.2.1 and 3.2.2. Five dialysis tubes for replicate measurements were prepared for each treatment using the procedure discussed in section 3.2.3 for setting and evaluating gel contraction with respect to time exposed to the osmotic stressing solution.

4.2.2 Osmotic Pressure Assessment in Prepared Brines

Three different treatments were developed to evaluate the effects of different osmotic pressure differentials and solute type on the syneresis behaviour: high salt, low salt, and low non-diffusing substance. The high salt treatment was intended to more closely mimic the conditions created in surface brine during dry salting, where a concentrated brine would form at the surface of the curd before commencing transport into the curd. Brines were deemed more appropriate for evaluating the effect of changing osmotic pressure differentials as there was decreased risk compared with dry salting of creating uneven application of the salt across the gel surface. Although sodium chloride has a solubility of approximately 26% (w/w) at room temperature, the presence of whey proteins and other compounds in the whey decrease the solubility of the sodium chloride (Y. Luo & Roux, 2010). A brine concentration of 20% NaCl dissolved in whey was established to ensure both high induced osmotic pressure differential conditions and minimized risk of salt spontaneously precipitating out of solution.

The low salt brine case was established in tandem with the non-salt osmotic pressure inducing treatment. Solutions of dissolved salt in whey and 6 kD polyethylene glycol (PEG)

(Sigma-Aldrich Chemical Co., USA) dissolved in whey were prepared in different concentrations and tested for their osmolality using an Osmomat 030 (Gonotec, Germany) osmometer. This osmometer assessed osmolality using a freezing point depression and was therefore limited to assessing osmolality in samples with less than 2.5 osmoles per kilogram of solution. Samples were evaluated in triplicate for each concentration and multiplied by the solution density at 40 °C, the ideal gas constant, and the experimental temperature in Kelvin units to determine the osmotic pressure.

Curves were fitted to describe the changing osmotic pressure as a function of the concentration of whey in each solution and a value of 2.5% NaCl in whey was established as low salt concentration treatment. This value fit within a range of low salt concentrations that demonstrated a linear relationship between salt concentration and osmotic pressure. It was also the maximum concentration where the PEG-whey solutions with the same osmotic pressure could be consistently dissolved in the whey. The fitted curves were used to determine the concentrations of PEG to achieve the same osmotic pressure values for each whey pH as the osmotic pressure of the 2.5% NaCl-whey brines. The final values were 16.6%, 16.9%, and 16.8% PEG in whey, for the pH 6.25, 5.75, and 5.25 treatments, respectively. The starting induced osmotic pressure differential was 2.38, 2.47, and 2.75 kPa for the pH 6.25, 5.75, and 5.25 2.5% NaCl-whey brine or corresponding PEG-whey solution, respectively. The 20% NaCl-whey brines established for the high salt case could not be tested with the osmometer, as the values exceeding the testing range of the equipment. The data and curves used to evaluate the osmotic pressure of NaCl or PEG in whey are shown in Appendix C.

4.2.3 Sample Gel Preparation and Evaluation

Gels were prepared and imaged using the same procedure described in section 3.2.5., whereby prepared milk was renneted, deposited in 10 mL aliquots into prepared dialysis tubes, and imaged before the onset of gelation. The gels were set for thirty minutes and then exposed to whey prewarmed at 40 °C to undergo syneresis. Imaging using the imaging apparatus and the procedure detailed in section 3.2.5 continued for the first two hours of syneresis. After imaging at the two-hour time point, the tubes were removed from the regular whey conditions, drained of all free whey in the tubes, and exposed to 100 mL of solution prewarmed to 40 °C to induce an osmotic pressure differential. Approximately five millilitres of the new solution were added directly onto the surface of the gel inside the tube to prevent the possible physical crushing of the gel by the tube under the high induced

osmotic stress. The experiment continued using the same imaging procedure discussed in section 3.2.5, whereby the gels were imaged in fifteen-minute intervals for the first hour of osmotic stress induced syneresis, followed by two images collected in thirty-minute intervals, and images captured twice more at 24 and 48 hours. Gels were blotted dry and weighed before being discarded with the remaining used whey solutions.

4.3 Analysis Techniques

4.3.1 MATLAB ® Image Analysis Methods

Image analysis of the images captured throughout the exposure time to the osmotic pressure differential inducing conditions was completed using the code and techniques previously described in section 3.3.1. Gel volume and surface area data were compiled and used to model the gel surface area and accumulated whey volume as a function of osmotic pressure differential induced syneresis time. The accumulated whey volume expelled was determined using Equation 3-6, with the caveat being that the measurements were assessed at the onset of exposure to the osmotic pressure differential inducing solution. This means that the total accumulated whey volume during exposure to the osmotic pressure differential inducing solution is standardized from the onset of exposure, leading to equilibrium values significantly smaller than those modelled by Equation 3-7 in the previous chapter. Furthermore, the time variable used to model whey expulsion and contraction of the gel surface area is an adjusted value, denoted as t_{osm}, and shown in Equation 4-3.

$$t_{osm} = t - t_{RegSyn}$$

Equation 4-3: Adjusted osmotic time variable for modelling whey expulsion and gel contraction during exposure of osmotic pressure differential induced syneresis conditions.

In Equation 4-3, t_{osm} [s] is the osmotic pressure differential induced syneresis time and t_{RegSyn} [s] is the total time regular, bulk syneresis takes place. The MATLAB ® code introduced in section 3.3.3 and detailed in Appendix B was used to fit two biexponential functions for the changing accumulated whey volume and gel surface area using the MATLAB ® *lsqcurvefit* function to identify variable values that minimize the least-squares error. These values were then used to describe the syneresis behaviour observed as a whey flux. The models fitted to the data are shown in Equations 4-4 and 4-5.

$$V_{w,osm} = A_{w,osm} + B_{w,osm}e^{-p_{w,osm1}t_{osm}} + C_{w,osm}e^{-p_{w,osm2}t_{osm}}$$

Equation 4-4: Accumulated whey volume model under osmotic pressure differential conditions.

$$SA_{osm} = A_{SA,osm} + B_{SA,osm}e^{-p_{SA,osm1}t_{osm}} + C_{SA,osm}e^{-p_{SA,osm2}t_{osm}}$$

Equation 4-5: Gel surface area model under osmotic pressure differential conditions.

In Equations 4-4 and 4-5, $V_{W,osm}$ [mL] represents the volume of the of the accumulated whey expelled during osmotic exposure, SA_{osm} [mm^2] represents the surface area of the gel during osmotic exposure, and the *osm* subscripts refer to the osmotic pressure differential induced syneresis case. Equation 4-4 and 4-5 parallel Equations 3-7 and 3-8 to account for long-term and short-term mechanisms that may affect whey expulsion and gel contraction but are otherwise independent from those equations to evaluate the role of an induced osmotic pressure differential on the syneresis behaviour.

4.3.2 Statistical Analysis of Accumulated Whey Volume and Surface Area

The average accumulated whey volume and surface area for each gel at each time point, starting at the onset of exposure to the osmotic stressor was collected and assembled to form the complete results for each pH treatment tested. Results were then assessed using one-way analysis of variance (ANOVA) to determine if any statistically significant differences between the different pH gels within the different osmotic stressor treatments, within 95% confidence. One-way ANOVA was also conducted on each treatment to determine if there were any statistically significant differences between the gels tested within each treatment.

4.3.3 Modelling Whey Flux and Changing Average Gel Moisture Content

Whey flux during exposure to the osmotic pressure differential induced syneresis was calculated from the gel surface area and accumulated whey volume models as the rate of whey volume accumulation per surface area. The first derivative of the accumulated whey volume model is divided by the gel surface area model to produce the whey flux at any time during the exposure to the osmotic pressure differential. The equation describing the whey flux is shown below.

$$J_{W,osm} = \frac{\frac{dV_{W,osm}}{dt}}{SA_{osm}} = \frac{-B_{W,osm}p_{Wosm,1}e^{-p_{Wosm,1}t_{osm}} - C_{W,osm}p_{Wosm,2}e^{-p_{Wosm,2}t_{osm}}}{A_{SA,osm} + B_{SA,osm}e^{-p_{SAosm,1}t_{osm}} + C_{SA,osm}e^{-p_{SAosm,2}t_{osm}}}$$

Equation 4-6: Whey flux equation during osmotic pressure induced syneresis derived from the modelled gel surface area and accumulated whey volume.

In Equation 4-6, $J_{W,osm}$ [m^3 m^{-2} s^{-1}] is the osmotic pressure differential induced whey flux and $dV_{W,osm}/dt$ [mL s^{-1}] is the rate of the osmotically induced whey expulsion. Equation 4-6 corresponds to Equation 3-13 in form, but describes the whey flux under different conditions, namely osmotic induced syneresis instead of regular, bulk syneresis.

The average internal gel moisture content may be estimated using the whey expulsion models combined with the starting properties of each gel prior to the onset of osmotic pressure induced syneresis. If it is assumed that the whey expelled maintains moisture content consistency, and the relevant whey density is the same, Equation 4-7 may be used to estimate the average internal gel moisture content.

$$MMF_{osm} = \frac{M_{gel,tosm=0} MMF_{gel,tosm=0} - \rho_{whey} MMF_{whey} V_{W,osm}}{M_{gel,tosm=0} - \rho_{whey} V_{W,osm}}$$

Equation 4-7: Average internal gel moisture mass fraction, calculated from mass fractions during osmotic pressure differential induced syneresis.

In Equation 4-7, MMF_{osm} [dimensionless] represents the moisture mass fraction of the gel, $MMF_{gel,tosm=0}$ [dimensionless] is the moisture mass fraction of the gel at the onset of exposure to the osmotic pressure differential, $M_{gel,tosm=0}$ [kg] is the mass of the gel at the onset of exposure to the osmotic pressure differential. Equation 4-7 parallels Equation 3-14 to estimate the moisture mass fraction of the gel under osmotically induced syneresis conditions. It provides a simple estimate for the average overall internal moisture content but may not account for residual moisture at the surface of the gel which could affect the moisture content observed in a regular oven mass difference technique. It also does not account for salt or other solute uptake into the gel, and therefore may have limited application for estimating moisture mass fraction without modelling of the salt uptake. Nevertheless, this approach could be useful for relating the average internal moisture content to the osmotic pressure differential induced whey flux observed, as the gradient between the average internal moisture content and the moisture content at equilibrium would drive the whey expulsion.

4.4 Experimental Results and Discussion

4.4.1. Non-salt Induced Osmotic Pressure Syneresis

4.4.1.1 Statistical Analysis of Accumulated Whey Volume and Gel Surface Area Data

One-way ANOVA were conducted on the accumulated whey volume data and gel surface areas to determine if there was a significant difference between any of the gels evaluated within their respective treatments beginning at the onset of the PEG-whey exposure. Results showed no statistically significant differences between the values within each pH treatment, within 95% confidence. One-way ANOVA assessment also showed that there was no statistically significant difference in the accumulated whey volume data between pH treatments, within 95% confidence. These results indicate that the presence of the PEG-whey

solution produced remarkably similar whey expulsion accumulation between the gel pH treatments. However, statistically significant differences were detected in the gel surface area values between the pH treatments and are detailed in Table 4-1.

Table 4-1: One-way ANOVA statistically significant differences in gel surface area between pH treatments exposed to PEG-whey conditions, within 95% confidence. NS = No statistically significant difference, S = significant difference.

Treatment	pH 6.25	pH 5.75	pH 5.25
pH 6.25	-	NS	S
pH 5.75	NS	-	S
pH 5.25	S	S	-

The PEG-whey syneresis results indicated that there were statistically significant differences between the pH 5.25 treatment and the other two treatments, within 95% confidence. The syneresis behaviours were successfully modelled using Equations 4-4 and 4-5.

The following subsection details the accumulated whey volume and gel surface area data during PEG-whey osmotic pressure differential induced syneresis. It is important to note that PEG-whey osmotic induced syneresis occurs after two hours of regular syneresis to better simulate cheese production where salting occurs after limited syneresis times, and that several figures shown in this chapter only show the data and fitted models standardized at the onset of osmotically induced syneresis. Figure 4-1 provides context to the figures presented in the sections 4.4.1.2, 4.4.2.2, and 4.4.3.2, by showing a complete data set that includes the regular syneresis data and fitted model in addition to the osmotically induced syneresis data and fitted model, specifically in the case of pH 6.25 gels treated with PEG-whey.

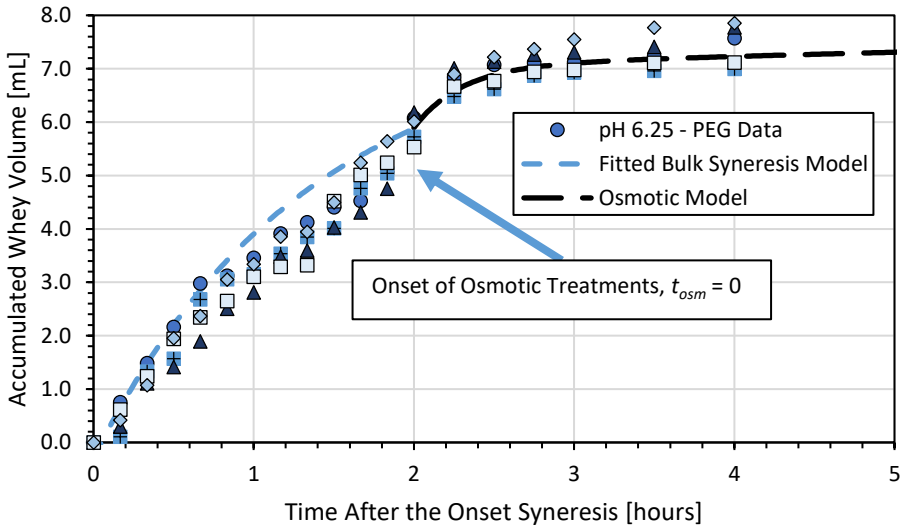

(a)

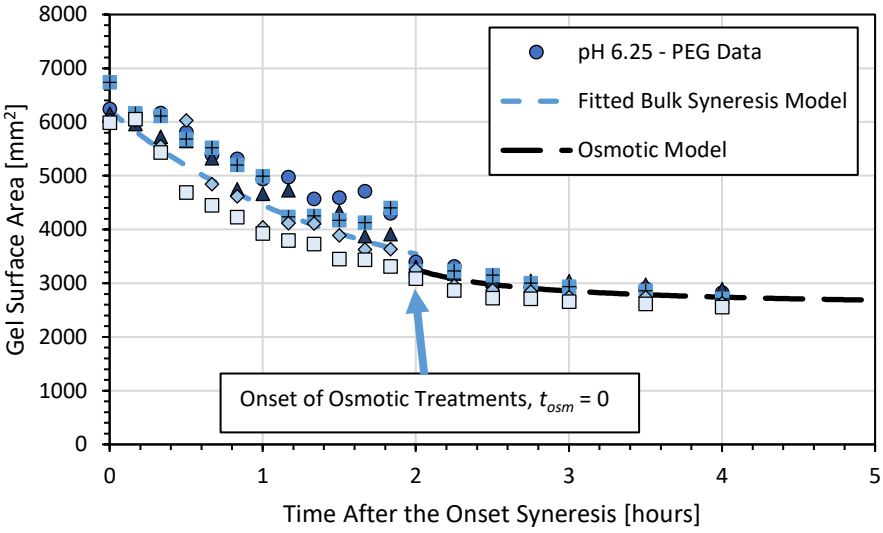

(b)

Figure 4-1: Demonstration of the PEG-whey osmotically induced syneresis (a) accumulated whey volume data and models, and (b) gel surface area data and models in the first five hours of total experimental evaluation time. Osmotic induced syneresis behaviour is analysed and modelled after two hours of regular syneresis, where the t_{osm} value is equivalent to 0 seconds (see arrow). Symbols represent the five different replicates evaluated.

The accumulated whey volume osmotic model equilibrium constant is adjusted in Figure 4-1(a) to match with all data presented. Figure 4-1 shows that at the onset of exposure to osmotic pressure differential inducing solutions the syneresis behaviours change from what was previously observed in Chapter 3, but their effect is restricted with respect to the total syneresis observed as most of the whey is lost during the regular, bulk syneresis conditions. Nonetheless, it is worthwhile to investigate how an induced osmotic pressure differential affects whey expulsion and gel contraction.

4.4.1.2 Accumulated Whey Volume and Gel Surface Area

Equation 3-6 was used to successfully convert the changing gel volume data to the accumulated whey volume. This data was fitted with Equation 4-4, a five-parameter biexponential curve, using the code listed in Appendix B to solve for the nonlinear and linear variables using a least squares approach. The biexponential fitting was used to describe two separate possible mechanisms that could affect the short and long-term expulsions behaviour under induced osmotic pressure conditions. Figures 4-2 through 4-4 show the changing accumulated whey volumes as a function of PEG-whey exposure time at 40 °C for the pH 6.25, 5.75, and 5.25 gel treatments, respectively.

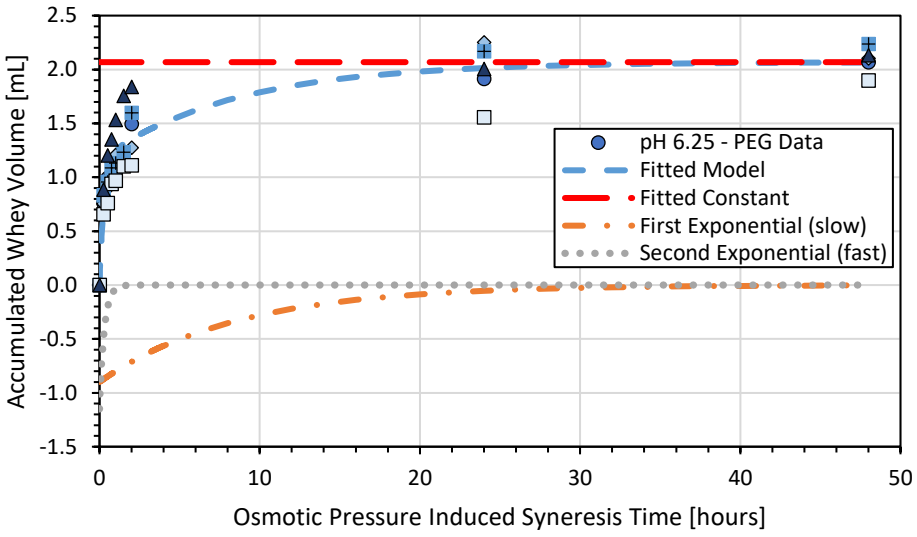

(a)

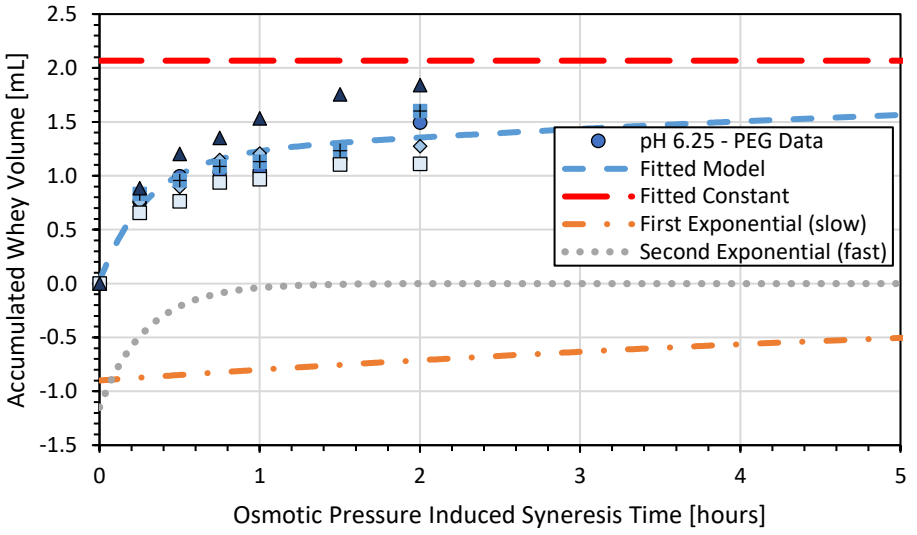

(b)

Figure 4-2: Accumulated whey volume and fitted model as a function of osmotic pressure induced syneresis time for (a) the whole experiment and (b) the first five hours of the experiment after exposure to the PEG-whey solution for five replicates of pH 6.25 gels held at 40 °C in 16.6% PEG-whey brine (equivalent to 2.5% NaCl-whey brine osmotic pressure). Symbols represent the five different replicates evaluated.

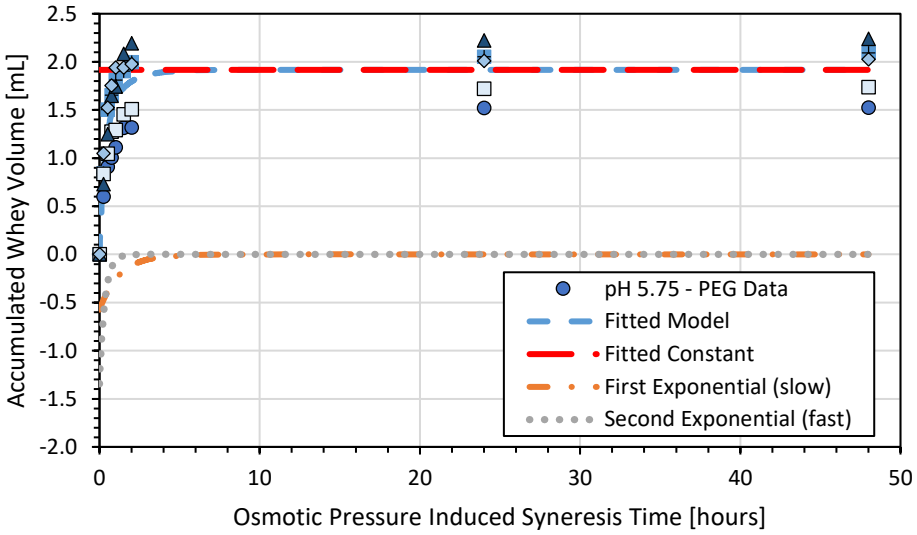

(a)

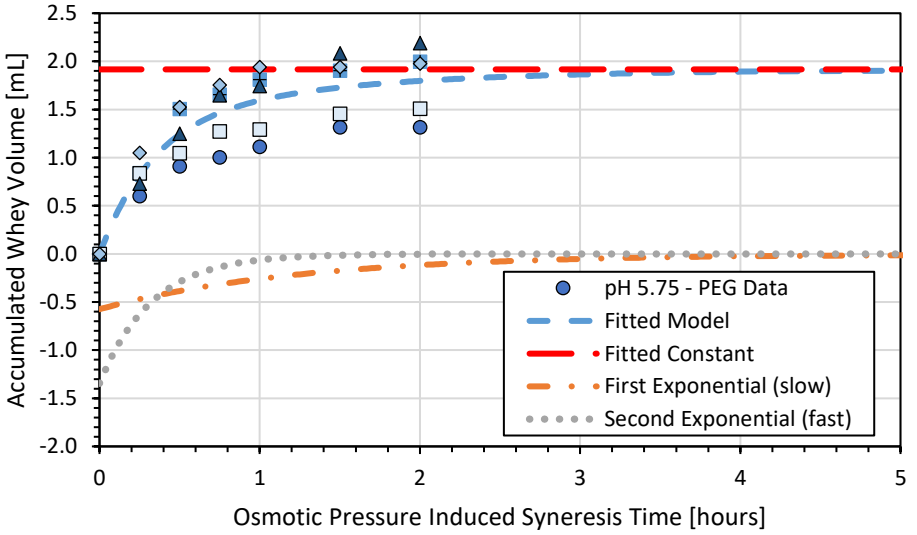

(b)

Figure 4-3: Accumulated whey volume and fitted model as a function of osmotic pressure induced syneresis time for (a) the whole experiment and (b) the first five hours of the experiment after exposure to the PEG-whey solution for five replicates of pH 5.75 gels held at 40 °C in 16.9% PEG-whey brine (equivalent to 2.5% NaCl-whey). Symbols represent the five different replicates evaluated.

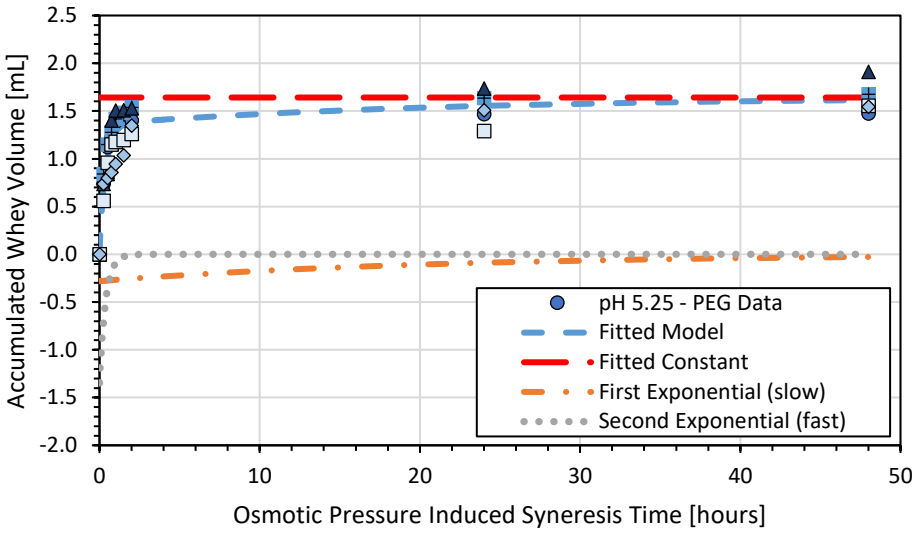

(a)

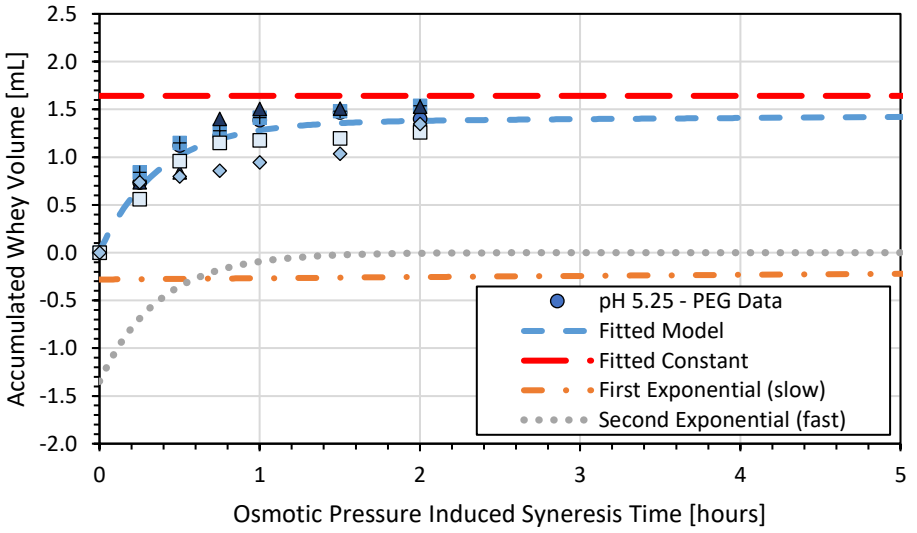

(b)

Figure 4-4: Accumulated whey volume and fitted model as a function of osmotic pressure induced syneresis time for (a) the whole experiment and (b) the first five hours of the experiment after exposure to the PEG-whey solution for five replicates of pH 5.25 gels held at 40 °C in 16.8% PEG-whey brine (equivalent to 2.5% NaCl-whey). Symbols represent the five different replicates evaluated.

Figures 4-2 through 4-4 demonstrate a rapid increase in accumulated whey volume, with some differences in the best-fit models. These differences are detailed in Table 4-2, which provides the values of the for the fitted linear and nonlinear variables, in addition to the coefficient of determination (r^2) and the root mean squared error (RMSE).

Table 4-2: Fitted linear and nonlinear variables in Equation 4-4 for accumulated whey volume with fitting statistics of root mean square error and coefficient of determination for each pH treatment under PEG-induced osmotic pressure differential conditions.

Treatment	$A_{w,osm}$ [mL]	$B_{w,osm}$ (slow) [mL]	$C_{w,osm}$ (fast) [mL]	$p_{w,osm1}$ (slow) [s^{-1}]	$p_{w,osm2}$ (fast) [s^{-1}]	RMSE [mL]	r^2 [ ]
pH 6.25	2.068	-0.900	-1.15	3.25E-05	9.41E-04	0.194	0.912
pH 5.75	1.917	-0.575	-1.35	2.21E-04	8.48E-04	0.272	0.843
pH 5.25	1.642	-0.281	-1.35	1.34E-05	7.43E-04	0.159	0.909

Statistics presented in Table 4-2 show a good degree of fit between the fitted model and the data collected. The RMSE values also show the average error in the accumulated volume at any point to not exceed 0.28 mL for any of the models. Although the RMSE value is small, there is a relative error of 9.38%, 14.2%, 9.68% for the pH 6.25, 5.75, and 5.25 treatments, respectively when evaluated at equilibrium, indicating there is considerable error to be considered while modelling the whey expulsion behaviour. The surface area data was successfully fitted with Equation 4-5 using the previously described least squares modelling approach detailed in section 3.3.2 for all three pH treatments. Figures 4-5 through 4-7 show the surface area data and fitted biexponential models.

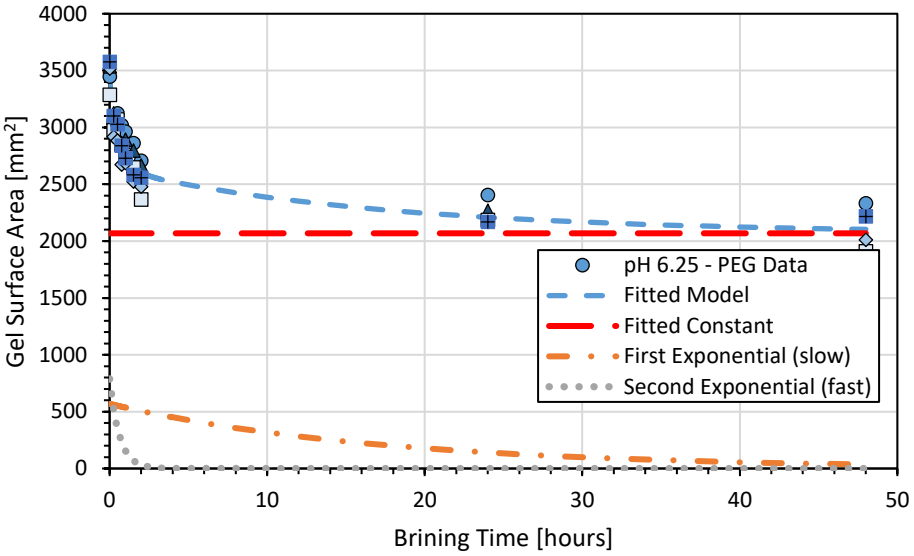

(a)

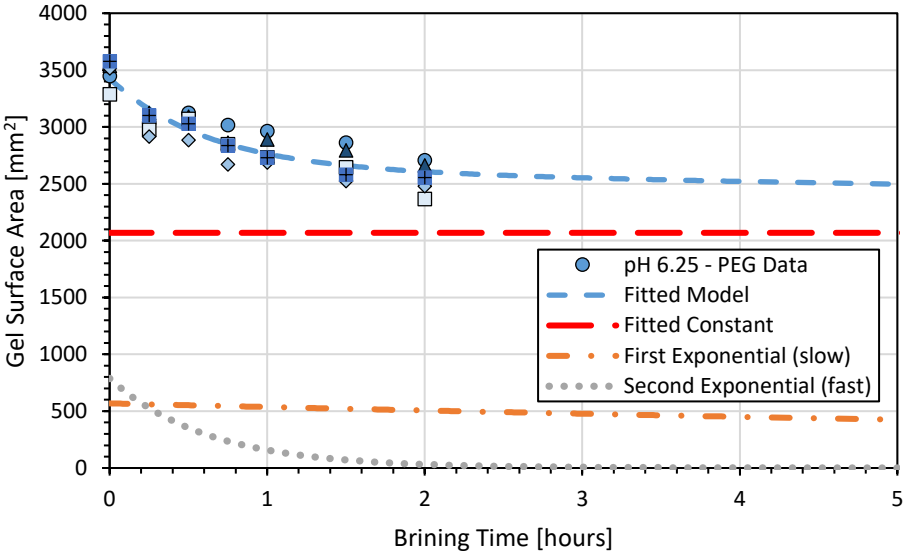

(b)

Figure 4-5: Gel surface area and fitted model as a function of osmotic pressure induced syneresis time for (a) the whole experiment and (b) the first five hours of the experiment after exposure to the PEG-whey solution for five replicates of pH 6.25 gels held at 40 °C in 16.6% PEG-whey brine (equivalent to 2.5% NaCl-whey). Symbols represent the five different replicates evaluated.

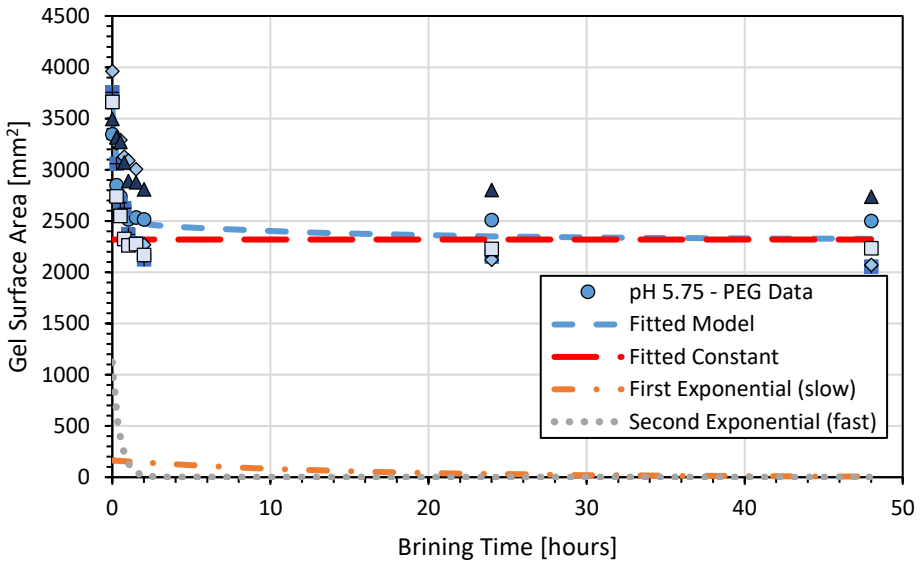

(a)

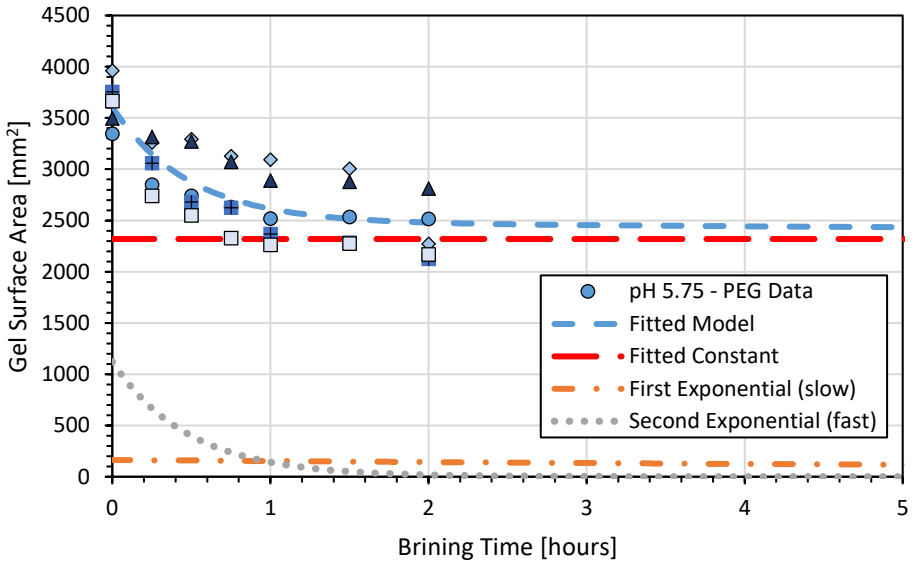

(b)

Figure 4-6: Gel surface area and fitted model as a function of osmotic pressure induced syneresis time for (a) the whole experiment and (b) the first five hours of the experiment after exposure to the PEG-whey solution for five replicates of pH 5.75 gels held at 40 °C in 16.9% PEG-whey brine (equivalent to 2.5% NaCl-whey). Symbols represent the five different replicates evaluated.

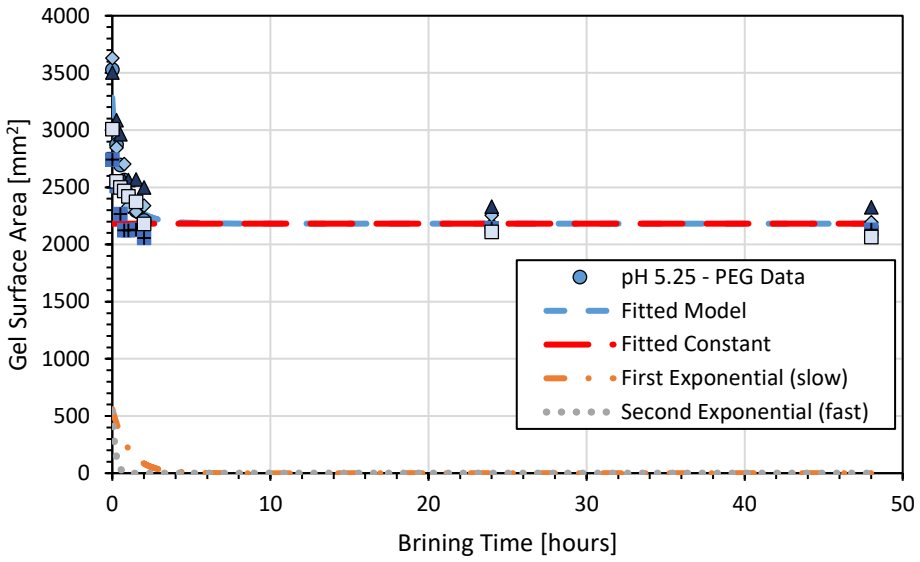

(a)

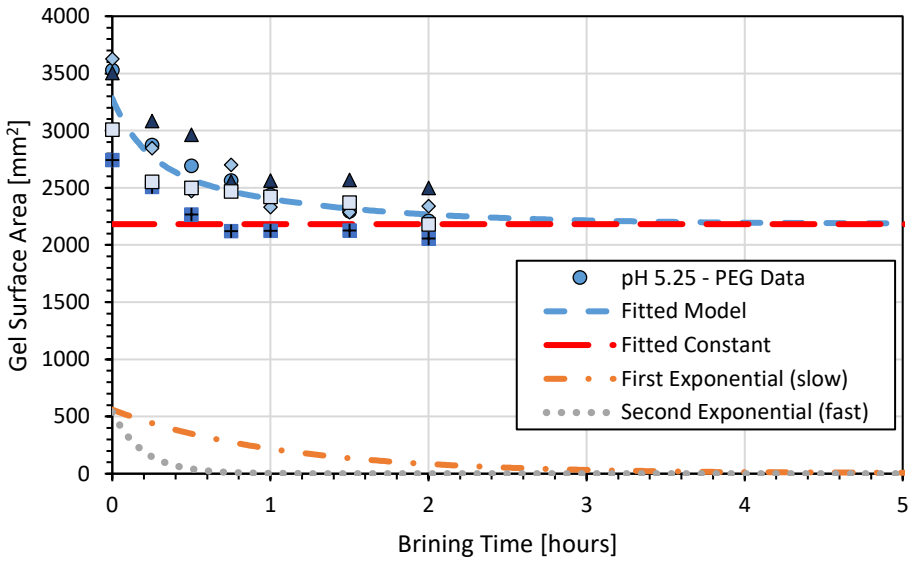

(b)

Figure 4-7: Gel surface area and fitted model as a function of osmotic pressure induced syneresis time for (a) the whole experiment and (b) the first five hours of the experiment after exposure to the PEG-whey solution for five replicates of pH 5.25 gels held at 40 °C in 16.8% PEG-whey brine (equivalent to 2.5% NaCl-whey). Symbols represent the five different replicates evaluated.

Figures 4-5 through 4-7 demonstrate a rapid decrease in gel surface area to the equilibrium values, with some differences in the best-fit models by pH treatment. The differences are detailed in Table 4-3, which provides the values of the for the fitted linear and nonlinear variables, in addition to the coefficient of determination (r^2) and the root mean squared error (RMSE).

Table 4-3: Fitted linear and nonlinear variables in Equation 4-5 for gel surface area with fitting statistics of root mean square error and coefficient of determination for each pH treatment under PEG-induced osmotic pressure differential conditions.

Treatment	$A_{SA,osm}$ [mm^2]	$B_{SA,osm}$ (slow) [mm^2]	$C_{SA,osm}$ (fast) [mm^2]	$p_{SA,osm1}$ (slow) [s^{-1}]	$p_{SA,osm2}$ (fast) [s^{-1}]	RMSE [mm^2]	r^2 [ ]
pH 6.25	2.07E+03	5.69E+02	7.88E+02	1.62E-05	4.46E-04	1.33E+02	0.909
pH 5.75	2.32E+03	1.64E+02	1.12E+03	1.91E-05	5.76E-04	2.97E+02	0.663
pH 5.25	2.18E+03	5.61E+02	5.40E+02	2.62E-04	1.43E-03	2.06E+02	0.745

Statistics presented in Table 4-3 show an adequate degree of fit between the fitted model and the data collected for the pH 6.25 and pH 5.25 treatments, with a less ideal fit associated with the pH 5.75 treatment. This may be due to uneven contraction induced by the PEG-whey solution to produce gels with slightly higher or lower surface area values relative to the gel volume values. The RMSE values also show the average error in the gel surface area at any point to not exceed 300 mm^2 for any of the models. Although the RMSE value is small, it produces a relative error of 6.42%, 12.8%, 9.45% for the pH 6.25, 5.75, and 5.25 treatments, respectively when evaluated at equilibrium. The differences between the fitted models for accumulated whey volume and gel surface area pH treatments are important to the mechanistic understanding of whey expulsion under different pH and external conditions, as observed in flux behaviour and gel moisture mass fraction.

4.4.1.3 Average Internal Gel Moisture Content Estimation

The estimated average internal moisture mass fraction was calculated using Equation 4-7 for each pH treatment. The average internal gel moisture mass fraction was calculated using the predicted starting moisture mass fraction and gel mass values of the gels after two hours of regular syneresis using the model presented in section 3.4.3. Gels were assumed to weigh 4.22, 2.92, and 3.06 grams and have starting moisture mass fractions of 0.817, 0.764, and 0.771, for the pH 6.25, 5.75, and 5.25 treatments, respectively. Whey was assumed to have a constant density of 1.04 g mL^{-1} and 0.94 moisture mass fraction. The results for all three pH treatments are shown as a function of osmotic pressure induced syneresis time in Figure 4-8.

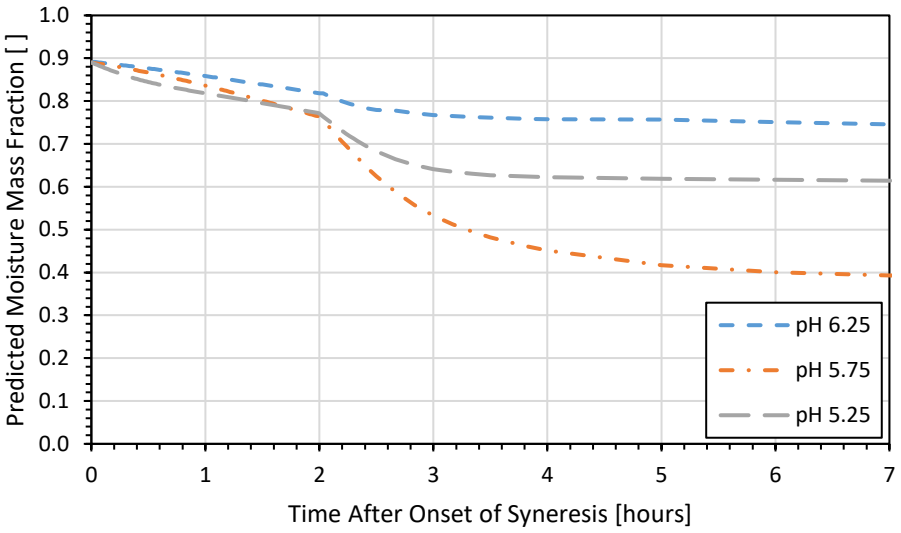

Figure 4-8: Simulated moisture mass fraction of gels with respect to brining time for the first seven hours of after onset of bulk syneresis, with exposure to PEG-whey producing osmotic pressure differentials equal to 2.5% NaCl-whey solutions beginning after two hours of regular syneresis.

The modelled moisture mass fraction quickly decreases with respect to time exposed to the PEG-whey solution during the early stages osmotically induced syneresis, before gradually slowing the moisture mass fraction decline. Lower pH gels decrease in moisture mass fraction at a faster rate early during the syneresis process due to higher whey mass loss relative to the gel mass. It is interesting to note that the pH 5.75 treatment was predicted to achieve a lower equilibrium moisture mass fraction than the pH 5.25 gels. This may be partially explained by the pH, where the more acid-type gels (pH 5.25) resist whey expulsion due to differences in the structure and water holding capacity of the formed casein matrix, thereby maintaining a higher moisture mass fraction (Lucey et al., 1997a, 1997b).

4.4.2 Low Salt Induced Osmotic Pressure Syneresis

4.4.2.1 Statistical Analysis of Accumulated Whey Volume and Gel Surface Area Data

One-way ANOVA were conducted on the accumulated whey volume data and gel surface area to determine if there was a significant difference between any of the gels evaluated within their respective pH treatments beginning at the onset of exposure to the 2.5% NaCl-whey brine. Results showed no statistically significant differences between the accumulated whey volume values within each pH treatment or in two of the gel surface area data sets, within 95% confidence. Only the pH 5.25 gel surface area data showed any statistically significant differences within the data set, which is evidenced by the data spread shown in Figure 4-14. These findings indicate that the gels treated with 2.5% NaCl-whey undergo

relatively consistent contraction behaviours, except at lower pH values where there is more variation in gel surface area.

One-way ANOVA assessment also showed that there were statistically significant differences in the accumulated whey volume data and gel surface area data between pH treatments, within 95% confidence. These results indicate that the presence of the 2.5% NaCl-whey solution produced different syneresis behaviour between the gel pH treatments. The differences are detailed in Tables 4-4 and 4-5.

Table 4-4: One-way ANOVA statistically significant differences in accumulated whey volume between pH treatments exposed to 2.5% NaCl-whey conditions, within 95% confidence. NS = No statistically significant difference, S = significant difference.

Treatment	pH 6.25	pH 5.75	pH 5.25
pH 6.25	-	NS	S
pH 5.75	NS	-	S
pH 5.25	S	S	-

Table 4-5: One-way ANOVA statistically significant differences in gel surface area between pH treatments exposed to 2.5% NaCl-whey conditions, within 95% confidence. NS = No statistically significant difference, S = significant difference.

Treatment	pH 6.25	pH 5.75	pH 5.25
pH 6.25	-	S	NS
pH 5.75	S	-	S
pH 5.25	NS	S	-

The statistically significant differences between different pH treatments indicate that the presence of 2.5% NaCl-whey brine does not produce the same, highly consistent syneresis behaviour observed in the case of PEG-whey producing the same starting osmotic pressure differential. Despite variation in gel surface area results, the syneresis behaviours were modelled using Equations 4-4 and 4-5.

4.4.2.2 Accumulated Whey Volume and Gel Surface Area

Figures 4-9 through 4-11 show the changing accumulated whey volumes as a function of 2.5% NaCl-whey brining time at 40 °C for the pH 6.25, 5.75, and 5.25 gel treatments, respectively.

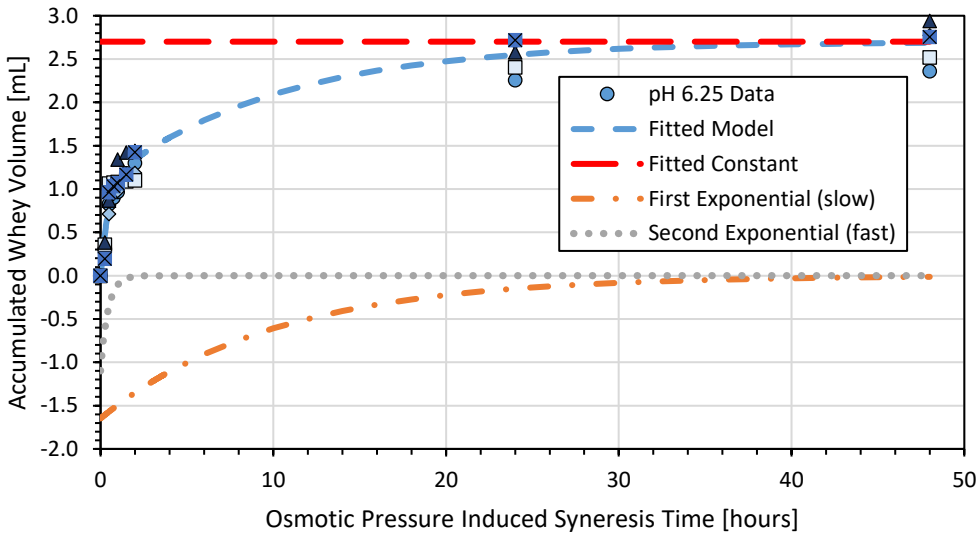

(a)

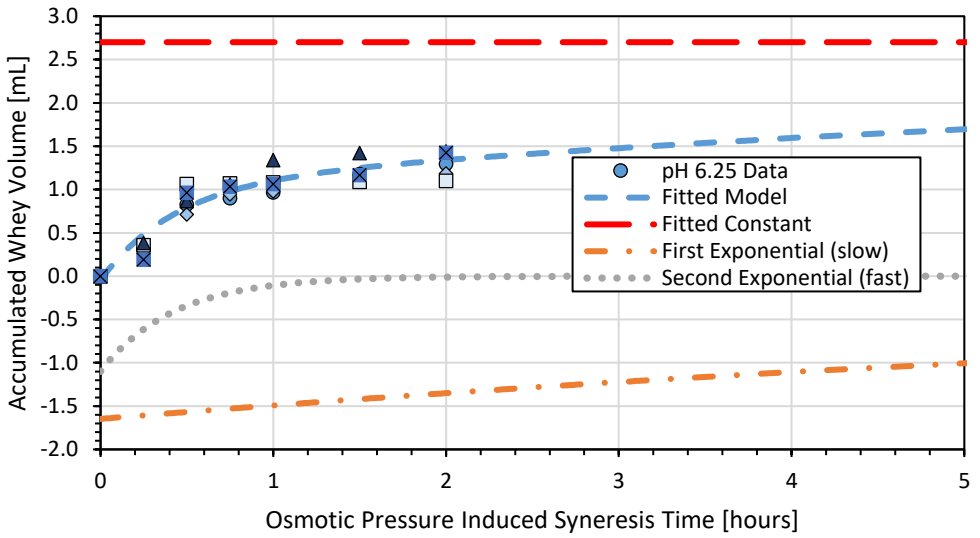

(b)

Figure 4-9: Accumulated whey volume and fitted model as a function of osmotic pressure induced syneresis time for (a) the whole experiment and (b) the first five hours of the experiment after exposure to the 2.5% NaCl-whey solution for five replicates of pH 6.25 gels held at 40 °C in 2.5% NaCl-whey brine. Symbols represent the five different replicates evaluated.

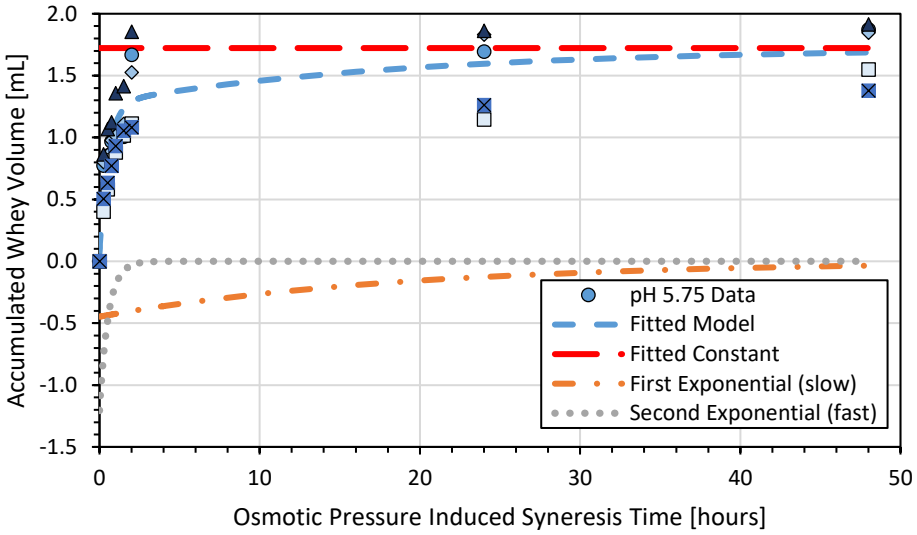

(a)

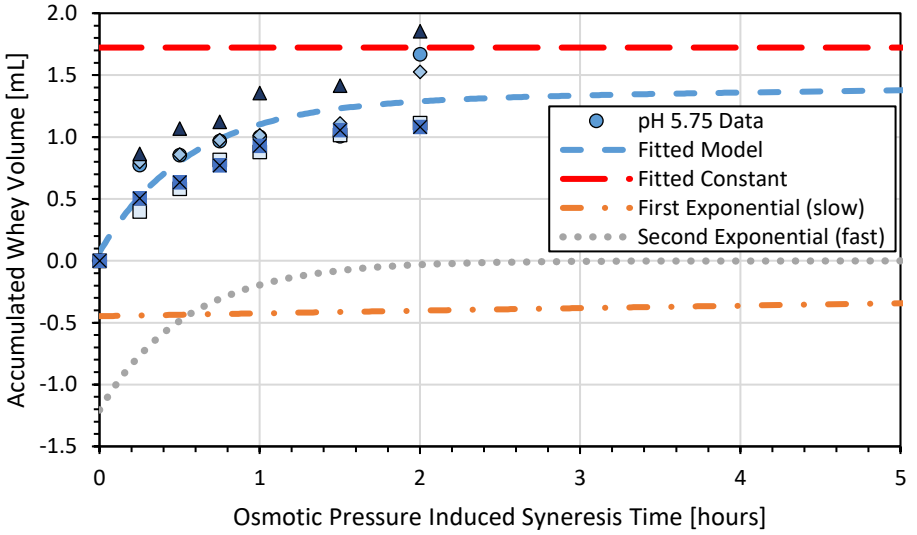

(b)

Figure 4-10: Accumulated whey volume and fitted model as a function of osmotic pressure induced syneresis time for (a) the whole experiment and (b) the first five hours of the experiment after exposure to the 2.5% NaCl-whey for five replicates of pH 5.75 gels held at 40 °C in 2.5% NaCl-whey brine. Symbols represent the five different replicates evaluated.

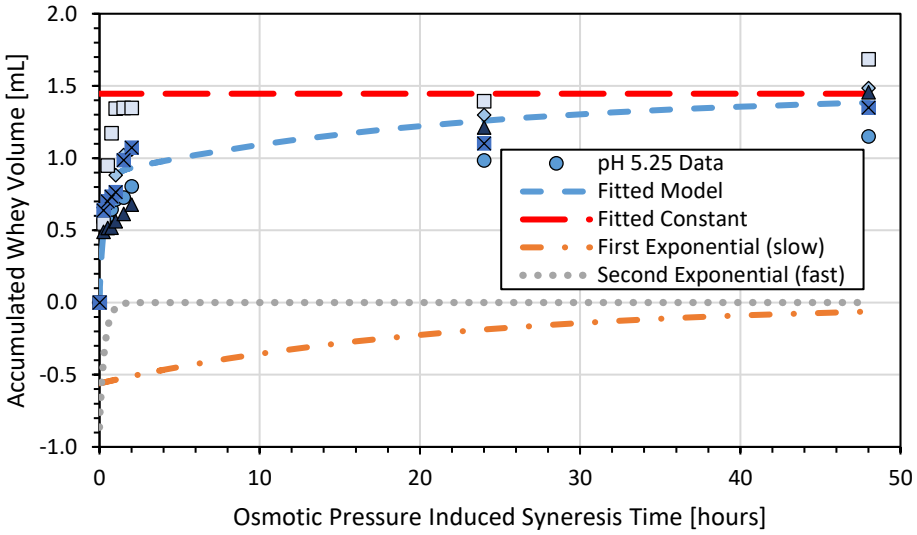

(a)

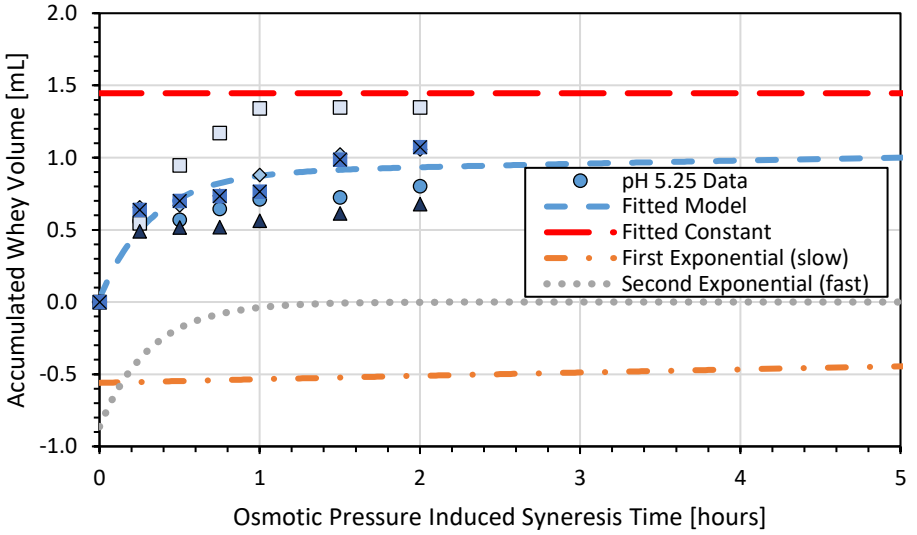

(b)

Figure 4-11: Accumulated whey volume and fitted model as a function of osmotic pressure induced syneresis time for (a) the whole experiment and (b) the first five hours of the experiment after exposure to the 2.5% NaCl-whey for five replicates of pH 5.25 gels held at 40 °C in 2.5% NaCl-whey brine. Symbols represent the five different replicates evaluated.

Figures 4-9 through 4-11 show a slower increase in accumulated whey volume during the early stages of osmotic induced syneresis, compared to the results observed in the PEG-whey treatments. Table 4-6 provides greater detail regarding the model fitted linear and nonlinear variables, in addition to the coefficient of determination (r^2) and the root mean squared error (RMSE).

Table 4-6: Fitted linear and nonlinear variables in Equation 4-4 for accumulated whey volume with fitting statistics of root mean square error and coefficient of determination for each pH treatment under 2.5% NaCl-whey induced osmotic pressure differential conditions.

Treatment	$A_{W,osm}$ [mL]	$B_{W,osm}$ (slow) [mL]	$C_{W,osm}$ (fast) [mL]	$p_{W,osm1}$ (slow) [s^{-1}]	$p_{W,osm2}$ (fast) [s^{-1}]	RMSE [mL]	r^2 [ ]
pH 6.25	2.70	-1.10	0.00	6.48E-04	6.48E-04	0.145	0.974
pH 5.75	1.72	-0.45	-1.21	1.46E-05	5.06E-04	0.233	0.830
pH 5.25	1.45	-0.56	-0.86	1.27E-05	8.70E-04	0.206	0.792

Statistics presented in Table 4-6 show an adequate degree of fit between the fitted model and the data collected. The RMSE values also show the average error in the accumulated volume at any point to not exceed 0.25 mL for any of the models. The RMSE show a relative error of 5.37%, 13.5%, 14.2% in the accumulated whey volume for the pH 6.25, 5.75, and 5.25 treatments, respectively when evaluated at equilibrium.

The 2.5% NaCl-whey osmotic treatment surface area data was fitted with Equation 4-5 for all three pH treatments. Figures 4-12 through 4-14 show the surface area data and fitted biexponential models.

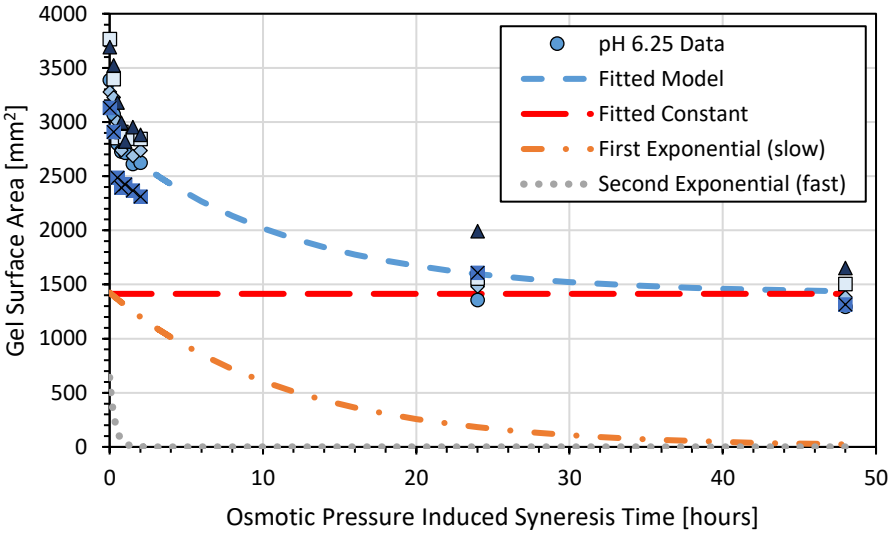

(a)

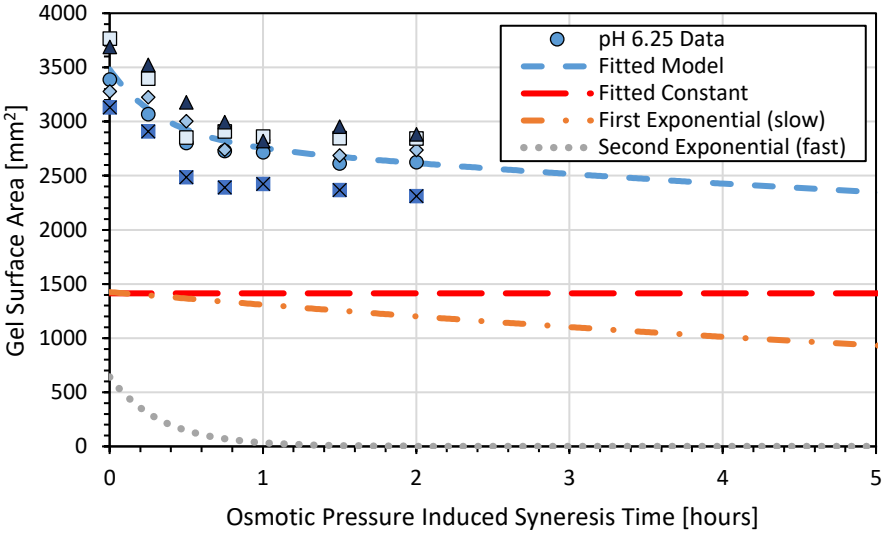

(b)

Figure 4-12: Gel surface area as a function of osmotic pressure induced syneresis time for (a) the whole experiment and (b) the first five hours of the experiment after exposure to the 2.5% NaCl-whey for five replicates of pH 6.25 gels held at 40 °C in 2.5% NaCl-whey brine. Symbols represent the five different replicates evaluated.

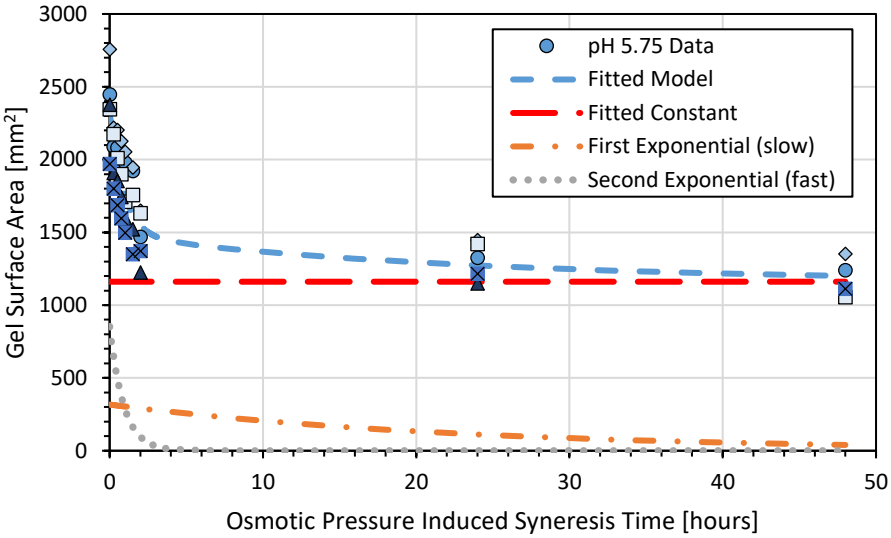

(a)

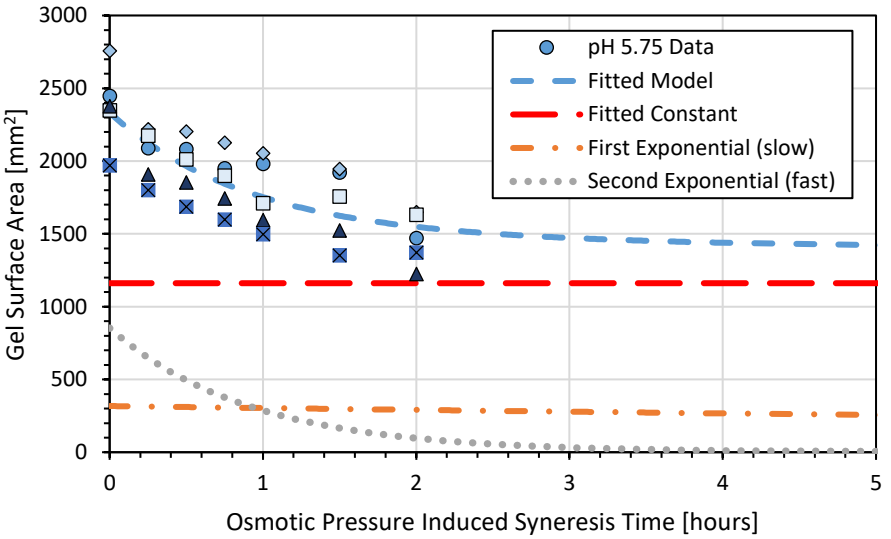

(b)

Figure 4-13: Gel surface area as a function of osmotic pressure induced syneresis time for (a) the whole experiment and (b) the first five hours of the experiment after exposure to the 2.5% NaCl-whey for five replicates of pH 5.75 gels held at 40 °C in 2.5% NaCl-whey brine. Symbols represent the five different replicates evaluated.

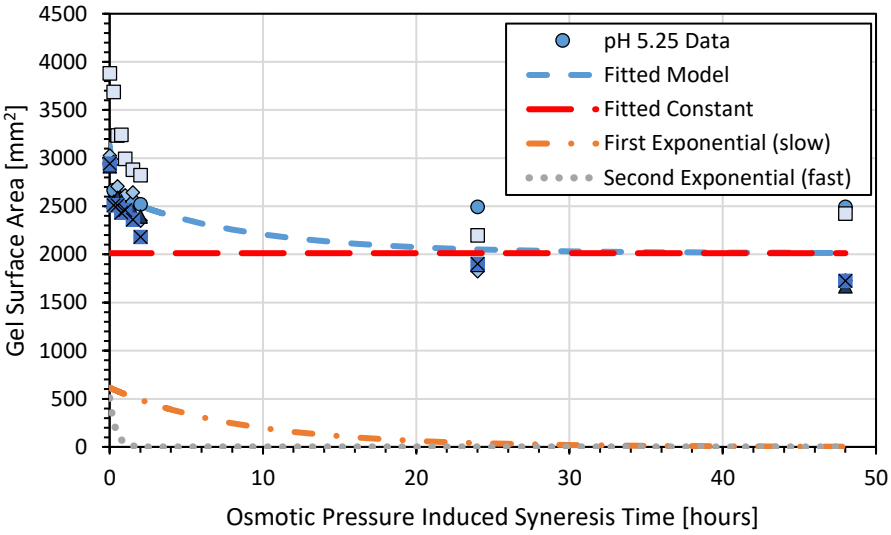

(a)

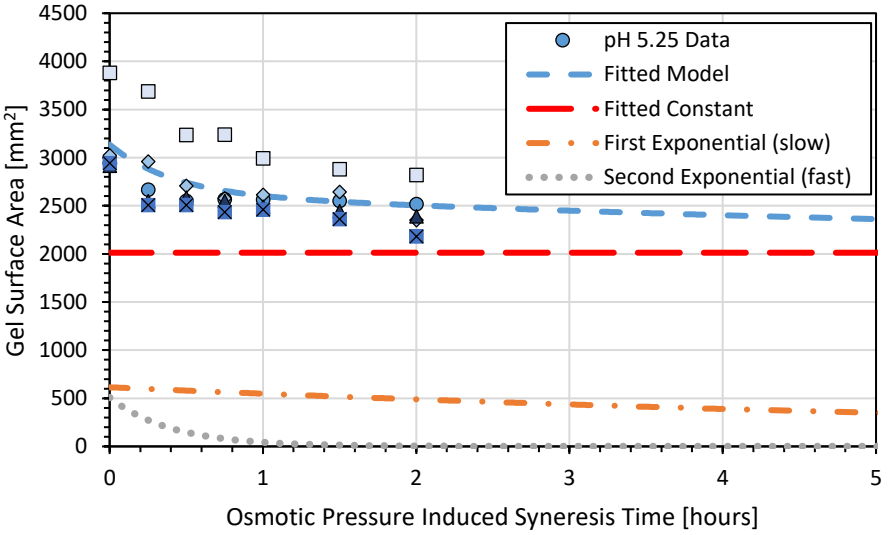

(b)

Figure 4-14: Gel surface area as a function of osmotic pressure induced syneresis time for (a) the whole experiment and (b) the first five hours of the experiment after exposure to the 2.5% NaCl-whey for five replicates of pH 5.25 gels held at 40 °C in 2.5% NaCl-whey brine. Symbols represent the five different replicates evaluated.

Figures 4-12 through 4-14 show the contraction of the gel surface area with respect to time exposed to 2.5% NaCl-whey solution. The behaviour modelled in these figures showed that pH 5.25 gels underwent a limited and slow contraction compared to the other two pH treatments evaluated. Table 4-7 provides the values of the for the fitted linear and nonlinear variables, in addition to the coefficient of determination (r^2) and the root mean squared error (RMSE).

Table 4-7: Fitted linear and nonlinear variables in Equation 4-5 for gel surface area with fitting statistics of root mean square error and coefficient of determination for each pH treatment under 2.5% NaCl-whey induced osmotic pressure differential conditions.

Treatment	$A_{SA,osm}$ [mm^2]	$B_{SA,osm}$ (slow) [mm^2]	$C_{SA,osm}$ (fast) [mm^2]	$p_{SA,osm1}$ (slow) [s^{-1}]	$p_{SA,osm2}$ (fast) [s^{-1}]	RMSE [mm^2]	r^2 [ ]
pH 6.25	1.41E+03	1.43E+03	6.42E+02	2.38E-05	8.17E-04	224	0.900
pH 5.75	1.16E+03	3.17E+02	8.53E+02	1.20E-05	3.03E-04	203	0.773
pH 5.25	2.01E+03	6.14E+02	5.08E+02	3.17E-05	6.90E-04	317	0.563

The statistics presented in Table 4-7 show an adequate degree of fit between the fitted model and the data collected for the pH 6.25 and pH 5.75 treatments, with a poor fit associated with the pH 5.25 treatment. This was likely due to uneven contraction induced by the 2.5% NaCl-whey solution to produce gels with slightly higher or lower surface area values relative to the gel volume values, as evidenced by the degree of variation in the data. The RMSE values also show the average error in the gel surface area at any point to not exceed 320 mm^2 for any of the models. The RMSE values produce a relative error in the modelled gel surface area of 15.9%, 17.5%, and 15.8% for the pH 6.25, 5.75, and 5.25 treatments, respectively when evaluated at equilibrium. The effects of the variation in the fitted accumulated whey volume and gel surface area models are clearer in whey flux and gel moisture mass fractions discussed in the following subsection and section 4.4.4.

4.4.2.3 Average Internal Gel Moisture Content Estimation

The estimated average internal moisture mass fraction for gels undergoing exposure to 2.5% NaCl-whey was calculated using Equation 4-7 for each pH treatment. The average internal gel moisture mass fraction was calculated using the details previously provided in section 4.4.1.3. The results for all three pH treatments are shown as a function of osmotic pressure induced syneresis time in Figure 4-15.

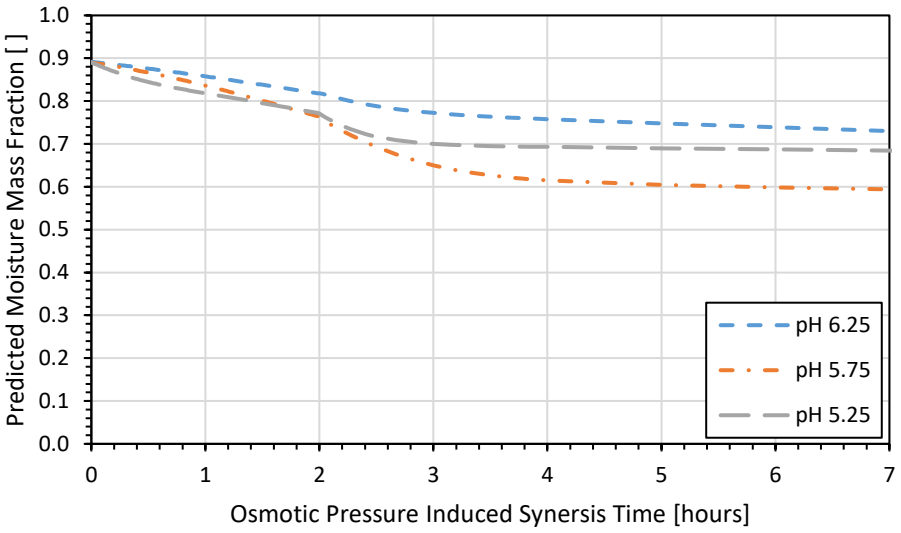

Figure 4-15: Estimated moisture mass fraction of gels with respect to brining time for the first seven hours of after onset of syneresis, with exposure to 2.5% NaCl-whey solutions beginning after two hours of regular syneresis.

The modelled moisture mass fraction decreases at a faster rate with respect to time exposed to the 2.5% NaCl-whey brine during the early stages of osmotic pressure differential induced syneresis, compared to the moisture mass fraction reduction observed during bulk syneresis. As observed in the PEG-whey case, lower pH gels decrease in moisture mass fraction at a faster rate early during the syneresis process due to higher whey mass loss relative to the gel mass. This model does not account for the uptake of salt into the gels, which could affect the average osmotic pressure differential between the residual free whey trapped in the gel and the brine at the surface. The effect of salt interaction with the gel matrices may also be one of the reasons why there are significant differences between the pH treatments in the 2.5% NaCl-whey testing regime.

4.4.3 High Salt Induced Osmotic Pressure Syneresis

4.4.3.1 Statistical Analysis of Accumulated Whey Volume and Gel Surface Area Data

A one-way ANOVA was conducted on the accumulated whey volume and gel surface area data within each pH treatment to determine if there was a significant difference between any of the gels evaluated within their respective treatments beginning at the onset of the 20% NaCl-whey brining. Results indicated that there was no statistically significant difference between the values ascertained in each pH treatment for the accumulated whey volume data, within 95% confidence. However, there were statistically significant differences found within the gel surface area data for the pH 6.25 and 5.25 cases. These findings indicate that although the accumulated whey volume data showed more limited variability, there was

significant variability in the surface area data for two of the pH treatments, indicating inconsistent gel contraction behaviour.

One-way ANOVA assessment also showed no statistically significant differences in the accumulated whey volume data between the pH treatments, within 95% confidence. These results indicate that the high osmotic pressure differential produces approximately the same whey volume expulsion behaviour, regardless of gel pH under these conditions. However, one-way ANOVA on the gel surface area values indicate that all the pH treatments are significantly different from each other, within 95% confidence. This finding indicates that although the net loss of whey volume was consistent between the treatments, there were significant differences in how the gels underwent contraction.

4.4.3.2 Accumulated Whey Volume and Gel Surface Area

The accumulated whey volume data was fitted using Equation 4-4 to model the whey expulsion behaviour of the gels under high osmotic pressure differential induced conditions with 20% NaCl-whey solution. Figures 4-16 through 4-18 show the changing accumulated whey volumes as a function of 20% NaCl-whey exposure time at 40 °C for the pH 6.25, 5.75, and 5.25 gel treatments, respectively.

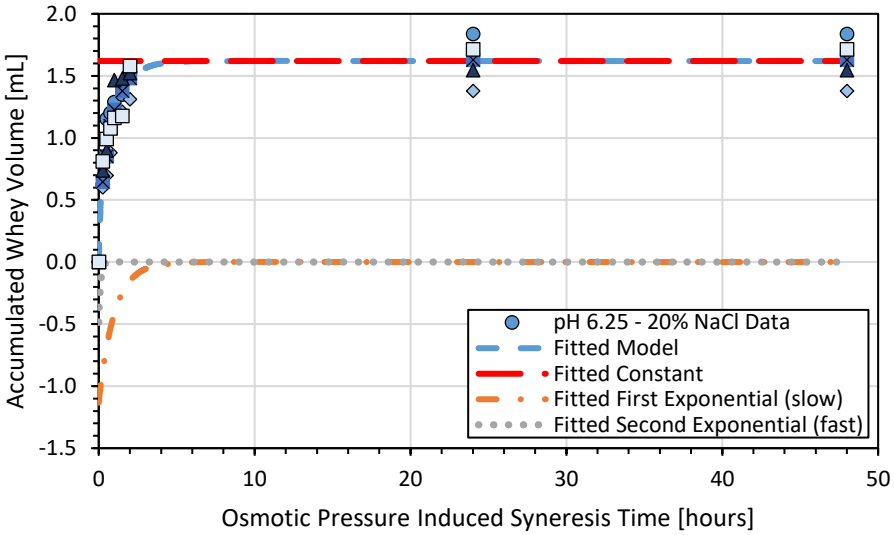

(a)

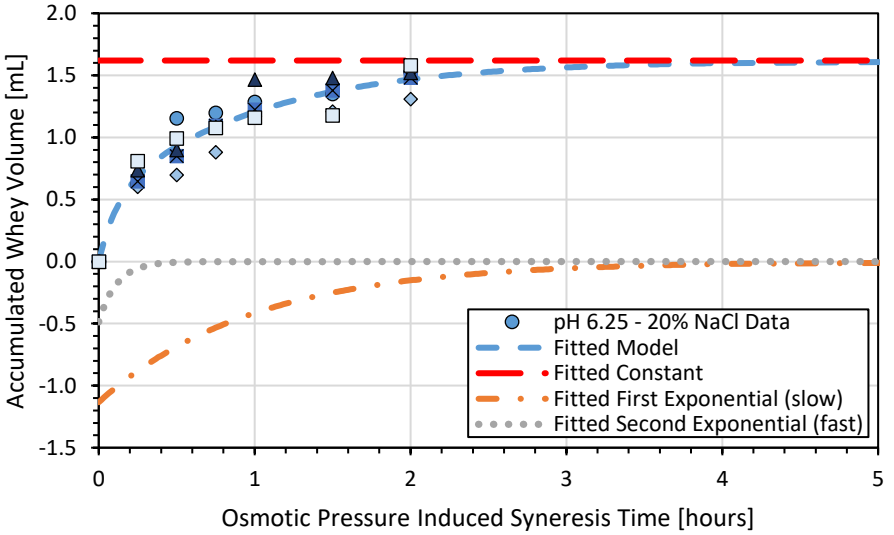

(b)

Figure 4-16: Accumulated whey volume and fitted model as a function of osmotic pressure induced syneresis time for (a) the whole experiment and (b) the first five hours of the experiment after exposure to the 20% NaCl-whey solution for five replicates of pH 6.25 gels held at 40 °C in 20% NaCl-whey brine. Symbols represent the five different replicates evaluated.

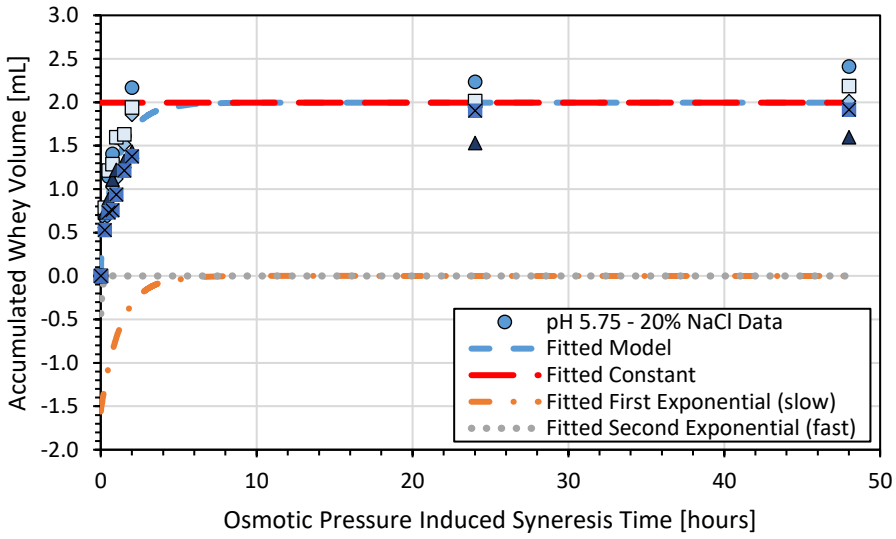

(a)

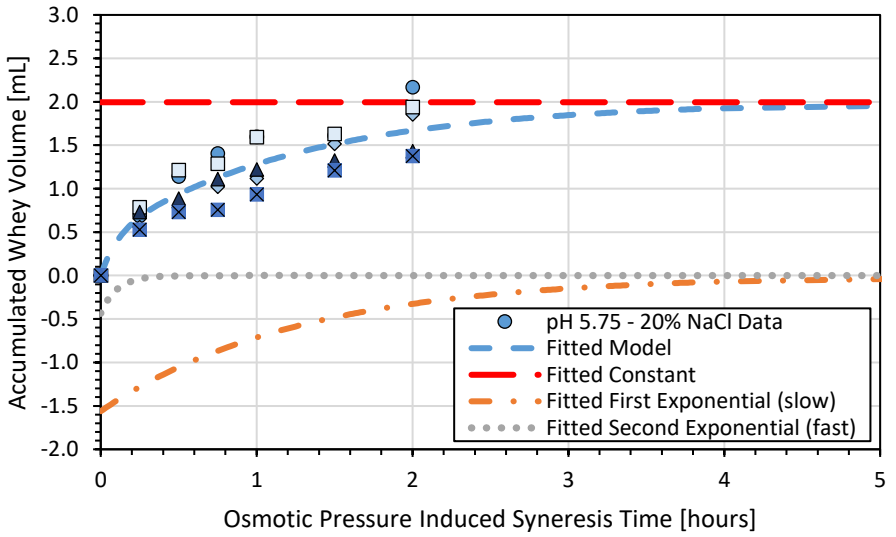

(b)

Figure 4-17: Accumulated whey volume and fitted model as a function of osmotic pressure induced syneresis time for (a) the whole experiment and (b) the first five hours of the experiment after exposure to the 20% NaCl-whey solution for five replicates of pH 5.75 gels held at 40 °C in 20% NaCl-whey brine. Symbols represent the five different replicates evaluated.

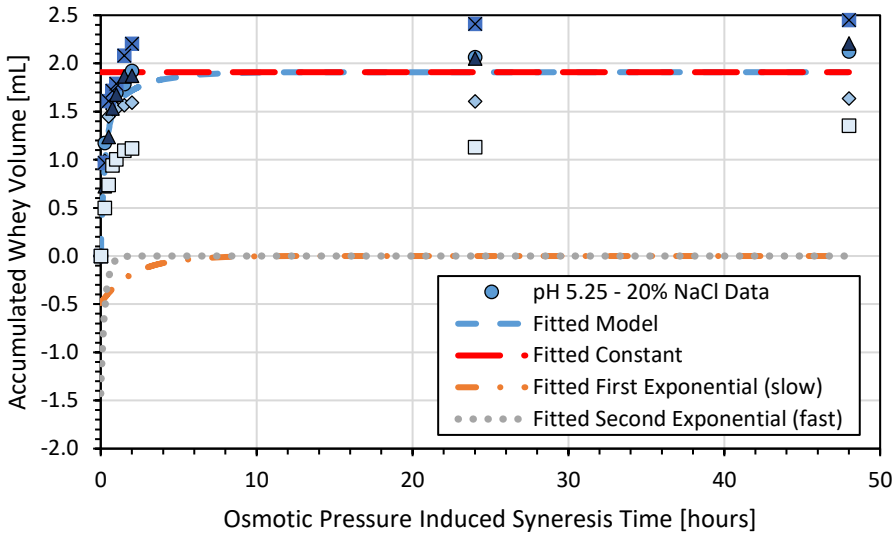

(a)

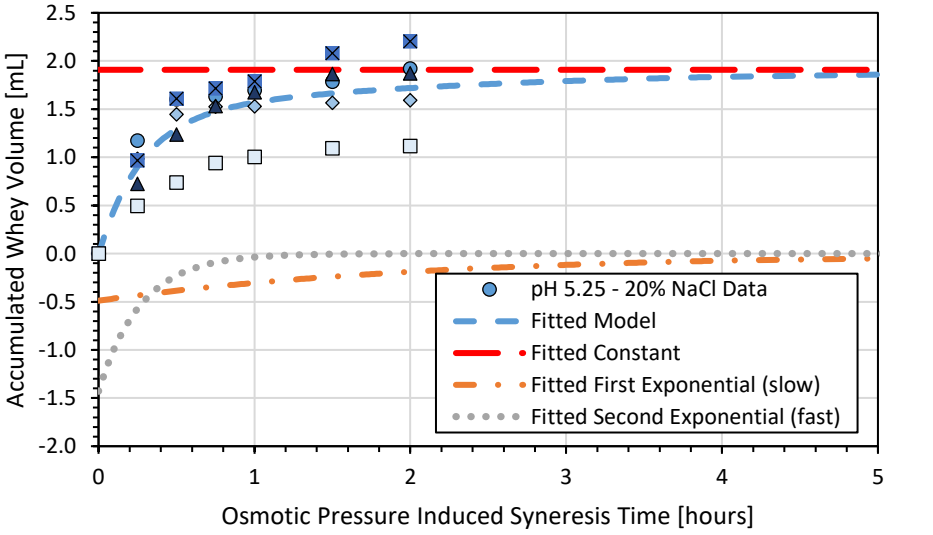

s

(b)

Figure 4-18: Accumulated whey volume and fitted model as a function of osmotic pressure induced syneresis time for (a) the whole experiment and (b) the first five hours of the experiment after exposure to the 20% NaCl-whey solution for five replicates of pH 5.25 gels held at 40 °C in 20% NaCl-whey brine. Symbols represent the five different replicates evaluated.

Figures 4-16 through 4-18 show the fast whey expulsion occurring immediately after exposure to the 20% NaCl-whey solution. This result is expected as the induced osmotic pressure gradient is at least an order of magnitude larger than the two previous tests completed with lower osmotic pressure differentials. Table 4-8 provides the values of the for the fitted linear and nonlinear variables, the coefficient of determination (r^2) and the root mean squared error (RMSE).

Table 4-8: Fitted linear and nonlinear variables in Equation 4-4 for accumulated whey volume with fitting statistics of root mean square error and coefficient of determination for each pH treatment under 20% NaCl-whey induced osmotic pressure differential conditions.

Treatment	$A_{W,osm}$ [mL]	$B_{W,osm}$ (slow) [mL]	$C_{W,osm}$ (fast) [mL]	$p_{W,osm1}$ (slow) [s^{-1}]	$p_{W,osm2}$ (fast) [s^{-1}]	RMSE [mL]	r^2 [ ]
pH 6.25	1.62	-1.13	-0.49	2.79E-04	2.40E-03	0.126	0.945
pH 5.75	1.99	-1.56	-0.43	2.18E-04	2.68E-03	0.232	0.887
pH 5.25	1.91	-0.49	-1.43	1.32E-04	1.02E-03	0.340	0.762

Statistics presented in Table 4-8 show a good degree of fit between the fitted model and the data collected. The RMSE values also show the average error in the accumulated volume at any point to not exceed 0.35 mL for any of the models. The RMSE values indicate that there is a relative error of 7.78%, 11.7%, 17.8% in the accumulated whey volume for the pH 6.25, 5.75, and 5.25 treatments, respectively when evaluated at equilibrium. The 20% NaCl-whey surface area data was fitted with Equation 4-5 for all three pH treatments. Figures 4-19 through 4-21 show the surface area data and fitted models.

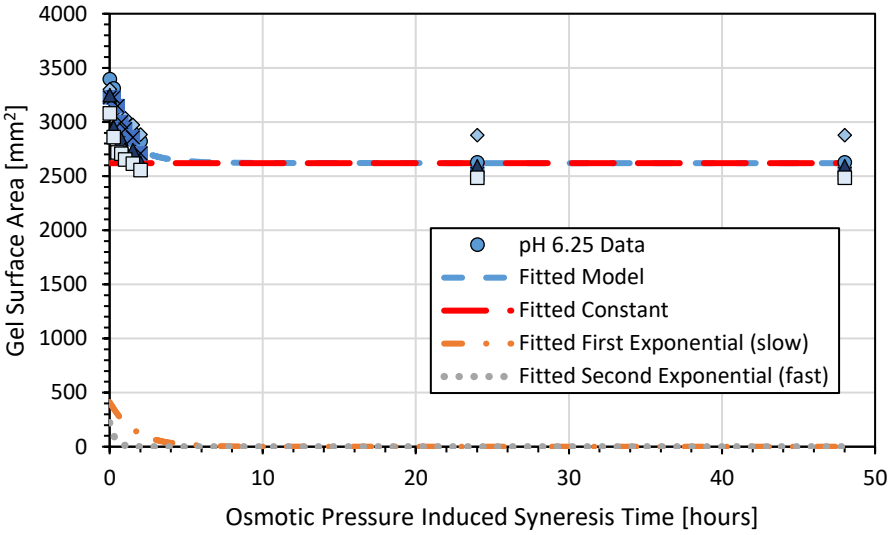

(a)

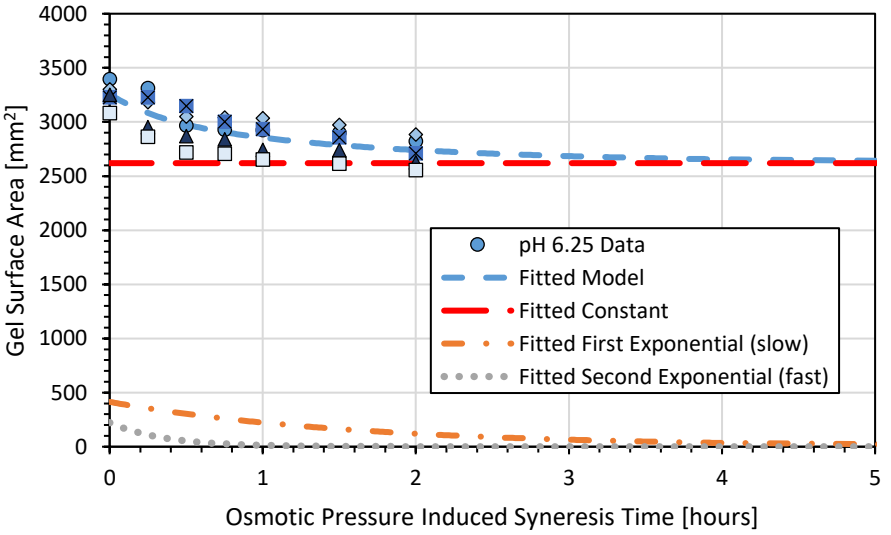

(b)

Figure 4-19: Gel surface area as a function of osmotic pressure induced syneresis time for (a) the whole experiment and (b) the first five hours of the experiment after exposure to the 20% NaCl-whey solution for five replicates of pH 6.25 gels held at 40 °C in 20% NaCl-whey brine. Symbols represent the five different replicates evaluated.

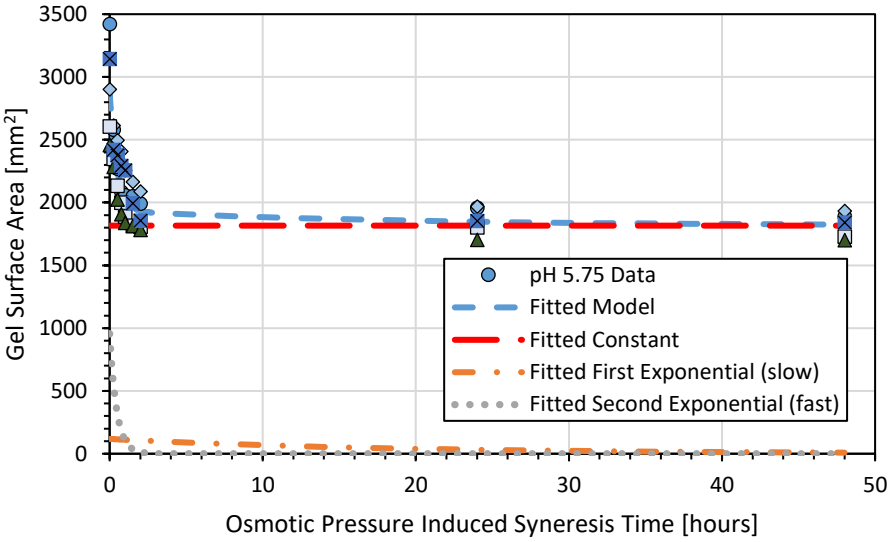

(a)

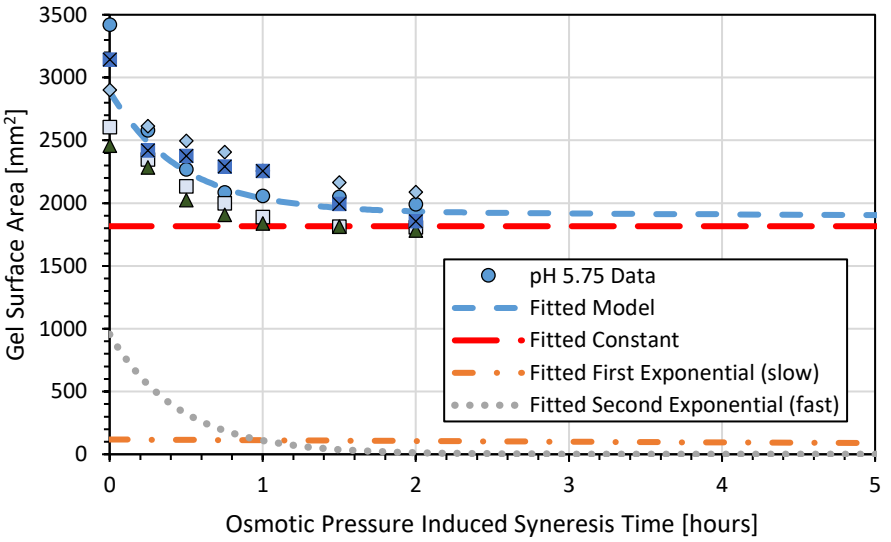

(b)

Figure 4-20: Gel surface area as a function of osmotic pressure induced syneresis time for (a) the whole experiment and (b) the first five hours of the experiment after exposure to the 20% NaCl-whey solution for five replicates of pH 5.75 gels held at 40 °C in 20% NaCl-whey brine. Symbols represent the five different replicates evaluated.

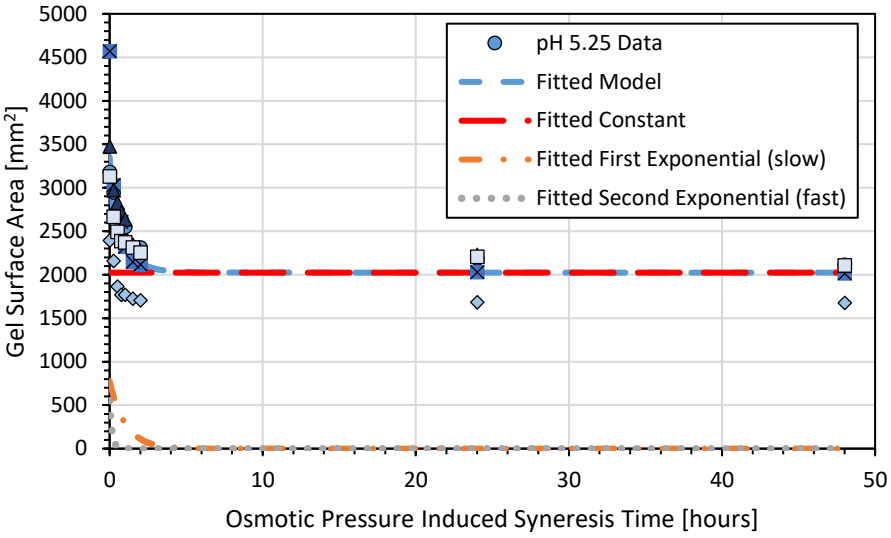

(a)

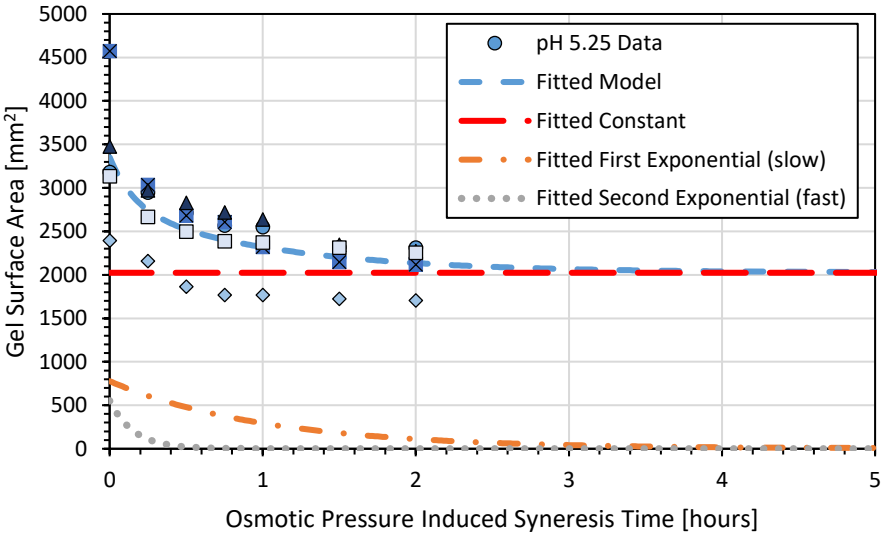

(b)

Figure 4-21: Gel surface area as a function of osmotic pressure induced syneresis time for (a) the whole experiment and (b) the first five hours of the experiment after exposure to the 20% NaCl-whey solution for five replicates of pH 5.25 gels held at 40 °C in 20% NaCl-whey brine. Symbols represent the five different replicates evaluated.

Figures 4-19 through 4-21 show the changing gel surface area with respect to time exposed to the 20% NaCl-whey brine. The lower pH treatments show a fast contraction while the higher pH gels undergo a more gradual reduction in value. Table 4-9 provides the values of the for the fitted linear and nonlinear variables, in addition to the coefficient of determination (r^2) and the root mean squared error (RMSE).

Table 4-9: Fitted linear and nonlinear variables in Equation 4-5 for gel surface area with fitting statistics of root mean square error and coefficient of determination for each pH treatment under 20% NaCl-whey induced osmotic pressure differential conditions.

Treatment	$A_{SA,osm}$ [mm^2]	$B_{SA,osm}$ (slow) [mm^2]	$C_{SA,osm}$ (fast) [mm^2]	$p_{SA,osm1}$ (slow) [s^{-1}]	$p_{SA,osm2}$ (fast) [s^{-1}]	RMSE [mm^2]	r^2 [ ]
pH 6.25	2.62E+03	4.13E+02	2.22E+02	1.72E-04	7.94E-04	145	0.658
pH 5.75	1.82E+03	1.18E+02	9.56E+02	1.53E-05	6.01E-04	189	0.771
pH 5.25	2.02E+03	7.77E+02	5.52E+02	2.70E-04	1.79E-03	372	0.565

Statistics presented in Table 4-9 show an adequate degree of fit between the fitted model and the data collected for the pH 5.75 treatment, with a poor fit associated with the pH 5.25 and pH 6.25 treatments, likely due to the variability in the surface area data. This variation may be attributed to uneven contraction induced by the strong osmotic pressure gradient or the effect of diffusing salt on the structure of the gel matrix, thereby affecting surface area values relative to the gel volumes. The RMSE values also show the average error in the gel surface area at any point to not exceed 380 mm^2 for any of the models, but there is a relative error of 5.55%, 10.4%, and 18.4% error in the surface area values for the pH 6.25, 5.75, and 5.25 treatments, respectively when evaluated at equilibrium. These results indicate that Equation 4-5 does not model the pH 5.25 and pH 6.25 surface area values well in the 20% NaCl-whey solution conditions due to the amount of data variability in the pH 5.25 treatment and the rapid contraction of the pH 6.25 treatment to the equilibrium surface area, respectively.

4.4.3.3 Average Internal Gel Moisture Content Estimation

The estimated average internal moisture mass fraction was calculated using Equation 4-7 for each pH treatment. The average internal gel moisture mass fraction was calculated using the same assumptions listed in section 4.4.1.3. The results for all three pH treatments are shown as a function of osmotic pressure induced syneresis time in Figure 4-22.

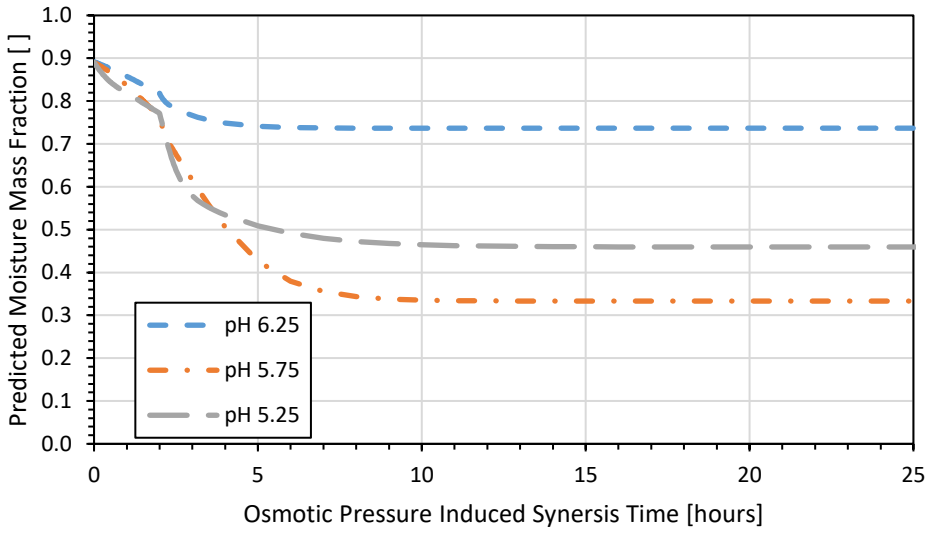

Figure 4-22: Simulated moisture mass fraction of gels with respect to brining time for the first seven hours of after onset of syneresis, with exposure to 20% NaCl-whey solutions beginning after two hours of regular syneresis.

The modelled moisture mass fraction shows a rapid decrease in estimated moisture content upon exposure to the 20% NaCl-whey solution after two hours of regular syneresis, before gradually slowing towards an equilibrium value. Again, as in the previous osmotic stress treatments, the lower pH gels decrease in moisture mass fraction at a faster rate early during the syneresis process due to the higher whey mass loss relative to the gel mass. This is due, in part, to their smaller starting mass at the onset of brining, whereby any whey losses have a larger effect on the moisture mass fraction than on larger gels with high moisture mass fractions. It is also important to note, that this model is limited by not accounting for the uptake of salt into the gels. The presence of salt diffusing into the gels could affect the strength of the gel or average osmotic pressure differential between the residual free whey trapped in the gel and the brine at the surface, thereby affecting whey expulsion and degree of surface area contraction. Inclusion of the salt uptake behaviour in the moisture mass fraction model would improve understanding of the role of salt uptake on the movement of moisture through the gel.

4.4.4 Comparison of Induced Osmotic Pressure Differential Syneresis Results

Comparison of the short-term dominating rate constants of the accumulated whey volume model ($p_{w,osm2}$ in Equation 4-4) in each osmotic pressure and pH treatment shows insights to the mechanisms that may be governing whey expulsion. Figure 4-23 shows the different best-fit short-term dominating rate constant for all three osmotic pressure treatments presented in this chapter as a function of gel pH.

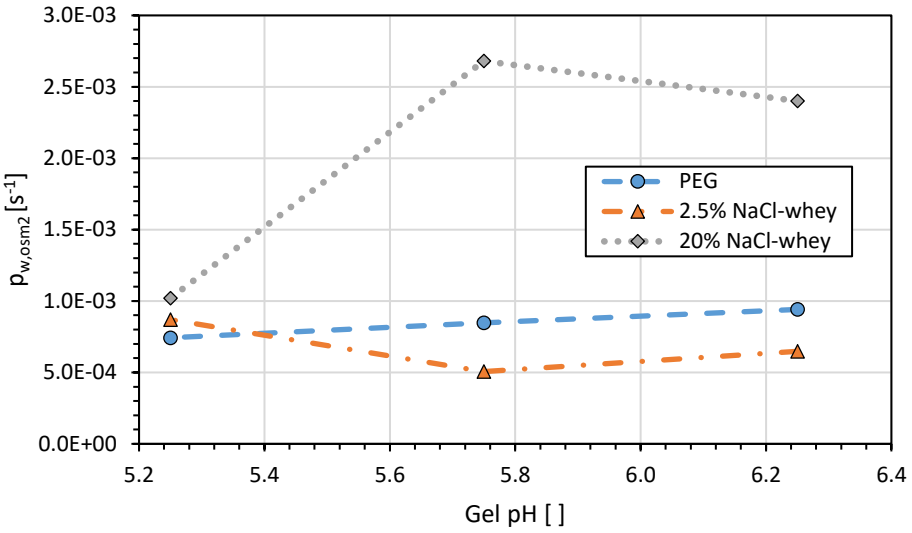

Figure 4-23: Short-term dominating rate constants for the whey expulsion models with respect to gel pH for each induced osmotic pressure differential treatment. Lines connecting the values at each pH are included for ease of evaluation.

Figure 4-23 shows that the presence of a larger osmotic pressure differential (20% NaCl-whey) creates a larger short-term rate constant for all gel pH values assessed, particularly for the pH 5.75 and 6.25 cases. A larger short-term rate constant allows for faster expulsion of whey during the earliest stages of syneresis, specifically in the first hour of syneresis. This finding indicates that more of the trapped whey may be available for fast expulsion for higher pH gels treated with 20% NaCl-whey brining conditions. This is makes sense because the higher pH gels have more moisture available for expulsion at the time of exposure to the osmotic pressure differential, as shown in Figure 4-22. This behaviour is presumed to occur due to the presence of additional stabilizing free calcium for the higher pH gels, which limit interactions between the protein matrix and diffusing salts that would otherwise improve moisture retention in the gel (T. Guinee & Fox, 2017).

Whey flux results for all treatments demonstrated the effect of the osmotic pressure differential on the whey flux behaviour, with differing levels of affect. Figures 4-24 through 4-26 compare the whey flux results for all the osmotic pressure differential treatments to the regular syneresis case for the pH 6.25, 5.75, and 5.25 treatments, respectively.

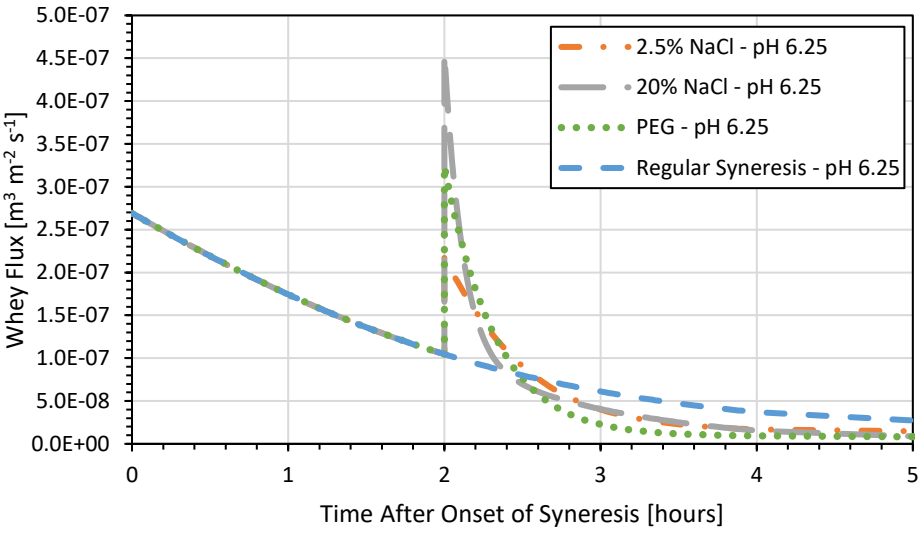

Figure 4-24: Comparison of simulated whey flux behaviours under different osmotic pressure induced syneresis treatments for pH 6.25 gels held at 40 °C and undergoing regular syneresis for two hours prior to the onset of the osmotic pressure induced syneresis conditions.

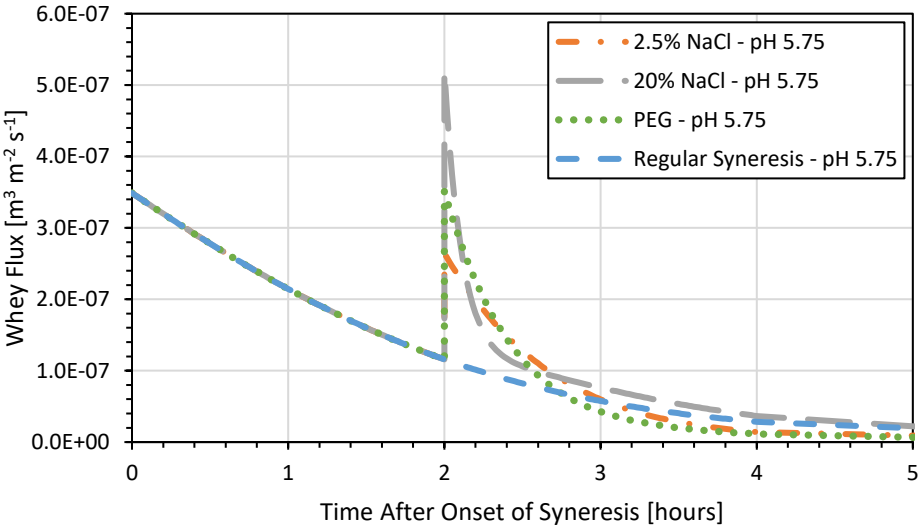

Figure 4-25: Comparison of simulated whey flux behaviours under different osmotic pressure induced syneresis treatments for pH 5.75 gels held at 40 °C and undergoing regular syneresis for two hours prior to the onset of the osmotic pressure induced syneresis conditions.

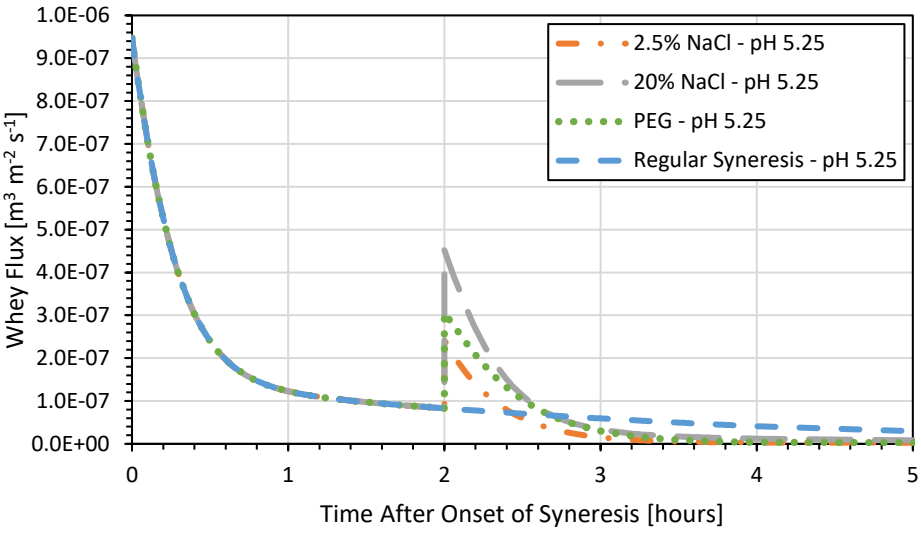

Figure 4-26: Comparison of simulated whey flux behaviours under different osmotic pressure induced syneresis treatments for pH 5.25 gels held at 40 °C and undergoing regular syneresis for two hours prior to the onset of the osmotic pressure induced syneresis conditions.

Results from all the treatments show that the 20% NaCl-whey treatment produced the largest starting whey flux behaviour, which rapidly decreased within the first thirty minutes of brining for all pH treatments. This is expected as the amount of free whey available for expulsion would be quickly depleted, causing the whey flux to decrease. Interestingly, the whey flux behaviour at the onset of osmotic pressure differential induced syneresis of the 20% NaCl-whey was roughly 1.5-2.0 times that of the whey flux for the 2.5% NaCl-whey treatments. This is significantly less than what would be predicted from an induced osmotic pressure differential at several orders of magnitude larger, indicating that after most of the whey has been expelled there is a constrained effect of the osmotic pressure differential at the surface to promote whey expulsion. This may be due to the degree of binding between the moisture and the para-casein matrix forming the gel, or the inhibited transport of the whey out of the gels through the porous matrix.

The data also showed that for equivalent starting osmotic pressure differentials with the PEG-whey and 2.5% NaCl-whey solutions, the PEG-whey solutions consistently produced a slightly larger starting whey flux values at the onset of exposure. This could be explained by the differences in the solutes producing the osmotic pressure differential. Salt would be expected to interact with the gel matrix as it gradually diffused into the gel matrix, while the PEG would not diffuse into the gel or interact at the surface. This would ultimately decrease the osmotic pressure differential between the trapped whey in the gel and the surface brine,

thereby decreasing the effect of the starting osmotic pressure differential on the whey flux behaviour.

4.5 Conclusions

This chapter applied the image analysis and modelling techniques described in the previous chapter to investigate and model syneresis under osmotic pressure differential conditions as a whey flux. The findings from the experiment discussed in this chapter have shown that (1) induced osmotic pressure differentials create change in the whey flux behaviour of renneted milk gels, (2) higher starting osmotic pressure differential conditions yield larger whey flux to a limit, and (3) the type of solute used to create the osmotic pressure differential affects the whey expulsion behaviour due to possible interactions with the gel matrix. These achievements provide the foundation to understand and model the effect of induced osmotic pressure effects on syneresis behaviour and changes in the internal microstructure of the gels. The following chapters assess salt uptake and the internal structural changes of gels exposed to different osmotic pressure differential conditions using image analysis and modelling techniques.

Chapter 5 Salt Transport in Gel Systems

5.1 Introduction

Assessment and mathematical modelling of salt uptake is important for optimizing the uptake of salt in cheese curds, while minimizing losses in expelled whey to attain target cheese properties. Section 2.3 provides detail about the specific roles salt plays in the developing of cheeses with desirable qualities. The following subsections provide a brief introduction to the physical mechanisms involved in the transport of salt in cheese curds and methods to model salt uptake.

5.1.1 Salt Uptake Mechanisms

Salt uptake into cheese curds is governed primarily by diffusion mechanisms, where the concentrated brine at the surface of the curd creates the driving concentration gradient for mass transfer of the salt ions into the curd structure (Floury, Rouaud, et al., 2009; T. Guinee & Fox, 2017; Morris, Guinee, & Fox, 1985; Turhan & Kaletunc, 1992). Under normal diffusion behaviour the salt ions would slowly diffuse into the gel structure via the free whey within the gel until an equilibrium is established with the surrounding brine. However, salt ions are not inert, and they interact with the para-casein curd matrix to create noticeably stronger gels at the macro-scale (Fucà et al., 2012; McCarthy, Wilkinson, Kelly, & Guinee, 2016). The combination of the strong, possibly adsorptive interactions between the salt ions and the para-casein matrix and the expulsion of salt from the gel into the free fluid expelled due to osmotic pressure differential induced syneresis make the modelling of salt transport via diffusion more complicated than simple Fickian models would suggest (Melilli et al., 2005; Sutherland, 1974). Figure 5-1 provides a visual representation of the complexities involved in the transport of salt ions into individual cheese curds.

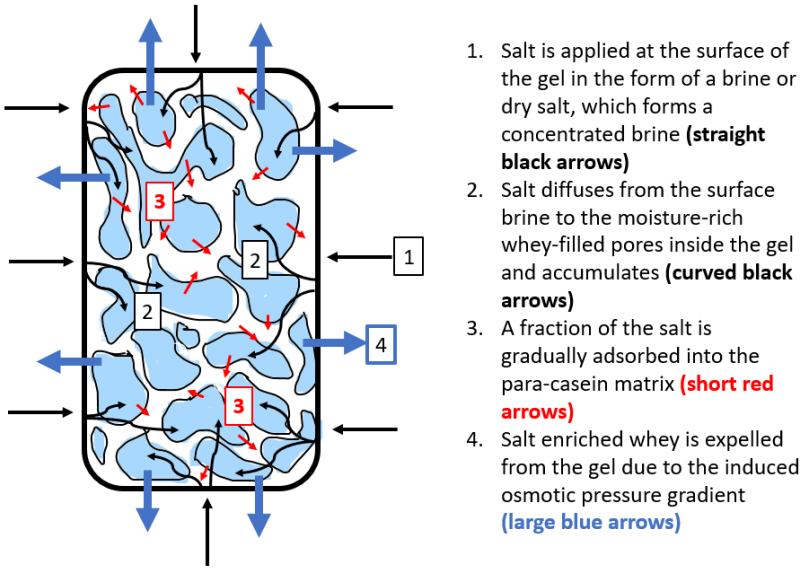

Figure 5-1: Demonstration of the mechanisms occurring during salt uptake and osmotic pressure gradient induced syneresis, where salt is first is transported from the surface into the moisture-rich regions in the gel before it begins to adsorb to the gel protein or is expelled in the whey expelled from the gel due to syneresis. Blue regions represent the whey-filled porous regions, while white represents the para-casein matrix.

Figure 5-1 provides a simplified demonstration of the different mechanisms happening during the mass transfer of salt into a cheese curd. Although salt diffusion into cheese matrices has previously been modelled using the Fickian mass diffusion approach, it is important to note that the calculation of an effective diffusion coefficient must also account for possible adsorption-like behaviours and salt expulsion via osmotic pressure differential induced syneresis.

5.1.2 Fickian Diffusion Modelling

The most common approach to modelling salt uptake into cheese systems has consisted of Fickian diffusion modelling, usually in the form of unsteady-state diffusion described using Fick's first and second laws, previously described in Equations 2-1 and 2-2. Section 2.6.1 details the Fickian unsteady-state mass transport of salt into slabs of semi-infinite slabs. Fick's laws have also been applied to describe unsteady-state diffusion in infinite cylinders. Equation 5-1 shows the Fick's second law adapted for an infinite cylinder with an outer radius of r_{max} [m].

$$\frac{\partial C_i}{\partial t_D} = D_i \frac{\partial^2 C_i}{\partial r^2} + \frac{D_i}{r}\frac{\partial C_i}{\partial r} \quad \text{for } t_D > 0 \text{ and } 0 < r < r_{max}$$

Equation 5-1: Fick's second law of diffusion for cylindrical coordinates.

The two boundary conditions and the initial condition required for solving the partial differential equation regarding salt uptake into the curd are shown below.

$$C = C_\infty \text{ for } t_D \geq 0 \text{ at } r = r_{max}$$

$$\frac{\partial C_i}{\partial r} = 0 \text{ for } t_D \geq 0 \text{ at } r = 0$$

$$C = C_i \text{ at } t_D = 0 \text{ for } 0 \leq r < r_{max}$$

Crank (1975) used a separation of variables approach to develop a solution for the concentration of diffusing solute at any radius, r_i, within the maximum radius of an infinite cylinder under unsteady-state diffusion, which is shown in Equation 5-2.

$$\frac{C - C_\infty}{C_0 - C_\infty} = \sum_{m=1}^{\infty} \frac{2J_0\left(\beta_m \frac{r_i}{r_{max}}\right)}{\beta_m J_1(\beta_m)} e^{(-\beta_m{}^2 F_{0,cyl})}$$

Equation 5-2: Analytical solution for unsteady-state diffusion into an infinite cylinder.

In Equation 5-2, J_0 and J_1 [dimensionless] are the first-order Bessel's functions, β_m [dimensionless] are the roots of the first-order Bessel function, and C_∞ [kg m^{-3}] is the concentration in ambient surroundings at equilibrium. The Fourier number for diffusion into a cylinder, F_0 [dimensionless], is shown in Equation 5-3.

$$F_0 = \frac{D_{eff} t_D}{r_{max}{}^2}$$

Equation 5-3: Fourier number equation for diffusion into the radial dimension of an infinite cylinder.

Calculations for the average concentration throughout the gel, C_{avg} [kg m^{-3}], can also be determined analytically, as shown in the equation below.

$$\frac{C_{avg} - C_\infty}{C_0 - C_\infty} = \sum_{m=1}^{\infty} \left(\frac{4e^{-\beta_m{}^2 F_0}}{\beta_m{}^2}\right)$$

Equation 5-4: Analytical solution for the average concentration in an infinite cylinder undergoing unsteady-state diffusion.

Equation 5-4 serves an important function when modelling the net salt uptake into the fluid fraction of gels and determining the best-fit effective diffusion coefficient for salt transport. It is important to note that modelling salt transport into cheese curds using a Fickian model relies on the transport occurring within the evenly distributed whey fraction within the gel. It does not account for interactions between the diffusing salt ions and the para-casein matrix that may otherwise remove or prevent the free movement of salt ions in the gel fluid. The next section provides different methodologies to model the possible salt adsorption-like

behaviours that may occur between the solids fraction of a cheese curd and the diffusing dissolved salt ions.

5.1.3 Modelling Hypothesized Salt Adsorption-Like Behaviour

Interactions between the dissolved salt ions and the proteinaceous para-casein matrix have been discussed regarding changes in the macro-scale rheological properties of curds (Henneberry et al., 2015; Lucey et al., 2003; McCarthy et al., 2016). The reason for the observed increase in gel firmness is attributed to an increase in protein-protein interactions facilitated by the presence of the salt ions that reduce the electrostatic forces between the proteins (Lucey et al., 2003). Previous studies have also explained the behaviour between the salt ions and the para-casein network as a calcium-sodium ion exchange takes place between the free sodium ions and the calcium ions associated with the para-casein matrix (Gal & Bankay, 1971; Hardy & Steinberg, 1984). However, this work has focused on determining the isotherm behaviours regarding moisture and salt in para-casein matrixes and not the kinetics of interest that govern the transition of salt ions to a state of close interaction with the para-casein network.

Adsorption kinetics are usually modelled with pseudo first-order (PFO) or pseudo second-order (PSO) rate equations (Haerifar & Azizian, 2012; Liu & Shen, 2008; Marczewski, 2010). Equations 5-5 and 5-6 show the PFO and PSO equations, respectively.

$$\frac{dq}{dt} = k_1(q_e - q)$$

Equation 5-5: Pseudo first-order kinetic adsorption model.

$$\frac{dq}{dt} = k_2 q_e (q_e - q)^2$$

Equation 5-6: Pseudo second-order kinetic adsorption model.

In Equations 5-5 and 5-6, q [dimensionless] is the mass adsorbed per mass of the adsorbent, q_e [dimensionless] is the mass adsorbed per mass of the adsorbent at equilibrium, and k_1 and k_2 [s^{-1}] represent the rate constants for the PFO and PSO equations, respectively. The differential form of the PFO and PSO may be reorganized in the integrated forms of PFO and PSO, shown below.

$$q = q_e(1 - e^{-k_1 t})$$

Equation 5-7: Integrated pseudo first-order kinetic adsorption model.

$$q = \frac{k_2 {q_e}^2 t}{1 + k_2 q_e t}$$

Equation 5-8: Integrated pseudo second-order kinetic adsorption model.

Modelling adsorption kinetics with the PFO or PSO models are good choices for when the mechanism controlling adsorption is well understood. However, the hypothesized adsorption kinetics of salt to para-casein matrix solids is not well understood and other models must be considered when fitting data. An adsorption model that accounts for the changing effective distances solute must travel to adsorb is a fractal adsorption model, whereby the rate constant associated with adsorption changes as a function of time, which could be related to the accessibility of binding sites for adsorbing solutes (Haerifar & Azizian, 2012). Figure 5-2 provides a visual demonstration of how the changing effective path for solutes to travel would create a fractal-type change in the adsorption kinetic rate constant with respect to time.

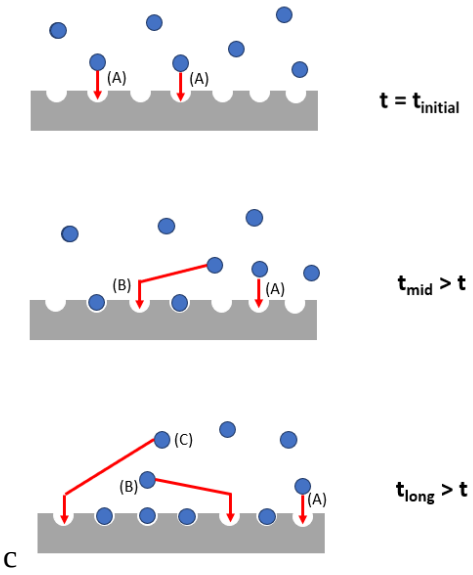

Figure 5-2: Schematic representation of adsorption process as a function of time. (A), (B), and (C) are the possible paths for sorption of adsorbate particles on surface under different time regimes, with the onset of adsorption occurring in the top panel and the second and third panels proceeding sequentially, adapted from Haerifar and Azizian (2012).

Figure 5-2 provides a visual example of how the changing effective pathway for solutes to travel to adsorb onto available binding sites in the adsorbent would effectively change the overall kinetic rate constant with respect to time. Figure 5-2 depicts a gradual change in the dominating pathway for adsorption, with different pathways accounting for a certain number of the adsorbed solutes with respect to time. The shortest pathways provide the greatest contribution to the binding of the solutes at the initial stages of adsorption, until the readily available sites are saturated and different pathways become more important to the adsorption

behaviour. Haerifar and Azizian (2012) provided an approach to model the adsorption behaviour for fractal-like binding conditions for adsorbing solutes, and the Fractal Integrated Kinetic Langmuir (fractal IKL) equation developed is shown in Equation 5-9.

$$q = \frac{q_e\left(1 - \exp\left(-k'_{1,0}t^{\alpha}\right)\right)}{1 - f_{eq}\exp\left(-k'_{1,0}t^{\alpha}\right)}$$

Equation 5-9: Fractal Integrated Kinetic Langmuir equation.

In Equation 5-9, α [dimensionless] represents the fractional time index that alters the adsorption behaviour as a function of time and is less than one in value, $k'_{1,0}$ [$s^{-\alpha}$] is the kinetic rate constant for the fractal IKL equation, and f_{eq} [dimensionless] is the Langmuir equilibrium batch value. Both the Langmuir equilibrium batch value and kinetic rate constant are described in Equations 5-10 and 5-11.

$$f_{eq} = \left(1 - \frac{C_{\infty}}{C_{0,brine}}\right)\left(\frac{q_e}{q_m}\right)$$

Equation 5-10: Langmuir equilibrium batch equation.

$$k'_{1,0} = \frac{k_{a,0}}{\alpha} C_{0,brine}\left(1 - \frac{C_{\infty}}{C_{0,brine}}\right)\left(\frac{1 - f_{eq}}{f_{eq}}\right)$$

Equation 5-11: Rate coefficient for the Integrated Kinetic Langmuir Equation.

In Equations 5-10 and 5-11, $C_{0,brine}$ [kg m^{-3}] is the starting brine concentration, q_m [dimensionless] is the maximum adsorbed mass per mass of adsorbent or adsorption capacity, and $k_{a,0}$ [$s^{-\alpha}$] is the kinetic rate constant for the fastest route of adsorption, as shown in Figure 5-2 in the top panel. The kinetic rate constant for the fastest route of adsorption may also be related to an observable kinetic rate constant, $k_{a,obs}$ [s^{-1}] for the adsorption behaviour using the fractional time index, as shown in Equation 5-12.

$$k_{a,obs} = k_{a,0}t^{\alpha-1}$$

Equation 5-12: Observed rate coefficient of adsorption as a function of the rate constant for the shortest pathway to achieve adsorption (shown in Figure 5-2) and the fractional time index.

The PFO, PSO, and the Fractal IKL all provide approaches to model the possible adsorption-like behaviour that is hypothesized to occur between a fraction of the salt ions diffused into the gel and the para-casein matrix solids. However, the mechanisms that govern the interactions, ion exchange, or possible adsorptive-like behaviours are not well understood in the terms of the kinetics governing salt uptake and losses during the dynamic stages of salting and syneresis in cheesemaking. One step to ascertain how the close interactions of the salt

ions with the para-casein matrix change the properties of the para-casein matrix at the molecular scale is to assess changes in the Carbon-13 Nuclear Magnetic Resonance (^{13}C NMR) spectra and the T_1 longitudinal relaxation time constant. The next section provides a brief introduction to ^{13}C NMR and its possible uses in assessing cheese curds at different stages of salting.

5.1.4 Carbon-13 NMR

True adsorption behaviour is difficult to confirm in the case of cheese systems, which are extremely dynamic and may not maintain permanent adsorption-like properties. ^{13}C NMR may be used to provide insight to the changing behaviour of the para-casein matrix under different salting conditions. Carbon-13 NMR is analogous to proton NMR, where an external magnetic field causes a change in the spin of the carbon-13 atoms to reach a higher energy state. The amount of time required for the net magnetization vector (average angular momenta from all the spins within the sample) to achieve 63% of the maximum value parallel to the external magnetic field is the T_1 longitudinal relaxation constant (Boisard et al., 2013; Song, 2009). Reduction in of the net magnetisation vector is achieved via energy loss in the form of heat loss through collisions with nearby nuclei or rotation (Boisard et al., 2013; Song, 2009). Larger T_1 longitudinal relaxation constants indicate that the carbon-13 nuclei are undergoing fewer collisions or are otherwise restricted even in their ability to rotate. The T_1 longitudinal relaxation constant provides an indicator to the effect that salt ions have on the relative mobility of the para-casein matrix molecules.

The purpose of this chapter is four-fold: (1) to evaluate and model salt uptake in both fluid and solids fractions of milk gels as a function of brining time, (2) determine the best-fit Fickian effective diffusion coefficient to describe the salt uptake behaviour in the fluid fraction, (3) evaluate and model the hypothesized adsorption-like behaviour of salt to the para-casein matrix, and (4) assess the changing para-casein matrix mobility with respect to salt uptake using Carbon-13 NMR to calculate the T_1 longitudinal relaxation constant. The following sections provide the experimental design and results from brining experiments evaluating the changing distribution of fluid and solids fractions and allotment of salt in each fraction as a function of brining time. It also provides insight to the salt uptake behaviours that deviate from the standard Fickian diffusion case, including expulsion of salted whey from the gel due to the induced osmotic pressure differential from the surrounding brine, possible adsorptive behaviour of salt ions to the solids fraction of the gels, and the changing

mobility state of the para-casein matrix as assessed via carbon-13 NMR T_1 longitudinal relaxation constant assessment.

5.2 Experimental Design

An experiment was designed to evaluate salt uptake with respect to starting NaCl-whey brine concentrations and diffusion time, by combining previously described image analysis and gel evaluation techniques from Chapters 2 and 3 with ion chromatography analysis, as a destructive method to assess salt uptake in different fractions of the brined gels.

5.2.1 Experimental Material Preparation

Milk, rennet, whey, imaging apparatus, and dialysis tubing preparation was conducted following the procedures described in sections 3.2.1 through 3.2.4. Brines were prepared to evaluate salt uptake under high salt (20% NaCl-whey brine) and low salt (2.5% NaCl-whey brine) conditions using the procedure detailed in section 4.2.2. All brines were prepared with salt and pre-acidified whey with the same pH as the gels, thereby preventing calcium salt concentration gradients across the curd and surrounding brines.

5.2.2 Sample Gel Preparation and Evaluation

Tests were designed to evaluate salt uptake in individual gels undergoing brining at different points in time using a destructive assessment. Gels were poured, set, and allowed to undergo regular bulk syneresis in dialysis tubing using the procedure detailed in section 4.2.2 for two hours at 40 °C. Images were taken of the gel before the onset of syneresis and after two hours of regular syneresis to confirm adherence to the net gel contraction and whey expulsion behaviour observed in sections 3.4.2 and 3.4.3. No additional images were captured during the bulk syneresis phase as the models for syneresis had previously been established in section 3.4. Free whey in the tubes was removed and the gels were exposed to pre-warmed NaCl-whey brines to commence salt uptake and osmotically induced whey expulsion, following the procedures listed in section 4.2.3. Samples were removed in triplicate at 1, 5, 10, 20, 30, 60, 120, 300, and 1440 minutes to evaluate salt uptake as a function of brining time at 40 °C with either 2.5% NaCl-whey solution or 20% NaCl-whey solution.

Gels were removed from the brine solution at the predetermined sampling times, dipped into Milli-Q water to remove any surface brine that had not diffused into the gel, blotted dry, and weighed. The gels were then placed in 3 mL centrifuge tubes and centrifuged for an hour at a rotational speed of 1.45×10^4 revolutions per minute using an Eppendorf MiniSpin Plus (Eppendorf AG, Germany) to produce a relative centrifugal force of 1.4×10^3 N at room

temperature. The rate of rotation produced approximately 1.76 x 10^3 kPa pressure on the gels, leading to the separation of the gel into pellet and free fluid fractions. The fluid fraction was decanted and weighed before being diluted with 100 mL of pre-weighed Milli-Q water at room temperature. The diluted fluid fraction underwent another 100-fold dilution in Milli-Q water before being filtered with a 40-micron syringe filter in final sample preparation for ion exchange chromatography. The pellet fraction was removed from the centrifuge tube, weighed, and blended in a Multipro Excel Food Processor FPM910 (Kenwood Limited, United Kingdom) with 100 mL of pre-weighed Milli-Q water at the maximum blending speed (speed 8) for a minute at room temperature. The slurry produced was gravimetrically filtered through a 40-micron filter for ten minutes to remove any particulates and before undergoing an additional two serial dilutions. The final diluted sample was then filtered with a 40-micron syringe filter as final sample preparation for analysis with ion chromatography, under the assumption that all free chloride derived from the presence of salt in the pellet fraction had been desorbed into the water.

5.2.3 ^{13}C NMR Gel Preparation

Investigation of changing nature of the protein structure of the gel matrices was done using Carbon-13 Nuclear Magnetic Resonance (NMR). Gels undergoing brining in 20% NaCl-whey solution were selected for sampling in duplicate at 15, 30, 45, 60, 90, 120, and 1440 minutes of total brining at 40 °C. Gels were gently removed from the NaCl-whey solutions via a combination of pouring and use of tweezers to remove the gel from the dialysis tube while minimizing gel structure damage. Freed gels were immediately frozen via immersion in approximately 50 mL of liquid nitrogen (-196 °C) until completely frozen and approximately 90% of the liquid nitrogen had evaporated. Frozen gels were stored in -40 °C freezers until undergoing freeze drying. Samples were freeze dried and stored at room temperature before ^{13}C NMR analysis of the naturally occurring ^{13}C in the gels.

5.3 Analysis Techniques

5.3.1 MATLAB® Image Analysis Methods

The dimensions of the starting gels, after two hours of regular bulk syneresis, and at the sampling time were determined using the image analysis techniques described in section 3.3.1. The average D_{Disk} values were reported for each image and used to assess the average governing diameter for each gel at the time of sampling. The average governing gel diameters were used to evaluate major changes in gel diameter with respect to brining time.

5.3.2 Salt Content Evaluation

Samples were evaluated for total salt uptake and distribution using ion exchange chromatography. Prepared fluid fraction and pellet samples were assessed using a Thermofisher Dionex ICS-2000 with electrical conductivity detector (Thermo Fisher Scientific, USA), with a Dionex IonPac AS11-HC column with Dionex IonPac AG11-HC guard column. The chloride content for both the fluid and pellet fractions in unsalted gels were evaluated to determine the background chloride content innate to the renneted milk gel fluid and pellet fractions. Chloride content for each phase were adjusted to account for the background chloride in the gels before converting the chloride content to sodium chloride content by multiplying the chloride mass calculated in each phase by the ratio of sodium chloride molar mass to chloride molar mass. The mass fraction of salt was then calculated for the gel fluid fraction and the pellet fraction, as well as the salt mass dissolved in each fraction.

A mass balance of the gel was used to estimate the total salted whey mass in the pellet fraction, given that a significant fraction of salted whey was likely to be trapped in the pellet fraction. The non-salted whey mass was determined from the equation below.

$$M_{non-NaCl\ whey,PF} = M_{Gel} - M_{FF} - M_{non-wheyDS} - M_{NaCl,P}$$

Equation 5-13: Mass balance to determine mass of unsalted whey in pellet fraction.

In Equation 5-13, *M* [kg] represents the mass, with the subscripts *Gel*, *FF*, *non-wheyDS*, *NaCl,P*, and *non-NaCl whey,PF* representing the whole gel, the free fluid fraction, the non-whey dairy solids making up the matrix of the gel, the salt present in the pellet fraction, and the unsalted whey mass in the pellet fluid, respectively. The mass of the non-whey dairy solids was known from the starting gel composition. The mass fraction of salt in the pellet fluid was assumed to be equivalent to the mass fraction assessed in the free fluid fraction. Excess salt assessed in the pellet that exceeded the amount allowed for the given whey mass in the pellet was assumed to be adsorbed to the pellet phase, and therefore unavailable for diffusion or to affect the concentration gradient driving the diffusion of salt. The mass of salt adsorbed to the solids was determined using a mass balance using Equation 5-14.

$$M_{NaCl,S} = M_{NaCl,P} - \left(\frac{M_{non-NaCl\ whey,PF} MF_{NaCl,PF}}{1 - MF_{NaCl,PF}}\right)$$

Equation 5-14: Mass balance calculation of salt adsorbed to the pellet solids.

In Equation 5-14, $M_{NaCl,S}$ [kg] is the mass of salt adsorbed to the gel solids and $MF_{NaCl,PF}$ [dimensionless] is the mass fraction of salt in the pellet fluid fraction. Following the determination of all the free fluid, pellet fluid, and pellet solids masses and their respective salt mass fractions, modelling of the salt uptake behaviour using Fickian diffusion or adsorption models was possible.

5.3.3 Statistical Analysis of Salt Uptake and Phase Mass Fraction

The gel fluid, pellet fluid, and pellet solids mass fractions of the whole gels were assessed using one-way ANOVA to determine if there were any statistically significant differences between the pH treatments for each of the two brining conditions tested, within 95% confidence. One-way ANOVA was also conducted on each treatment to determine if there were any statistically significant differences between the salt mass fractions in the free gel fluid, pellet fluid, and pellet solid phase of all three gel pH conditions tested for each brining case.

5.3.4 Modelling Salt Uptake and Moisture Mass Fractions

Previous analysis of gels undergoing salt uptake and osmotic pressure induced whey expulsion demonstrated that the gels undergoing contraction maintained a roughly cylindrical shape, with the length of the cylinder ranging between seven and twenty times the average diameter of the gel, depending of the time of assessment. Given the length of the cylindrical gel dominated the surface through which salt transport would occur, the salt uptake into the fluid phase of the gel was modelled as unsteady-state Fickian diffusion in an infinite cylinder. The gel samples proved to be too small to assess uptake at different locations within the radius of the gel, so Fickian modelling had to be done using the average salt mass fraction in the gel fluid phase, shown in Equation 5-4. The best-fit effective diffusion coefficient and equilibrium mass fraction of salt in the surrounding brine were determined from salt mass fraction data in the gel fluid phase collected throughout the experiment using a MATLAB® script detailed in Appendix D to minimize the least squares error. The adsorbed salt uptake was modelled using a biexponential model to provide an initial evaluation of the uptake behaviour, before being modelled with a fractal IKL model using a least squares error approach shown in Appendix E.

Determining the changing moisture mass fraction of the gel required assessment of the fluid expelled from the gel during the osmotic pressure differential induced syneresis. An assumption was made that once the salt entered the gel fluid, it was immediately evenly

distributed within all the gel fluid. This meant that the fluid expelled had the same salt mass fraction as the fluid remaining within the gel. Although this assumption is unlikely to represent the system, it provides a first estimate to account for possible salt expulsion via osmotic pressure differential induced syneresis without knowledge of the exact salt concentration-distance curve. The density of the expelled gel fluid was assumed to have a linear relationship with the salt mass fraction, as shown in Equation 5-15.

$$\rho_{NaCl-whey} = \rho_{whey} + 764(MF_{NaCl-whey})$$

Equation 5-15: Density of NaCl-whey solution as a function of the salt mass fraction.

In Equation 5-15, $\rho_{NaCl\text{-}whey}$ [kg m^{-3}] is the density of the NaCl-whey solution, ρ_{whey} [kg m^{-3}] is the density of whey, $MF_{NaCl\text{-}whey}$ [dimensionless] is the mass fraction of salt in the NaCl-whey solution, and the 764 [kg m^{-3}] is the constant describing the linear increase in the density of salt water brines as a function of the mass fraction of salt (*CRC Handbook of Chemistry and Physics* 2005). The density function shown in Equation 5-15 and the volume expulsion models developed in section 4.4.2.2 and 4.4.3.2 were combined with the modelled changing mass fraction of salt in the gel fluid (described by Equation 5-4) to determine the whey mass and salt mass expelled, as a function of brining time. The mass of moisture lost in the expelled pellet fluid was assumed to be 94% of the non-salt whey mass lost.

A complete mass balance of the whole gel and a salt mass balance was achieved once the expulsion losses were determined and the salt adsorption behaviour was established, allowing for the calculation of the total salt mass entering the gel to compensate for the accumulated salt in both the gel fluid fraction and solids fraction, in addition to expelled losses. Determining the influx of salt into the gel allowed for a complete knowledge of the changing moisture mass and gel mass, allowing for the successful calculation of the moisture mass fraction from the fitted models. Figure 5-1 provided an appropriate visual reference to describe the changing flows of salt and whey into and out of the gel fluid fraction.

5.3.5 Assessment of ^{13}C NMR Spectrographs

Carbon-13 NMR spectra were acquired on a Bruker BioSpec spectrometer (Elektronik GmbH, Rheinstetten, Germany) operating at a ^{1}H frequency of 200.32 MHz. Approximately, 150 – 200 milligrams of freeze-dried brined gel sample were packed into a sealed 4-millimetre rotor. Samples were measured in a Bruker 4-mm double resonance H/X SB-MAS (small bore-magic angle spinning) probe with temperature control. The 90° pulse of ^{1}H was 3.4 μs and the rotor spinning speed was maintained at 5000 Hz ± 10 Hz.

All chemical shifts were referenced externally to glycine and the spectra processing and relaxation constant curve fitting were undertaken with MNova version 9.02 (Mestrelabs, Spain). The carbon spectra were acquired with 894 data points, spectral width of 18 kHz, 4096 data points, 2048 scans, a ^{1}H-^{13}C CP contact pulse of 1000 ms and a recycle time of one second. A 55 kHz dipolar proton decoupling with decoupling sequence "spinal64" was used during all acquisitions. The carbon longitudinal relaxation constants ($T_1(^{13}C)$) were measured with the standard Bruker pulse sequence "cpxt1" which uses the CP inversion recovery (Torchia) method. The inversion time was varied from 50 ms to 15 s with 8 steps. Carbon spectra were zero filled to 2048 data points, baselined corrected and windowed with an exponential factor of 30 Hz. The relaxation curves were fitted with a single exponential decay to derive the T_1 longitudinal relaxation constants. The T_1 longitudinal relaxation constants were assessed with respect to brining time and salt mass fraction in the different fractions of the gel.

5.4 Experimental Results and Discussion

5.4.1 Low Salt Brining Conditions

5.4.1.1 Gel Radius and General Observations

Gels of all three pH values tested showed similar contraction behaviour to what was observed in the previous chapter, as was expected. The average gel radius reported for the whole experiment was 3.06, 3.05, and 2.63 mm, for the pH 6.25, 5.75, and 5.25 gels, respectively. No statistically significant differences or trends were observed in the gel radius values with respect to brining time, and the standard error for each average radius did not exceed 9.10 x 10^{-3} mm for the experiment, therefore the average gel radius for each gel was considered constant for modelling purposes.

Gels undergoing brining under low (2.5% NaCl-whey) brining conditions showed both gel contraction and uptake of salt at every evaluation time for the pH 6.25 and 5.75 gels. These gels gradually contracted while salt was taken into the gel, making the gels slightly firmer to handle. The combination of an increase in gel firmness providing resistance to centrifugation force and syneresis induced by the osmotic pressure gradient continued, decreased amounts of free whey were expressed from centrifugation with respect to brining time. However, the pH 5.25 gels showed a marked decrease in gel firmness as the brining progressed after the first hour.

The pH 5.25 gels became extremely soft and impossible to handle after two hours of brining in 2.5% NaCl-whey at 40 °C, preventing analysis of salt uptake or the distribution of each phase after two hours of brining. The pH 5.25 gels continued to undergo contraction and presumably the uptake of salt with respect to brining time, but the gels became extremely soft, gelatinous, and no longer maintained a contiguous gel structure required for processing. Centrifugation of gels produced limited free whey as brining time progressed. This behaviour was not necessarily due to an increase in the stiffness of the gel and resistance to compression, such as with the other gels. It is speculated that the gel matrix had changed sufficiently to stabilize the water-protein emulsion much like a sodium caseinate, thereby producing limited free serum for expression. The mechanisms governing this change likely relate to the lack of free calcium to stabilize the cleaved κ-casein polar domain (due to whey losses of free calcium in the expelled whey during bulk syneresis). The lack of stabilizing free calcium, as would be in the case of a regular renneted gel, creates a more acid-like gel susceptible to interactions with salts. The addition of sodium chloride to the system produces free sodium ions that can (1) interact with the casein matrix through ion exchange with calcium ions, or (2) salt-in the protein, thereby making the matrix more soluble and difficult to process for this experiment. The same phenomena with renneted milk gels of differing pH values was observed by Guinee, O'Kennedy, and Mullins in unpublished results (T. Guinee & Fox, 2017). Although salt uptake and phase distribution were modelled for the pH 5.25 gels, the results provided in this section are limited given the lack of a complete data set.

5.4.1.2 Statistical Analysis of Gel Phase Distribution and Salt Uptake

One-way ANOVA was conducted on the phase distribution and salt uptake in each phase to determine if there were any significant differences between gel pH treatments brined in 2.5% NaCl-whey at 40 °C. ANOVA results showed that only the pH 5.25 treatment was significantly different from the other two gel pH values for the gel fluid and pellet fluid mass fractions. There were no statistically significant differences between the pH treatments regarding the pellet solids mass fraction in the final gel mass.

One-way ANOVA of the salt mass fraction in each phase of the gel showed that there was no statistically significant difference between the pH treatments on the salt mass fraction in the free gel fluid (or pellet fluid), when analysed over the entire experimental time of twenty-four hours of brining. Upon analysis of only the first two hours of data (the total data collected for the pH 5.25 treatment), there were statistically significant differences between the pH 5.25 and pH 5.75 salt mass fractions in the gel fluid. One-way ANOVA also showed there was a

statistically significant difference between the salt mass fraction in the pellet solids of the pH 5.25 and pH 5.75 gel treatments. These findings indicate that the gels treated with 2.5% NaCl-whey undergo relatively consistent changes in the mass fractions of each phase in the whole gel, except for pH 5.25 gels which may be explained by the structural changes observed. The findings also show that there were differences in the salt uptake into each phase between the pH 5.75 and 5.25 gels, which may also be partially due to the changing state of the low pH gel structure. Tables 5-1 through 5-5 summarize the findings of one-way ANOVA assessments completed.

Table 5-1: One-way ANOVA statistically significant differences in the gel fluid mass fractions from gels undergoing 2.5% NaCl-whey brining conditions after two hours of regular syneresis, within 95% confidence. NS = No statistically significant difference, S = significant difference.

pH Treatment	pH 6.25	pH 5.75	pH 5.25
pH 6.25	-	NS	S
pH 5.75	NS	-	S
pH 5.25	S	S	-

Table 5-2: One-way ANOVA statistically significant differences in the pellet fluid mass fractions from gels undergoing 2.5% NaCl-whey brining conditions after two hours of regular syneresis, within 95% confidence. NS = No statistically significant difference, S = significant difference.

pH Treatment	pH 6.25	pH 5.75	pH 5.25
pH 6.25	-	NS	S
pH 5.75	NS	-	S
pH 5.25	S	S	-

Table 5-3: One-way ANOVA statistically significant differences in the pellet solids mass fractions from gels undergoing 2.5% NaCl-whey brining conditions after two hours of regular syneresis, within 95% confidence. NS = No statistically significant difference, S = significant difference.

pH Treatment	pH 6.25	pH 5.75	pH 5.25
pH 6.25	-	NS	NS
pH 5.75	NS	-	NS
pH 5.25	NS	NS	-

Table 5-4: One-way ANOVA statistically significant differences in the salt mass fractions in the gel fluid gels undergoing 2.5% NaCl-whey brining conditions after two hours of regular syneresis, within 95% confidence. NS = No statistically significant difference, S = significant difference.

pH Treatment	pH 6.25	pH 5.75	pH 5.25
pH 6.25	-	NS	NS
pH 5.75	NS	-	S
pH 5.25	NS	S	-

Table 5-5: One-way ANOVA statistically significant differences in the salt mass fractions in the gel solids undergoing 2.5% NaCl-whey brining conditions after two hours of regular syneresis, within 95% confidence. NS = No statistically significant difference, S = significant difference.

pH Treatment	pH 6.25	pH 5.75	pH 5.25
pH 6.25	-	NS	NS
pH 5.75	NS	-	S
pH 5.25	NS	S	-

5.4.1.3 Salt Mass Fraction in Gels

Figures 5-3, 5-4, and 5-5 show the mass fraction of salt in the whole gel, the pellet, and free fluid expelled via centrifugation with respect to time in 2.5% NaCl-whey at 40 °C, for the pH 6.25, 5.75, and 5.25 gels, respectively.

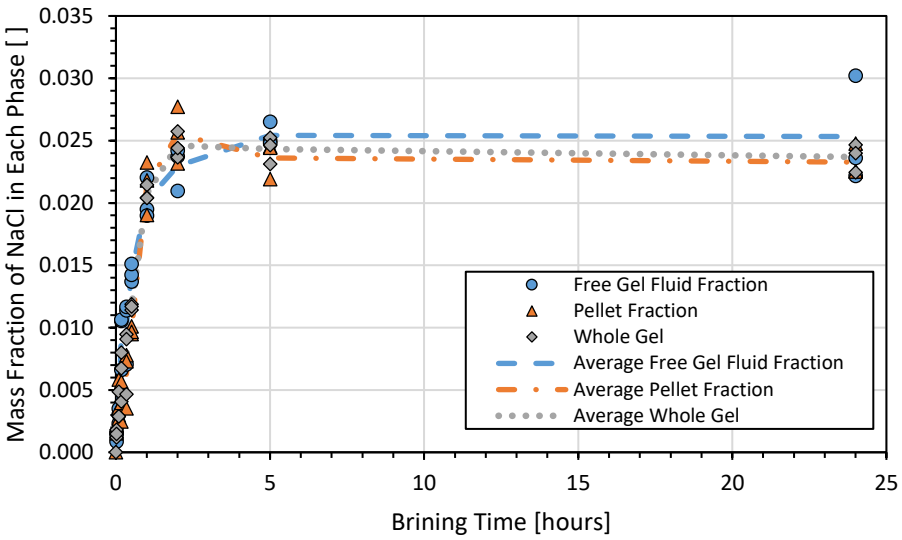

(a)

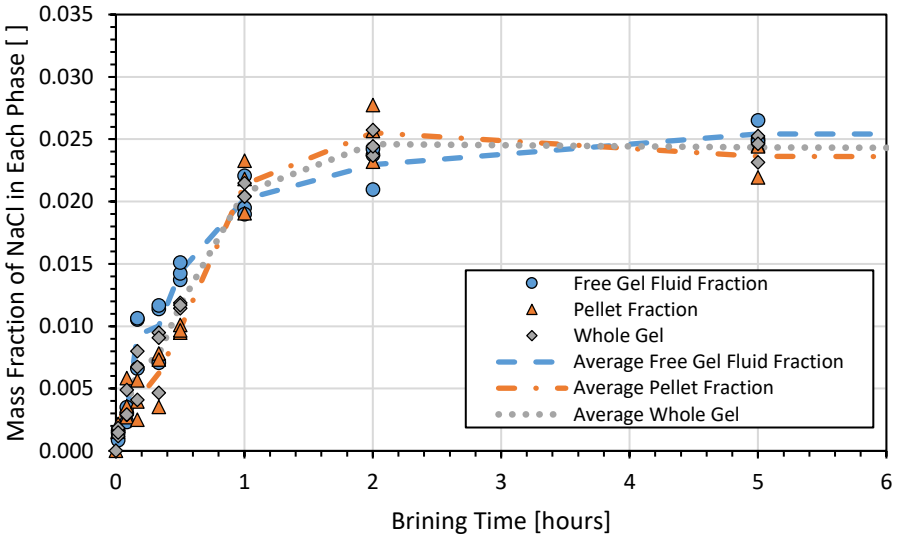

(b)

Figure 5-3: Mass fraction salt in the free gel fluid fraction, pellet fraction, and in the whole gel as a function of brining time for (a) the whole experiment and (b) the first six hours of the experiment after exposure of pH 6.25 gels to 2.5% NaCl-whey brine held at 40 °C assessed in triplicate for each time point. The average values from three replicates are plotted to provide a guiding line for evaluation.

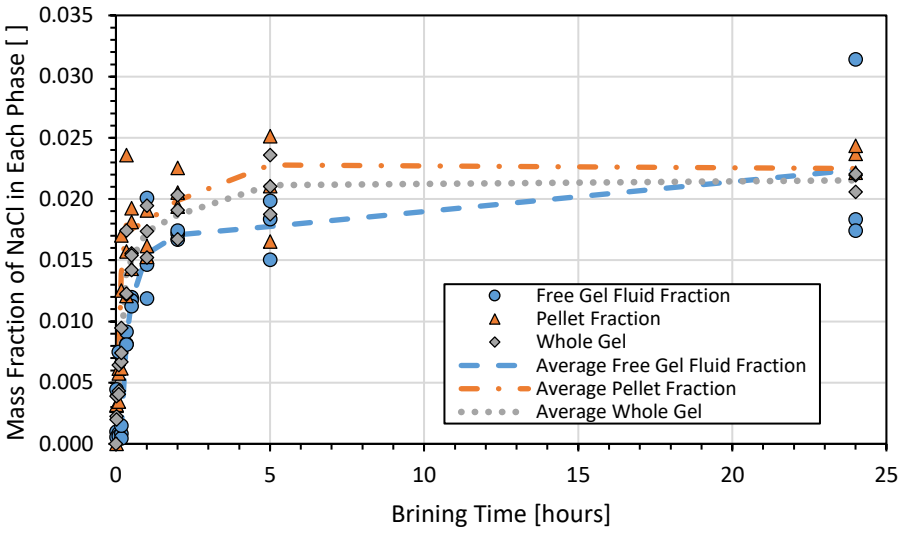

(a)

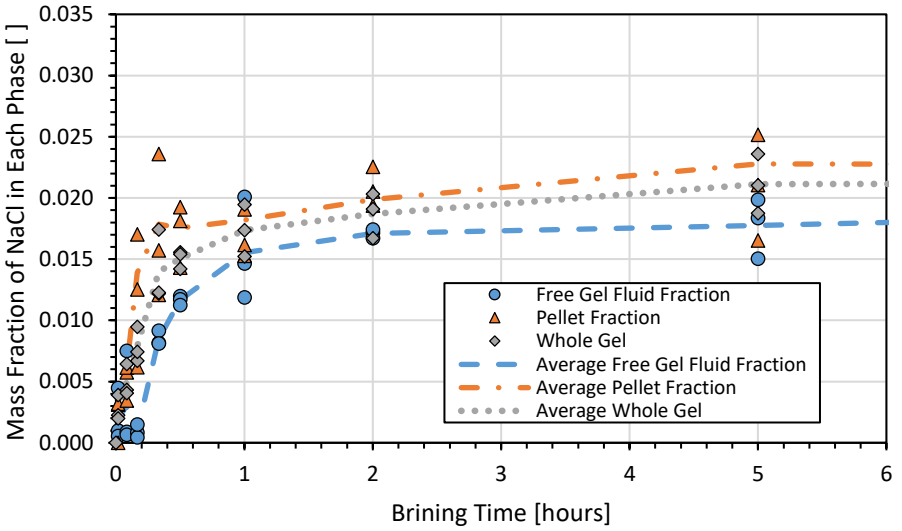

(b)

Figure 5-4: Mass fraction salt in the free gel fluid fraction, pellet fraction, and in the whole gel as a function of brining time for (a) the whole experiment and (b) the first six hours of the experiment after exposure of pH 5.75 gels to 2.5% NaCl-whey brine held at 40 °C assessed in triplicate for each time point. The average values from three replicates are plotted to provide a guiding line for evaluation.

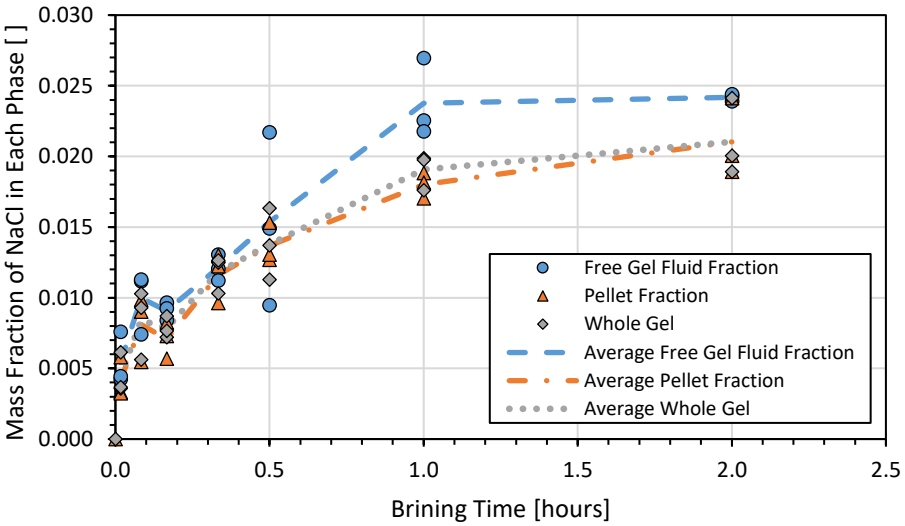

Figure 5-5*:* Mass fraction salt in the free gel fluid fraction, pellet fraction, and in the whole gel as a function of brining time for the first 2.5 hours of the experiment after exposure of pH 5.25 gels to 2.5% NaCl-whey brine held at 40 °C assessed in triplicate for each time point. The average values from three replicates are plotted to provide a guiding line for evaluation.

Figures 5-3 through 5-5 show the rapid uptake of salt into the different fractions of the gel with respect to time, with near equilibrium reached within approximately two hours of brining time for all three pH treatments evaluated. The salt mass fraction in the pellet fraction, free gel fluid fraction, and in the whole gel show similar values at each timepoint during brining. This may be partially explained by the presence of gel fluid within the pellet fractions affecting salt uptake in the pellet fraction, as shown in the following section.

5.4.1.4 Mass Fraction of Free Fluid and Solid Phases in Gels

Figures 5-6, 5-7, and 5-8 show the distribution of the free fluid, pellet fluid, and pellet solids fraction with respect to brining time in 2.5% NaCl-whey at 40 °C, for the pH 6.25, 5.75, and 5.25 gels, respectively.

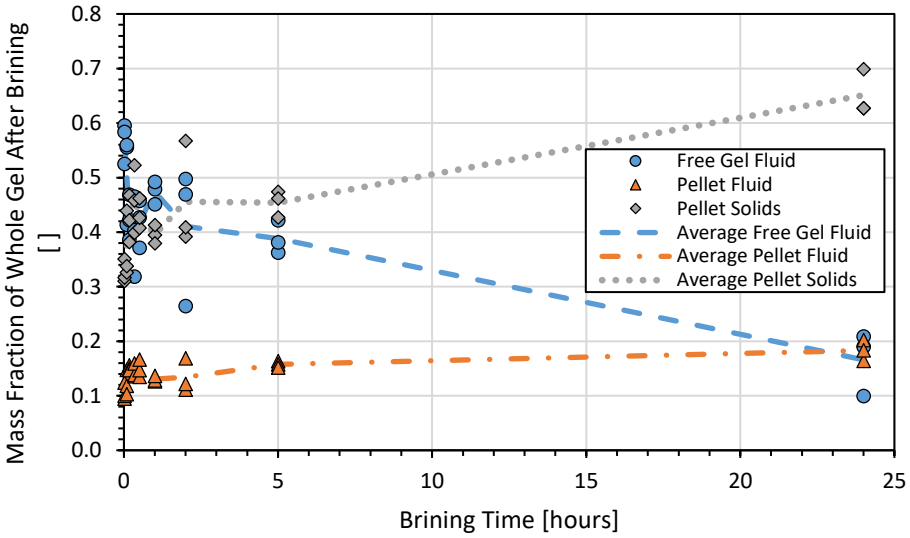

(a)

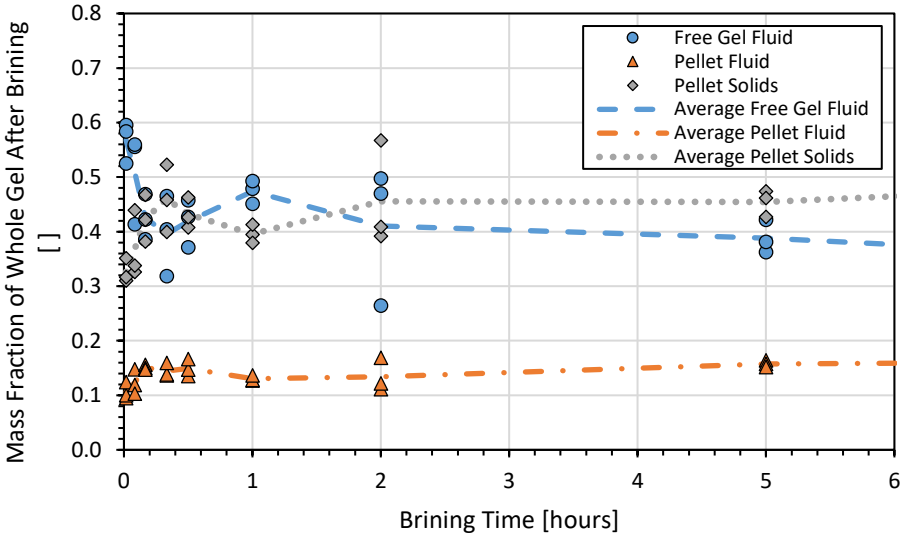

(b)

Figure 5-6: Phase distribution as a function of brining time for (a) the whole experiment and (b) the first six hours of the experiment after exposure of pH 6.25 gels to 2.5% NaCl-whey brine held at 40 °C assessed in triplicate for each time point. The average values from three replicates are plotted to provide a guiding line for evaluation.

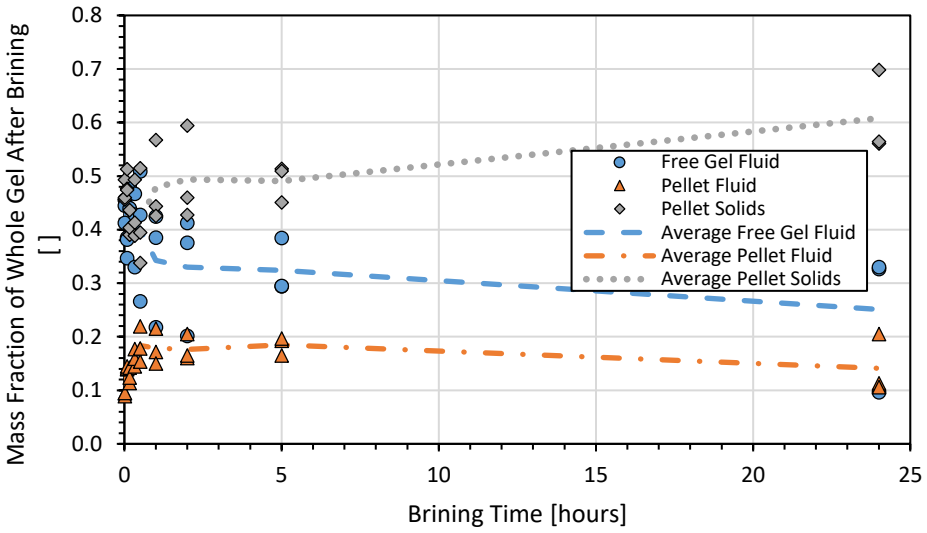

(a)

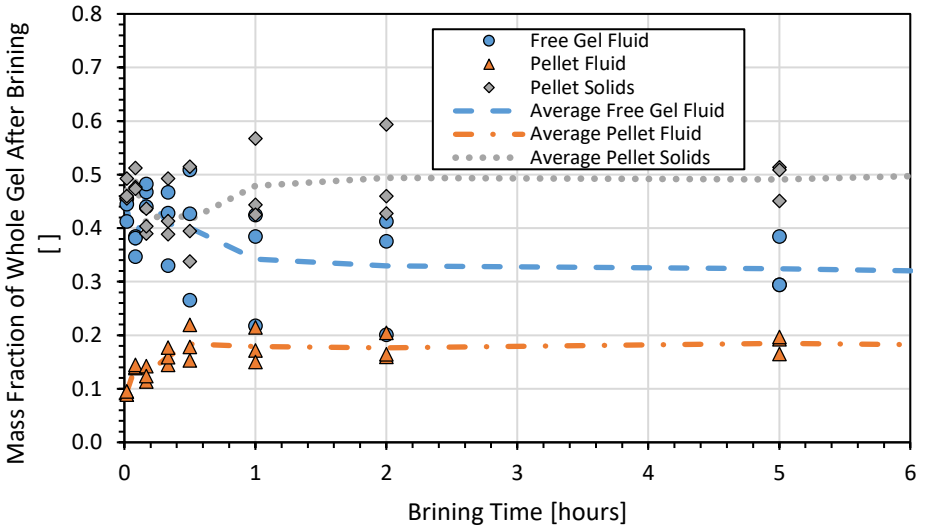

(b)

Figure 5-7: Phase distribution as a function of brining time for (a) the whole experiment and (b) the first six hours of the experiment after exposure of pH 5.75 gels to 2.5% NaCl-whey brine held at 40 °C assessed in triplicate for each time point. The average values from three replicates are plotted to provide a guiding line for evaluation.

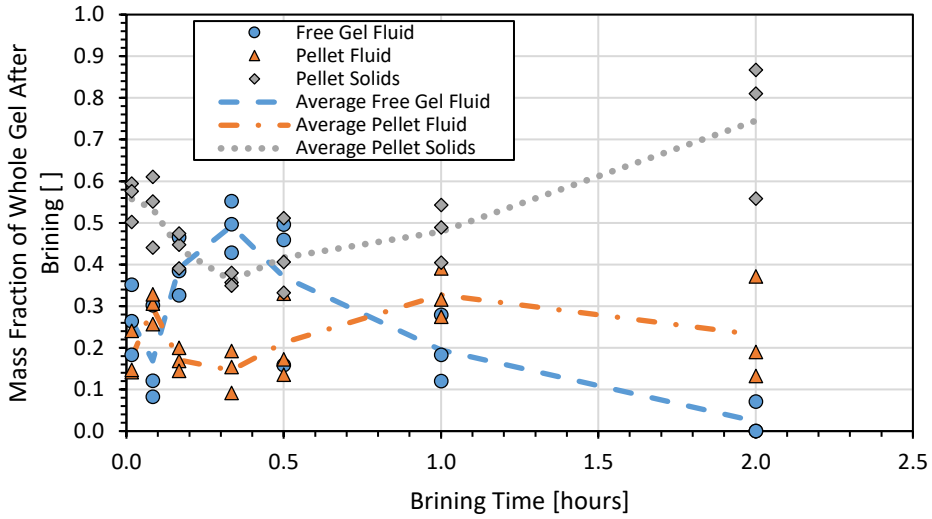

Figure 5-8: Phase distribution as a function of brining time for the first 2.5 hours of the experiment after exposure of pH 5.25 gels to 2.5% NaCl-whey brine held at 40 °C assessed in triplicate for each time point. The average values from three replicates are plotted to provide a guiding line for evaluation.

Figures 5-6 through 5-8 demonstrate a high degree of variability in the composition of the gel, especially within the first thirty minutes of brining. The variability was likely due to the natural variance in the gels evaluated and to the changing state of the gel, whereby whey is being expelled from the gel at the fastest rate in the earliest brining times simultaneously with the protein matrix undergoing changes due to the presence of salt diffusing into the gel. Eventually there was enough whey lost to reduce the free whey fraction contribution in the whole gel and thereby increase the contribution of the pellet fluid and pellet solids fraction with respect to brining time.

5.4.1.5 Salt Uptake in Fluid and Solids Fraction

Figures 5-9, 5-10, and 5-11 show the salt mass fraction in the fluid fraction and pellet solids fraction with respect to brining time in 2.5% NaCl-whey at 40 °C, for the pH 6.25, 5.75, and 5.25, respectively.

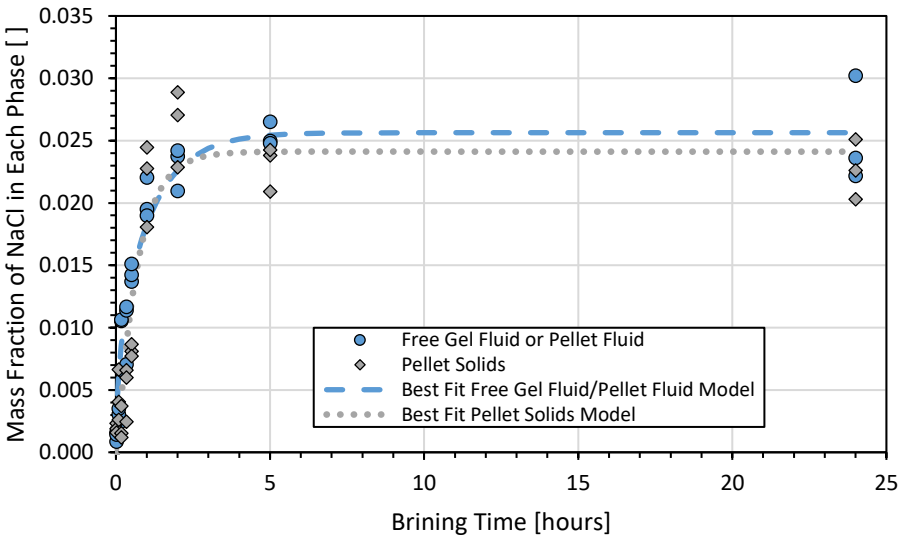

(a)

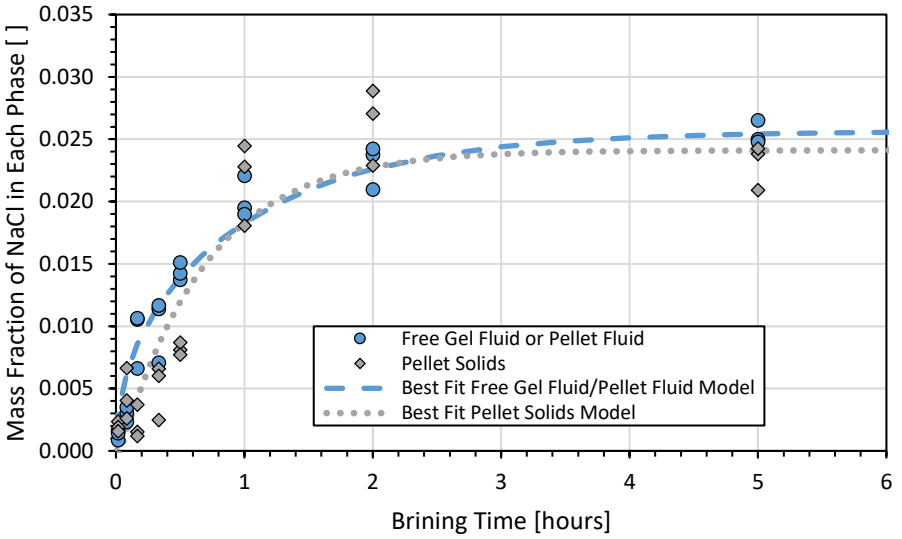

(b)

Figure 5-9: Mass fraction of NaCl in fluid and dairy solid phases and fitted models as a function of brining time for (a) the whole experiment and (b) the first six hours of the experiment after exposure of pH 6.25 gels to 2.5% NaCl-whey brine held at 40 °C assessed in triplicate for each time point. The blue dashed line represents the Fickian fitting while the grey dotted line represents the biexponential fitting for the pellet solids case. The free fluid and pellet fluid were assumed to have the same salt mass fraction.

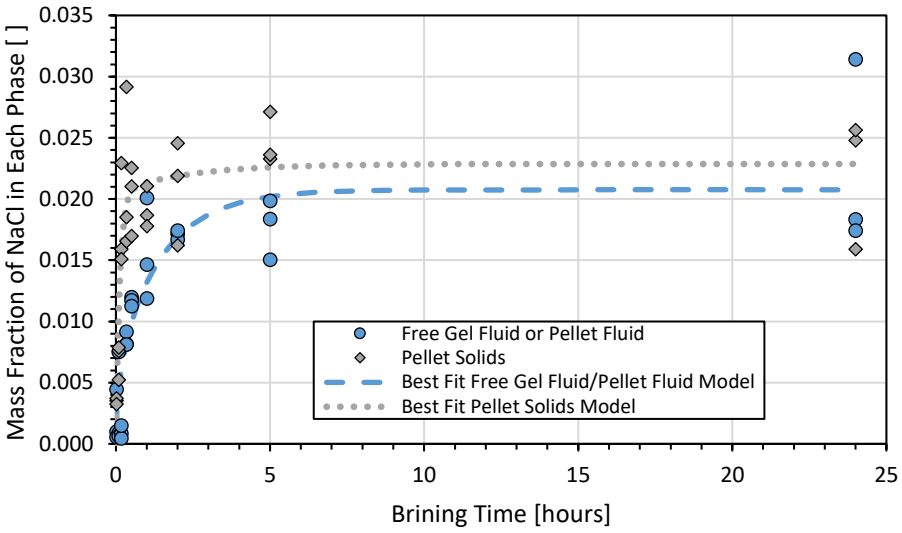

(a)

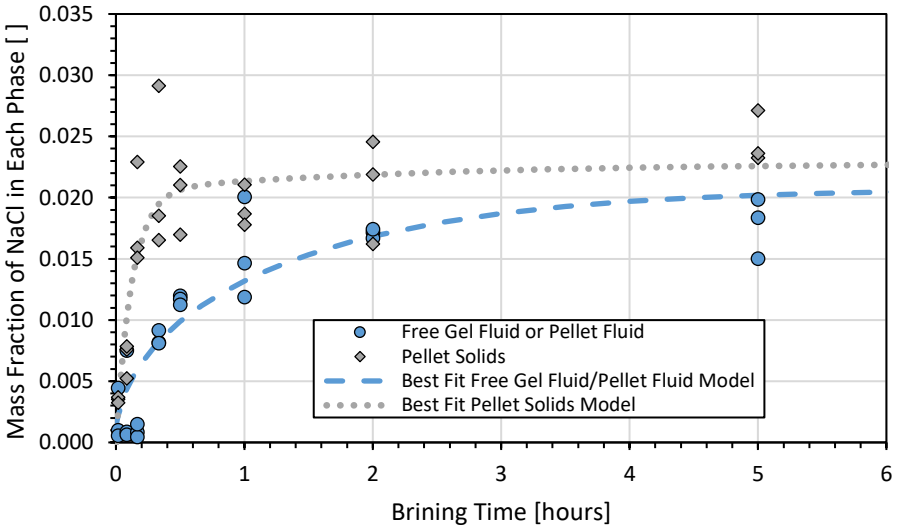

Figure 5-10: Mass fraction of NaCl in fluid and dairy solid phases and fitted models as a function of brining time for (a) the whole experiment and (b) the first six hours of the experiment after exposure of pH 5.75 gels to 2.5% NaCl-whey brine held at 40 °C assessed in triplicate for each time point. The blue dashed line represents the Fickian fitting while the grey dotted line represents the biexponential fitting for the pellet solids case. The free fluid and pellet fluid were assumed to have the same salt mass fraction.

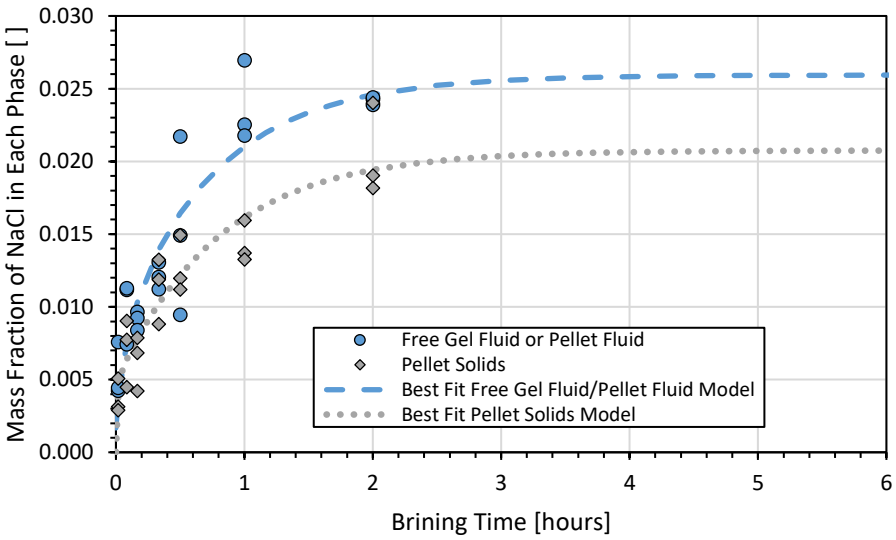

Figure 5-11: Mass fraction of NaCl in fluid and dairy solid phases and fitted models as a function of brining time for the first six hours of the experiment after exposure of pH 5.25 gels to 2.5% NaCl-whey brine held at 40 °C assessed in triplicate for each time point. The blue dashed line represents the Fickian fitting while the grey dotted line represents the biexponential fitting for the pellet solids case. The free fluid and pellet fluid were assumed to have the same salt mass fraction.

Figures 5-9 through 5-11 show relatively consistent salt uptake behaviours in both fluid fractions and estimated salt adsorbed to the solids. The fitted biexponential models for salt uptake in the pellet solids and fitted Fickian models for uptake in the fluid fraction are shown in Tables 5-6 and 5-7, respectively.

Table 5-6: Fitted salt mass fraction in the pellet solids in a biexponential model as a function of brining time in 2.5% NaCl-whey solution.

Treatment	A [ ]	B [ ]	C [ ]	p_1 [s^{-1}]	p_2 [s^{-1}]	RMSE [ ]	r^2 [ ]
pH 6.25	0.0241	1.57E-03	-0.02543	0.0377	4.09E-04	3.46E-03	0.902
pH 5.75	0.0229	-0.0206	-2.31E-03	2.25E-03	1.17E-04	3.78E-03	0.847
pH 5.25	0.0208	-4.82E-03	-0.01592	0.0194	3.44E-04	2.16E-03	0.906

Table 5-7: Fitted average Fickian diffusion coefficient values for salt transport in 2.5% NaCl-whey solution.

Treatment	D_{eff} [$m^2 s^{-1}$]	C_∞ [ ]	RMSE [ ]	r^2 [ ]
pH 6.25	3.98E-10	0.0256	2.33E-03	0.947
pH 5.75	2.90E-10	0.0208	3.61E-03	0.824
pH 5.25	4.30E-10	0.0259	2.82E-03	0.892

The statistics presented in Tables 5-6 and 5-7 show a good degree of fit between the fitted models and the data collected for all three pH treatments, with RMSE values that do not exceed 0.38 % of the total mass fraction at any evaluation time. Salt uptake in each phase occurs at similar rates for the pH 6.25 case, while uptake is slower in the solids of the pH

5.25 gels and faster in the solids of the pH 5.75 gels. The fitted effective diffusion coefficients demonstrate a slightly lower value for the pH 5.75 case, but a faster uptake of salt into the pellet solids fraction than the pH 5.25 and 6.25 cases. The high degree of fit between the biexponential model and estimated adsorbed salt mass fraction in the solids data shows that should a standard adsorption kinetics model not be used to describe the estimated adsorptive behaviour between the salt and gel solids, the biexponential model approach is sufficient to describe the behaviour.

The behaviour shown in Figure 5-9 shows that salt uptake is consistent between the fluid fraction and the solids fraction, indicating that adsorptive behaviours may not contribute as prominently to the total salt uptake performance in pH 6.25 gels under low concentration salting conditions. However, Figure 5-10 shows a marked difference in the salt uptake between the fluid fraction and solids fraction, where the salt mass fraction in the solids exceeds the salt mass fraction in the fluid fraction. This behaviour indicates that adsorptive behaviours may be affecting the overall salt uptake behaviour in the pH 5.75 gels, which could be related to the calcium-sodium ion exchange hypothesis posited by Hardy and Steinberg (1984). Figure 5-11 shows the opposite behaviour to what was observed in Figure 5-10, where the salt mass fraction in the fluid fraction of the gel exceeds the value of the salt mass fraction in the solids fraction of the gel. This indicates that any adsorption behaviour is slowed in the case of pH 5.25 gels, which is likely related to the changing structure of the gel to be more like a calcium caseinate viscoelastic material (Creamer, 1985; Gal & Bankay, 1971).

5.4.1.6 Salt Distribution in Each Phase

Figures 5-12, 5-13, and 5-14 show the mass fraction of all the salt in the system in the free fluid, pellet fluid, and pellet solids fraction with respect to brining time for pH 6.25, 5.75, and 5.25 gels treated with 2.5% NaCl-whey at 40 °C, respectively.

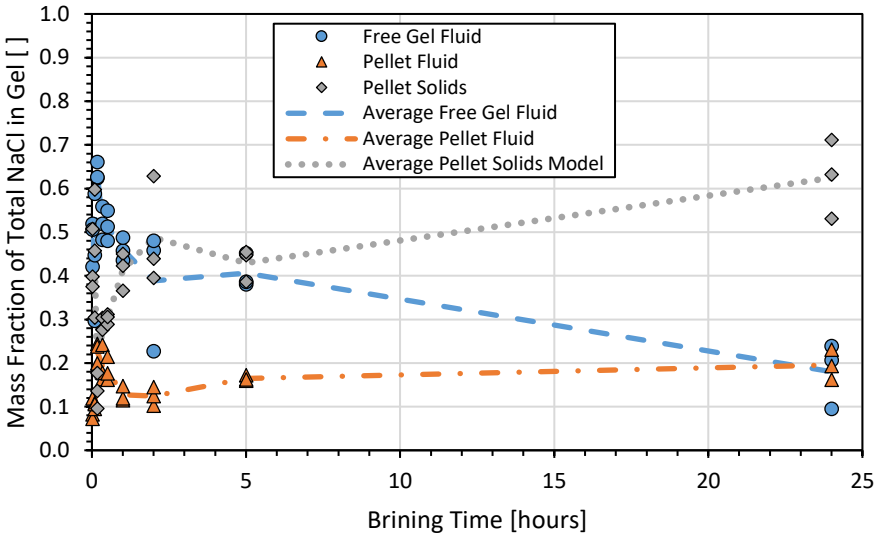

(a)

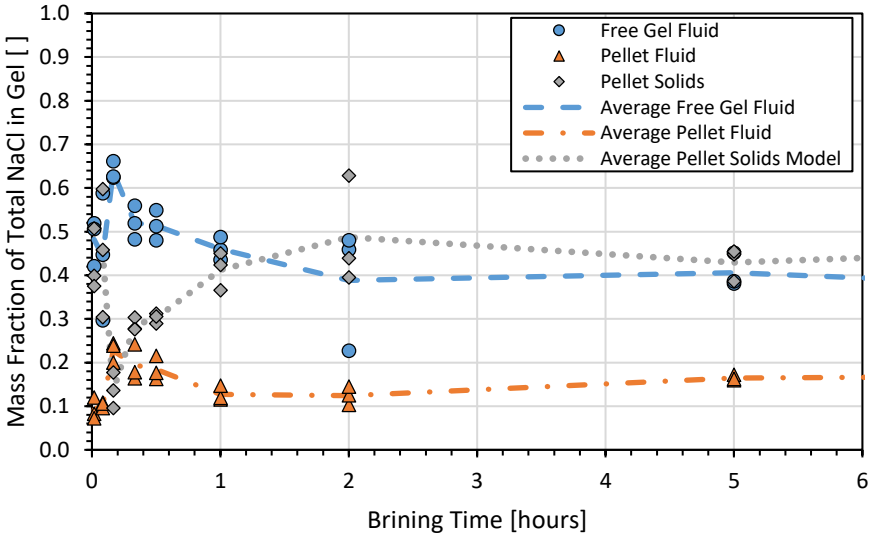

(b)

Figure 5-12: Salt distribution between phases as a function of brining time for (a) the whole experiment and (b) the first six hours of the experiment after exposure of pH 6.25 gels to 2.5% NaCl-whey brine held at 40 °C assessed in triplicate for each time point. The average values from three replicates are plotted to provide a guiding line for evaluation.

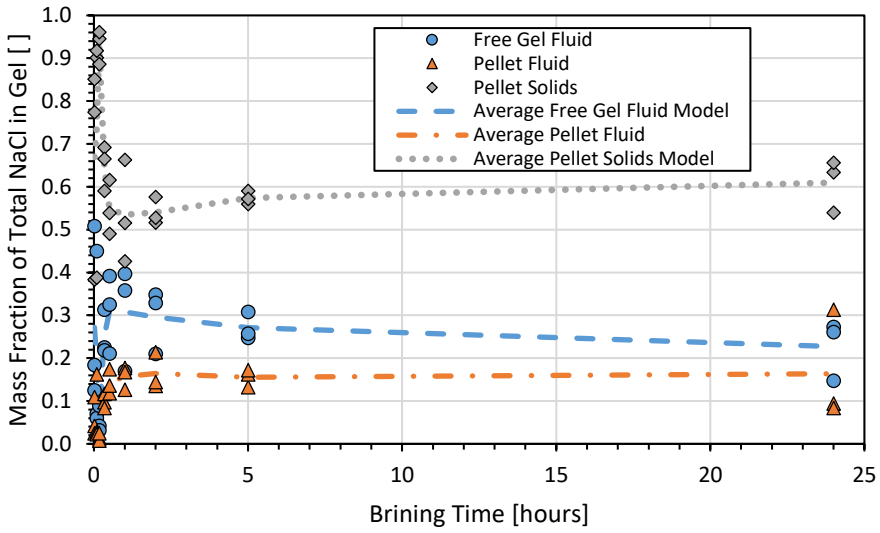

(a)

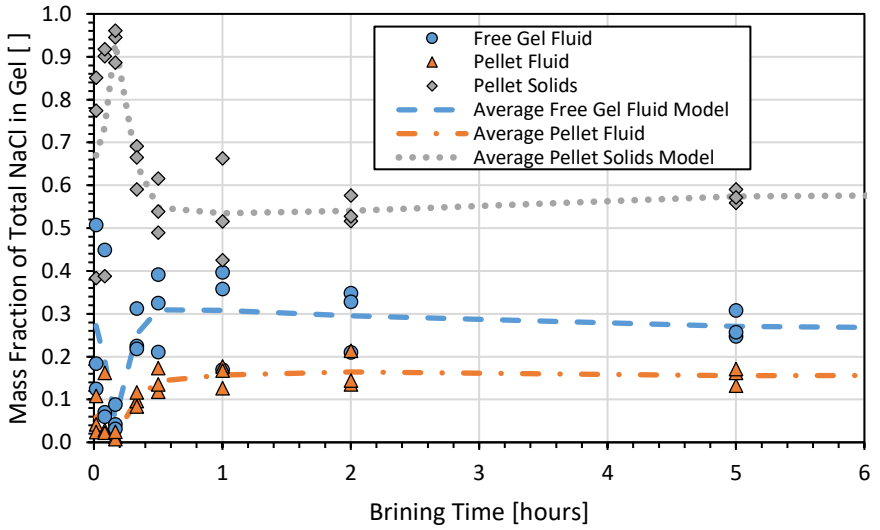

(b)

Figure 5-13: Salt distribution between phases as a function of brining time for (a) the whole experiment and (b) the first six hours of the experiment after exposure of pH 5.75 gels to 2.5% NaCl-whey brine held at 40 °C assessed in triplicate for each time point. The average values from three replicates are plotted to provide a guiding line for evaluation.

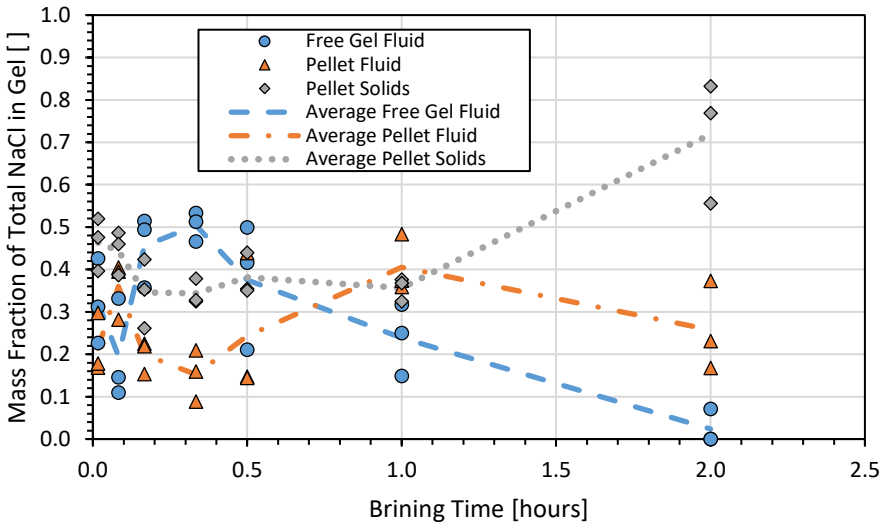

Figure 5-14: Salt distribution between phases as a function of brining time for the first 2.5 hours of the experiment after exposure of pH 5.25 gels to 2.5% NaCl-whey brine held at 40 °C assessed in triplicate for each time point. The average values from three replicates are plotted to provide a guiding line for evaluation.

Figures 5-12 through 5-14 show a significant degree of variability in the location of salt within the gel with respect to brining time. Most salt in the pH 6.25 gels was in the free fluid fraction of the gel during the first two hours of brining. This finding is reasonable, given that higher pH gels are expected to have a higher starting moisture mass fraction than the other pH treatments. That allowed for more of the net salt total in the gel to be in the fluid fraction, although the total mass fraction of the fluid in the gel could be modest. However, as brining time increased, gradually more of the total salt was found in the solids fraction. This was also realistic as the free fluid mass fraction of the gel decreases due to losses during syneresis and possible increase in salt adsorption to the solids.

Most salt in the pH 5.75 gels was positioned in the pellet solids during the early stages of brining, before rapidly decreasing to a constant fraction of the total salt in the gel. This behaviour was nearly the inverse for the salt situated in the fluid fraction of the gel. A rapid whey expulsion experienced early during exposure to the 2.5% NaCl-whey decreased the amount of the total salt mass fraction in the gel fluid, before enough salt diffusion into the gel once more increased the total share of the salt in the fluid fraction. The high concentration of the total salt in the solids fraction indicates that there may have been a high degree of adsorptive behaviour occurring, such as the postulated calcium-sodium ion exchange (Hardy & Steinberg, 1984).

Salt was more evenly distributed between the different phases of the pH 5.25 gels during the early stages of brining. However, this rapidly changed as the gel underwent structural

changes to convert it from a contiguous gel to a soft, gelatinous material. The amount of free whey spun off during centrifuging rapidly decreased and most of the salt in the gel was calculated to be in the solids fraction.

Results from Figures 5-12 through 5-14 show that the fraction of the total salt in the gel at risk of being lost due to external pressing of the gels is in the free fluid fraction, which decrease with respect to brining time. This insight may be useful for limiting salt losses in gels that are expected to undergo pressing, where most of the salt located in the free fluid fraction would be pressed from the gel. The results indicate that after thirty minutes of brining 50, 30, and 40 % of all the salt in the gels would be at risk of being expelled via pressing actions from pH 6.25, 5.75, and 5.25 gels, respectively.

5.4.2 High Salt Brining Conditions

5.4.2.1 Gel Radius and Observations

Gels of all three pH values tested showed similar contraction behaviour to what was observed in the 20% NaCl-whey data of the previous chapter, as was expected. The average gel radius reported for the whole experiment was 3.03, 2.52, and 2.55 mm, for the pH 6.25, 5.75, and 5.25 gels, respectively. No statistically significant differences or trends were observed in the gel radius values with respect to brining time, and the standard error for each average radius did not exceed 7.44×10^{-3} mm for the experiment, hence the average gel radius for each gel was considered constant for modelling purposes.

Gels undergoing brining under high concentration salt brining conditions showed both gel contraction and uptake of salt at every evaluation time for all three gel pH values tested. These gels gradually contracted while salt was taken into the gel, making the gels increase in stiffness and brittleness upon handling with respect to brining time. No softening of the pH 5.25 gels was observed, and all gels maintained structural integrity during processing. All gels treated with 20% NaCl-whey were remarkably stiffer than the gels treated under low brining conditions, which was expected due to the effects of high levels of salt on casein hydration and aggregation (Euston, Piska, Wium, & Qvist, 2002; Floury, Camier, et al., 2009).

5.4.2.2 Statistical Analysis of Gel Phase Distribution and Salt Uptake

One-way ANOVA was conducted on the phase distribution and salt uptake in each phase to determine if there were any significant differences between gel pH treatments brined in 20% NaCl-whey at 40 °C. ANOVA results showed that only the pH 6.25 and pH 5.75 treatments

was significantly different each other for the gel fluid mass fractions, within 95% confidence. There were no statistically significant differences between the pH treatments regarding the pellet fluid mass fractions in the final gel mass for any of the pH treatments. One-way ANOVA results showed a statistically significant differences between the pH 6.25 and the other two pH treatments in the solids mass fraction in the final gel mass.

One-way ANOVA assessment of the salt mass fraction in each phase of the gel showed there were no statistically significant differences between the salt content in the gel fluid fraction or gel solids fraction between the pH treatments, within 95% confidence. These findings indicate that the gels treated with 20% NaCl-whey undergo consistent changes in phase fractions, except for the pH 6.25 gels, and that salt uptake is relatively consistent between the pH treatments regarding salt mass fractions in both solid and fluid phases. Tables 5-8 through 5-12 summarize the findings of one-way ANOVA assessments completed.

Table 5-8: One-way ANOVA statistically significant differences in the gel fluid mass fractions from gels undergoing 20% NaCl-whey brining conditions after two hours of regular syneresis, within 95% confidence. NS = No statistically significant difference, S = significant difference.

pH Treatment	pH 6.25	pH 5.75	pH 5.25
pH 6.25	-	S	NS
pH 5.75	S	-	NS
pH 5.25	NS	NS	-

Table 5-9: One-way ANOVA statistically significant differences in the pellet fluid mass fractions from gels undergoing 20% NaCl-whey brining conditions after two hours of regular syneresis, within 95% confidence. NS = No statistically significant difference, S = significant difference.

pH Treatment	pH 6.25	pH 5.75	pH 5.25
pH 6.25	-	NS	NS
pH 5.75	NS	-	NS
pH 5.25	NS	NS	-

Table 5-10: One-way ANOVA statistically significant differences in the pellet solids mass fractions from gels undergoing 20% NaCl-whey brining conditions after two hours of regular syneresis, within 95% confidence. NS = No statistically significant difference, S = significant difference.

pH Treatment	pH 6.25	pH 5.75	pH 5.25
pH 6.25	-	S	S
pH 5.75	S	-	NS
pH 5.25	S	NS	-

Table 5-11: One-way ANOVA statistically significant differences in the salt mass fractions in the gel fluid in gels undergoing 20% NaCl-whey brining conditions after two hours of regular syneresis, within 95% confidence. NS = No statistically significant difference, S = significant difference.

pH Treatment	pH 6.25	pH 5.75	pH 5.25
pH 6.25	-	NS	NS
pH 5.75	NS	-	NS
pH 5.25	NS	NS	-

Table 5-12: One-way ANOVA statistically significant differences in the salt mass fractions in the gel solids in gels undergoing 20% NaCl-whey brining conditions after two hours of regular syneresis, within 95% confidence. NS = No statistically significant difference, S = significant difference.

pH Treatment	pH 6.25	pH 5.75	pH 5.25
pH 6.25	-	NS	NS
pH 5.75	NS	-	NS
pH 5.25	NS	NS	-

5.4.2.3 Salt Mass Fraction in Gels

Figures 5-15, 5-16, and 5-17 show the mass fraction of salt in the whole gel, the pellet, and free fluid expelled via centrifugation with respect to time in 20% NaCl-whey at 40 °C, for the pH 6.25, 5.75, and 5.25 gels, respectively.

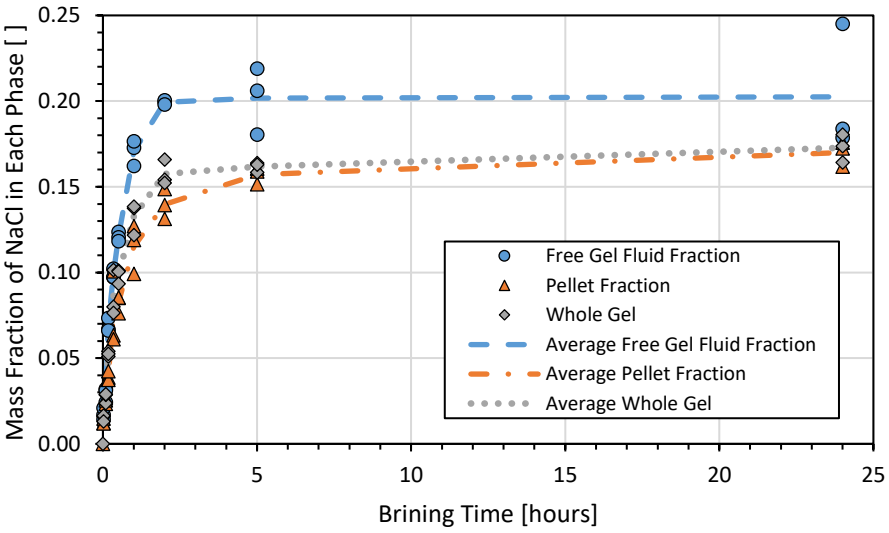

(a)

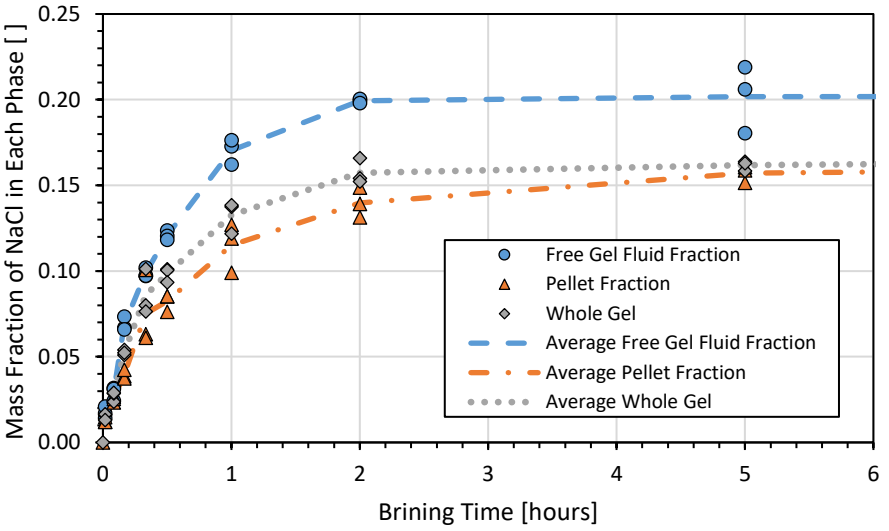

(b)

Figure 5-15: Mass fraction salt in the free gel fluid fraction, pellet fraction, and in the whole gel as a function of brining time for (a) the whole experiment and (b) the first six hours of the experiment after exposure of pH 6.25 gels to 20% NaCl-whey brine held at 40 °C assessed in triplicate for each time point. The average values from three replicates are plotted to provide a guiding line for evaluation.

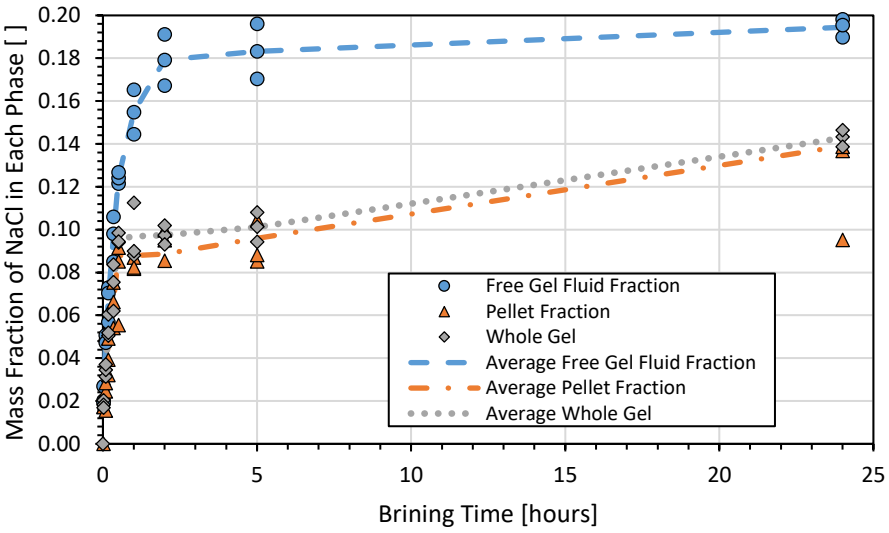

(a)

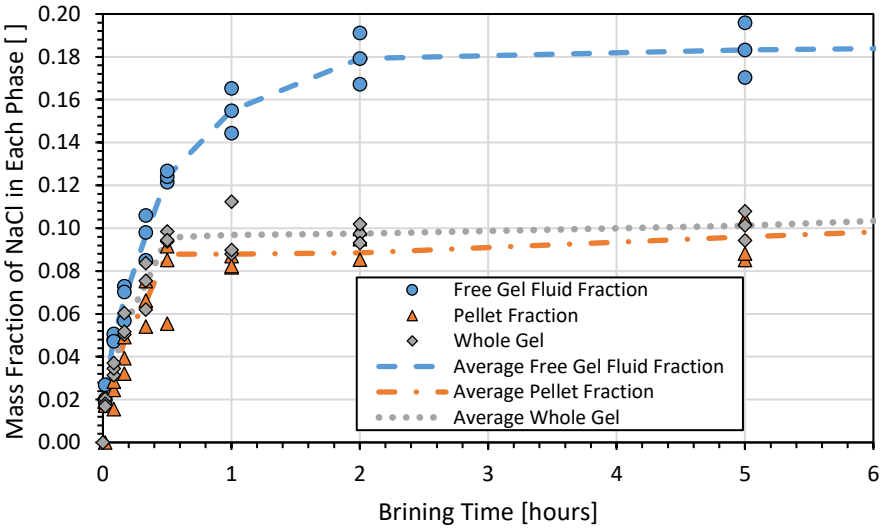

(b)

Figure 5-16: Mass fraction salt in the free gel fluid fraction, pellet fraction, and in the whole gel as a function of brining time for (a) the whole experiment and (b) the first six hours of the experiment after exposure of pH 5.75 gels to 20% NaCl-whey brine held at 40 °C assessed in triplicate for each time point. The average values from three replicates are plotted to provide a guiding line for evaluation.

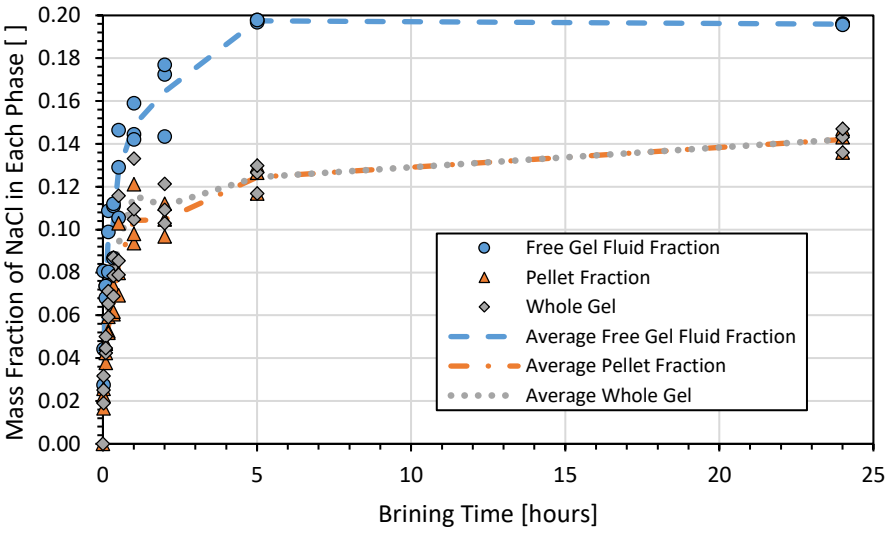

(a)

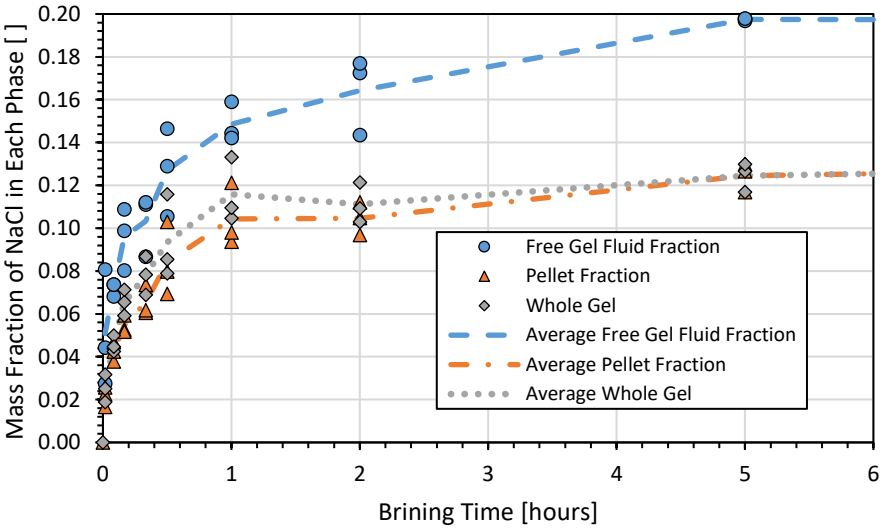

(b)

Figure 5-17: Mass fraction salt in the free gel fluid fraction, pellet fraction, and in the whole gel as a function of brining time for (a) the whole experiment and (b) the first six hours of the experiment after exposure of pH 5.25 gels to 20% NaCl-whey brine held at 40 °C assessed in triplicate for each time point. The average values from three replicates are plotted to provide a guiding line for evaluation.

Figures 5-15 through 5-17 show the rapid uptake of salt into the different fractions of the gel with respect to time for gels treated with 20% NaCl-whey at 40 °C, with near equilibrium values reached within approximately five hours of brining time for all three pH treatments evaluated. The salt mass fraction in the pellet fraction, free gel fluid fraction, and in the whole gel show rapid uptake of salt with respect to brining time, with the salt mass fraction in the free fluid showing the fastest rate of uptake and value with respect to brining time, for all three pH treatments. However, the salt mass fraction in the whole gel closely follows the salt

mass fraction in the pellet fraction, indicating that the total salt uptake is largely affected by the salt uptake behaviour in the pellet fraction. This is a reasonable finding as the amount of free fluid in the gel rapidly decreases with respect to brining time due to the osmotic pressure differential induced syneresis that expels large amounts of whey from the gel, as shown in the following section. Interestingly, the salt uptake in the pellet fraction does not follow the same behaviour observed in the 2.5% NaCl-whey brining case, denoting that there may be limits to the amount of salt that may be taken up in the pellet fraction under high salting conditions.

5.4.2.4 Mass Fraction of Free Fluid and Solids Phases in Gels

Figures 5-18, 5-19, and 5-20 show the distribution of the free fluid, pellet fluid, and pellet solids fraction with respect to brining time in 20% NaCl-whey at 40 °C, for the pH 6.25, 5.75, and 5.25, respectively.

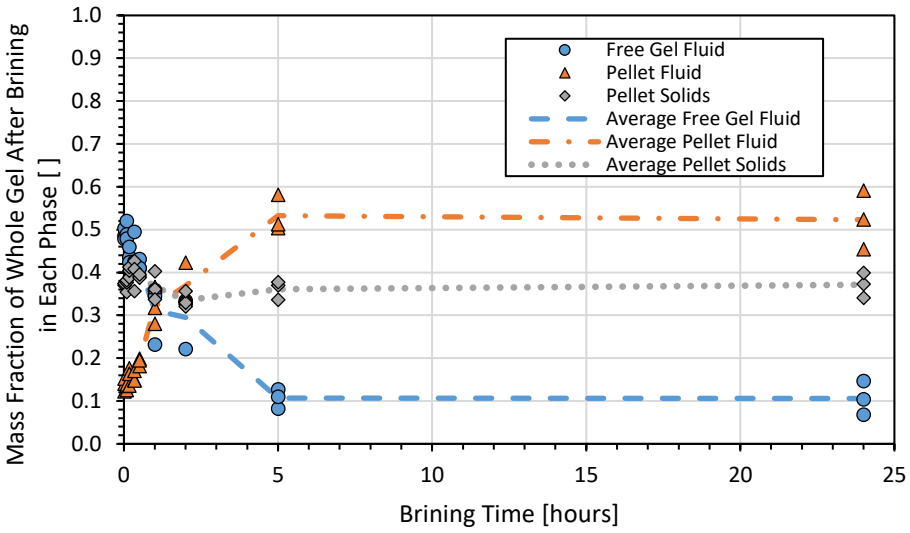

(a)

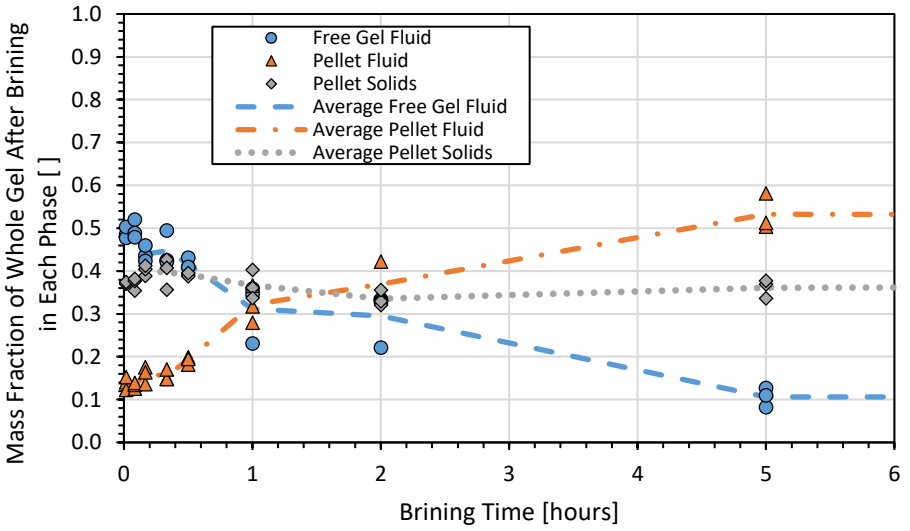

(b)

Figure 5-18: Phase distribution as a function of brining time for (a) the whole experiment and (b) the first six hours of the experiment after exposure of pH 6.25 gels to 20% NaCl-whey brine held at 40 °C assessed in triplicate for each time point. The average values from three replicates are plotted to provide a guiding line for evaluation.

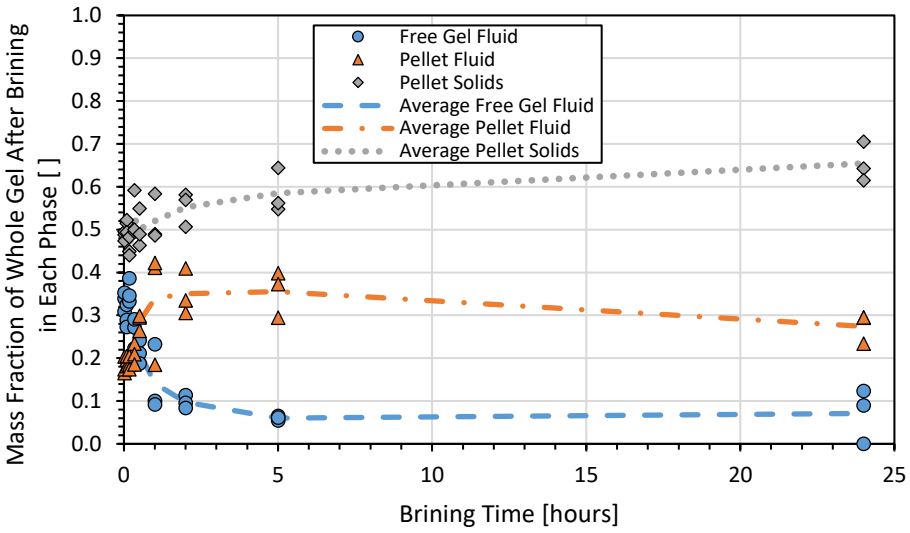

(a)

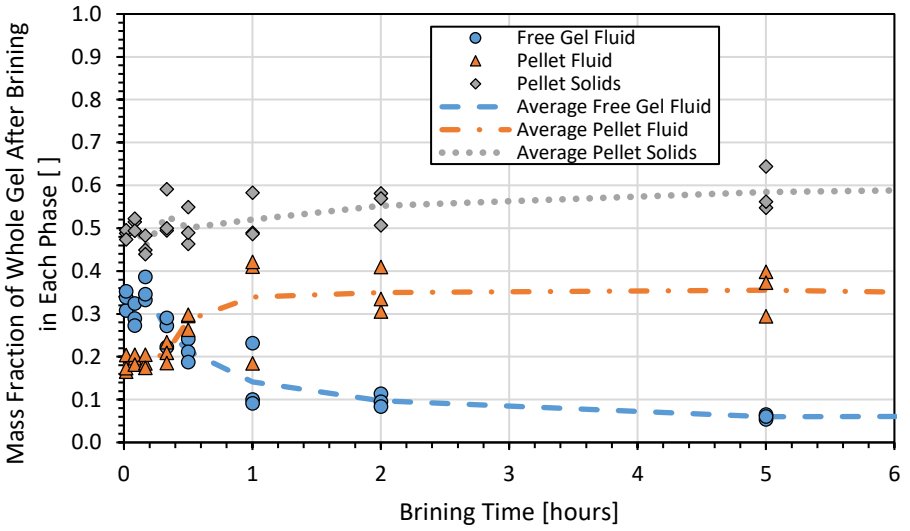

(b)

Figure 5-19: Phase distribution as a function of brining time for (a) the whole experiment and (b) the first six hours of the experiment after exposure of pH 5.75 gels to 20% NaCl-whey brine held at 40 °C assessed in triplicate for each time point. The average values from three replicates are plotted to provide a guiding line for evaluation.

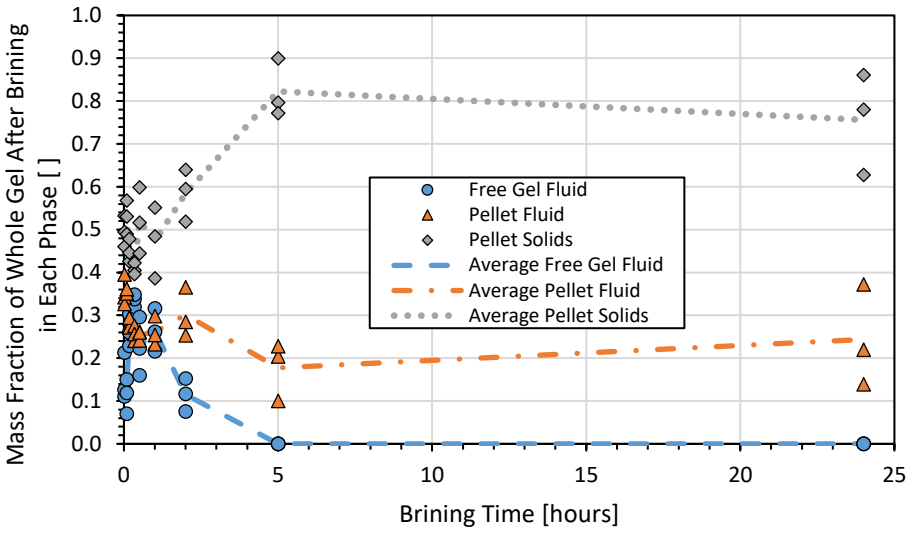

(a)

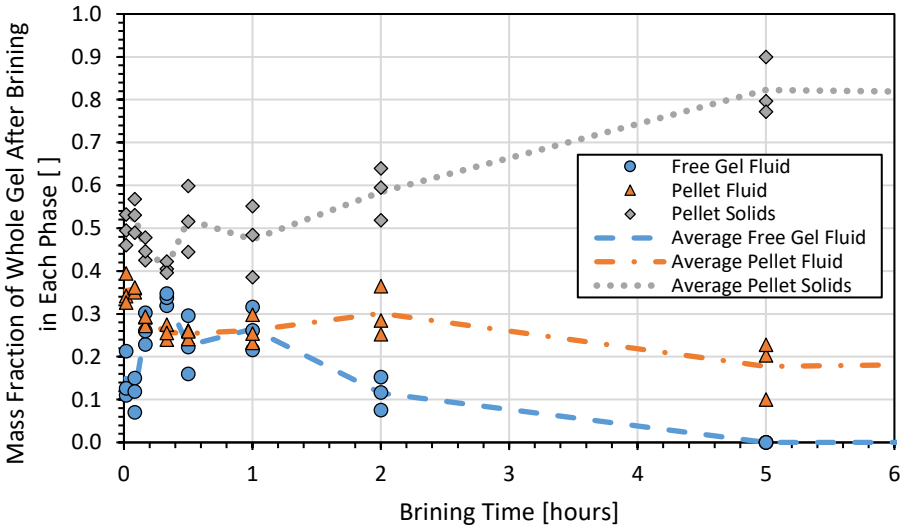

(b)

Figure 5-20: Phase distribution as a function of brining time for (a) the whole experiment and (b) the first six hours of the experiment after exposure of pH 5.25 gels to 20% NaCl-whey brine held at 40 °C assessed in triplicate for each time point. The average values from three replicates are plotted to provide a guiding line for evaluation.

Figures 5-18 through 5-20 demonstrate some degree of variability in the composition of the gel, but less than the results shown in section 5.4.1.3. The free fluid fraction greatly contributes to the starting composition of the gel before gradually decreasing in value to approximately 10% of the gel mass, for the pH 6.25 and 5.75 gels. This behaviour is expected as the syneresis continues through the brining process, thereby decreasing the total amount of fluid in the gel available for separation via centrifugation. However, this behaviour is not matched in the pH 5.25 case, where the free fluid fraction increases slightly

in the first thirty minutes of brining, before decreasing to negligible values at long brining times. This behaviour is likely due to natural variation in the gels evaluated and the extent of change occurring in the gel structure and expelled whey during the early stages of brining.

The pellet fluid fraction also gradually increases in value with respect to time for the pH 6.25 and 5.75 gels, due to continued syneresis behaviour throughout the brining process that decrease the amount of the fluid in the gel that could be separated from the gel solids via centrifugation. Likewise, the solids fraction gradually increased with respect to brining time as the total amount of fluid in the gel decreased due to syneresis. The pellet fluid fraction, however, remained consistent throughout the experiment. This is likely due in part to the limited mobility of moisture located near the protein matrix, participating in hydration of the casein (T. Guinee & Fox, 2017).

5.4.2.5 Salt Uptake in Fluid and Solids Fraction

Figures 5-21, 5-22, and 5-23 show the salt mass fraction in the free fluid and pellet solids fraction with respect to brining time in 20% NaCl-whey at 40 °C, for the pH 6.25, 5.75, and 5.25, respectively.

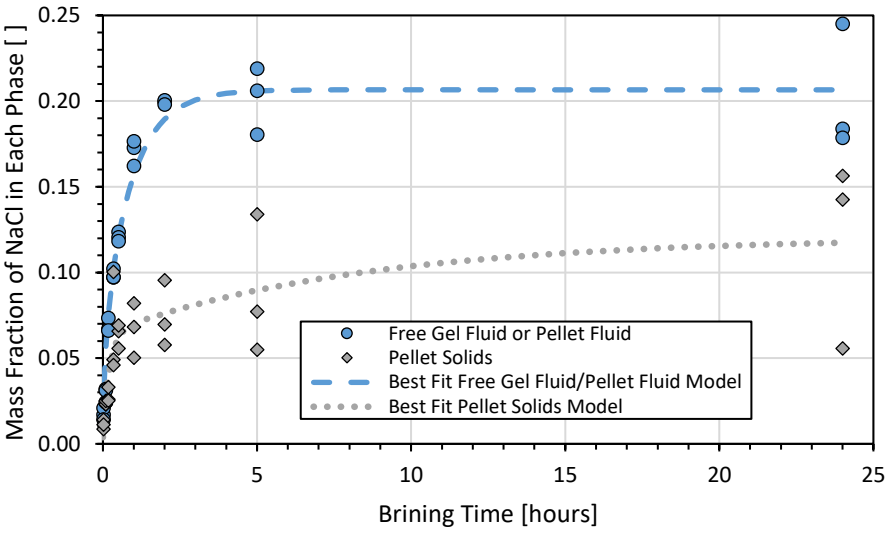

(a)

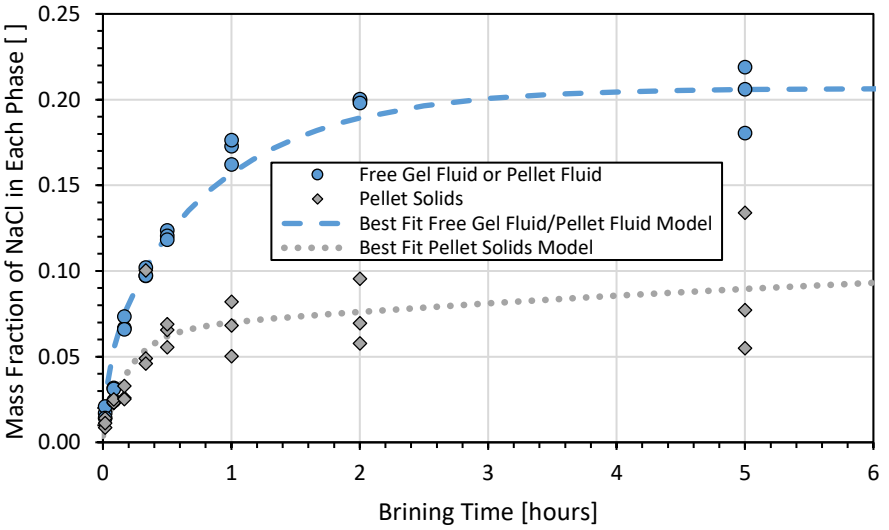

(b)

Figure 5-21: Mass fraction of NaCl in fluid and dairy solid phases and fitted models as a function of brining time for (a) the whole experiment and (b) the first six hours of the experiment after exposure of pH 6.25 gels to 20% NaCl-whey brine held at 40 °C assessed in triplicate for each time point. The blue dashed line represents the Fickian fitting while the grey dotted line represents the biexponential fitting for the pellet solids case. The free fluid and pellet fluid were assumed to have the same salt mass fraction.

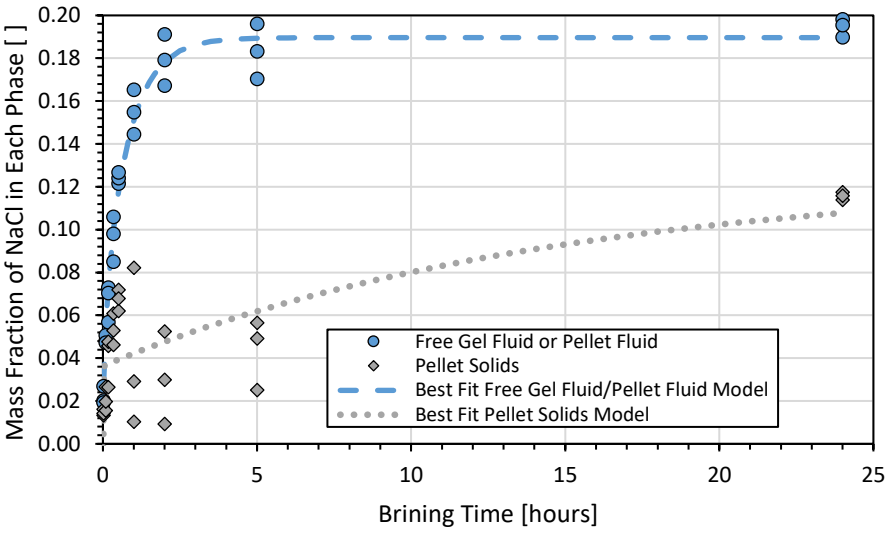

(a)

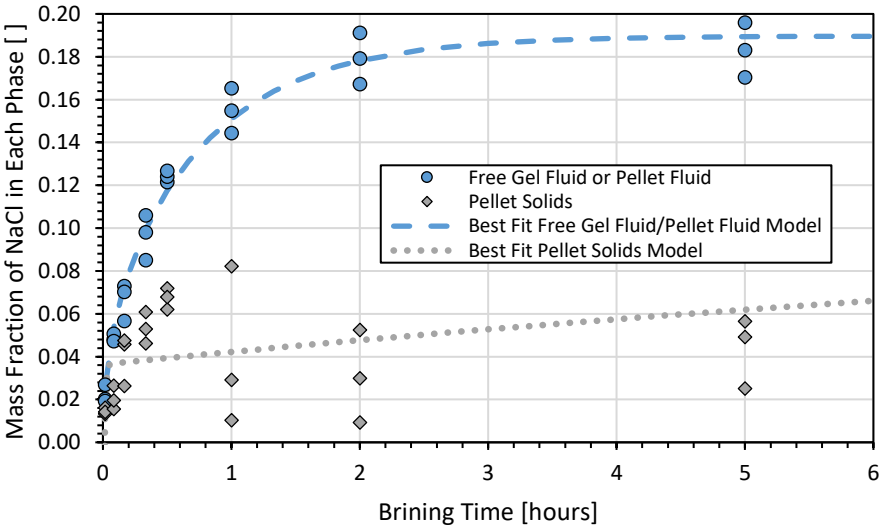

(b)

Figure 5-22: Mass fraction of NaCl in fluid and dairy solid phases and fitted models as a function of brining time for (a) the whole experiment and (b) the first six hours of the experiment after exposure of pH 5.75 gels to 20% NaCl-whey brine held at 40 °C assessed in triplicate for each time point. The blue dashed line represents the Fickian fitting while the grey dotted line represents the biexponential fitting for the pellet solids case. The free fluid and pellet fluid were assumed to have the same salt mass fraction.

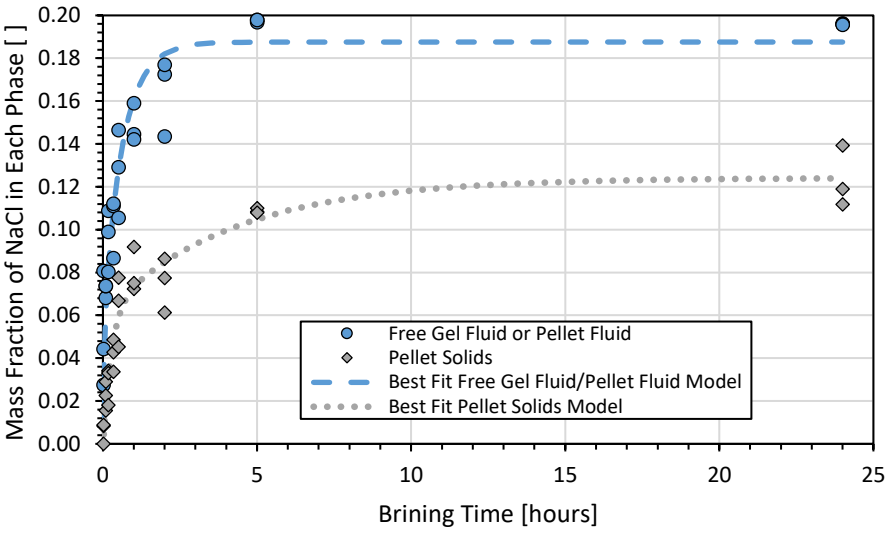

(a)

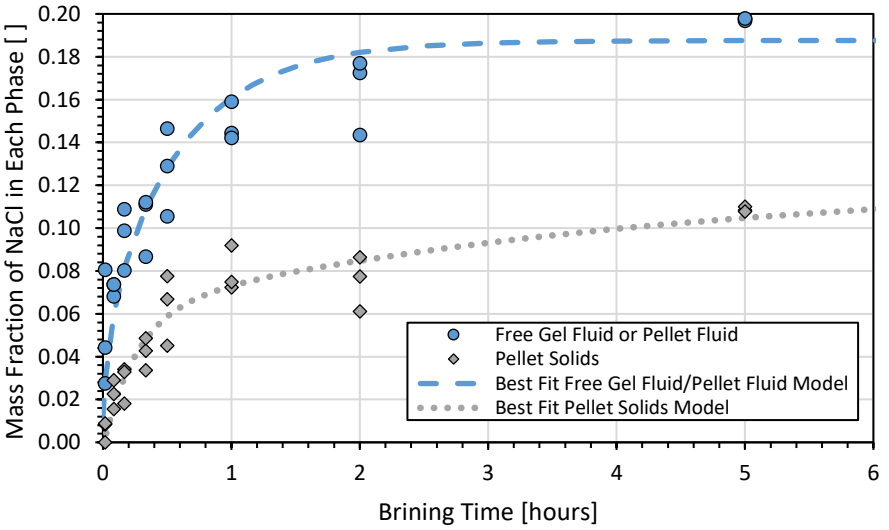

(b)

Figure 5-23: Mass fraction of NaCl in fluid and dairy solid phases and fitted models as a function of brining time for (a) the whole experiment and (b) the first six hours of the experiment after exposure of pH 5.75 gels to 20% NaCl-whey brine held at 40 °C assessed in triplicate for each time point. The blue dashed line represents the Fickian fitting while the grey dotted line represents the biexponential fitting for the pellet solids case. The free fluid and pellet fluid were assumed to have the same salt mass fraction.

Figures 5-21 through 5-23 show greatly differing salt uptake behaviours in both fluid fractions and estimated salt adsorbed to the solids. The fitted biexponential models and fitted Fickian models for uptake in the solids fraction and fluid fraction are shown in Tables 5-13 and 5-14, respectively.

Table 5-13: Fitted salt mass fraction in the pellet solids as a function of brining time in 20% NaCl-whey solution.

Treatment	A [ ]	B [ ]	C [ ]	p_1 [s^{-1}]	p_2 [s^{-1}]	RMSE [ ]	r^2 [ ]
pH 6.25	0.120	-0.0601	-0.0565	1.33E-03	3.36E-05	0.0246	0.669
pH 5.75	0.125	-0.146	-0.0888	0.0316	1.89E-05	0.022	0.600
pH 5.25	0.124	-0.0630	-0.0630	1.06E-03	6.57E-05	0.0119	0.926

Table 5-14: Fitted average Fickian diffusion coefficient values for salt transport in 20% NaCl-whey solution.

Treatment	D_{eff} [$m^2 s^{-1}$]	C_∞ [ ]	RMSE [ ]	r^2 [ ]
pH 6.25	4.67E-10	0.207	0.0170	0.949
pH 5.75	3.72E-10	0.189	9.37E-03	0.983
pH 5.25	4.92E-10	0.188	0.0190	0.876

The statistics presented in Table 5-13 only show a good degree of fit for the salt mass fraction in solids model for the pH 5.25 gels, likely due to the lower degree of variability in the gels at one, two, and five hours of brining time at this pH. Table 5-14 shows a good degree of fit between the fitted diffusion models and the data collected for all three pH treatments, with RMSE values that do not exceed 1.90% of the total mass fraction at any evaluation time. Salt uptake in the fluid phase occurred at a faster rate and yielded a higher equilibrium mass fraction in the fluid phase of all gel pH treatments tested, compared to the salt mass fraction in the solids phase. This finding indicates that there may be a limit to the salt adsorption capacity in the solids phase to approximately 0.12 salt mass fraction in solids, particularly for the pH 5.75 and 5.25 gels. The equilibrium salt mass fraction in the pH 6.25 solids is approximately 0.118, but there is significant variance from the data points shown in Figure 5-21 which must be considered.

The slow uptake of salt into the gel solids fraction after the first hour of brining may indicate that the number of available binding sites decreased and the average pathway length to the available sites may have increased sufficiently by that point to slow the rate of adsorption. Fitting fractal adsorption kinetics to the adsorption data may provide some insights the changing adsorption behaviour. Nonetheless, should a standard adsorption kinetics model not be successfully established to describe the estimated adsorptive behaviour between the salt and gel solids, the biexponential model approach is sufficient to describe the behaviour.

5.4.2.6 Salt Distribution in Each Phase

Figures 5-24, 5-25 and 5-26 show the mass fraction of all the salt in the system in the free fluid, pellet fluid, and pellet solids fraction with respect to brining time for pH 6.25, 5.75, and 5.25 gels treated with 20% NaCl-whey at 40 °C, respectively.

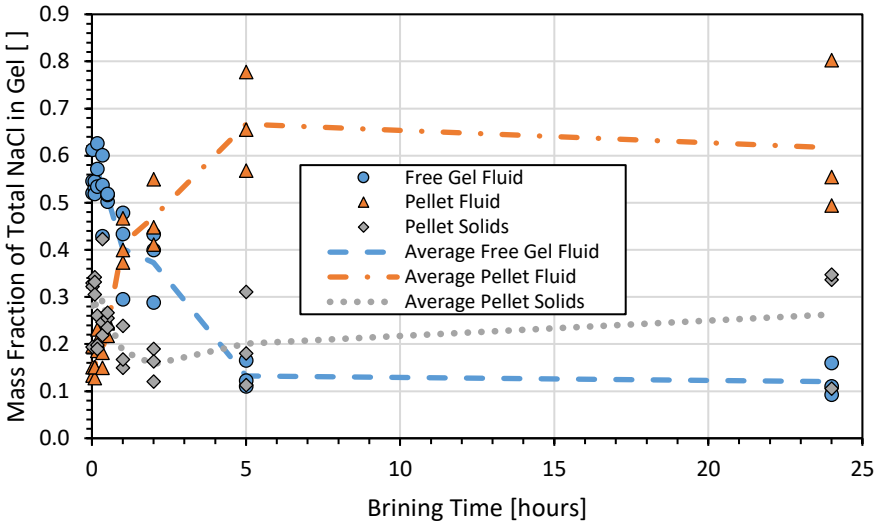

(a)

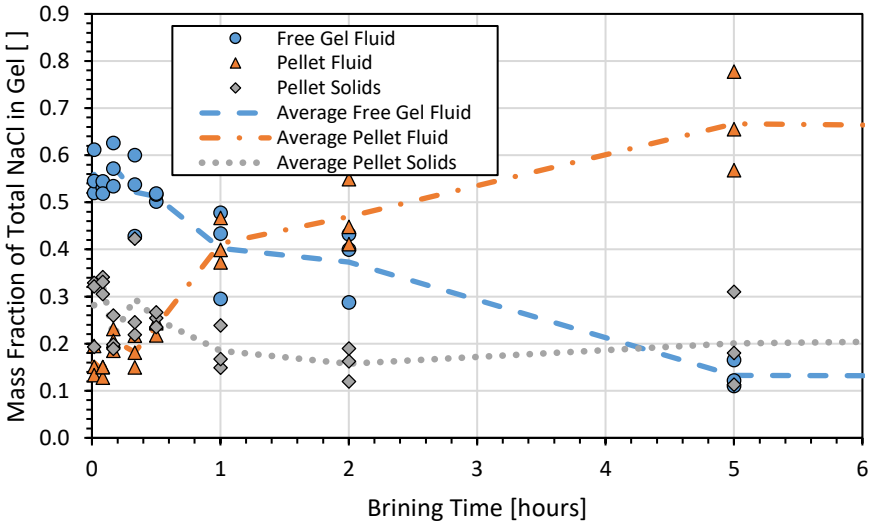

(b)

Figure 5-24: Salt distribution between phases and fitted models as a function of brining time for (a) the whole experiment and (b) the first six hours of the experiment after exposure of pH 6.25 gels to 20% NaCl-whey brine held at 40 °C assessed in triplicate for each time point. The average values are plotted to provide a guiding line for evaluation.

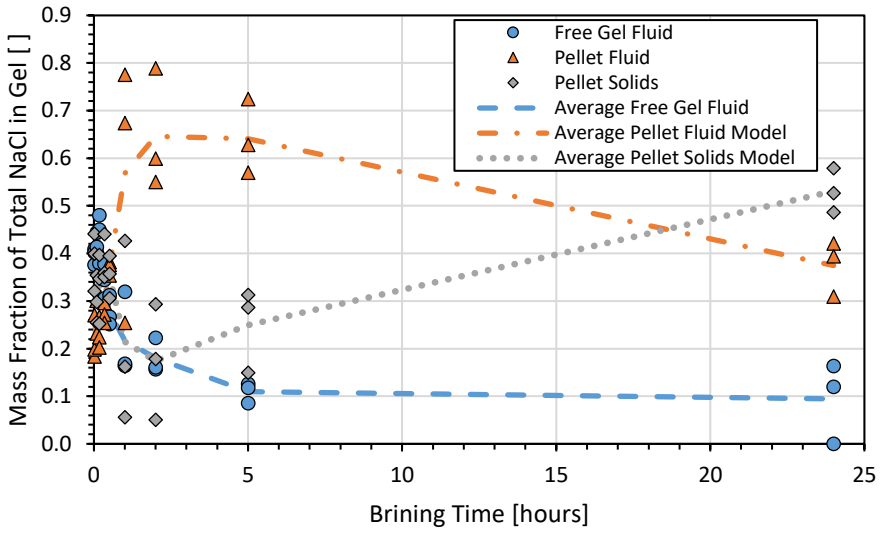

(a)

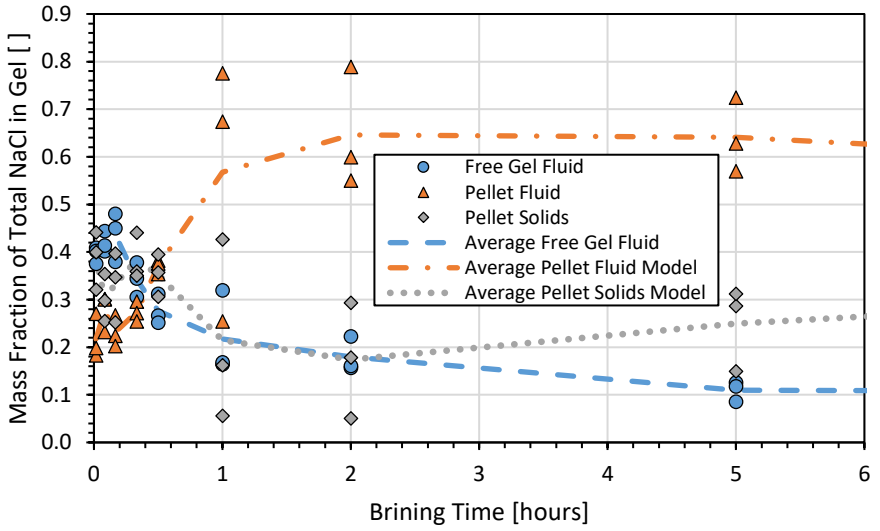

(b)

Figure 5-25: Salt distribution between phases and fitted models as a function of brining time for (a) the whole experiment and (b) the first six hours of the experiment after exposure of pH 5.75 gels to 20% NaCl-whey brine held at 40 °C assessed in triplicate for each time point. The average values from three replicates are plotted to provide a guiding line for evaluation.

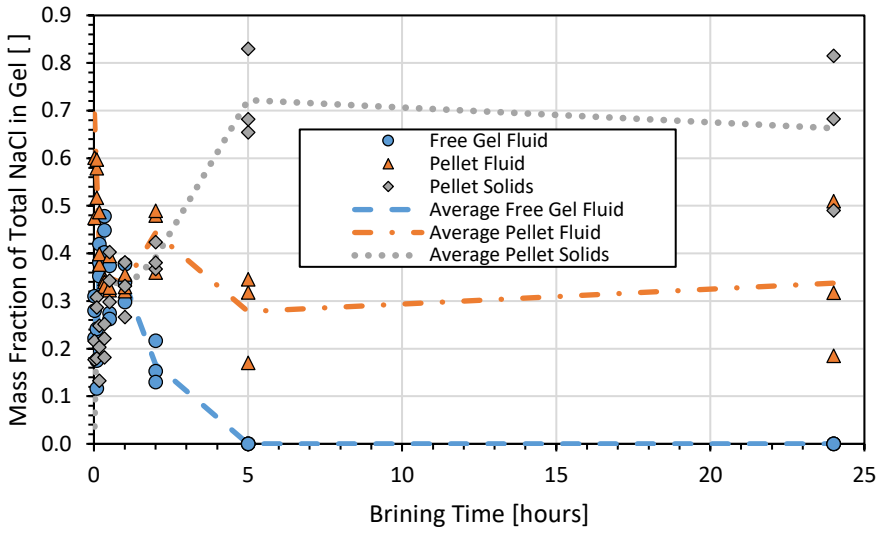

(a)

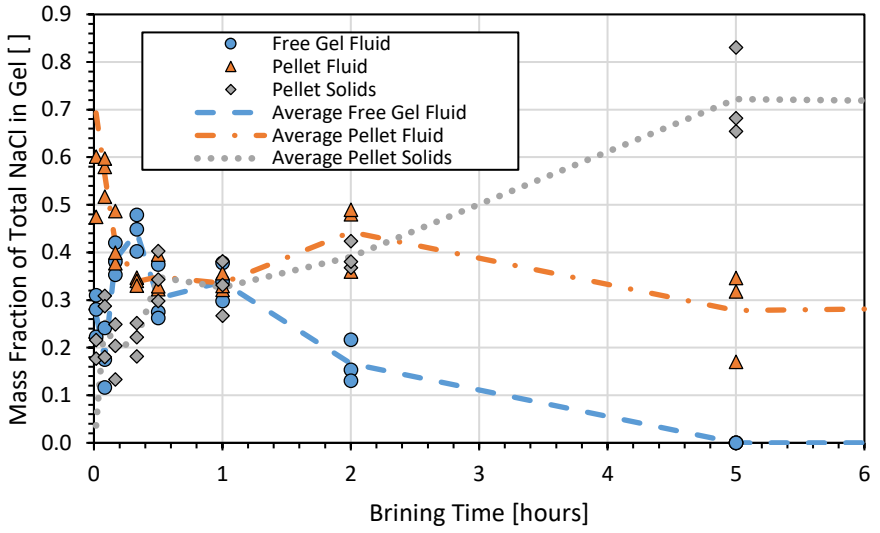

(b)

Figure 5-26: Salt distribution between phases and fitted models as a function of brining time for (a) the whole experiment and (b) the first six hours of the experiment after exposure of pH 5.25 gels to 20% NaCl-whey brine held at 40 °C assessed in triplicate for each time point. The average values from three replicates are plotted to provide a guiding line for evaluation.

Figures 5-24 through 5-26 show a moderate degree of variability in the location of salt within the gel with respect to brining time. Most salt in the pH 6.25 gels was in the free fluid fraction of the gel during the first hour of brining, which proved reasonable as higher pH gels are expected to have a higher starting moisture mass fraction than the other pH treatments. The fraction of the total salt in the free fluid fraction decreased as brining time increased due to the continued syneresis and expulsion of whey from the free fluid fraction during the

brining process and the resulting increase in the contribution of the pellet fluid and solids fraction to the total salt in the gel.

Most of the salt in the pH 5.75 gels was split evenly between the free fluid, pellet fluid, and solids fraction during the first thirty minutes of brining. This changed rapidly afterwards, with most of the salt in the gel being found in the pellet fluid fraction, before once more shifting much of the salt in the gel to the solids fraction. The reduction of the total salt present in the free fluid fraction was due to the syneresis of the whey that continued throughout brining. The rapid increase in the total salt present in the pellet fluid relative to the whole gel demonstrates the fast uptake of salt from the surrounding brine into the fluid phase of the gel. The increased concentration of the total salt in the gel in the solids fraction is due to a combination of the decrease of the total whey fraction with salt in the gel and increased salt adsorption. Similar behaviour was also observed with the pH 5.25 gels, except that the contribution of the solids fraction to the whole of the salt content in the gel was achieved earlier than in the pH 5.75 case, due to the rapid decrease in the free fluid fraction in the gel.

Results from the Figures 5-24 through 5-26 show that the fraction of the total salt in the gel at risk of being expelled from the gel to external pressing forces is in the free fluid fraction, which naturally decreases with respect to brining time. This finding provides guidance for limiting salt losses in gels that undergo pressing, whereby salt located in the mobile free fluid phase would be at risk of being pressed from the gel. The results indicate that after thirty minutes of brining, 51, 28, and 30 % of the salt in the gels would be at risk of being expelled through external pressing from pH 6.25, 5.75, and 5.25 gels, respectively.

5.4.3 Effective Diffusion Coefficient Modelling

Sections 5.4.1.4 and 5.4.2.4 successfully modelled the salt uptake behaviour in the gel fluid fractions of the gel. The fitted effective diffusion coefficients were 20.5, 14.9, and 22.2% of the ideal salt diffusion coefficient of 1.94×10^{-10} m^2 s^{-1} for 2.5% NaCl-water solution at 40 °C, for the pH 6.25, 5.75, and 5.25 gels, respectively. Likewise, the fitted effective diffusion coefficients for the pH 6.25, 5.75, and 5.25 gels treated in 20% NaCl-whey were 21.0, 16.7, and 22.1% of the ideal salt diffusion coefficient of 2.22×10^{-10} m^2 s^{-1} for 20% NaCl-water solution at 40 °C, respectively. The fitted effective diffusion coefficients also correspond within the expected range of effective diffusion coefficients for salt in cheese or cheese

analogues reported, indicating that the gels follow the observed salt uptake behaviours in other cheese systems noted by Floury et al. (2010).

However, it should be noted that the salt mass fraction assessed in the free gel fluid fraction was the net accumulated salt in the gel fluid, which does not account for the accumulated salt in the gel presumably adsorbed to the gel solids or the loss of salt in the expelled salted gel whey. Therefore, the effective diffusion coefficient reported in the sections 5.4.1.4 and 5.4.2.4 maybe considered the "net effective diffusion coefficient". If all salt in the gels is assumed to be in the fluid fraction of the gel and adsorption does not occur, then a new net effective diffusion coefficient may be determined to describe the total salt uptake, while also accounting for the salt expelled during the osmotic pressure differential induced syneresis.

Figures 5-27 and 5-28 show the salt mass fraction in the gel fluid for the previously modelled data and new data and Fickian model, fitted under the assumption that all salt in the gel was in the fluid fraction for the 2.5% NaCl-whey and 20% NaCl-whey treatments, respectively. Interestingly, if adsorption is not assumed to occur, the salt mass fraction in the gel rapidly exceeds the surrounding brine composition, which would be thermodynamically untenable. This finding confirms that some adsorption-like behaviours must occur to effectively remove salt ions from the solution state in the gel. A re-modelling of the data was conducted to determine the change in the diffusion coefficient if all salt detected in the gels were assumed to be in the fluid fraction of the gel. The findings are presented in the following figures with the salt mass fractions from the surrounding brine replacing the calculated salt mass fractions when the calculated salt mass fraction would exceed the surrounding brine concentration. The data points that were calculated to exceed the surrounding brine mass fraction are included for reference.

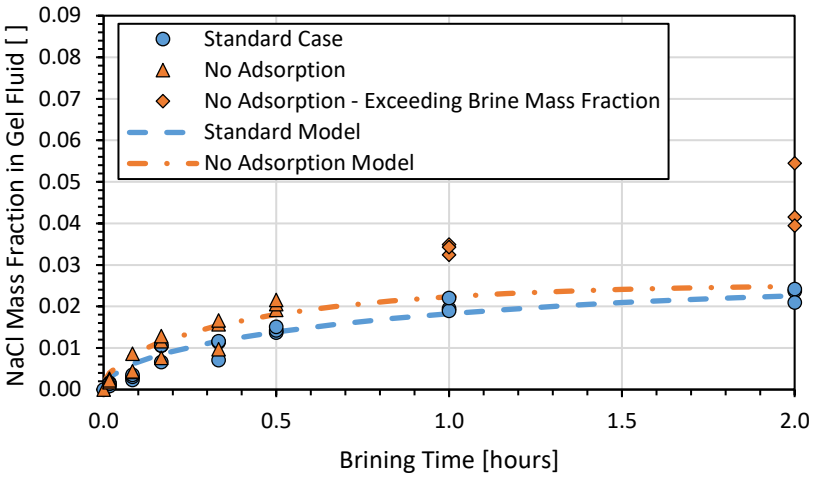

(a)

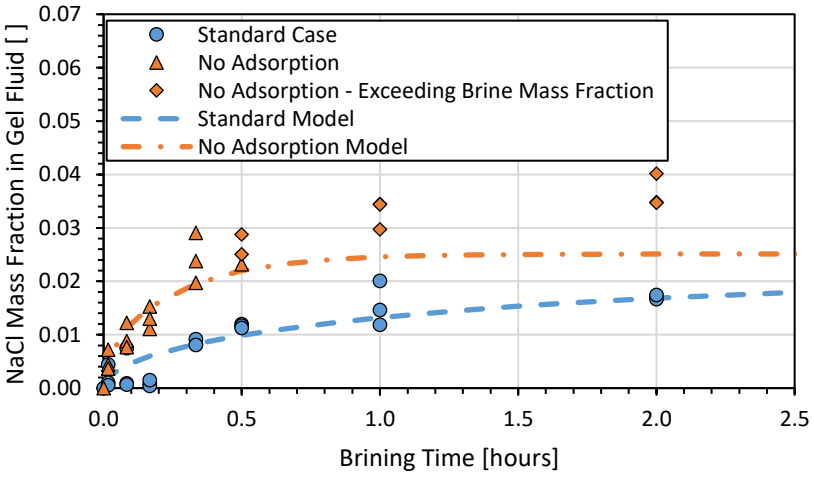

(b)

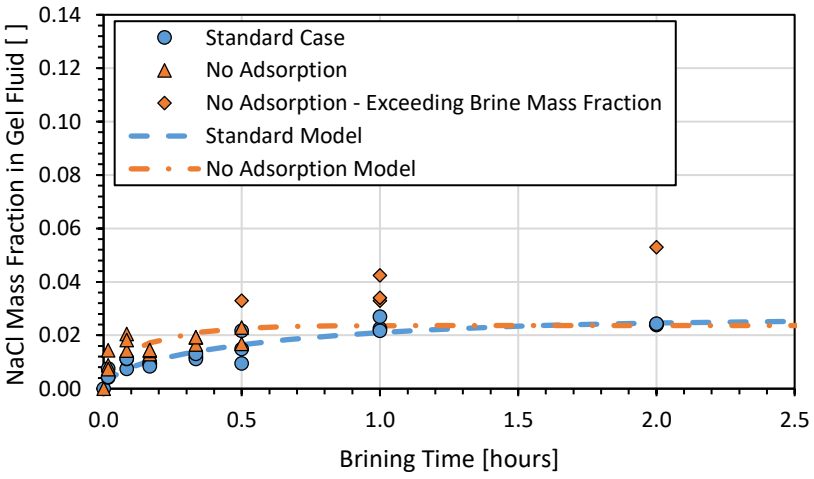

(c)

Figure 5-27: Salt uptake in fluid fractions of (a) pH 6.25, (b) pH 5.75, and (c) pH 5.25 gels exposed to 2.5% NaCl-whey at 40 °C assessed in triplicate for each time point for the first 2.5 hours of brining and fitted diffusion models assuming that adsorption occurs or does not occur. Diamond symbols represent the salt mass fraction in the gel fluid assuming that solubility of salt in whey is not a limiting factor on salt uptake.

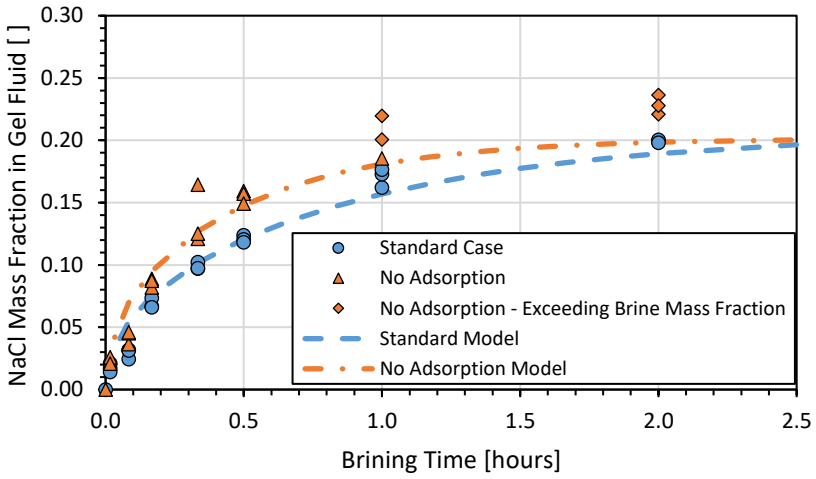

(a)

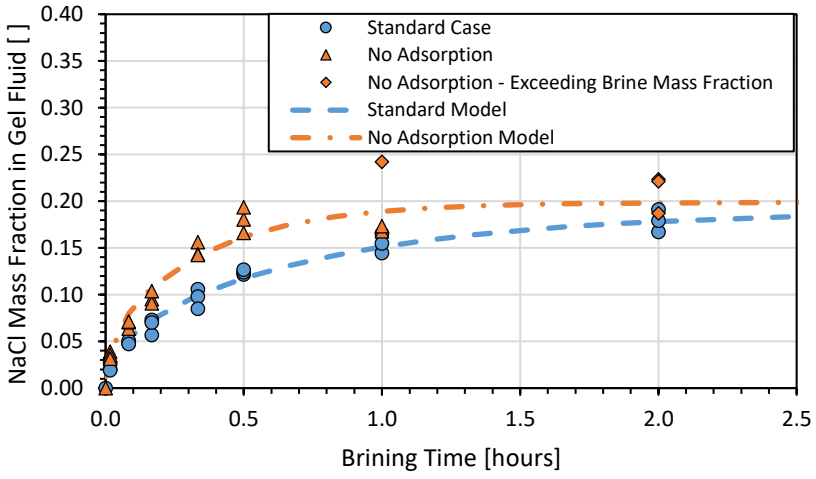

(b)

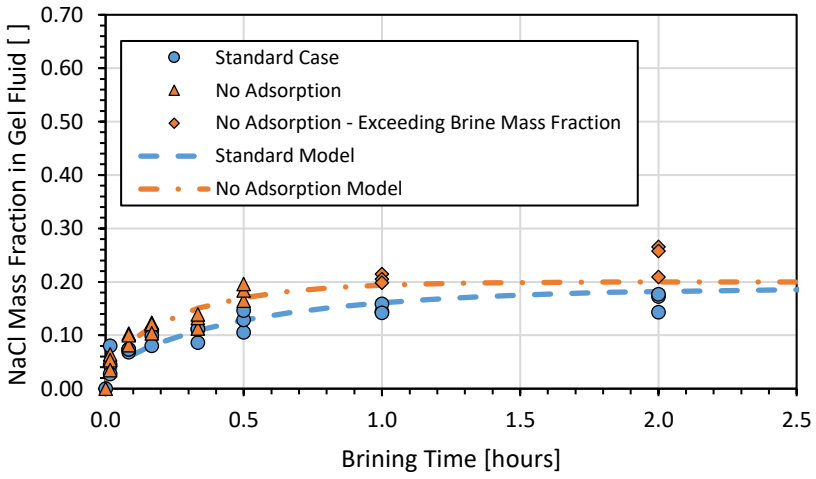

(c)

Figure 5-28: Salt uptake in fluid fractions of (a) pH 6.25, (b) pH 5.75, and (c) pH 5.25 gels exposed to 20% NaCl-whey at 40 °C assessed in triplicate for each time point for the first 2.5 hours of brining and fitted diffusion models assuming that adsorption occurs or does not occur. Diamond symbols represent the salt mass fraction in the gel fluid assuming that solubility of salt in whey is not a limiting factor on salt uptake.

Figures 5-27 and 5-28 demonstrate different salt uptake behaviours in gels under the assumption of both adsorption occurring and not occurring during the brining process in 2.5% NaCl-whey and 20% NaCl-whey solutions, respectively. The fitted Fickian models for uptake in the solids fraction and fluid fraction for the 2.5% NaCl-whey and 20% NaCl-whey treatments are shown in Tables 5-15 and 5-16, respectively.

Table 5-15: Fitted average Fickian diffusion coefficient values for salt transport in 2.5% NaCl-whey solution, assuming no adsorption occurs and salt in the gel remains in the gel fluid.

Treatment	$D_{eff,\ no\ ads}$ [$m^2\ s^{-1}$]	C_∞ [ ]	RMSE [ ]	r^2 [ ]	Ratio $D_{eff,\ no\ ads}/D_{eff}$ [ ]
pH 6.25	8.01E-10	0.0253	2.29E-03	0.949	2.01
pH 5.75	1.53E-09	0.0251	1.88E-03	0.963	5.27
pH 5.25	1.84E-09	0.0236	3.58E-03	0.826	4.28

Table 5-16: Fitted average Fickian diffusion coefficient values for salt transport in 20% NaCl-whey solution, assuming no adsorption occurs and salt in the gel remains in the gel fluid.

Treatment	$D_{eff,\ no\ ads}$ [$m^2\ s^{-1}$]	C_∞ [ ]	RMSE [ ]	r^2 [ ]	Ratio $D_{eff,\ no\ ads}/D_{eff}$ [ ]
pH 6.25	8.46E-10	0.201	0.0145	0.966	1.81
pH 5.75	1.17E-09	0.199	0.0118	0.975	3.13
pH 5.25	9.66E-10	0.200	0.0134	0.965	1.96

The new Fickian models describing salt uptake assuming that no adsorption had occurred in the gels were well fitted in all treatment pH and brining solution cases, with the RMSE never exceeding 0.0145 salt mass fraction in gel fluid. The new models showed a significant increase in the fitted effective diffusion coefficients, with the gels treated with 2.5% NaCl-whey conditions showing the highest increase in the effective diffusion coefficient. Furthermore, whereas pH 5.75 gels in both brining conditions had previously shown the lowest effective diffusion coefficients, assuming no adsorption takes place promotes the effective diffusion coefficient to the largest value compared to the other two pH treatments in the 20% NaCl-whey brining condition. This exercise provides insight to the role adsorption is contributing to the evaluation of salt transport and the of fitting effective diffusion coefficients. Use of the original effective diffusion coefficient alone would underestimate the total mass of salt taken into the gel because it already accounts for adsorption behaviour. An additional adsorption model would be required to accurately describe the total salt uptake into the gel. The next section provides some insight to the modelling of the hypothesized adsorption behaviours.

5.4.4 Salt Adsorption Modelling in Dairy Solids Fraction

The ratio of estimated adsorbed salt mass to dairy solids (all non-water components such as protein, lactose, and mineral content) was assessed from the data and fitted to with the fractal integrated kinetic Langmuir (IKL) equation, previously shown as Equation 5-9. Figures 5-29, 5-30, and 5-31 show the 20% NaCl-whey treatment adsorption data and fitted model for pH 6.25, 5.75, and 5.25 gels, respectively.

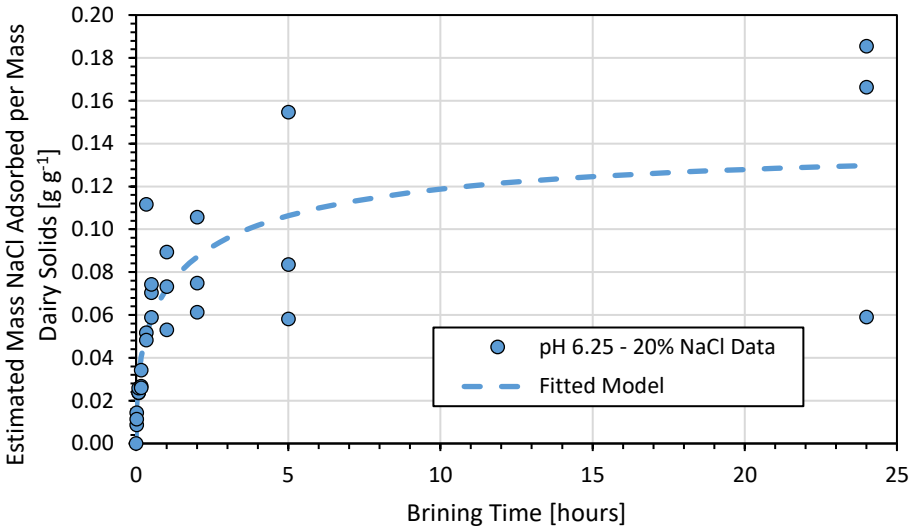

Figure 5-29: Estimated mass of adsorbed salt per gram of dairy solids in the gel, modelled with a fractal integrated kinetic Langmuir equation for pH 5.25 gels treated with 20% NaCl-whey at 40 °C assessed in triplicate for each time point.

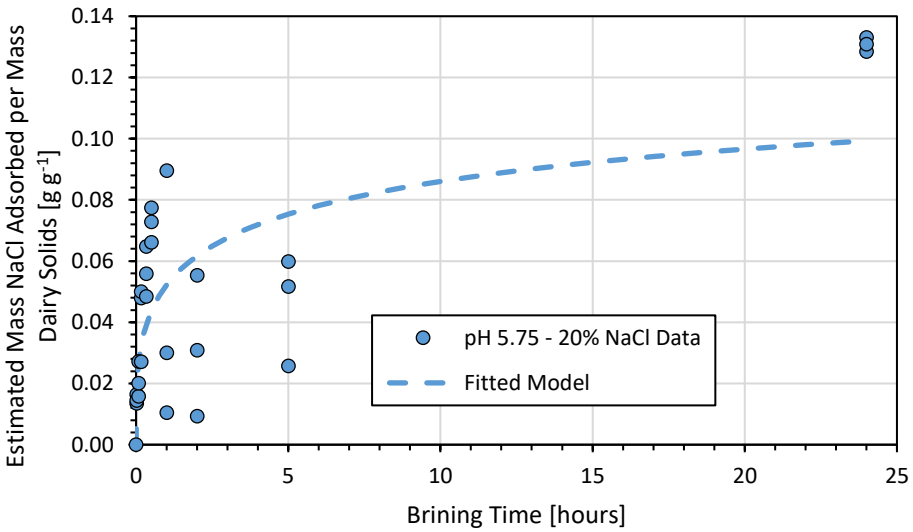

Figure 5-30: Estimated mass of adsorbed salt per gram of dairy solids in the gel, modelled with a fractal integrated kinetic Langmuir for pH 5.75 gels treated with 20% NaCl-whey at 40 °C assessed in triplicate for each time point.

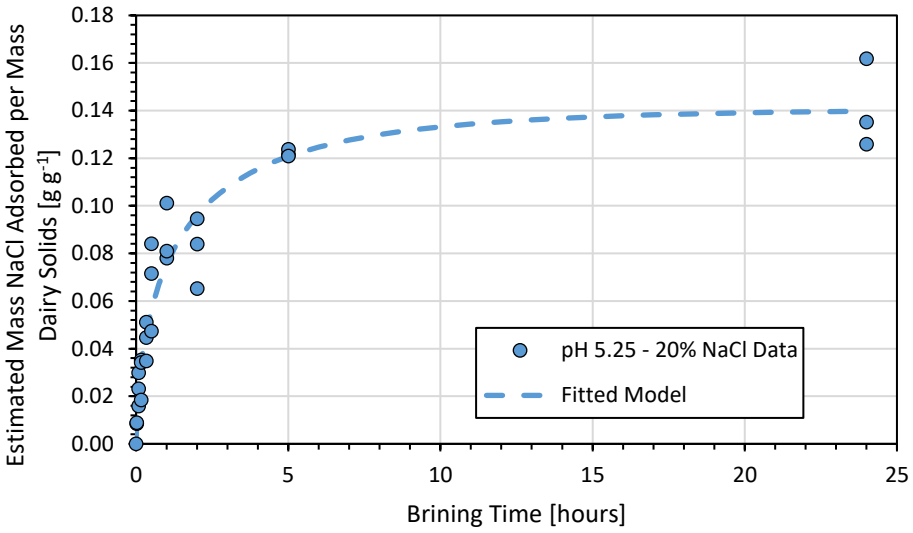

Figure 5-31: Estimated mass of adsorbed salt per gram of dairy solids in the gel, modelled with a fractal integrated kinetic Langmuir equation for pH 5.25 gels treated with 20% NaCl-whey at 40 °C assessed in triplicate for each time point.

Figures 5-29 through 5-31 show greatly differing salt adsorption data and fitted models using the fractal integrated kinetic Langmuir equation. The fitted fractal IKL models for uptake in the solids fraction are shown in Table 5-7.

Table 5-17: Fitted fractal integrated kinetic Langmuir Equation values and degree of fitting for gels of different pH values treated with 20% NaCl-whey for 24 hours.

Treatment	α [ ]	$k'_{1,0}$ [$s^{-\alpha}$]	$k_{a,obs}$ [s^{-1}]	f_{eq} [ ]	RMSE [ ]	r^2 [ ]
pH 6.25	0.431	0.0218	0.188	7.46E-03	0.0280	0.688
pH 5.75	0.324	0.0359	0.548	5.16E-03	0.0257	0.570
pH 5.25	0.580	6.62E-03	0.0499	3.96E-03	0.0134	0.928

The fitting results from the fractal IKL models shown in Table 5-7 demonstrate good to poor fitting for the adsorbed salt mass per mass of solids data. The poor fitting shown especially in the case of the pH 5.75 gels is due to the degree of data variability for data collected after the first hour of brining, similar to the findings discussed in section 5.4.2.5. The differences in the $k_{a,obs}$ values provide insight to the rate of salt adsorption occurring at the onset of gel protein exposure to the salt brine treatment, with pH 5.75 gels showing the fastest uptake. Although the fractal IKL equation may be used to model salt uptake behaviour under the high salt mass fraction brining conditions, it may not be appropriate to apply it to the low salt mass fraction brining conditions. This is due to the apparent salt uptake mass fractions in the low mass fraction salting regime (shown in section 5.4.1.5) where there is significant variation in the salt uptake behaviour in the solids fraction, with pH 6.25 and 5.75 gels achieving roughly

the same or higher salt mass fractions in the solids fraction than the fluid fraction, respectively. These results indicate that there may be additional mechanisms occurring that govern the adsorptive behaviour not accounted for in the fractal IKL model or more likely, due to an accumulation of errors from the small sampling size.

Given the lack of fitting and incomplete knowledge regarding the changing state of the para-casein matrix binding sites for the sodium ions or the exact mechanisms of "binding" that occurs between the salt ions and the protein matrix, future work should be conducted to evaluate the apparent adsorption behaviour between the salt taken into the gel and the protein matrix. Literature sources have suggested an ion exchange behaviour between the free sodium ions and calcium ions around the protein matrix, but these findings should be investigated to a larger degree to confirm the behaviour before a formal adsorption model is assigned to describe the specific sodium chloride adsorption kinetics behaviour with para-casein matrices (Creamer, 1985; Gal & Bankay, 1971; Hardy & Steinberg, 1984). The establishment of the exact adsorption model is outside the direct purview of this thesis.

5.4.5 Moisture Content and Salt Transport

The estimated average internal moisture mass fraction was calculated using the mass balance discussed in section 5.3.4 for each pH treatment and brining condition. The average internal gel moisture mass fraction was calculated using the same assumptions listed in section 4.4.1.3, except that the whey expelled did not have a constant density due to the presence of salt expelled with the free gel fluid. Instead, Equation 5-15 was used as the density equation to determine the mass of whey and salt loss from the gels with respect to brining time. Figures 5-32 and 5-33 show the predicted salt and whey expulsion behaviour and the net mass fraction of salt in the whey expelled with respect to time for the 2.5% NaCl-whey 20% NaCl-whey brining conditions, respectively.

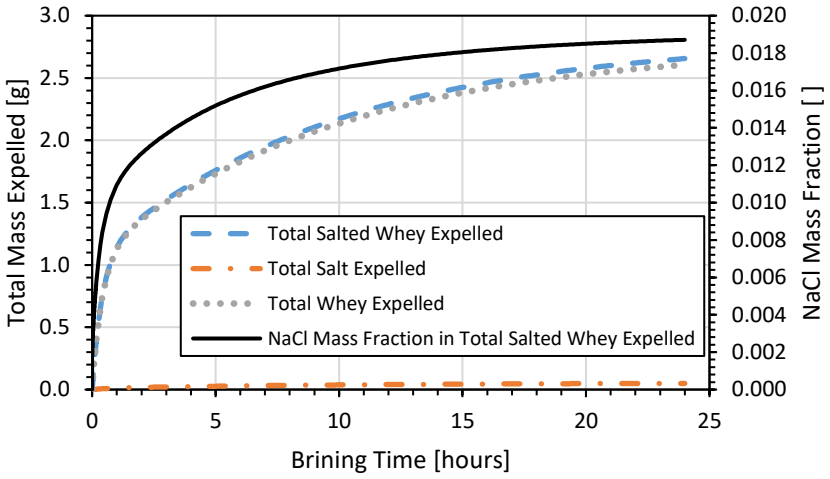

(a)

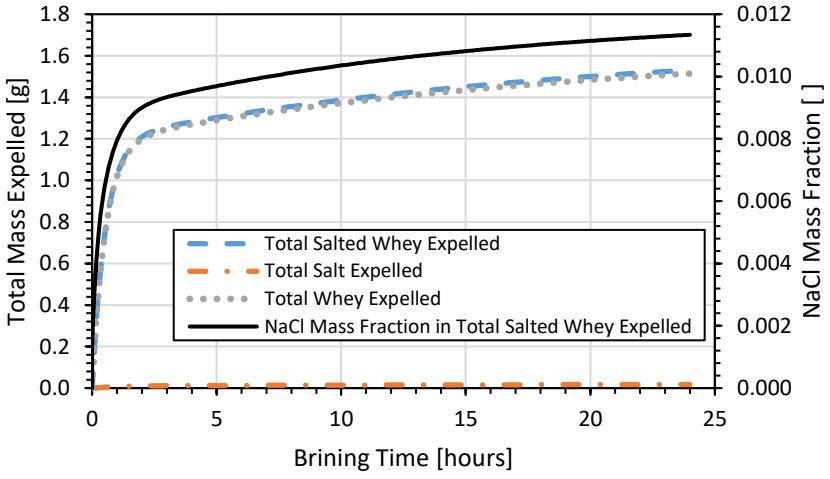

(b)

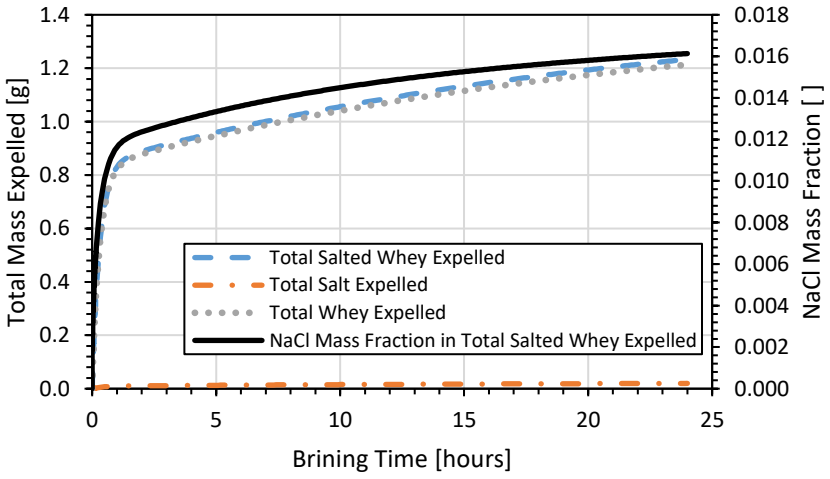

(c)

Figure 5-32: Simulated whey and salt mass expulsion, and net expelled salted whey solution salt mass fraction for gels treated with 2.5% NaCl-whey brine at 40 °C for 24 hours total brining time with (a) pH 6.25, (b) pH 5.75, and (c) pH 5.25 gels, respectively. The solid black line shows the total salt mass fraction of all the expelled salted whey using the right vertical axis.

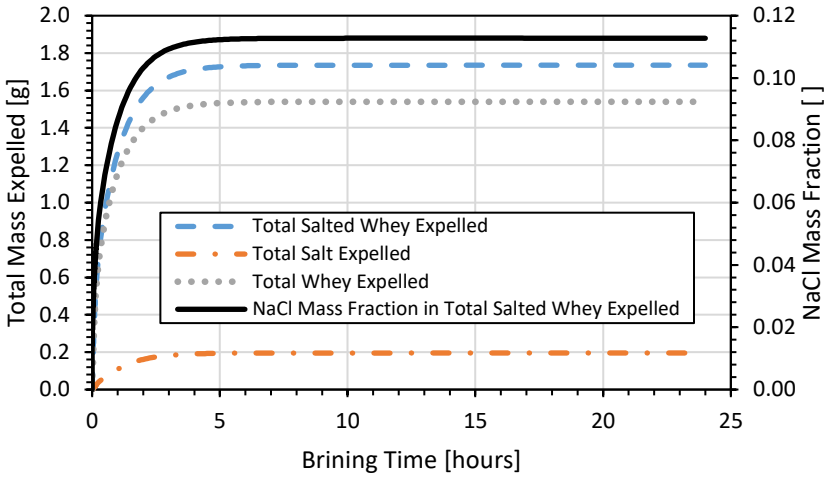

(a)

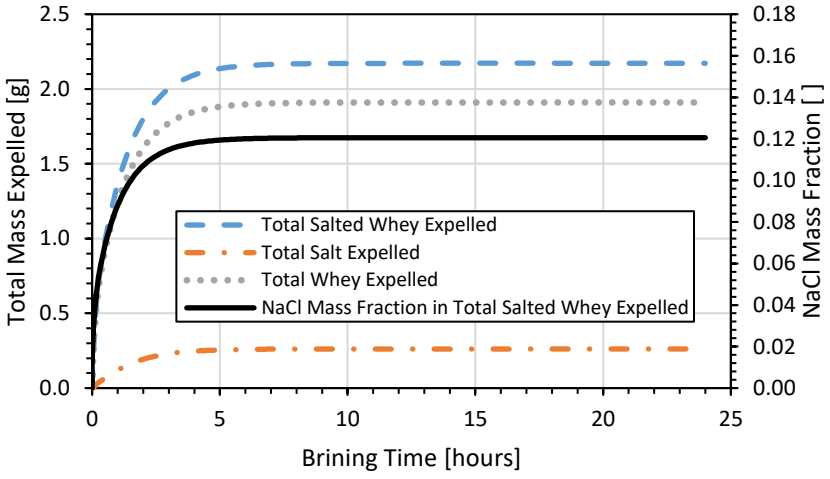

(b)

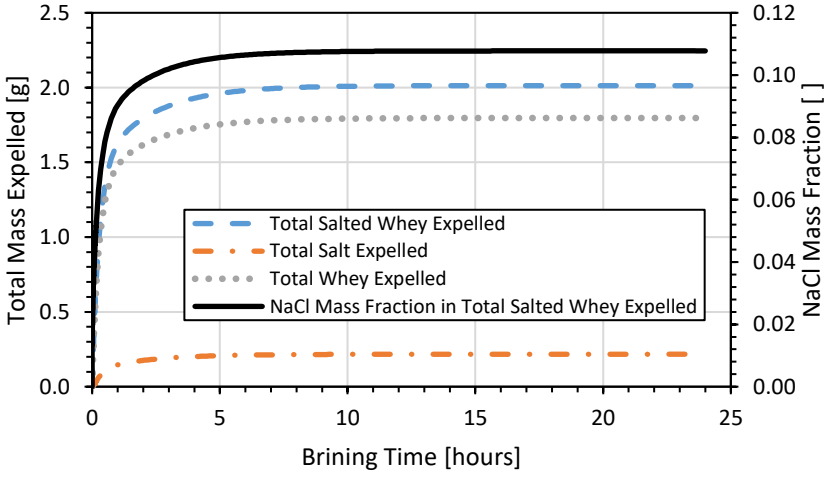

(c)

Figure 5-33: Simulated whey and salt mass expulsion, and net expelled salted whey solution salt mass fraction for gels treated with 20% NaCl-whey brine at 40 °C for 24 hours total brining time with (a) pH 6.25, (b) pH 5.75, and (c) pH 5.25 gels, respectively. The solid black line shows the total salt mass fraction of all the expelled salted whey using the right vertical axis.

Figures 5-32 and 5-33 show the rapid expulsion of salted whey and the net salt mass fraction of the total amount of whey expelled as a function of brining time. The salt mass fraction reaches equilibrium after approximately five hours brining time for the 20% NaCl-whey expulsion case, but only gradually approaches the final mass fraction after the first hour of brining for the 2.5% NaCl-whey brining case. This is due to the different whey expulsion behaviours observed in sections 4.4.2.2 and 4.4.3.2 and the changing salt mass fraction in the gel fluid fraction with respect to brining time, detailed in sections 5.4.1.5 and 5.4.2.5, where whey expulsion is fastest at the onset of brining while the average salt mass fraction in the gel fluids only reaches its maximum after a significant amount of brining time.

A salt mass balance was conducted to determine the rate of salt entering the gel to achieve the accumulated salt in the fluid and solids fractions and the lost salt in the expelled salted whey. This information was combined with the salted whey expulsion models to model the changing moisture mass fraction of the gels with respect to brining time for all the pH and brining treatments. Figure 5-34 shows the predicted moisture mass fraction for each of pH treatments for gels treated with 2.5% NaCl-whey and 20% NaCl-whey.

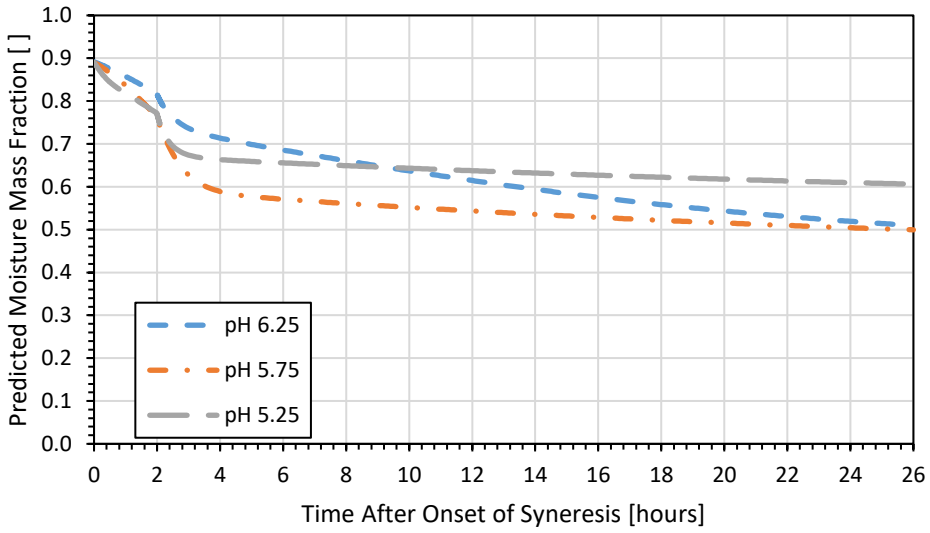

(a)

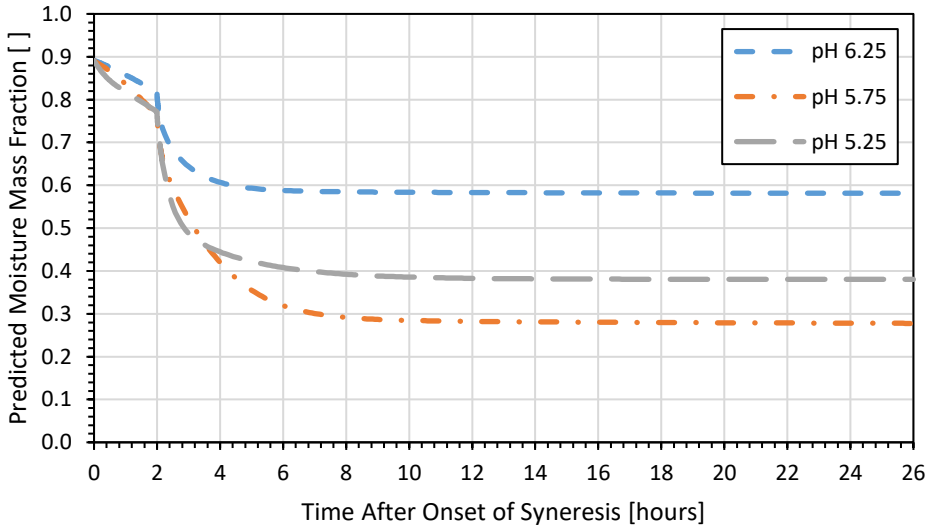

(b)

Figure 5-34: Simulated moisture mass fraction in pH 6.25, 5.75, and 5.25 gels treated at 40 °C with (a) 2.5% NaCl-whey and (b) 20% NaCl-whey, after two hours of regular syneresis for 26 hours of total syneresis time, including 24 hours of brining time.

Figure 5-34 shows improved predicted moisture mass fraction calculations than the simplified estimations in sections 4.4.2.3 and 4.4.3.3. Moisture mass is rapidly lost within the first two hours of brining for both brining cases, with the 20% NaCl-whey treatment leading to a greater reduction of moisture in the gel due to the larger osmotic pressure differential induced gradient. Once again, the lower equilibrium moisture mass fractions of the pH 5.75 gels were modelled to be lower than the other two pH values modelled. The reduction in the equilibrium moisture mass fraction is realistic from the combination of salt ion presence and gel pH reduction that reduces the electrostatic repulsion between proteins,

thereby increasing the protein-protein interactions that lead to greater syneresis behaviour (Dejmek & Walstra, 2004; van Dijk & Walstra, 1986; Walstra et al., 1985). The modelled moisture mass fraction data may be used to assess salt uptake behaviour, as well. Figures 5-35 and 5-36 show the changing salt mass fractions of gels exposed to the 2.5% NaCl-whey and 20% NaCl-whey brine conditions, respectively.

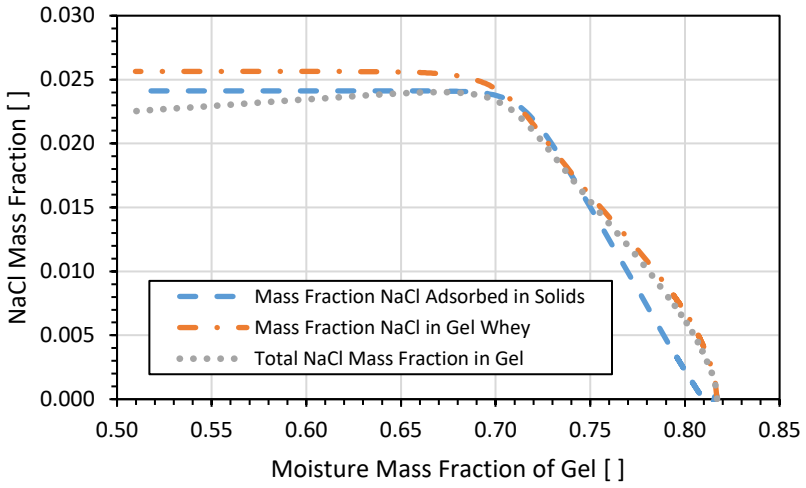

(a)

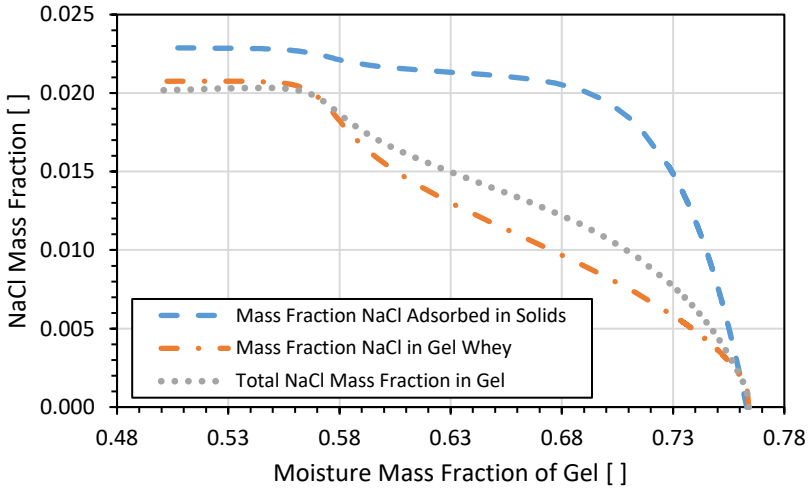

(b)

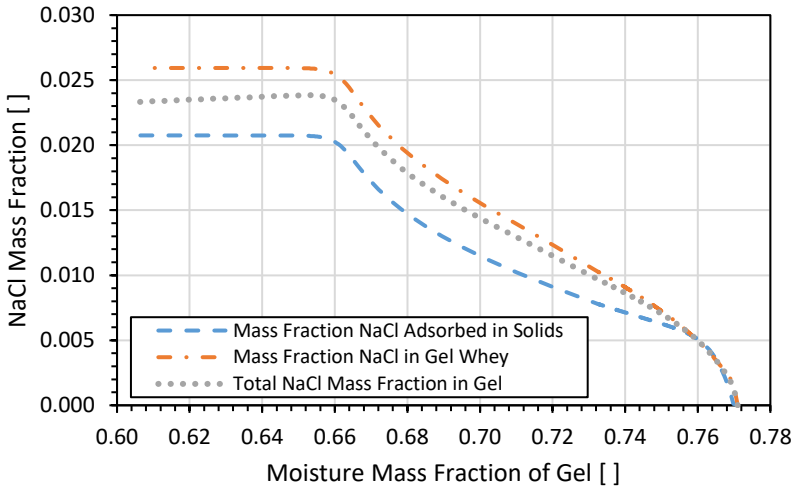

(c)

Figure 5-35: Simulated salt mass fraction in the whole gel, gel whey, and adsorbed to the gel matrix for (a) pH 6.25, (b) pH 5.75, and (c) pH 5.25 gels with respect to the calculated moisture mass fraction of the gel for gels treated with 2.5% NaCl-whey brine for 24 hours following two hours of regular syneresis at 40 °C.

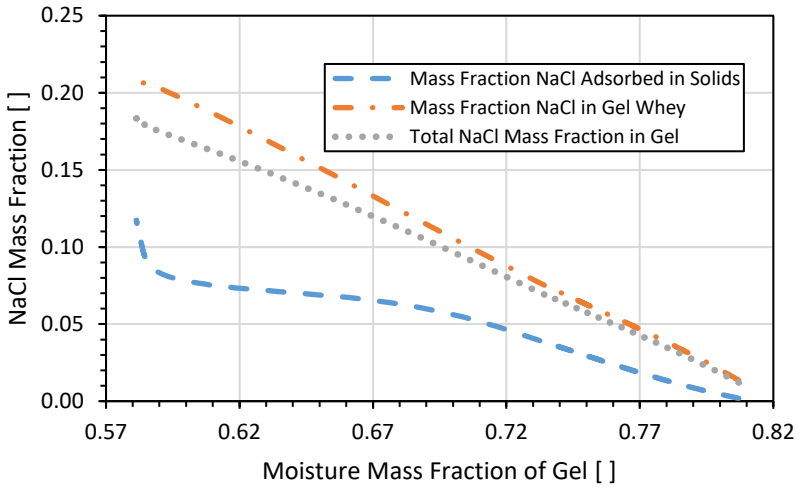

(a)

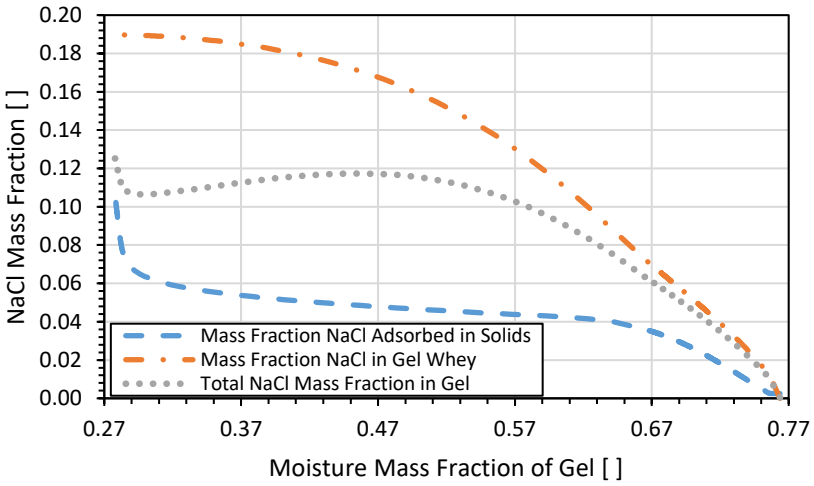

(b)

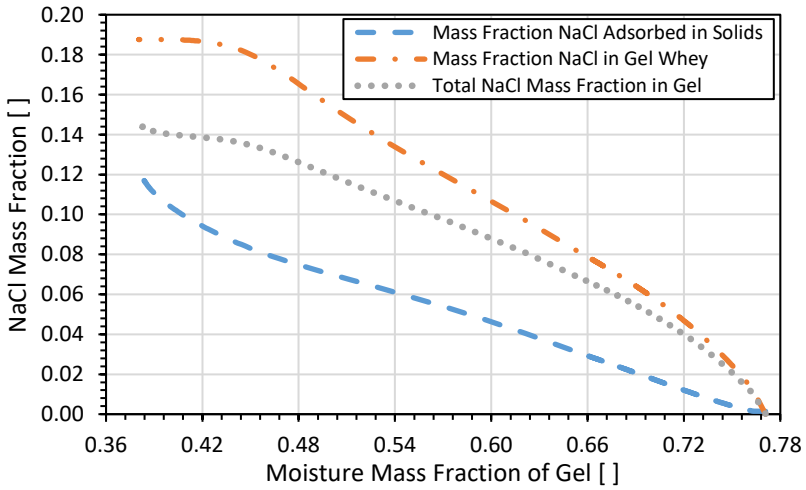

(c)

Figure 5-36: Simulated salt mass fraction in the whole gel, gel whey, and adsorbed to the gel matrix for (a) pH 6.25, (b) pH 5.75, and (c) pH 5.25 gels with respect to the calculated moisture mass fraction of the gel for gels treated with 20% NaCl-whey brine for 24 hours following two hours of regular syneresis at 40 °C.

Results from Figure 5-35 indicate that the pH 6.25, 5.75, and 5.25 gels reach achieve salt mass fraction equilibrium at approximately 0.70, 0.57, and 0.66 moisture mass fraction, respectively for gels treated with 2.5% NaCl-whey at 40 °C. Interestingly, approximately linear fits can be made between the salt mass fraction in the whole gel and the moisture mass fraction of the gels prior to when salt mass fraction equilibrium is achieved. Results from Figure 5-36 also show that the pH 6.25, 5.75, and 5.25 gels achieve salt mass fraction equilibrium at a point where the moisture mass fraction also reaches equilibrium at the end of brining. The relationships between the salt mass fraction in the whole gel and the moisture mass fraction for the pH 6.25 and 5.25 gels are linear, whereas the pH 5.75 gels show a nonlinear relationship with a local salt mass fraction maximum at a moisture mass fraction of 0.47. The relationships shown in these two figures may prove useful for modelling salt uptake behaviours for gels of differing sizes treated with different brine concentration conditions.

5.4.6 ^{13}C NMR Findings

The ^{13}C NMR spectrum of the freeze curd samples brined in 20% NaCl-whey for pre-determined times detailed in section 5.2.3 were analysed for shifts in the readings compared with unsalted samples. Although several distinct peak shifts were determined in the brined gels, the peak at 168 ppm chemical shift shown in Figure 5-37 is related to the "carbon backbone" of the para-casein matrix as it reflects the carbonyl groups of the amino acid chain. The T_1 longitudinal relaxation constant of this peak indicates the general molecular mobility of the primary structure of the protein.

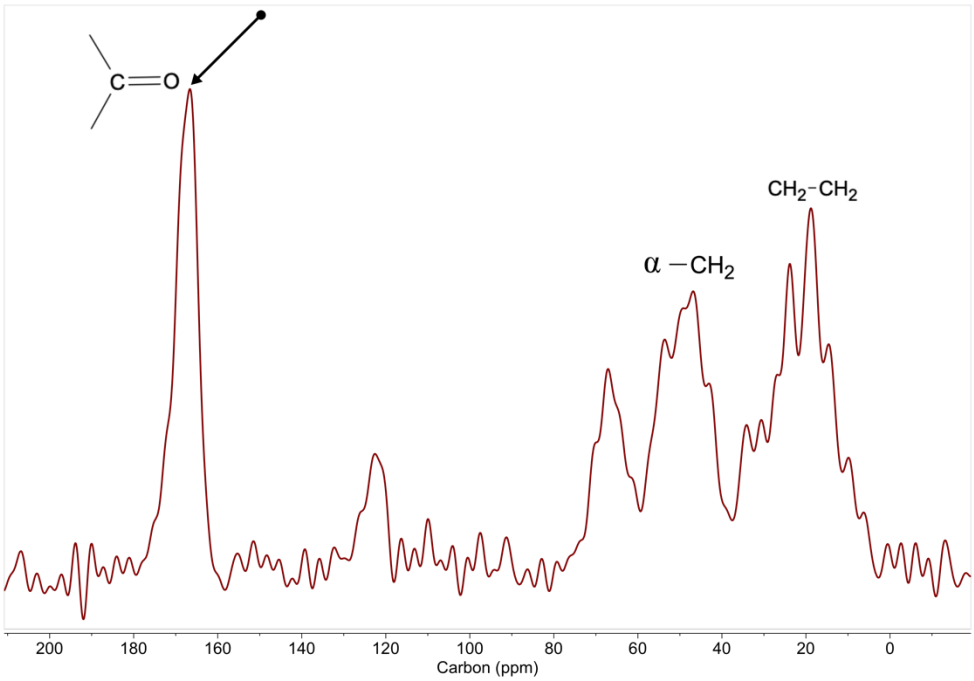

Figure 5-37: ^{13}C NMR spectrograph of an unsalted pH 5.25 gel after ninety minutes of regular syneresis. The peak of interest showing distinct differences in magnitude upon the uptake of salt into the gel is shown with the arrow.

Figures 5-38 and 5-39 show the T_1 longitudinal relaxation constants assessed using ^{13}C NMR for each gel pH treatment under 20% NaCl-whey brining conditions, as a function of brining time and the salt mass fraction in different fractions of the gels.

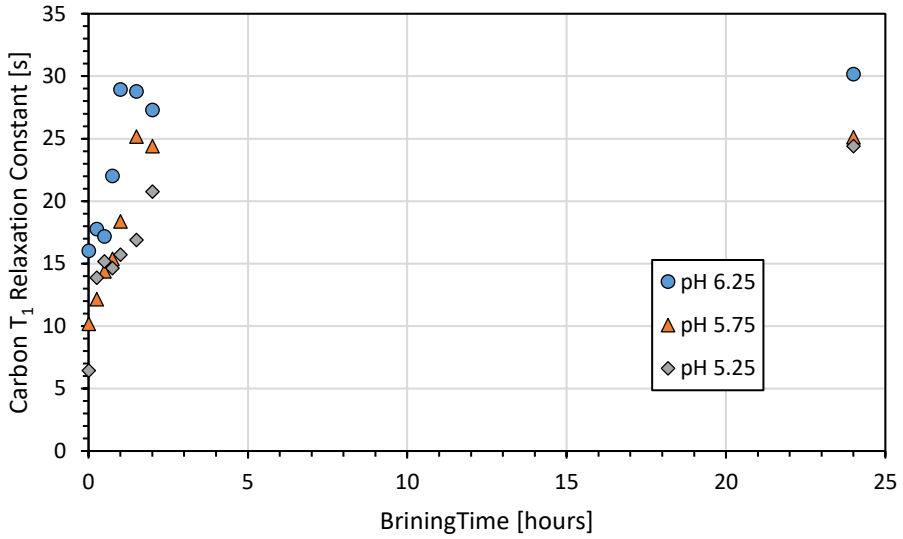

(a)

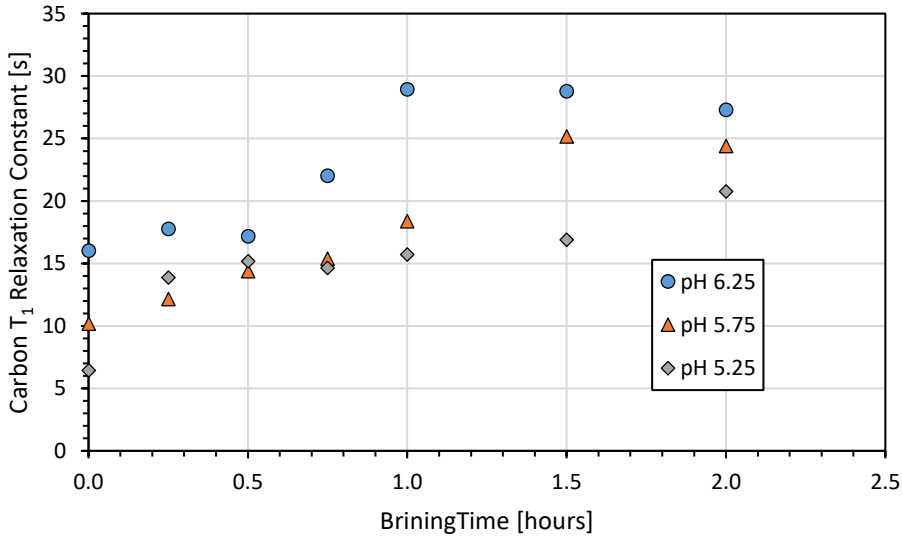

(b)

Figure 5-38: Carbon T_1 relaxation constant as a function of brining time for (a) the whole experiment and (b) the first 2.5 hours of the experiment after exposure of pH 6.25, 5.75, and 5.25 gels to 20% NaCl-whey brine..

Results from Figure 5-38 indicate that as brining time increases, the T_1 longitudinal relaxation constant gradually increases for all three pH values tested with respect to brining time. This increase indicates that the carbon backbone of the protein matrix in the gel becomes less mobile, likely due to the presence of the salt interacting with the para-casein matrix. However, evaluation of the T_1 relaxation constant as a function of the salt mass fraction in the different phases of the gel may provide insight to the effect of salt on the "mobility" of the gel proteins. Figure 5-39 shows the T_1 relaxation constant as a function of the average salt mass fraction in the whole gel, fluids fraction, and solids fraction.

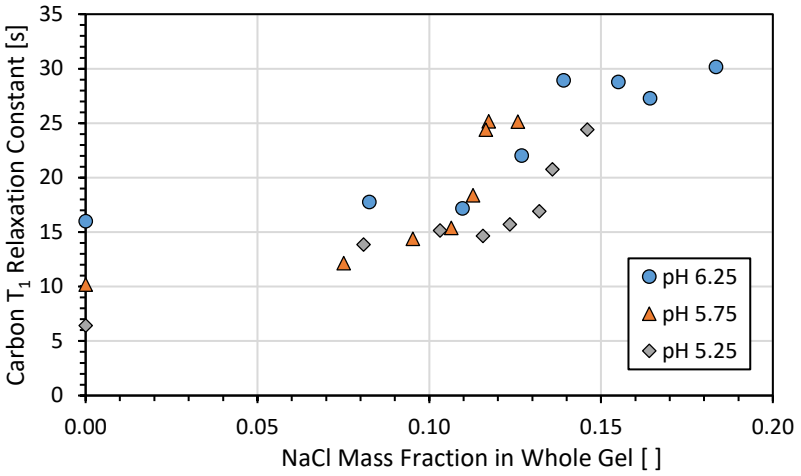

(a)

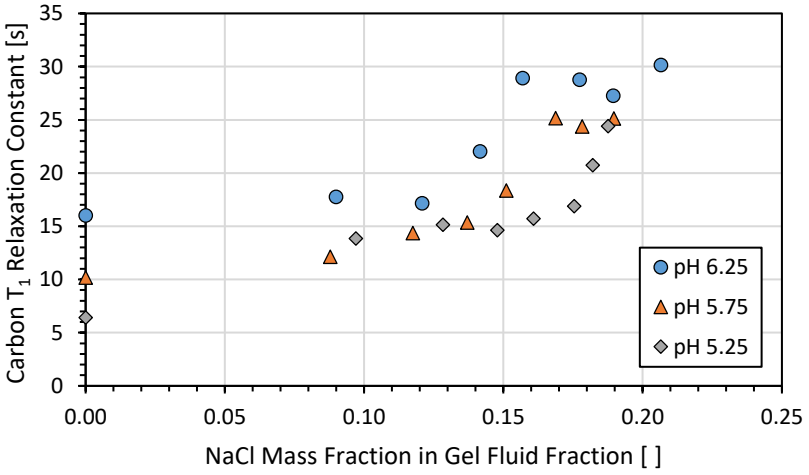

(b)

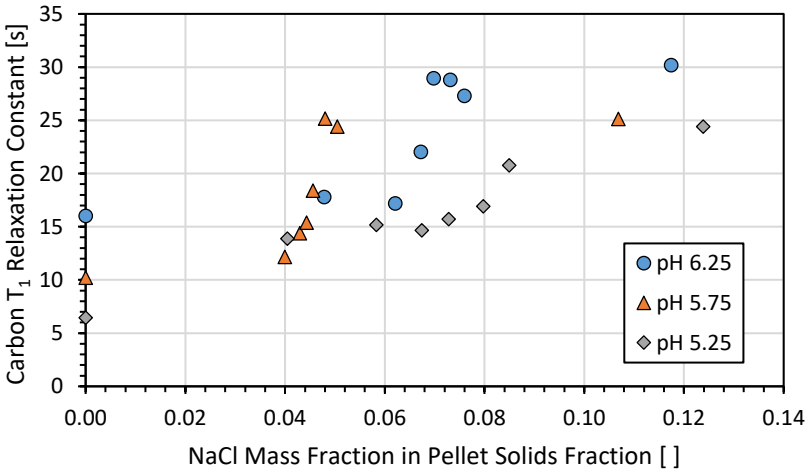

(c)

Figure 5-39: Carbon T_1 Relaxation Constant as a function of the modelled salt mass fraction in the (a) the whole gel, (b) the fluid fraction, and (c) the pellet solids fraction for pH 6.25, 5.75, and 5.25 gels treated with 20% NaCl-whey at 40 °C for 24 hours total brining time.

Figure 5-39 shows the increase in the T_1 relaxation constant with respect to any of the salt mass fraction in the whole gel, fluids fraction, or pellet fraction. The first two plots show a general increase in the T_1 relaxation constant with respect to mass fraction in the whole gel or gel fluid phases. However, it is the third plot that provides insight to the role of adsorption on the changing T_1 relaxation constant. The constant shows a rapid increase in value with respect to the salt mass fraction in the solids, with three distinct regimes observed for the pH treatments. While all three pH treatments achieve similar final T_1 relaxation constants and equilibrium salt mass fraction values in the solids, the rates of increase in the T_1 relaxation constants is fastest for the pH 5.75 gels, followed by the pH 6.25 and pH 5.25 gels. This finding indicates that the presence of salt, even in low mass fractions, yields a rapid change in the carbon backbone flexibility, probably due to the increased interactions or sodium-calcium ion exchange within the protein. The decrease in protein backbone flexibility with respect to salt adsorption, also explains the observed increase in gel firmness at the macro-scale with respect to brining time.

5.5 Conclusions

This chapter combined the image analysis techniques previously described in Chapters 2 and 3, with ion chromatography and modelling techniques to investigate salt uptake in renneted gels exposed to high and low salt brining conditions. Experiments showed the changing relative distribution of free fluid to dairy solids and the salt uptake behaviour in the fluid and solid fractions of three different gel pH values under two different brining conditions. Salt uptake was successfully modelled using a Fickian diffusion approach to describe the average salt uptake and modelling was completed to describe hypothesized adsorption behaviour between the diffusing salt and the para-casein matrix. Evaluation of preliminary ^{13}C NMR also provided insight to the changing "backbone" of the para-casein protein matrix upon interaction with salt. The next chapter will provide insight to the changing internal structure of the gels exposed to different brining conditions as a function of brining time and provide an approach to model the changing salted whey transport out of the gel.

Chapter 6 Evaluation and Modelling of Meso-Structure During Syneresis and Brining

6.1 Introduction

Control of curd meso-structure is important to the production of cheeses with desirable rheological and functional properties (Everett & Auty, 2017; Foegeding & Drake, 2007). While evaluation of meso-structure has been frequently used to evaluate a variety of dairy products at the latter stages of production, limited work has been conducted to evaluate the changing meso-structure of renneted milk gels during the most dynamic processes of cheesemaking. This has been due to an assortment of factors, particularly the rapid syneresis expulsion makes gels difficult to handle and evaluate using standard rheological or microscopy techniques (Fenoul, Le Denmat, Hamdi, Cuvelier, & Michon, 2008; Lucey, Tamehana, Singh, & Munro, 1998; Ong, Dagastine, Kentish, & Gras, 2011). However, understanding and modelling the changing curd meso-structure during the stages where the gel undergoes the most change, namely the syneresis and salting phases, may provide insight to the mechanisms regulating whey expulsion behaviours observed in freshly cut renneted gels and salted gels.

6.1.1 Gel Meso-structure Evaluation

Common methods to assess meso-structure in cheeses or cheese analogues consist of a combination of microscopy techniques, usually in conjunction with rheological analyses to provide insight between the meso-structural properties and the assessed functional or sensorial properties (El-Bakry & Sheehan, 2014; Everett & Auty, 2008). Confocal scanning laser microscopy (CSLM), scanning electron microscopy (SEM), and atomic force microscopy (AFM) are examples of microscopy techniques routinely used to assess meso-structure in food products, including cheeses and cheese analogues (Aguilera, 2005). Unfortunately, the nature of their operation usually restricts the real time evaluation of gels undergoing syneresis. Gels must have their structure essentially "frozen" in time for evaluation of the changing structure to occur. Flash freezing gels with liquid nitrogen meets this need, preventing the formation of ice crystals that would otherwise damage the structure. Freeze drying flash frozen gels provides a means to secure the structure without damaging it, allowing for assessment with SEM. Alternately, specific cryo-SEM techniques use a liquid nitrogen "slush" and other equipment such as vacuum transfer devices to assess frozen samples without requiring freeze drying (Ong et al., 2011).

6.1.2 Modelling Pressure Gradients Driving Syneresis

Limited work has been done to describe the induced pressure gradients driving whey expulsion during syneresis. A prevalent approach to understanding the pressure sources responsible for the syneresis observed in freshly cut, renneted curds was introduced by van Dijk (1982). This approach describes the total pressure driving syneresis as a function of the different pressure types on the gel, as shown in Equation 6-1.

$$p_{total} = p_s + p_g + p_p$$

Equation 6-1: Total pressure driving syneresis.

In Equation 6-1, p [Pa] is the pressure driving syneresis, and the subscripts of *total*, *s*, *g*, and *p* represent the total pressure in the gel, endogenous pressure, gravitational pressure, and external pressing pressure driving syneresis, respectively. The gravitational pressure is derived from the weight of the matrix pressing out the trapped whey within the gel, while the external pressure is produced via compression of the whole gel structure. The endogenous pressure describes the natural mechanisms causing the para-casein matrix to contract, thereby expelling the trapped whey out of the gel. Endogenous pressure has proven to be of interest to researchers assessing syneresis behaviour, but has yet to be determined outside of its order of magnitude due to its small value, of approximately 1 Pa (Fagan et al., 2017; Lucey et al., 1997b; van Dijk, 1982; van Dijk & Walstra, 1986; van Dijk, Walstra, & Geurts, 1979).

Assuming that the structure is isotropic, such that there is no variation in average porous structure with respect to dimension of evaluation or location within the gel, Poiseuille's law may be used to describe fluid flow through a cylindrical pore as a function of the driving pressure gradient. Poiseuille's law is shown in Equation 6-2, with Q [$m^3\ s^{-1}$] representing the volumetric flow rate and d [m] representing the diameter of the circular pore.

$$Q = -\frac{\pi d^4}{128\mu}\frac{dP}{dx}$$

Equation 6-2: Poiseuille's law describing volumetric flow through a single cylinder.

Poiseuille's law may also be used to describe flow through multiple circular tubes, as shown in Equation 6-3.

$$Q_{total\ pores} = -QA_{CS}n_A = -\frac{A_{CS}n_A\pi d^4}{128\mu}\frac{dP}{dx}$$

Equation 6-3: Adaption of Poiseuille's law for flow through multiple cylinders.

In Equation 6-3, $Q_{total\ pores}$ [$m^3\ s^{-1}$] represents the total volumetric flow rate through the pores, n_A [pores m^{-2}] number of pores per unit area, and A_{CS} [m^2] represents the cross-sectional area of the porous region. Dividing Equation 6-3 by the cross-sectional area of the porous region converts the equation from a volumetric flow rate to a flux, similar to what is described by Darcy's law in Equation 2-16. Therefore, the permeability describing flow through parallel circular pores may be described by Equation 6-4.

$$\kappa = \frac{n_A \pi d^4}{128}$$

Equation 6-4: Permeability equation for parallel circular pores.

Kozeny developed analytical solutions to describe permeability by using the Navier-Stokes equations to determine the fluid flow through pores (Bear, 2013). For straight, parallel pores, the permeability equation is shown in Equation 6-5.

$$\kappa = \frac{c\varepsilon^3}{s^2}$$

Equation 6-5: Kozeny permeability equation for parallel circular pores.

In Equation 6-5, c [dimensionless] represents the Kozeny constant shape factor (0.5 for circular pores), ε [dimensionless] represents the porosity of the structure, and s [m^{-1}] represents the specific surface of the pores. Porosity is calculated as the void volume divided by the total volume. Specific surface is calculated as the total pore interface area divided by the total volume. The more general Kozeny-Carman equation should be used to describe permeability in the case of non-cylindrical or tortuous pores, as shown in Equation 6-6.

$$\kappa = \frac{c\tau_h \varepsilon^3}{{s_0}^2(1-\varepsilon)^2}$$

Equation 6-6: Carman-Kozeny permeability equation for general flow through a porous network.

In Equation 6-6, s_0 [m^{-1}] represents the Carman-specific surface and τ_h [dimensionless] represents the hydraulic tortuosity of the pores. The Carman-specific surface is calculated as specific surface divided by the volume fraction of the non-porous media (equivalent to 1-ε). The hydraulic tortuosity is defined in Equation 6-7.

$$\tau_h = \left(\frac{L_{min}}{L_s}\right)^2$$

Equation 6-7: Tortuosity equation.

In Equation 6-7, L_{min} [m] is the minimum distance for contiguous transport along a tortuous path and L_s [m] is the straight path length.

The previous three chapters have focused upon evaluating the bulk transport of salt and whey into and out of renneted milk gels but have not investigated the changing microstructure of gels undergoing natural, bulk syneresis or osmotic pressure differential induced syneresis from brining conditions. The purpose of this chapter is to present a new method to evaluate and model the changing porous meso-structure to describe the permeability and calculate the pressure gradient driving the observed whey expulsion behaviours. The following sections provide the experimental design and results from experiments where gels underwent regular syneresis or osmotic pressure differential induced syneresis due to exposure to 2.5% or 20% NaCl-whey brining conditions.

6.2 Experimental Design

An experiment was designed to evaluate the changing internal meso-structure of gels undergoing syneresis during regular bulk syneresis conditions, and under two different brining conditions to create different induced osmotic pressure differential conditions. The experiment combined the previously described whey expulsion models in sections 3.4, 4.4.2, and 4.4.3 with SEM imaging and modelling techniques to provide a new approach for estimating the pressure gradient behaviours driving syneresis under different conditions.

6.2.1 Experimental Material Preparation

Milk, rennet, whey, imaging apparatus, and dialysis tubing preparation was conducted following the procedures described in sections 3.2.1 through 3.2.4 for pH 5.75 milk gels. Brine for pH 5.75 gels were prepared to evaluate salt uptake under high salt (20% NaCl-whey brine) and low salt (2.5% NaCl-whey brine) conditions using the procedure detailed in section 4.2.2.

6.2.2 Sample Gel Preparation and Evaluation

Tests were designed to evaluate the average changing internal structure of individual gels undergoing bulk syneresis or brining at different points in time. Gels evaluated under regular, bulk syneresis conditions freely underwent syneresis, as described in section 3.2.5 until their designated sampling times. Images were captured of the gels before the onset of syneresis and at the time of sample collection to confirm adherence to the net gel contraction and whey expulsion behaviour observed in sections 3.4.2 and 3.4.3. Samples were removed

from the whey in duplicate at 20, 40, 60, 90, 120, 150, and 1440 minutes to evaluate the general meso-structural changes as a function of syneresis time at 40 °C.

All gels evaluated under brining conditions were poured, set, and allowed to undergo regular bulk syneresis for two hours at 40 °C, before being transferred to brines, as described in section 4.2.2. Images of the gels were captured before the onset of syneresis, after two hours of regular syneresis for the brined gels to confirm adherence to the net gel contraction and whey expulsion behaviour observed in sections 3.4.2 and 3.4.3, and at the sampling time. No additional images were captured as the models for syneresis had previously been established in sections 3.4, 4.4.2, and 4.4.3. Samples were removed from brining conditions in duplicate at 15, 30, 45, 60, 90, 120 and 1440 minutes to evaluate the changes in the internal gel structure as a function of brining time at 40 °C with either 2.5% NaCl-whey solution or 20% NaCl-whey solution.

All gels sampled were gently removed from their respective dialysis tubes via a combination of pouring and use of tweezers to minimize gel structure damage. The freed gels were immediately frozen via immersion in approximately 50 mL of liquid nitrogen (-196 °C) until completely frozen and approximately 90% of the liquid nitrogen had evaporated. Frozen gels were stored in -40 °C freezers until undergoing freeze drying. Samples were freeze dried and stored at room temperature before undergoing analysis with SEM. Although cryo-SEM techniques would have been preferable for reducing risk of ice crystal formation or other artefacts which could affect SEM images, the dynamic nature of gels undergoing rapid syneresis, lack of access to a cryo-slushing station, and the limited access to the SEM, forced the use of simpler methods to prepare samples with care taken to limit the effect of ice crystal or artefact formation.

6.2.3 Scanning Electron Microscopy

Freeze dried gel samples were prepared for scanning electron microscopy by fracturing the gels approximately in half along natural fault lines to show the inner cross-sectional porous regions of the gel. Fractured samples were secured to aluminium stubs using double-sided tape and silver-based adhesive paint and sputter coated to a thickness of approximately 100 nm with gold using a Baltec SCD 050 sputter coater. Five SEM images were captured with a FEI Quanta 200 Environmental scanning electron microscope (Oregon, USA) at an accelerating voltage of 25 kV, at five randomly selected sites on the interior of the sample

surface for each sample. Images were captured under low contrast and brightness conditions to allow for greater flexibility in image analysis using MATLAB®.

6.3 Analysis Techniques

6.3.1 Scanning Electron Microscopy Image Analysis

Image pre-processing with MATLAB® started with the cropping of the SEM image and performing a transformation of the lightness of the pixels using histogram equalization followed by *imcomplementing* and filling in holes. The whole process was repeated once more before converting the image to binary using a threshold value. A structured disk element was established and used to perform a morphological opening on the binary image consisting of an erosion followed by a dilation. This process was conducted to smooth the edges of the gel image and remove possible errors due to slight differences in thresholding and lighting effects, smoothing features on the order of 0.2 μm or less. Assessment of each pore was conducted using the *regionprops* function and all properties for each pore, including area and perimeter, were converted from pixel-based units to micron-based units and stored in a table for ease of analysis. Pores within certain area ranges were also graphed using different colour outlines on the binary SEM image to provide a visual cue to the number and relative location of differently sized pores. The MATLAB® code used and the figures from a complete example run is included in Appendix F for reference.

The porosity from each image was determined by summing the entire area of the porous regions and dividing it by the image area. The specific surface was calculated by summing the perimeters of all the pores and dividing that value by the non-porous area of the image. The equations used to solve for porosity, specific surface, and the adapted specific surface of the pores are shown in Equations 6-8, 6-9, and 6-10, respectively.

$$\varepsilon = \frac{\sum_{i=1}^{i} A_{p,i}}{A}$$

Equation 6-8: Porosity equation as a function of pore areas in the total area of the 2D image.

$$s = \frac{\sum_{i=1}^{i} p_i}{A}$$

Equation 6-9: Specific surface equation as a function of pore perimeters total area in 2D images.

$$s_0 = \frac{s}{1-\varepsilon} = \frac{\sum_{i=1}^{i} p_i}{A(1-\varepsilon)}$$

Equation 6-10: Adapted specific surface equation relative to solids area in 2D images.

In Equations 6-8, 6-9, and 6-10, $A_{p,i}$ [m^2] represents the cross-sectional area of each pore, A [m^2] represents the image area, and p_i [m] represents the perimeter of each pore shown in the image. Evaluation of the relative pore size distribution was also conducted by evaluating pores sizes via the equivalent circular diameter, as shown in Equation 6-11 where the equivalent circular pore diameters is reported as $D_{equiv\text{-}circ}$ [μm].

$$D_{equiv-circ} = \sqrt{\frac{4A_p}{\pi}}$$

Equation 6-11: Equivalent circular pore diameter equation.

6.3.2 Statistical Analysis of Gel Porosity and Specific Surface Value

The calculated porosity and specific surface values were assessed using one-way ANOVA to determine if there were any statistically significant differences between the pH 5.75 un-brined and the two brining conditions tested, within 95% confidence.

6.3.3 Modelling the Average Induced Pressure Gradient Driving Syneresis

The porosity and Carman-specific surface values were fitted with a biexponential model to describe the porous contraction behaviour, specifically in the case where two different mechanisms may be governing the porous contraction mechanics. The porosity and Carman-specific surface equations fitted to the data are presented in Equation 6-12 and 6-13, respectively.

$$\varepsilon = A_\varepsilon + B_\varepsilon e^{-p_{1,\varepsilon}t} + C_\varepsilon e^{-p_{2,\varepsilon}t}$$

Equation 6-12: Biexponential model for average internal porosity.

$$s_0 = A_{s0} + B_{s0} e^{-p_{1,s0}t} + C_{s0} e^{-p_{2,s0}t}$$

Equation 6-13: Biexponential model for Carman-specific surface values.

In Equation 6-12, A_ε [dimensionless] is the equilibrium porosity, B_ε and C_ε [dimensionless] are the amplitude for the long-term dominating rate constant and short-term dominating rate constant for the porosity model, $p_{1,\varepsilon}$ and $p_{2,\varepsilon}$ [s^{-1}] are long-term dominating rate constant and the short-term dominating rate constant for the porosity model. In Equation 6-13, A_{s0} [m^{-1}] is the equilibrium Carman-specific surface, B_{s0} and C_{s0} [m^{-1}] are the amplitude for the long-term dominating rate constant and short-term dominating rate constant for the Carman-specific surface model, $p_{1,\varepsilon}$ and $p_{2,\varepsilon}$ [s^{-1}] are long-term dominating rate constant and the short-term

dominating rate constant for the Carman-specific surface model. The porosity and Carman-specific surface data are fitted using the MATLAB® code presented in Appendix B.

Other properties such as the calculated intrinsic permeability and the estimated pressure gradient driving syneresis were also modelled for each treatment. This was done by combining the porosity and Carman-specific surface models with the equations presented in section 6.1.2. Permeability requires the knowledge of the tortuosity of the porous network. Unfortunately, the tortuosity of the network could not be determined via image analysis techniques. The hydraulic tortuosity analytical model used in this chapter was developed by Duplessis and Masliyah (1991) using a volume-averaging approach to describe the tortuous pathways in isotropic, granular media. This model presents the hydraulic tortuosity as a function of the porosity, as shown in Equation 6-14.

$$\tau_h = \frac{\varepsilon}{1 - (1 - \varepsilon)^{2/3}}$$

Equation 6-14: Hydraulic tortuosity equation.

Equation 6-14 provides a starting approach for estimating the hydraulic tortuosity when an empirical relationship cannot be established. It should be noted that Vogt et al. (2015) have found different tortuosity values for finished cheddars and mozzarella melted under different temperatures using proton NMR, which may provide another means to evaluate pore tortuosity. Permeability was modelled by substituting Equations 6-12, 6-13, and 6-14 into Equation 6-6 for their corresponding variables. Assessment of the average pressure gradient driving syneresis reassembles Darcy's law to solve for the pressure gradient. This rearrangement is shown in Equation 6-15, where $J_{w,p}$ [m^3 m^{-2} s^{-1}] represents the whey flux through the porous regions.

$$\left(\frac{dP}{dx}\right)_{Est} = \frac{J_{w,p}\mu}{\kappa} = \frac{J_{w,p}\mu {s_0}^2 (1-\varepsilon)^2}{c\tau_h \varepsilon^3}$$

Equation 6-15: Estimated pressure gradient driving syneresis.

The whey flux through the porous regions was calculated by dividing the whey expulsion models shown in sections 4.4.4 by the fitted porosity model, Equation 6-12.

6.4 Results and Discussion

6.4.1 Meso-Structural Contraction

6.4.1.1 Statistical Analysis of the Results

One-way ANOVA was conducted to determine if there were any statistical differences between the porosities and Carman-specific surface values from the regular syneresis treatment, the 20% NaCl-whey brining treatment, and the 2.5% NaCl NaCl-whey brining case for pH 5.75 gels. A simplified view of the statistically significant differences as determined from one-way ANOVA is shown in Table 6-1 and 6-2, respectively.

Table 6-1: One-way ANOVA statistically significant differences in porosity values from gels undergoing different brining conditions after two hours of regular syneresis, within 95% confidence. NS = No statistically significant difference, S = significant difference.

Treatment	Regular Syneresis	2.5% NaCl-whey	20% NaCl-whey
Regular Syneresis	-	S	S
2.5% NaCl-whey	S	-	S
20% NaCl-whey	S	S	-

Table 6-2: One-way ANOVA statistically significant differences in Carman-specific surface values from gels undergoing different brining conditions after two hours of regular syneresis, within 95% confidence. NS = No statistically significant difference, S = significant difference.

Treatment	Regular Syneresis	2.5% NaCl-whey	20% NaCl-whey
Regular Syneresis	-	NS	NS
2.5% NaCl-whey	NS	-	S
20% NaCl-whey	NS	S	-

There was a statistically significant difference in porosity data collected during each treatment beginning at two hours after the onset of syneresis (and the start of the brining case) between each treatment, within 95% confidence. Results indicate that there were only statistically significant differences in the Carman-specific surface values between the brining treatments from the data collected beginning two hours after the onset of syneresis and the start of the brining treatment, within 95% confidence. This finding indicates that although the porosity values may have been significantly different between the different induced osmotic pressure differential treatments, the reported Carman-specific surface values were comparable except between the 2.5% and 20% NaCl-whey brining treatments, indicating similar pore properties such as size distribution.

6.4.1.2 Bulk Regular Syneresis

Figures 6-1 and 6-2 show the changing porosity and Carman-specific surface values with respect to syneresis time, respectively. Both figures include the fitted biexponential models from Equations 6-12 and 6-13 to describe the changing structure, respectively.

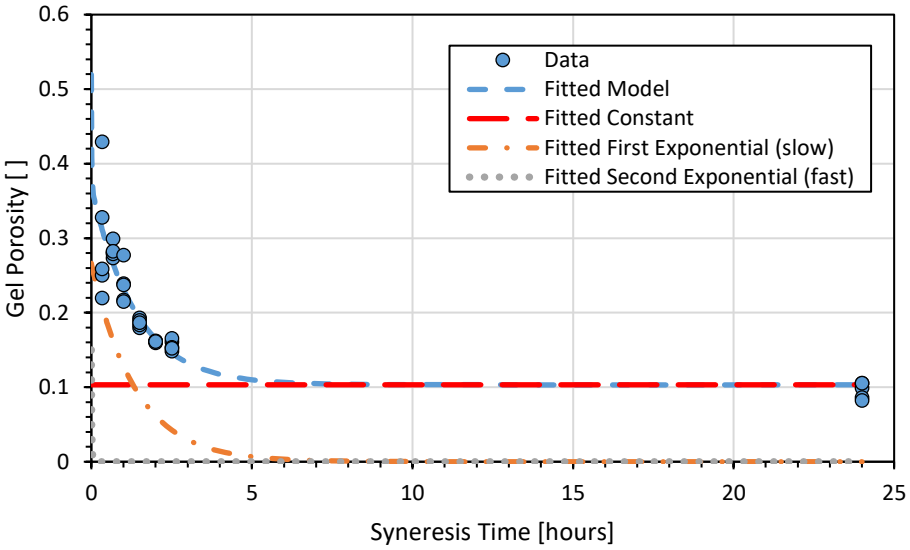

(a)

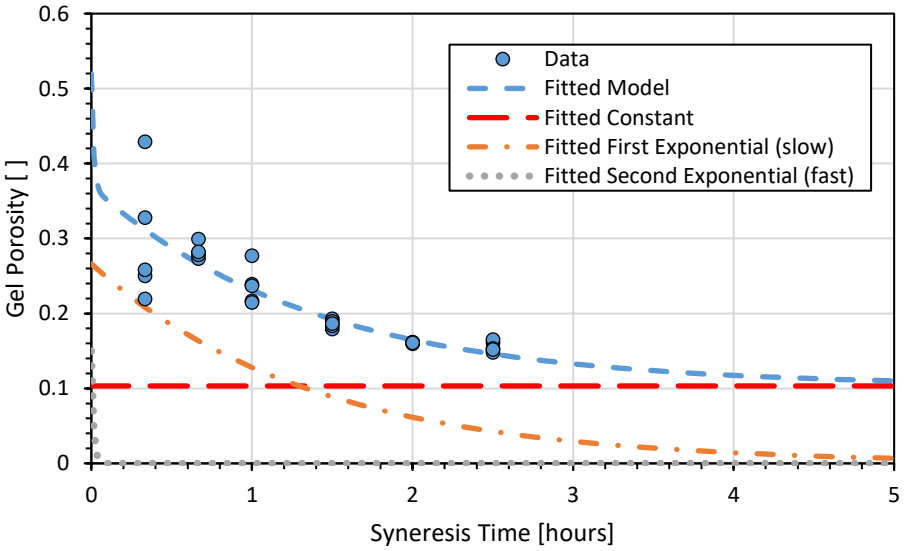

(b)

Figure 6-1: Gel porosity and fitted model as a function of syneresis time for (a) the whole experiment and (b) the first five hours of the experiment after onset of syneresis for five SEM images of the internal structure of pH 5.75 gels held at 40 °C and freeze dried for analysis for each time point.

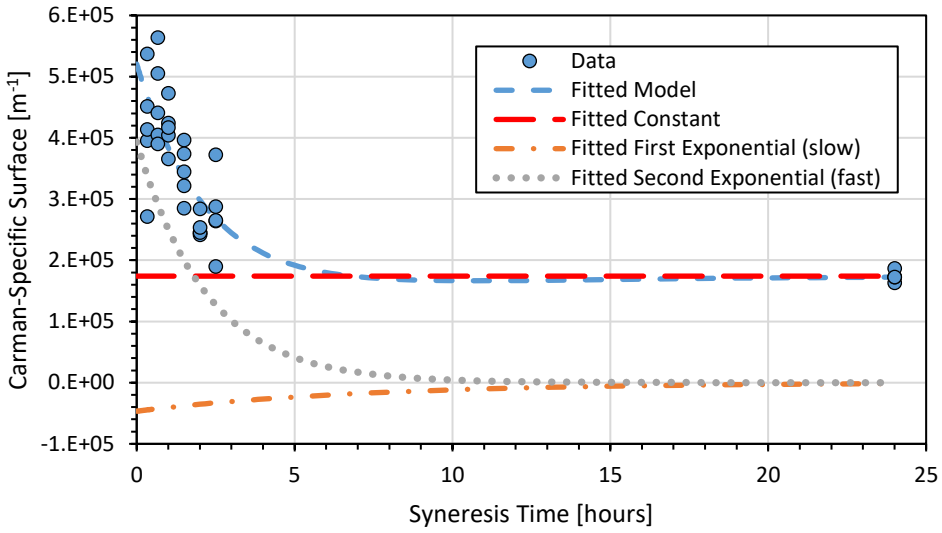

(a)

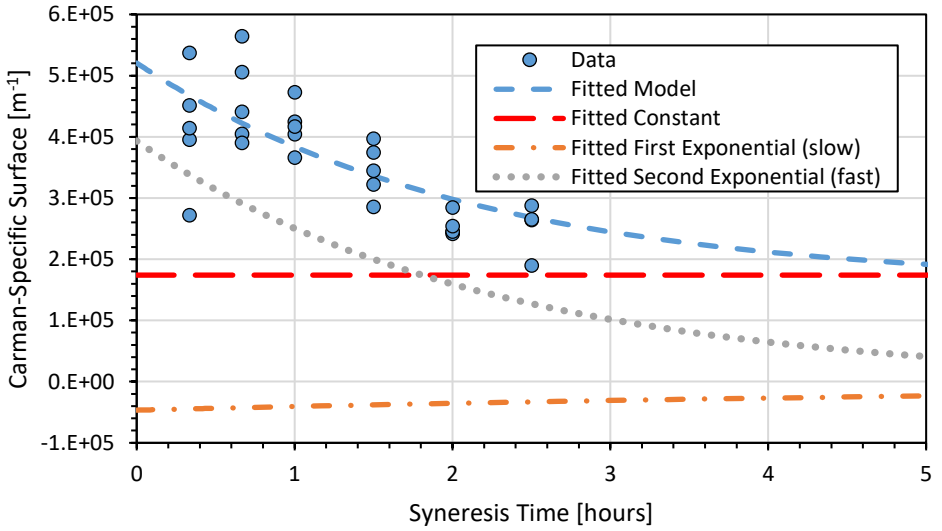

(b)

Figure 6-2: Gel Carman-specific surface and fitted model as a function of syneresis time for (a) the whole experiment and (b) the first five hours of the experiment after onset of syneresis for five SEM images of the internal structure of pH 5.75 gels held at 40 °C and freeze dried for analysis for each time point.

Figures 6-1 and 6-2 demonstrate the different meso-structural changes occurring within the porosity and Carman-specific surface values, respectively for pH 5.75 gels undergoing regular syneresis at 40 °C. The fitted models for the porosity and Carman-specific surface values are shown in Tables 6-3.

Table 6-3: Fitted linear and nonlinear variables in Equation 6-12 for gel porosity and Equation 6-13 for Carman-specific surface values with fitting statistics of root mean square error and coefficient of determination for each model under regular syneresis conditions for pH 5.75 gels.

Model of Interest	A [ ] OR [m^{-1}]	B (slow) [ ] OR [m^{-1}]	C (fast) [ ] OR [m^{-1}]	p_1 (slow) [s^{-1}]	p_2 (fast) [s^{-1}]	RMSE [ ] OR [m^{-1}]	r^2 [ ]
Porosity [ ]	0.103	0.266	0.150	2.04E-04	0.0211	0.0343	0.817
Carman-specific Surface [m^{-1}]	1.74E+05	-4.66E+04	3.93E+05	3.83E-05	1.25E-04	6.47E+04	0.705

The porosity values change according to a binomial exponential contraction, with limited error associated with the fitting. However, the Carman-specific surface values are not as well fitted by the biexponential model. This is due to the larger degree of variability in Carman-specific surface values, as shown in Figure 6-2. The high variability is expected as the pore sizes combine or are reduced due to the loss of free whey. The "fast" exponential section is predicted to be representative of a fast mechanism driving syneresis, likely the short distance between the gel surface and the whey-rich interior of the gel, while the second exponential describes the slow reorganizing of the porous structure in response to the rapid whey loss. Figure 6-3 provides insight to the changing equivalent circular diameter of the pores with respect to the changing syneresis time.

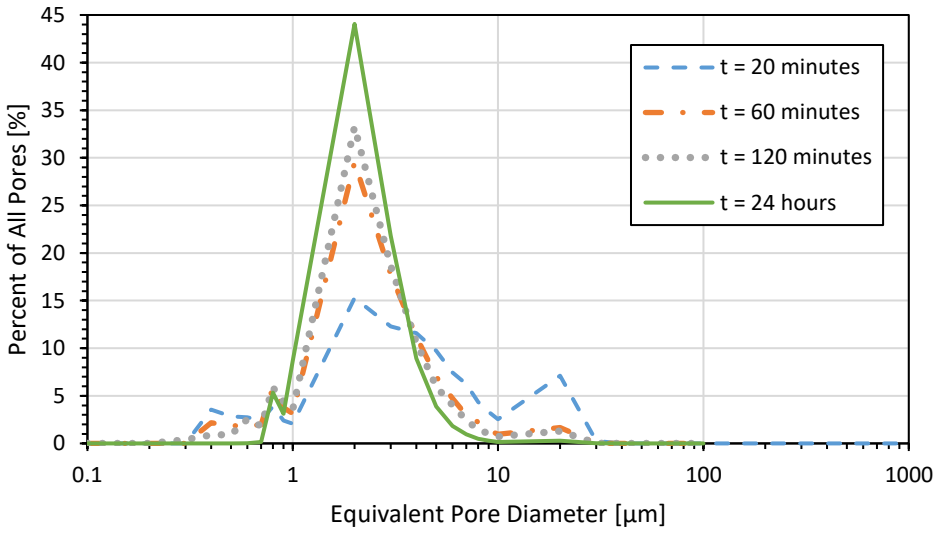

Figure 6-3: Equivalent circular pore diameter distribution of all pores analysed via SEM image analysis at 20, 60, 120, and 1440 minutes after the onset of syneresis for pH 5.75 gels undergoing regular syneresis at 40 °C.

Figure 6-3 shows the changing distribution of internal pore sizes with respect to time. Most pores become more uniform and achieve equivalent circular diameters within one to ten microns as syneresis time increases. This is a realistic finding as the meso-structure gradually contracts the larger pores into smaller, more evenly distributed pores as the amount

of free whey in the gel decreases. The next two sub-sections provide insight to the effect of induced osmotic pressure differentials and the presence of salt on the changing meso-structure.

6.4.1.3 Low Salt Induced Osmotic Pressure Syneresis

Figures 6-4 and 6-5 show the changing porosity and Carman-specific surface values for pH 5.75 gels exposed to 2.5% NaCl-whey brining conditions after undergoing regular syneresis for two hours with respect to osmotic pressure differential induced syneresis time, respectively. Both figures include the fitted biexponential models from Equations 6-12 and 6-13 to describe the changing structure, respectively.

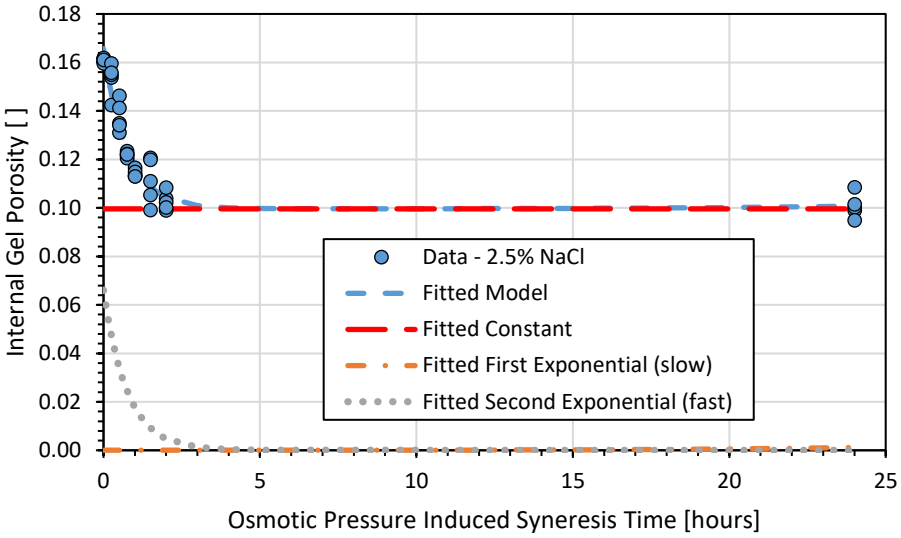

(a)

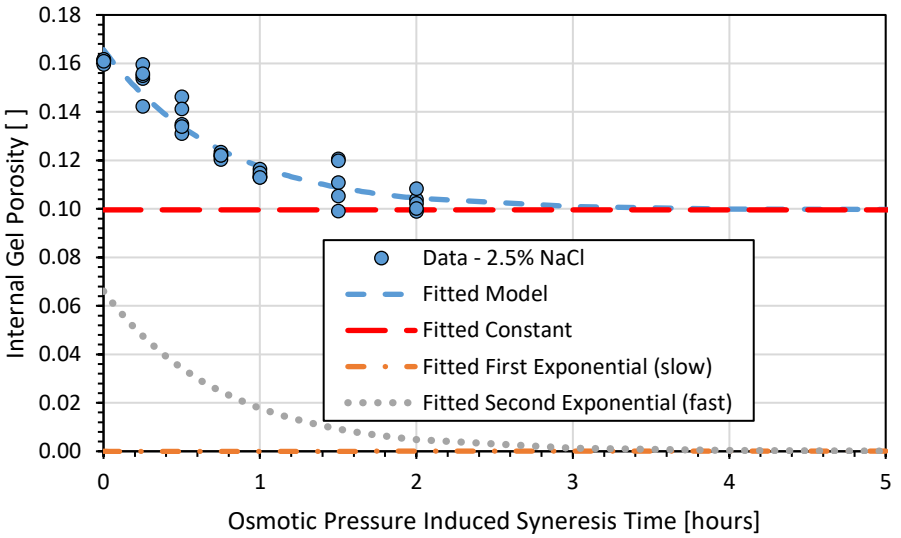

(b)

Figure 6-4: Gel porosity and fitted model as a function of osmotic pressure induced syneresis time for (a) the whole experiment and (b) the first five hours of the experiment after of exposure to 2.5% NaCl-whey conditions for five SEM images of the internal structure of pH 5.75 gels held at 40 °C and freeze dried for analysis for each time point.

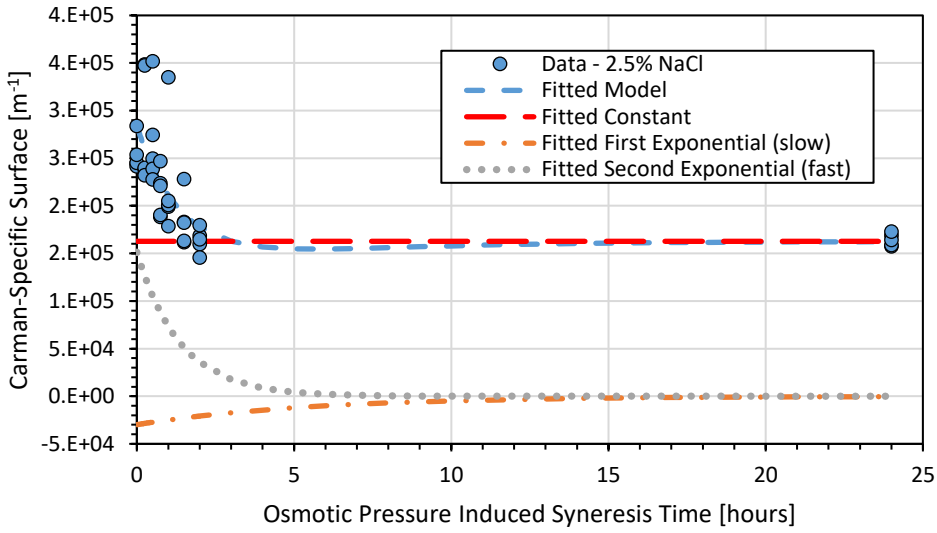

(a)

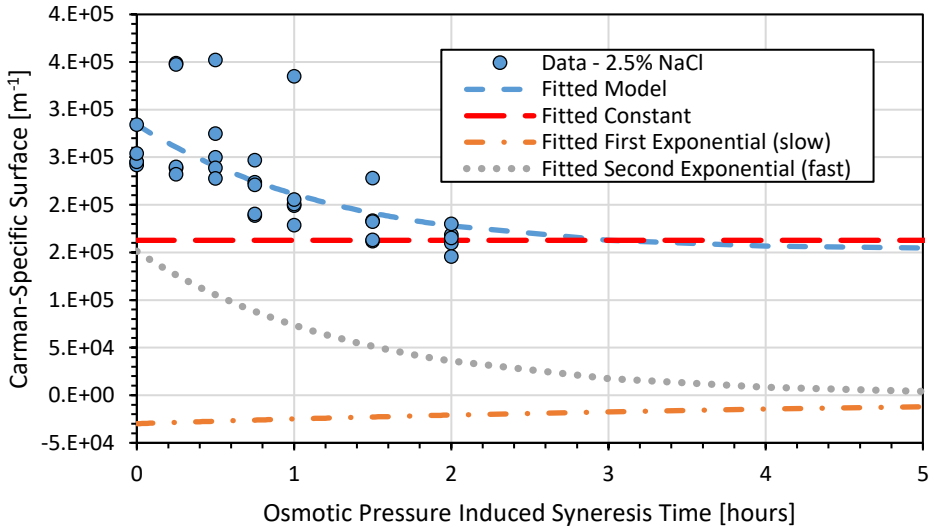

(b)

Figure 6-5: Gel Carman-specific surface and fitted model as a function of osmotic pressure induced syneresis time for (a) the whole experiment and (b) the first five hours of the experiment after of exposure to 2.5% NaCl-whey conditions for five SEM images of the internal structure of pH 5.75 gels held at 40 °C and freeze dried for analysis for each time point.

Figures 6-4 and 6-5 demonstrate the different meso-structural changes occurring within the porosity and Carman-specific surface values, respectively. The fitted models for the porosity and Carman-specific surface values are shown in Tables 6-4.

Table 6-4: Fitted linear and nonlinear variables in Equation 6-12 for gel porosity and Equation 6-13 for Carman-specific surface values with fitting statistics of root mean square error and coefficient of determination for each model for pH 5.75 gels undergoing 2.5% NaCl-whey brining conditions at 40 °C.

Model of Interest	A [ ] OR [m^{-1}]	B (slow) [ ] OR [m^{-1}]	C (fast) [ ] OR [m^{-1}]	p_1 (slow) [s^{-1}]	p_2 (fast) [s^{-1}]	RMSE [ ] OR [m^{-1}]	r^2 [ ]
Porosity [ ]	0.0996	1.02E-05	0.0661	-5.51E-05	3.64E-04	6.12E-03	0.931
Carman-specific Surface [m^{-1}]	1.63E+05	-2.99E+04	1.51E+05	5.00E-05	2.00E-04	4.18E+04	0.500

The porosity values were well fitted with the biexponential model, while the Carman-specific surface values were poorly fitted with the biexponential model. The poor fitting is due to the larger degree of variability in Carman-specific surface values, as shown in Figure 6-5. The high variability is predicted to be due in part to the induced osmotic pressure gradient that increases the rate of whey expulsion, as described in section 4.4.2.2. The extremely low values for the slow exponential function indicate that the internal porosity could be sufficiently modelled using a single exponential. Figure 6-6 provides insight to the changing equivalent circular diameter of the pores with respect to the time exposed to the 2.5% NaCl-whey brine.

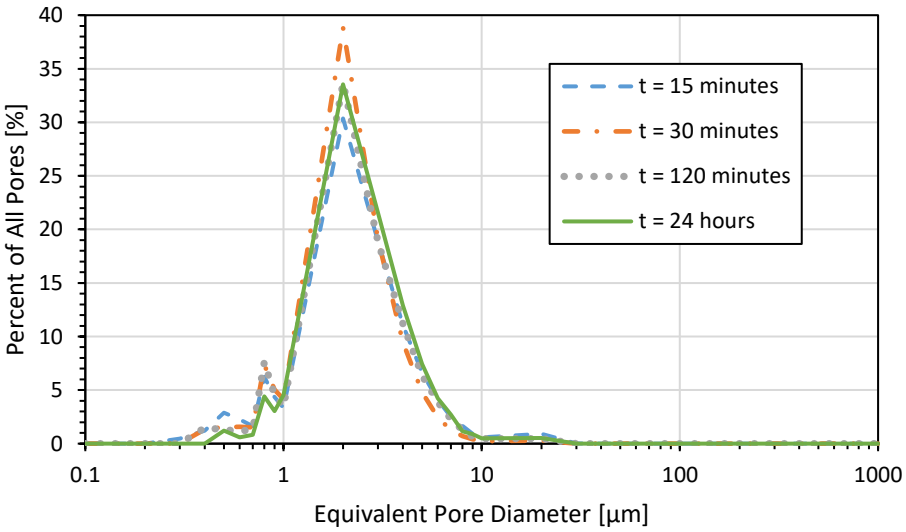

Figure 6-6: Equivalent circular pore diameter distribution of all pores analysed via SEM image analysis at 15, 30, 120, and 1440 minutes after the onset of exposure to 2.5% NaCl-whey for pH 5.75 gels undergoing regular syneresis at 40 °C, after undergoing regular syneresis for two hours.

The pore diameter distribution shown in Figure 6-6 follows the same general contraction behaviour observed in Figure 6-3, where the pore size distribution is dominated by pores with equivalent circular diameters in the one to ten-micron range. This is reasonable as most of the whey is lost during the initial two hours of regular syneresis, causing the pores to contract

to uniform sizes within a one to ten-micron diameter range. However, the gels exposed to the 2.5% NaCl-whey brine did have a slightly higher percentage of the total pores within the five to ten-microns diameter range. This created the statistically significant difference in the gel porosity between the unsalted and 2.5% NaCl-whey treatment, but no statistically significant differences in the Carman-specific surface values, due to the high degree of variability in those values from both the unsalted and 2.5% NaCl-whey treatments.

6.4.1.4 High Salt Induced Osmotic Pressure Syneresis

Figures 6-7 and 6-8 show the changing porosity and Carman-specific surface values for pH 5.75 gels exposed to 20% NaCl-whey brining conditions after undergoing regular syneresis for two hours with respect to osmotic pressure differential induced syneresis time, respectively. Both figures include the fitted biexponential models from Equations 6-12 and 6-13 to describe the changing structure, respectively.

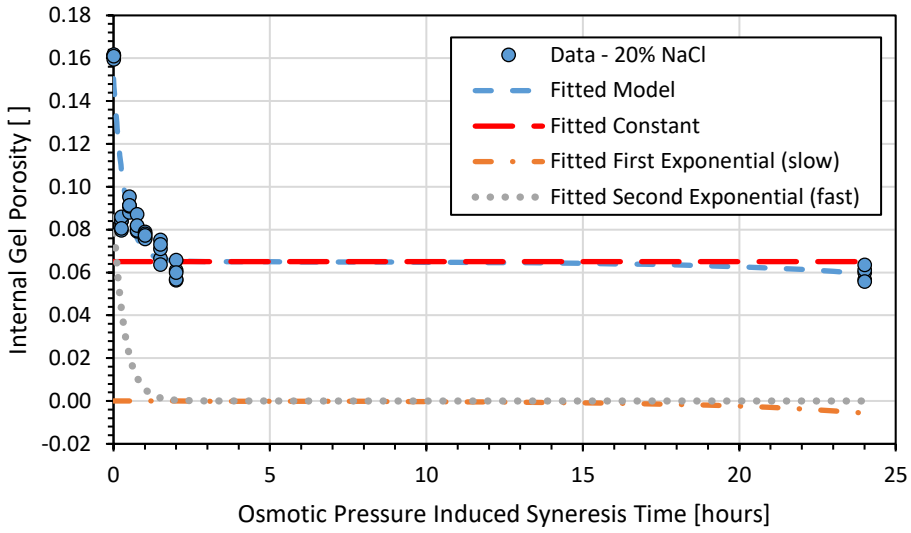

(a)

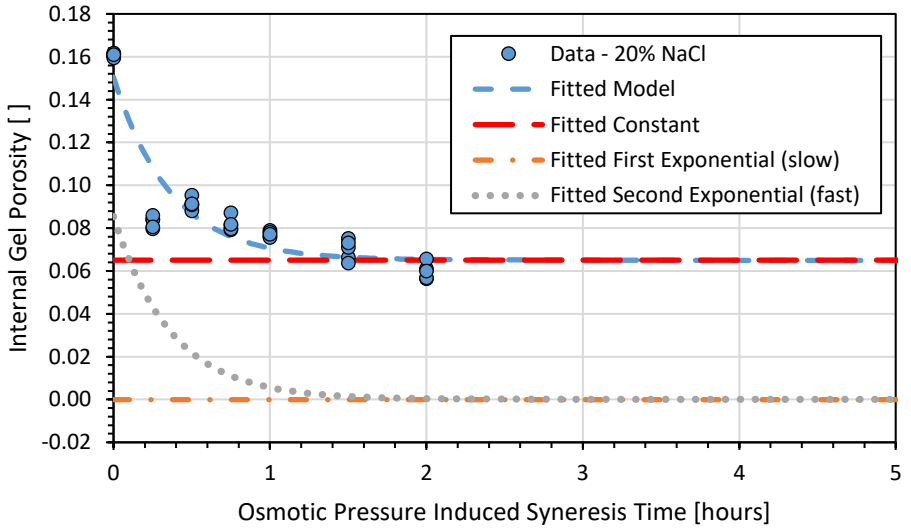

(b)

Figure 6-7: Gel porosity and fitted model as a function of osmotic pressure induced syneresis time for (a) the whole experiment and (b) the first five hours of the experiment after of exposure to 20% NaCl-whey conditions for five SEM images of the internal structure of pH 5.75 gels held at 40 °C and freeze dried for analysis for each time point.

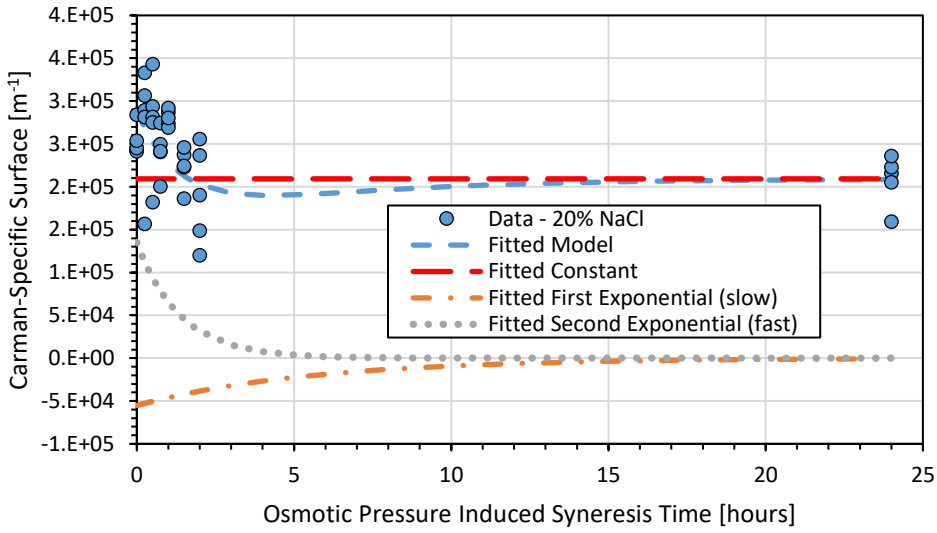

(a)

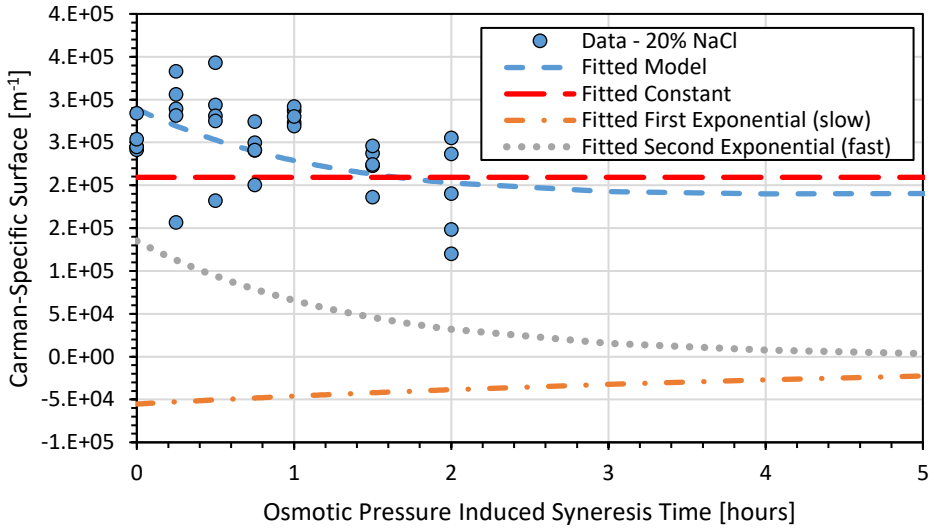

(b)

Figure 6-8: Gel Carman-specific surface and fitted model as a function of osmotic pressure induced syneresis time for (a) the whole experiment and (b) the first five hours of the experiment after of exposure to 20% NaCl-whey conditions for five SEM images of the internal structure of pH 5.75 gels held at 40 °C and freeze dried for analysis for each time point.

Figures 6-7 and 6-8 demonstrate the different meso-structural changes occurring within the porosity and Carman-specific surface values, respectively. The fitted models for the porosity and Carman-specific surface values are shown in Tables 6-5.

Table 6-5: Fitted linear and nonlinear variables in in Equation 6-12 for gel porosity and Equation 6-13 for Carman-specific surface values with fitting statistics of root mean square error and coefficient of determination for each model for pH 5.75 gels undergoing 20% NaCl-whey brining conditions at 40 °C.

Model of Interest	A [ ] OR [m^{-1}]	B (slow) [ ] OR [m^{-1}]	C (fast) [ ] OR [m^{-1}]	p_1 (slow) [s^{-1}]	p_2 (fast) [s^{-1}]	RMSE [ ] OR [m^{-1}]	r^2 [ ]
Porosity [ ]	0.0582	0.0392	0.140	2.28E-04	0.0296	0.0101	0.971
Carman-specific Surface [m^{-1}]	2.093E+05	-5.52E-04	1.350E+05	5.00E-05	2.00E-04	3.64E+04	0.420

The porosity values were well fitted with the biexponential model, while the Carman-specific surface values were poorly fitted with the biexponential model. Once again, the low value for the slow exponential in the porosity model indicates that the porosity model may be sufficiently modelled with only one exponential. This finding indicates that there may not be a second mechanism governing the changing overall porous contraction, and that the net contraction of the total porosity is only be due to the fast expulsion of whey from the structure. This finding implies that there may not be a strong mechanism governing "reorganisation" of the total porous area for the gel at equilibrium.

The poor fitting of the Carman-specific surface model is due to the larger degree of data, as shown in Figure 6-8. The high variability is predicted to be due in part to the induced osmotic pressure gradient that increases the rate of whey expulsion, as described in section 4.4.3.2. The slow exponential for the Carman-specific surface model indicates that although there is no observed second mechanism governing total porosity contraction, there is some redistribution of the pore sizes that occurs over a longer period as the gel approaches equilibrium. Figure 6-9 provides insight to the changing equivalent circular diameter of the pores with respect to the time exposed to the 20% NaCl-whey brine.

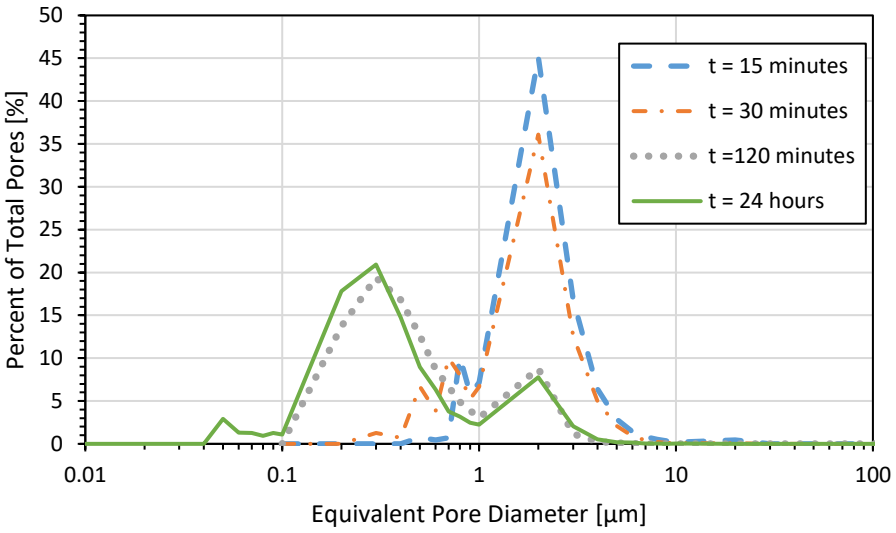

Figure 6-9: Equivalent circular pore diameter distribution of all pores analysed via SEM image analysis at 15, 30, 120, and 1440 minutes after the onset of exposure to 20% NaCl-whey for pH 5.75 gels undergoing regular syneresis at 40 °C.

The pore diameter distribution shown in Figure 6-9 shows a change in the pore diameter distribution, with pores undergoing significant changes in diameter between thirty minutes and two hours of exposure to the 20% NaCl-whey conditions. A shift in the pore diameter distribution favours the formation of pores within the 0.1 and one-micron size in the latter stages of brining conditions. This behaviour is unsurprising as the high induced osmotic pressure differential prompts a rapid increase in the rate of whey expulsion, causing a greater contraction of pores than pores exposed to lower induced osmotic pressure differentials. The next subsection compares the meso-structure contraction behaviours of all three treatments.

6.4.1.5 Comparison of Brining and Syneresis Treatments

Figures 6-10 and 6-11 show the changing porosity and Carman-specific surface value data and fitted models for each treatment, respectively.

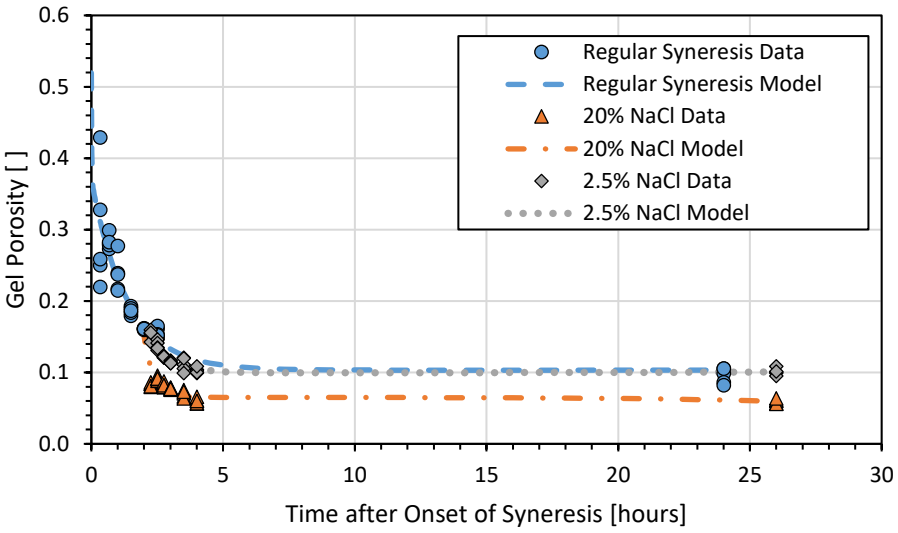

(a)

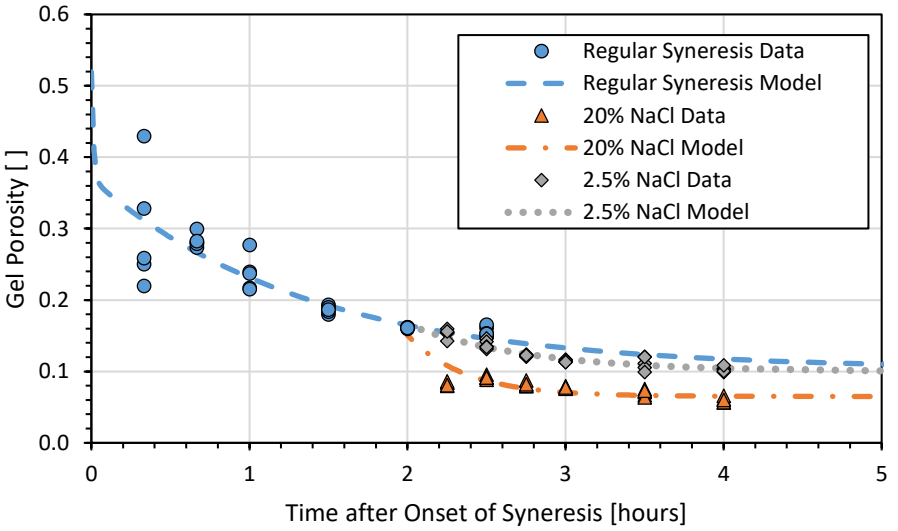

(b)

Figure 6-10: Gel porosity values and fitted models as a function of syneresis time for (a) the whole experiment and (b) the first five hours of the experiment after the onset of syneresis, with exposure to 20% NaCl-whey and 2.5% NaCl-whey conditions beginning two hours after the onset of syneresis for pH 5.75 gels at 40 °C syneresis temperature.

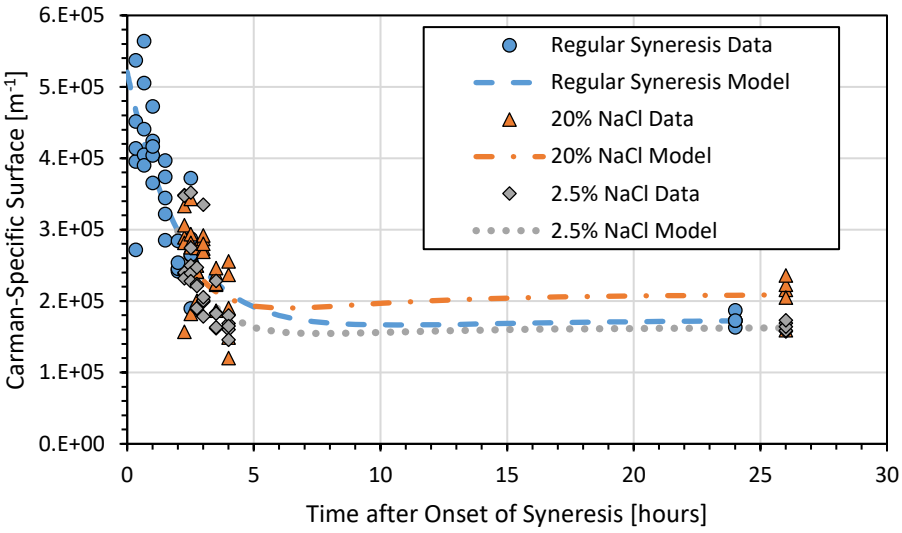

(a)

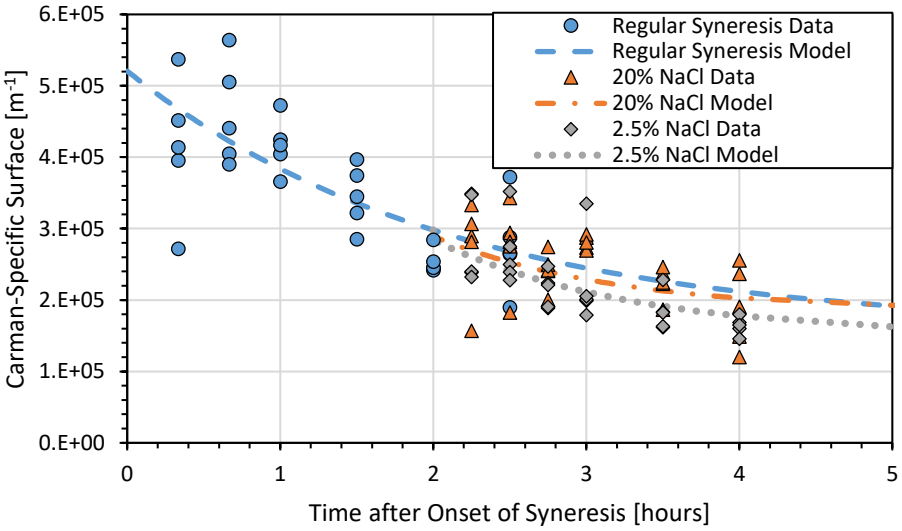

(b)

Figure 6-11: Gel Carman-specific surface values and fitted models as a function of syneresis time for (a) the whole experiment and (b) the first five hours of the experiment after the onset of syneresis, with exposure to 20% NaCl-whey and 2.5% NaCl-whey conditions beginning two hours after the onset of syneresis for pH 5.75 gels at 40 °C syneresis temperature.

Limited differences are observed between the regular syneresis and the 2.5% NaCl-whey brining treatment porosity or Carman-specific surface data, due to the high degree of data variability. Only the 20% NaCl-whey brining treatment produced a significant and clear differences from the other two treatments, especially in the gel porosity. It would therefore be unsurprising for the calculated pressure gradient driving syneresis for the 20% NaCl-whey treatment to produce significantly different values from the other two treatments. The following section uses the reported models describing the porosity and Carman-specific

surface values to estimate other flow parameters and pressure gradients governing whey expulsion.

6.4.2 Estimation of Tortuosity, Intrinsic Permeability, and Pressure Gradients

The first step to estimating the changing fluid flow properties in the gels is to convert the reported whey flux values from section 4.4 to whey flux from the whey-rich porous regions.

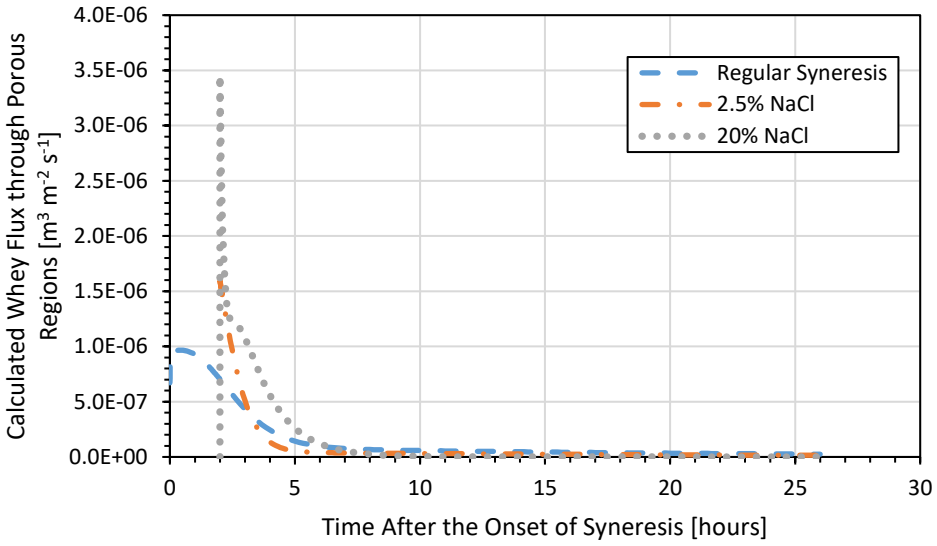

(a)

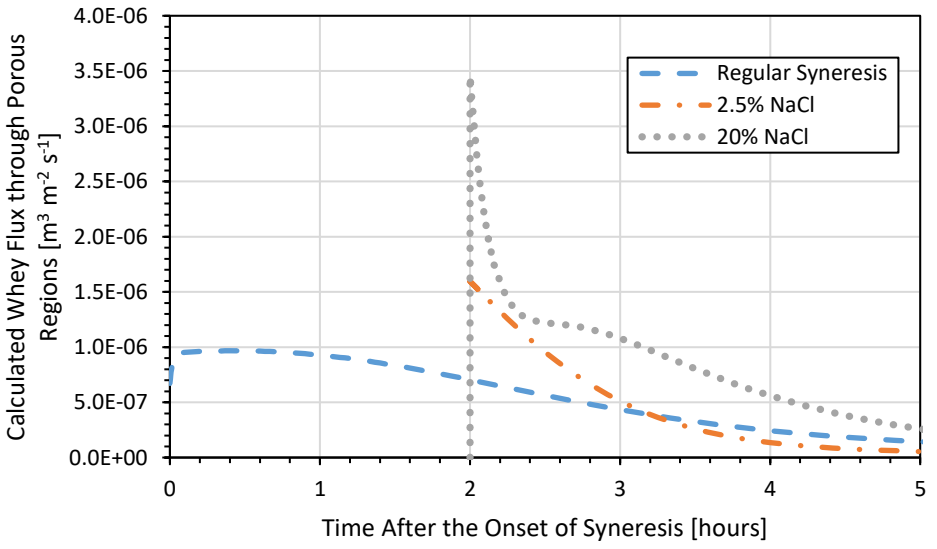

(b)

Figure 6-12: Simulated whey flux through porous region models as a function of syneresis time for (a) the whole experiment and (b) the first five hours of the experiment after the onset of syneresis, with exposure to 20% NaCl-whey and 2.5% NaCl-whey conditions beginning two hours after the onset of syneresis for pH 5.75 gels at 40 °C syneresis temperature.

Figure 6-12 shows how the changing porosity affects the calculated whey flux modelled in sections 4.4.2 and 4.4.3. The rapid reduction of the gel porosity in the 20% NaCl-whey

treatment increases the calculated whey flux through the porous regions, especially during the first thirty minutes of brining time. This is expected since the previously modelled whey flux was high due to the induced osmotic pressure differential.

Determination of the porous network's hydraulic tortuosity is not possible from the two-dimensional assessment of freeze-dried curd SEM images alone. Equation 6-14 was used to estimate the hydraulic tortuosity as a function of the modelled porosity in each treatment. The results are reported in Figure 6-13.

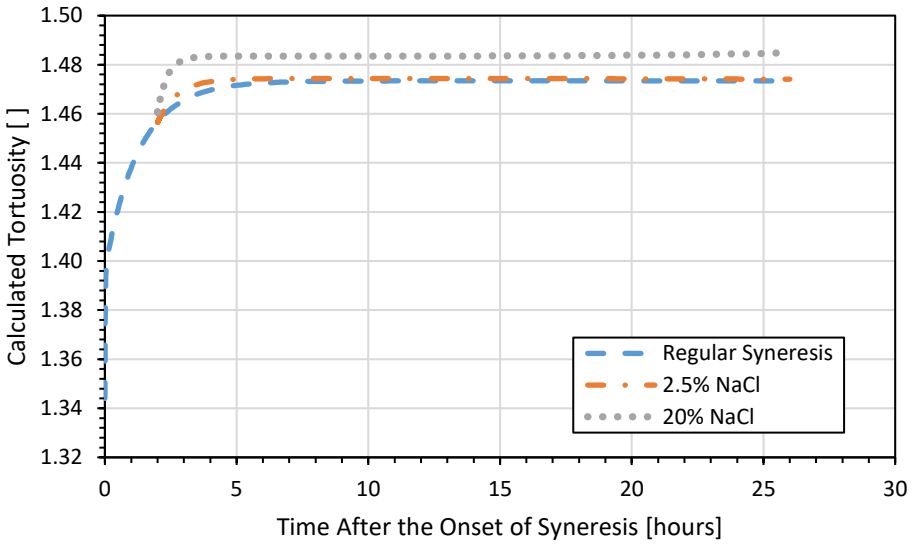

(a)

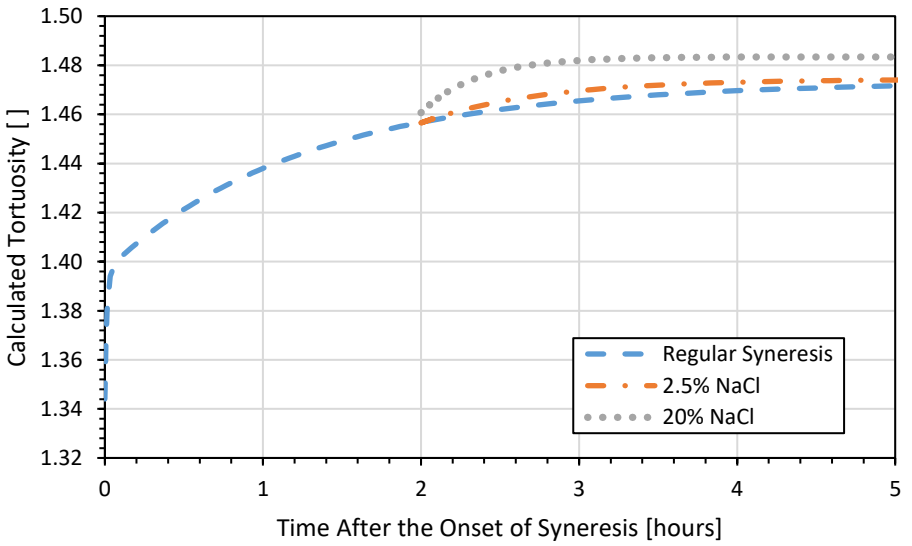

(b)

Figure 6-13: Simulated average hydraulic pore tortuosity models as a function of syneresis time for (a) the whole experiment and (b) the first five hours of the experiment after the onset of syneresis, with exposure to 20% NaCl-whey and 2.5% NaCl-whey conditions beginning two hours after the onset of syneresis for pH 5.75 gels at 40 °C syneresis temperature.

The calculated hydraulic tortuosity gradually increases as the porosity values decrease, with a possible reported hydraulic tortuosity range of between 1.0 and 1.5. These values are limited in scope and may require replacement with improved tortuosity models for biological structures. The modelled hydraulic tortuosity, Carman-specific surface, and porosity for each treatment were used with a circular shape factor of 0.5 and constant whey dynamic viscosity of 0.75 mPa s to calculate the Kozeny intrinsic permeability using Equation 6-6. The results are shown in Figure 6-14.

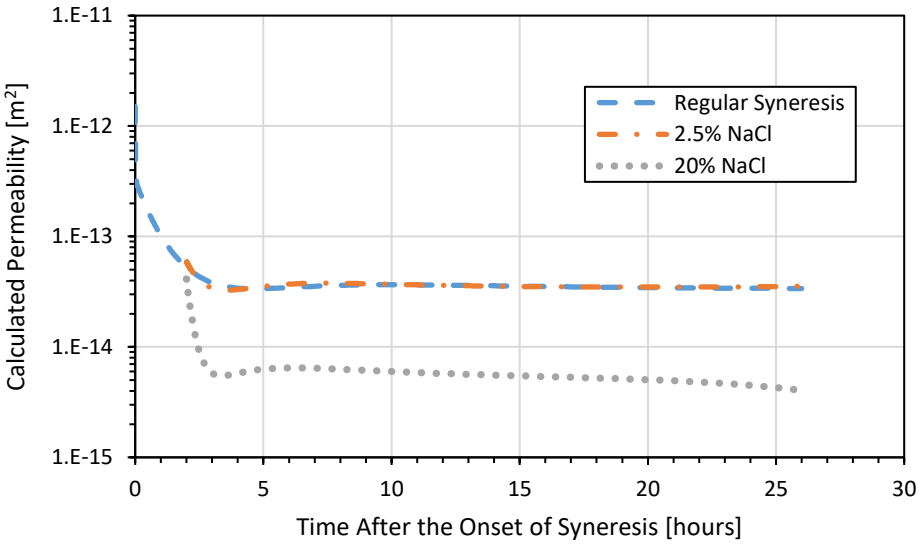

(a)

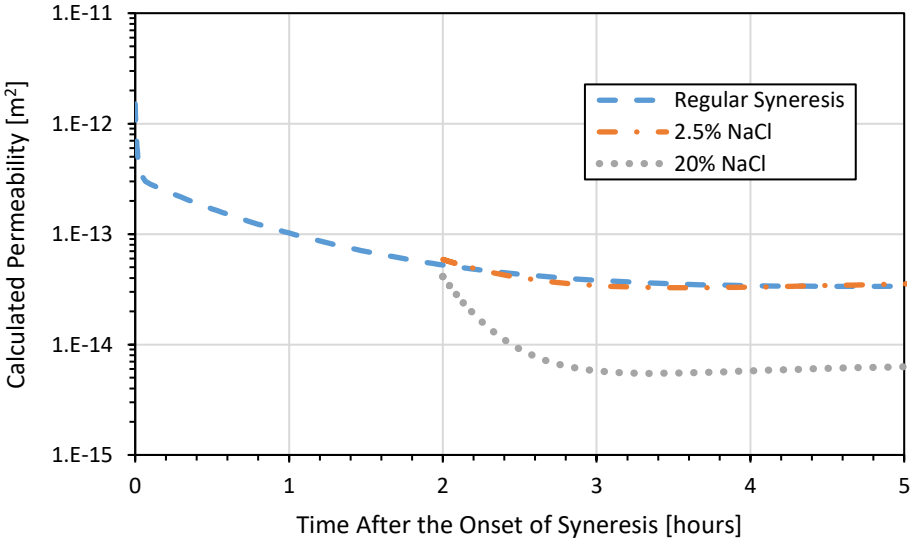

(b)

Figure 6-14: Simulated intrinsic permeability models as a function of syneresis time for (a) the whole experiment and (b) the first five hours of the experiment after the onset of syneresis, with exposure to 20% NaCl-whey and 2.5% NaCl-whey conditions beginning two hours after the onset of syneresis for pH 5.75 gels at 40 °C syneresis temperature.

Figure 6-14 shows the rapid reduction in the calculated intrinsic permeability of the gel structure for all treatments, with the 20% NaCl-whey treatment showing the greatest amount of change due to the rapid reduction of gel porosity. The porous structure of the gels undergoing the 2.5% NaCl-whey treatment produced similar permeability values to the regular syneresis permeability, as expected from the similar porosity and Carman-specific surface models. A similar rate of whey expulsion would therefore be expected from both the regular syneresis gels an the 2.5% NaCl-whey treatment gels, if the same pressure gradient driving syneresis was applied. The estimated pressure gradient driving syneresis was calculated using the intrinsic permeability and the porous area adjusted whey flux shown in Figure 6-12, using Equation 6-15. Figure 6-15 shows the estimated pressure gradient driving syneresis.

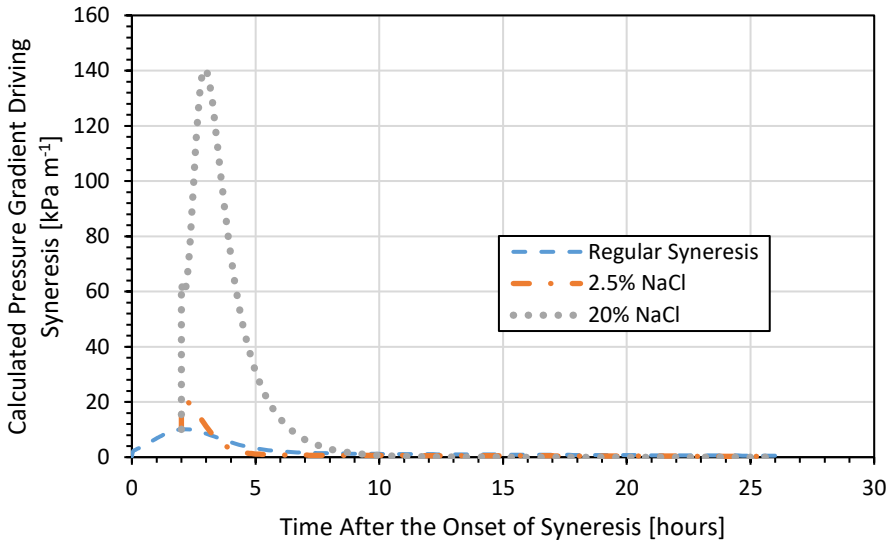

(a)

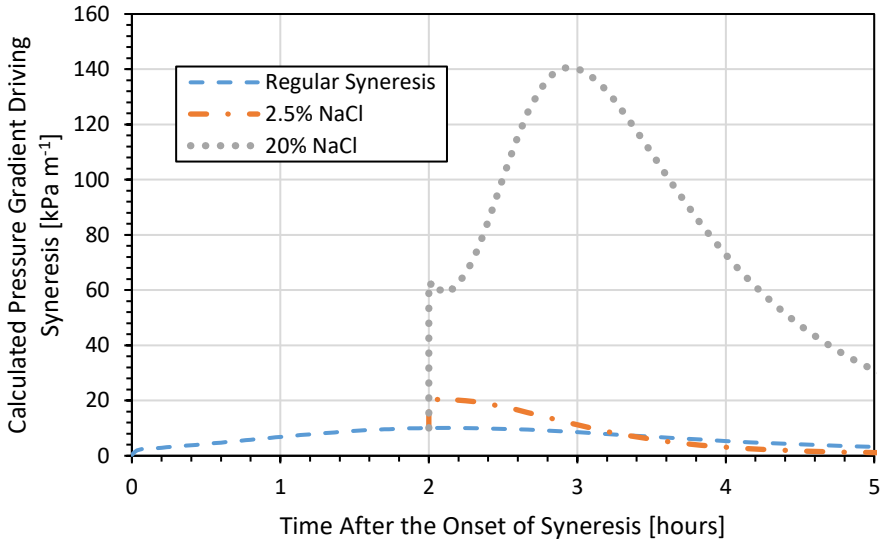

(b)

Figure 6-15: Simulated average pressure gradient models as a function of syneresis time for (a) the whole experiment and (b) the first five hours of the experiment after the onset of syneresis, with exposure to 20% NaCl-whey and 2.5% NaCl-whey conditions beginning two hours after the onset of syneresis for pH 5.75 gels at 40 °C syneresis temperature.

Figure 6-15 shows that the calculated pressure gradient driving syneresis gradually increases for the regular syneresis treatment for the first two hours of syneresis, before decreasing to values less than one tenth of the maximum pressure gradient at equilibrium. Assuming an average effective distance of five millimetres (approximately the average radius of gels undergoing regular syneresis within the first two hours of syneresis), the pressure driving the regular syneresis behaviour ranges between 1.67 and 50.5 Pa at the onset of syneresis and after two hours of regular syneresis. The slow increase in the pressure gradient is likely due

to the changing state of the gel and the changing strength of the intermolecular forces that govern the syneresis behaviour. This behaviour changes once enough whey has been expelled and a critical moisture concentration is achieved to attain equilibrium, reducing the pressure gradient to negligible levels.

The addition of the osmotic pressure induced differential from the 2.5% and 20% NaCl-whey treatments increases pressure gradient at the onset of exposure, before decreasing to 1.5% and approximately 0% of the maximum pressure gradient at equilibrium for the 2.5% and 20% NaCl-whey treatments, respectively. The pressure driving syneresis was calculated to range between 62.4 and 0.9 Pa after five minutes exposure to the 2.5% NaCl-whey and at equilibrium, respectively (assuming an average effective distance of 3.05 millimetres, reported in section 5.4.1.1). The pressure driving syneresis was calculated to range between 354 and 0 Pa after one hour of exposure to the 20% NaCl-whey and at equilibrium, respectively (assuming an average effective distance of 2.52 millimetres, reported in section and 5.4.2.1).

The changing driving pressure gradient is due to the presence of the induced osmotic pressure differential from the surface brine. While gels undergoing regular syneresis have only internal intermolecular forces govern whey expulsion behaviour, the addition of an osmotic pressure induced differential and the presence of salt ions that interact with the curd matrix affects the pressure gradient driving whey expulsion. As gels approach equilibrium (both of salt uptake and the whey expulsion), the pressure governing the syneresis behaviour approaches a negligible value. Another way to evaluate the changing pressure gradient driving syneresis is to observe the relationship between the average gel moisture content and both the intrinsic permeability and calculated pressure gradient, as shown in the next section.

6.4.3 Induced Pressure Gradients as a Function of Average Gel Moisture Content

The intrinsic permeability and pressure gradient driving syneresis may be evaluated with respect to the average gel moisture mass fraction. Figures 6-16 and 6-17 show the intrinsic permeability and pressure gradient with respect to the moisture mass fractions reported in sections 5.4.5, respectively.

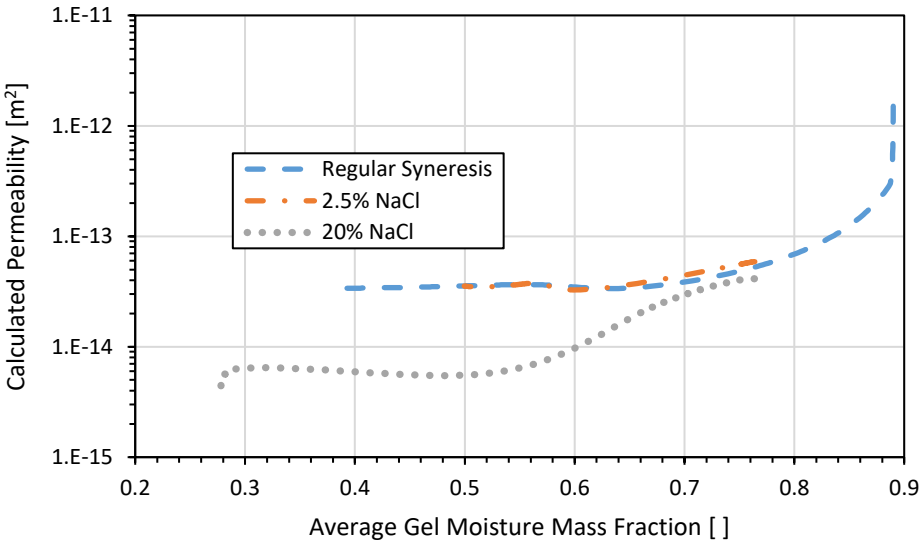

Figure 6-16: Simulated gel intrinsic permeability as a function of the average gel moisture mass fraction for pH 5.75 gels undergoing regular syneresis, 2.5% NaCl-whey, and 20% NaCl-whey brining treatments at 40 °C syneresis temperature.

Figure 6-16 shows the reduction of the gel intrinsic permeability as a function of the modelled average gel moisture mass fraction, where the fastest reduction in intrinsic permeability occurs during the early stages of syneresis when the gel undergoes the most contraction. Exposure to 2.5% NaCl-whey brine after two hours of regular syneresis continues the general intrinsic permeability reduction, achieving an equilibrium value beginning at approximately 0.65 moisture mass fraction. The 20% NaCl-whey brining treatment further reduces the equilibrium value of the intrinsic permeability, with equilibrium approximately achieved at 0.55 moisture mass fraction.

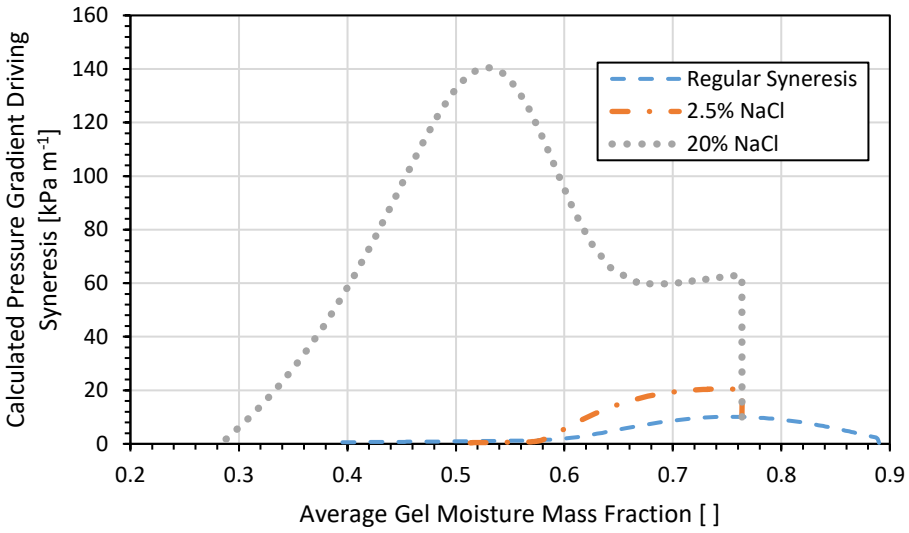

Figure 6-17: Simulated pressure gradient driving syneresis as a function of the average gel moisture mass fraction for pH 5.75 gels undergoing regular syneresis, 2.5% NaCl-whey, and 20% NaCl-whey brining treatments at 40 °C syneresis temperature.

Figure 6-17 shows that pressure gradient driving syneresis reaches its maximum value at approximately 0.75 moisture mass fraction for gels undergoing regular syneresis, before undergoing a gradual reduction to an equilibrium pressure gradient at approximately 0.6 moisture mass fraction. The 2.5% NaCl-whey treatment achieves a similar pressure gradient curve, with equilibrium being achieved at moisture mass fractions of approximately 0.58. The 20% NaCl-whey treatment shows an increase in the pressure gradient driving syneresis as the gel undergoes syneresis and meso-structural contraction, to a maximum pressure gradient at an average 0.53 moisture mass fraction. The pressure gradient undergoes rapid reduction as the gel approaches equilibrium after this moisture content is achieved, as a new equilibrium is established requiring minimal additional whey expulsion.

6.5 Conclusions

This chapter evaluated and modelled the internal meso-structure of pH 5.75 gels undergoing regular syneresis and osmotic pressure differential induced syneresis via exposure to 2.5% NaCl-whey and 20% NaCl-whey brining conditions. The fitted porosity and Carman-specific surface models were used with the Carman-Kozeny intrinsic permeability equation to assess the changing permeability of the gel as a function of the changing meso-structure. The permeability models were combined with the whey flux behaviours modelled in section 4.4.4 to estimate the pressure gradient driving syneresis. Results showed that exposure to high salt brining conditions significantly reduced the average porosity and pore properties within gels, leading to a higher calculated pressure gradient driving the syneresis behaviours previously

observed in Chapter 4. While there were several assumptions and limitations presented in this work, this exercise provided a new approach to evaluating the changing permeability of the gel meso-structure and estimating the pressure gradient driving syneresis using engineering principles. The next chapter combines the findings from Chapters 4 and 5 to present a comprehensive mathematical model to describe simultaneous salt uptake and whey expulsion for individual curds and its application to theoretical and real curd beds.

Chapter 7 Plant Experiment and Application of Mathematical Models

7.1 Introduction

Chapters 3 through 5 showed the complex whey expulsion and salt uptake behaviours of renneted milk gels exposed to differing brining conditions. The purpose of this chapter is to apply the models developed in those chapters to describe the proposed syneresis and salt uptake in different curd systems. Unlike the previous chapters, this chapter seeks to model salt uptake in dry salting conditions using the insight from the previous brine-based models. It also models the effects of curd size and relative shape on whey expulsion and salt uptake. These models are then related to the observed curd size distribution, salt content, and moisture content of curd samples collected from different beds of curds at an industrial cheesemaking facility.

7.2 Proposed Syneresis and Salt Uptake in Different Curd Sizes and Shapes

7.2.1 Adapting Brining Syneresis and Salt Uptake Models to Dry Salting Conditions

Chapters 3 through 5 provided a first stage in mechanistically modelling whey expulsion and salt uptake behaviour in renneted milk gels exposed to different brining conditions. The gels assessed and their models, however, have little application on their own for modelling the variety of different curd sizes and types undergoing syneresis and salt uptake. Furthermore, the brining techniques used to model salt uptake and osmotic pressure differential induced syneresis behaviours do not produce the exact same conditions as experienced with dry salting. That means that care must be taken to adjust the Fickian diffusion derived models to the rapidly changing surface brine conditions created during dry salting. The following sections seek to adapt the existing models describing whey expulsion and salt uptake for differently sized and shaped gels, while also providing a step-wise approach to combining whey expulsion and diffusion modelling under dry salting conditions for individual gels.

7.2.2 Curd Shape Surface Area and Volume Relationships

Chapters 3 through 5 have evaluated the whey expulsion and salt uptake behaviours of pH 6.25, 5.75, and 5.25 gels with starting volumes of ten millilitres in long, cylindrical shapes that would undergo relatively uniform contraction. These models are important to evaluating general whey expulsion behaviour but may be limited in application to very similar gels structures. It is therefore necessary to establish a method to apply the previously established whey expulsion models to gel systems with different starting volumes or shapes. This is achieved by ascertaining the relationship between the surface area and volume of any three-

dimensional shape that undergoes uniform contraction. A simple way of establishing the relationship may be completed using Equation 7-1.

$$SA_{Shape} = K_{Shape}(V_{Shape})^{2/3}$$

Equation 7-1: Gel surface area and volume relationship using a shape factor, K.

In Equation 7-1, SA_{Shape} [mm^2] is the surface area for any three-dimensional shape that undergoes relatively uniform contraction, V_{Shape} [mm^3] is the volume of that shape, and K_{Shape} [dimensionless] is the shape factor that defines the surface area and volume relationship for each specific shape. Plotting the surface area as a function of the curd volume taken to the two-thirds power yields a straight line fit to determine the value of the constant. Spherically shaped curds that would undergo uniform contraction in all dimensions are easily calculated to have a fitting constant of $(36\pi)^{1/3}$, the smallest possible surface area to volume ratio for a unit volume. Fortunately, the experimental gels tested in this thesis have also been shown to undergo relatively consistent contraction behaviour. Figure 7-1 uses the surface area and volume data from all the gels tested in the third and fourth chapter.

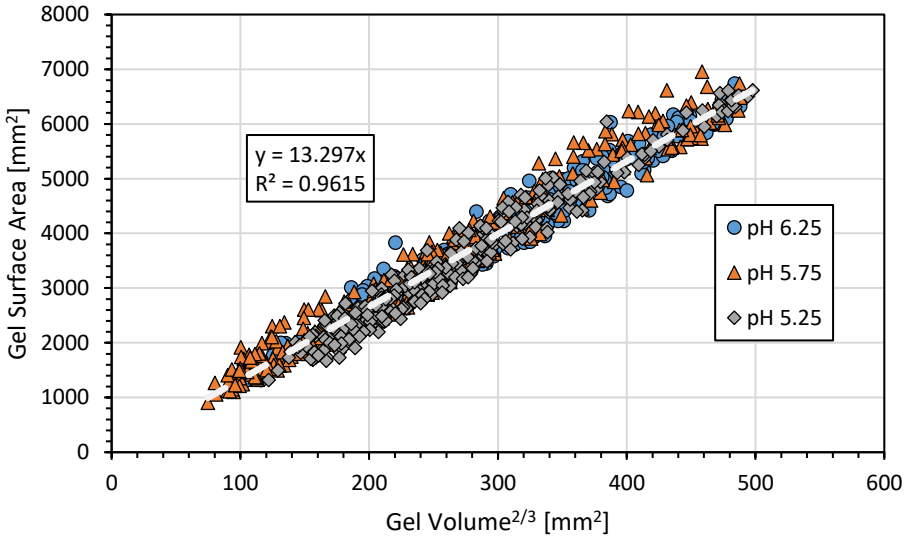

Figure 7-1: Experimental gel surface area and volume relationship for all tested gels, with the linear fitting included as a white dashed line. The high degree of fit (r^2 = 0.962 and RMSE = 270 mm^2) shows that Equation 7-1 was successfully used to describe the gel volume and surface area relationship, with slope of 13.3 representing the shape factor, *K*.

The fitted shape constant for the gels evaluated in this thesis was 13.3, indicating that the experimental gel shapes previously tested consistently have a larger surface area to volume ratio than other standardized shapes like spheres or cubes, providing a more extreme representative of possible real-world curd shapes. Most curd shapes produced during the

cheesemaking process end up having irregular ellipsoidal shapes, frequently with pitting and uneven surfaces. Figure 7-2 provides a visual example of the shape irregularity in curds sampled from an industrial cheese salting belt.

Figure 7-2: Monterey jack curd samples removed midway along the salting belt (approximately fifteen minutes into salting time) and separated onto the 6.35 mm sieve. The curds show irregular ellipsoidal-like shapes, indicating that the general shape factor relating the surface area and volume likely exists between the extremes of the experimentally evaluated gels in Chapters 3 through 5, and perfectly spherical curds.

Figure 7-2 suggests that the most appropriate shape factor to describe most curd shapes may lie between the experimental shape factor and the spherical shape factor. Therefore, evaluating and modelling syneresis and salt uptake using the long cylindrical curd shape previously evaluated and theoretical spherical curds provide two extremes for modelling curd beds, with the exact performance for each curd and curd bed performing somewhere in between.

7.2.3 Regular Syneresis Modelling

Modelling regular syneresis with differently shaped gels or starting gel sizes is achieved by adapting the flux definition in Equation 3-13 with Equation 7-1. The rate of whey expulsion previously used in calculating flux is equal and opposite to the rate of gel volume contraction, thereby maintaining a volume balance. The new equation for describing whey flux as a function of the gel volume is shown as Equation 7-2.

$$J_w = \frac{1}{SA_{Gel}}\frac{dV_w}{dt} = \frac{-1}{K_{Gel}{V_{Gel}}^{2/3}}\frac{dV_{Gel}}{dt}$$

Equation 7-2: Whey flux equation as a function of gel volume and shape factor.

Equation 7-2 may be solved to determine the volume of the gel at any time, *t*, since the whey flux values may be calculated from the previously developed models. The gel volume at any point during regular syneresis may be calculated by solving Equation 7-3.

$$\frac{-1}{V_{Gel}^{\,2/3}}\,dV_{Gel} = K_{Gel} J_w dt$$

Equation 7-3: Changing gel volume as a function of previously described whey flux and gel shape factor.

The change in the volume of the gel at any time point allows for the successful calculation of the whey volume or mass expelled and moisture content loss. Figures 7-3 and 7-4 show the expected changing gel volume and moisture mass fraction of gels undergoing regular syneresis at 40 °C for two hours, with the whey flux model parameters detailed in Tables 3-1 and 3-2. The hypothetical gels shown have three different starting gel sizes and two different shape factor constants to demonstrate the effect of starting gel size and shape factor on whey expulsion behaviour, assuming that the whey flux model is applicable to all the gels.

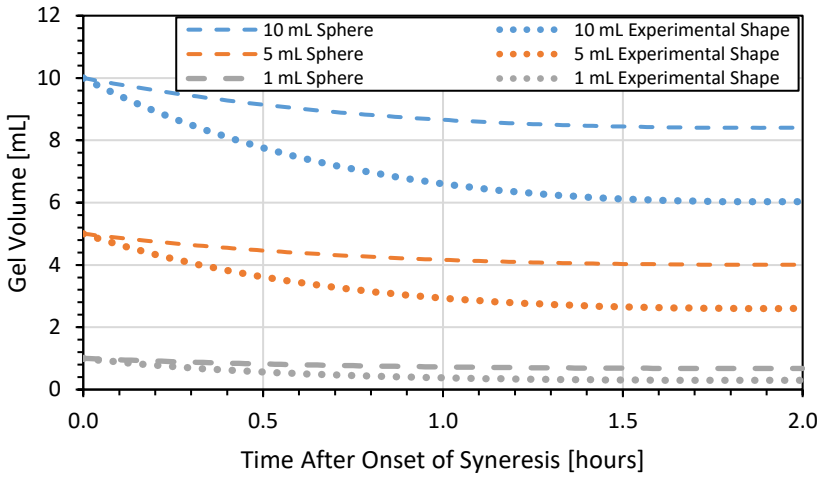

(a)

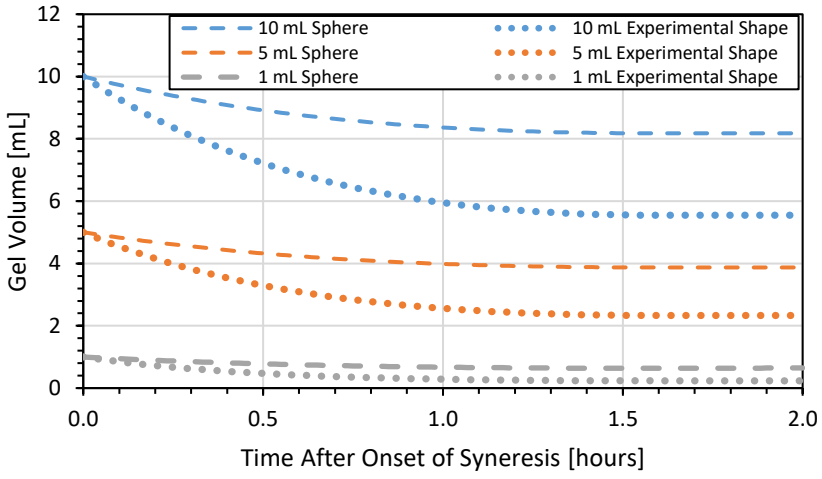

(b)

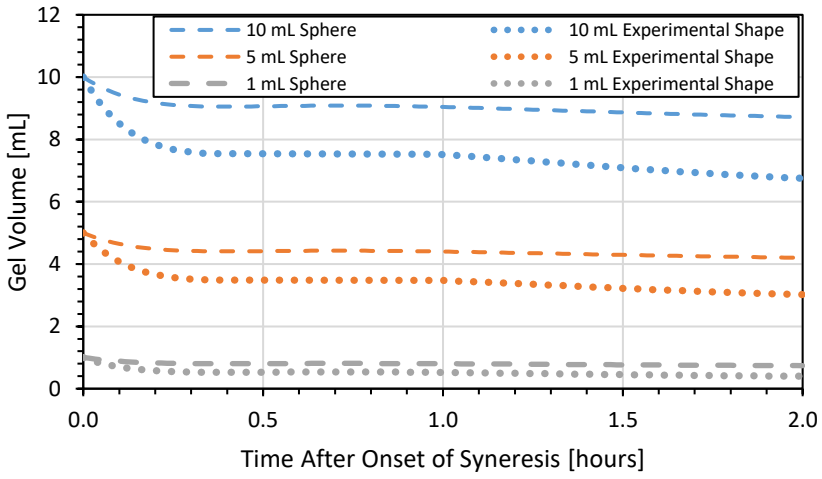

(c)

Figure 7-3: Simulated gel volume with respect to regular syneresis time at 40 °C for spherically shaped and long, cylindrical experimentally shaped gels with (a) pH 6.25, (b) pH 5.75, and (c) pH 5.25 values.

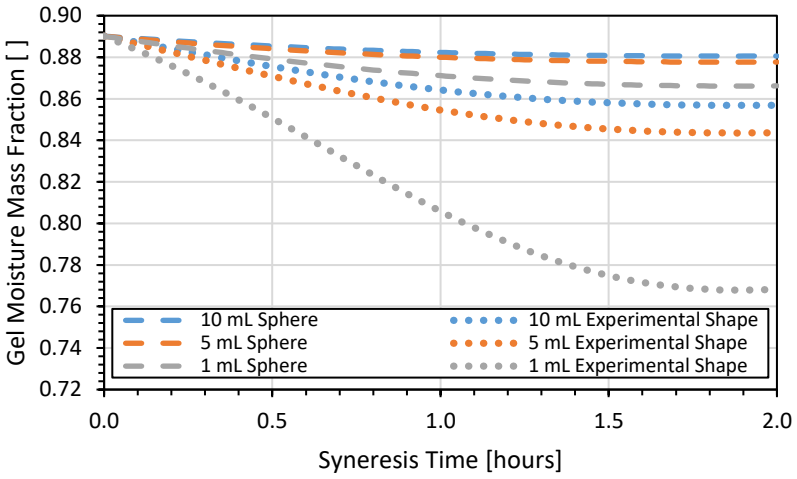

(a)

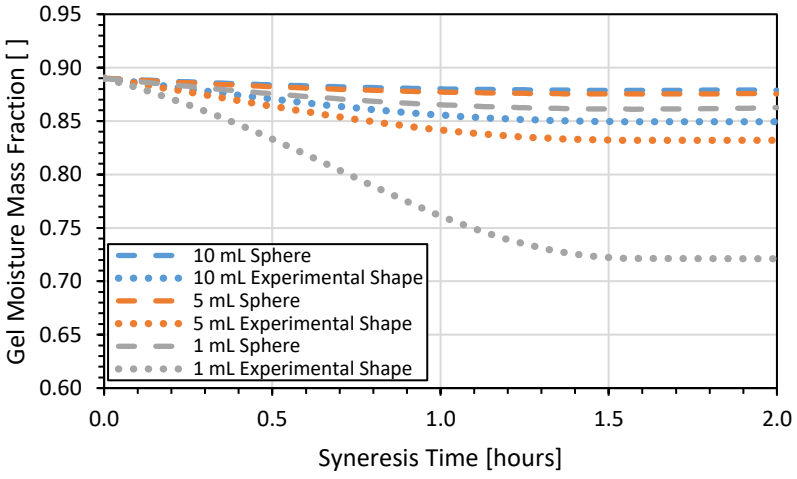

(b)

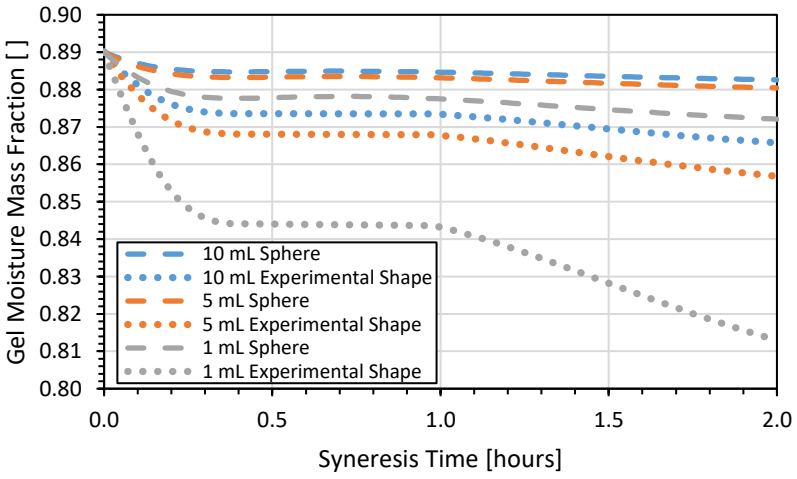

(c)

Figure 7-4: Simulated gel moisture mass fraction as a function syneresis time at 40 °C for spherically shaped and long, cylindrical experimentally shaped gels with (a) pH 6.25, (b) pH 5.75, and (c) pH 5.25 values.

Figures 7-3 and 7-4 demonstrate the effect of starting curd volume and shape on the whey expulsion behaviour of different pH gels undergoing regular syneresis, using Equation 7-3. Gels with larger starting volumes undergo slower reduction in the moisture mass fraction as more moisture would need to be expelled to significantly contribute to loss in the total mass of the gel. The shape factor significantly contributed to the rate of gel volume contraction, with the "experimental" shaped gels (K_{Shape} = 13.3) showing greater volume loss compared to the equivalent starting volume sphere shaped gel. This finding is expected as larger shape factors indicate higher surface area to the volume ratios, allowing for increased total volume transport of whey out of the gel.

The application of Equation 7-3 to different size and shaped curds was successful in this case as the gels were undergoing a limited, syneresis time. Obviously, without including moisture mass fraction restrictions, smaller gels would be mathematically expected to continue to undergo syneresis even though there would be insufficient whey in the gel for that to occur. Therefore, for models where regular syneresis stage is expected to be extended, gels are extremely small, or the gel shape factor is large, other moisture mass fraction restrictions should be included to slow or stop the whey expulsion behaviour at critical points. The next section details the combination of salt uptake and syneresis modelling for pH 6.25, 5.75, and 5.25 renneted milk gels of different sizes and shapes treated with different salting regimes.

7.2.4 Combined Syneresis and Salt Uptake Evaluation

Adapting brining models to dry salting conditions presents challenges. The mechanisms involved in the uptake of salt and expulsion of whey during dry salting consists of (1) application of dry salt to the surface of the curd, (2) dissolution of salt in any free surface whey to form a concentrated solution, (3) diffusion of dissolved salt ions into the gel, and (4) continued whey expulsion from the gel due to the induced osmotic pressure gradient or expulsion due to states (T. Guinee & Fox, 2017; Sutherland, 1974). While the concepts are essentially the same regarding diffusion and whey expulsion under regular brining conditions, dry salting speeds up the process of reaching salt concentration equilibrium between the surface whey and salted gel whey. This is primarily due to less salt being applied to the gel system and the salt brine formed at the gel surface tends to be more concentrated due to surface whey being the only solvent source (T. Guinee & Fox, 2017; Sutherland, 1974). This means that the majority of salt uptake and fastest rate of whey expulsion occurs within the first few minutes of salting, as the concentrated surface brine induces optimal conditions for

increased salt uptake (larger effective diffusion coefficient and salt concentration gradient) and whey expulsion (large induced osmotic pressure differential).

The first step to preparing the models to describe salt uptake and whey expulsion in dry salting conditions is to establish relationships between the whey flux behaviour and the salt concentration differential between the surface brine and salted internal gel whey. One approach is to plot the whey flux from the regular syneresis, 2.5% NaCl-whey brining, and 20% NaCl-whey brining cases at distinct time points and fit a curve between the three points as a function of the salt mass fraction differential between the surface brine and the internal salted whey. This process is best suited for time points early during the brining process, where the concentration differentials are at their largest and the relationships are more linear. The curves become far less valuable after longer salting times because the decreased salt concentration differentials. However, under normal dry salting application, this typically means any additional whey expulsion behaviour reverts to the regular syneresis case, which yields very slow whey flux. A visual example of this process is shown in Figure 7-5, whereby the observer would determine the coordinates where the time curve of interest corresponds to the appropriate salt mass fraction differential to determine the expected whey flux.

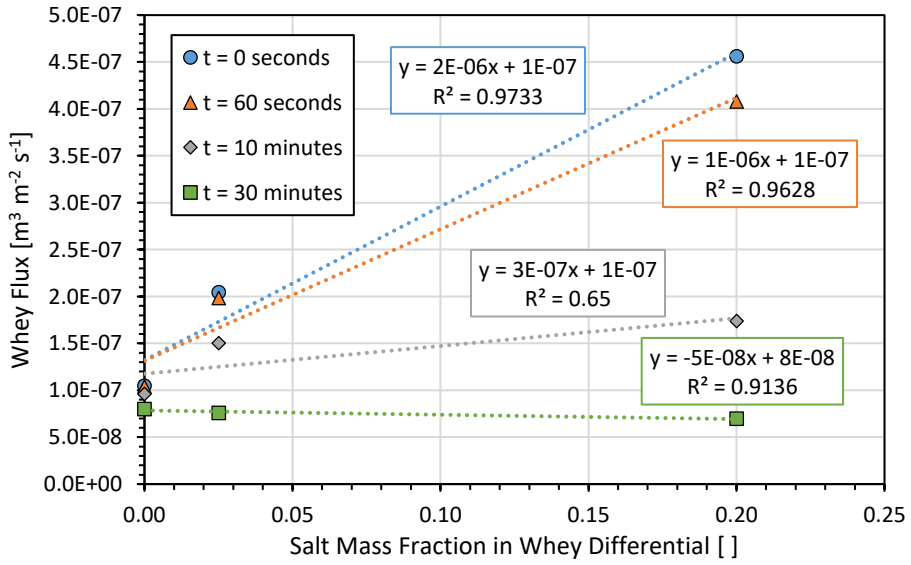

Figure 7-5: Whey flux from pH 6.25 gels as a function of the salt mass fraction differential between the brine and the internal gel whey for different evaluation times. Linear trendlines were fitted to describe the relationship at any distinct timepoint, with the slope gradually decreasing with respect to time as the gels approach equilibrium.

Figure 7-5 shows that as the salting time increases, the slope describing the relationship between the salt mass fraction differential and the whey flux decreases to approach the

regular syneresis value. This is due to the gels gradually approaching equilibrium due to adequate salt uptake or approaching limits on whey expulsion. As the salting time progresses, the salt mass fraction differential would decrease, and whey flux would be increasingly evaluated towards the lower left-hand corner of the figure. While a linear fit is used in this example, other curves may be more appropriate with additional data points from different brining evaluations.

Once the whey expulsion behaviour is established as a function of the salt mass fraction differential, the next step is to establish the effective salt diffusion coefficient as a function of the surface brine concentration, preferably with a linear relationship or other simple curve. This thesis has evaluated salt transport under two different brining conditions, making a linear relationship most appropriate. The geometry best represented by the curd should be selected to evaluate the salt transport via Fickian diffusion. Previous modelling in Chapter 5 has used an infinite cylinder model, but spherical geometries may be more appropriate for other curds. The application of Fick's diffusion model under unsteady-state conditions to a spherical geometry is detailed in Equation 7-4.

$$\frac{\partial C_i}{\partial t_D} = D_i \frac{\partial^2 C_i}{\partial r^2} + \frac{2D_i}{r}\frac{\partial C_i}{\partial r} \text{ for } t_D > 0 \text{ and } 0 < r < r_{max}$$

Equation 7-4: Fick's second law of diffusion for spherical coordinates.

The two boundary conditions and the initial condition required for solving the partial differential equation regarding salt uptake into the curd are shown below.

$$C = C_\infty \text{ for } t_D \geq 0 \text{ at } r = r_{max}$$

$$\frac{\partial C_i}{\partial r} = 0 \text{ for } t_D \geq 0 \text{ at } r = 0$$

$$C = C_i \text{ at } t_D = 0 \text{ for } 0 \leq r < r_{max}$$

Crank (1975) used a separation of variables approach to develop a solution for the concentration of diffusing solute at any radius, *r*, within the maximum radius of a sphere under unsteady-state diffusion, which is shown in the following equation.

$$\frac{C - C_\infty}{C_0 - C_\infty} = \sum_{m=1}^{\infty} \frac{2r_{\max}(-1)^{m-1}}{\pi r m} \sin\left(m\pi \frac{r}{r_{max}}\right) e^{-m^2\pi^2 F_0}$$

Equation 7-5: Analytical solution for unsteady-state diffusion into a sphere.

The analytical solution for unsteady-state diffusion into a spherical structure has also been adapted to calculate the average concentration within the sphere, as shown in Equation 7-6.

$$\frac{C_{Avg} - C_{\infty}}{C_0 - C_{\infty}} = \sum_{m=1}^{\infty} \frac{6}{\pi^2 m^2} e^{-m^2 \pi^2 F_0}$$

Equation 7-6: Analytical solution for the average concentration in a sphere undergoing unsteady-state diffusion.

After the establishment of the whey flux parameters, gel geometry, and relevant effective diffusion coefficient model as a function of the surface brine mass fraction, the next step is to determine the required salt mass uptake at different times within the first minute of brining in a concentrated brine. Given the known surface salt mass fraction, effective diffusion coefficient, and expected whey flux behaviour, this should be evaluated via a mass balance. Determining the required mass uptake provides an important limit to distinguish between expected salt uptake from the diffusion model and achievable salt transport in the early stages of salt exposure. Dry salting creates distinct limits for salt uptake during the earliest stages of salting as the whey expelled from the gel to form the surface brine is insufficient to dissolve the necessary amount of salt required by the diffusion model. Approximately the first fifteen to sixty seconds of exposure to dry salt will yield insufficient dissolved salt to achieve the expected salt mass uptake as predicted by diffusion under brining conditions.

The assumption made in this section is that all the dissolved salt available is absorbed into the gel during the early stages of dry salting until enough expelled whey is available to dissolve enough salt to meet the "Fickian diffusion demand". Figure 7-6 shows the limited salt uptake and its effect on the internal salt mass fraction in gel whey for a pH 6.25 gel example evenly coated with a salt mass equivalent to two percent of the gel mass at the onset of salting. The first ten seconds show limited salt mass uptake due to insufficient whey expulsion to dissolve the salt on the surface, but the salt uptake is large enough to achieve a gel whey salt mass fraction of approximately 0.02 in this time. The salt mass fractions undergo some variation in the following fifteen seconds (as evaluated in one second evaluation time) as the salt mass fraction differential approaches zero, to achieve a final salt mass fraction of 0.023 in both the gel whey and surface brine.

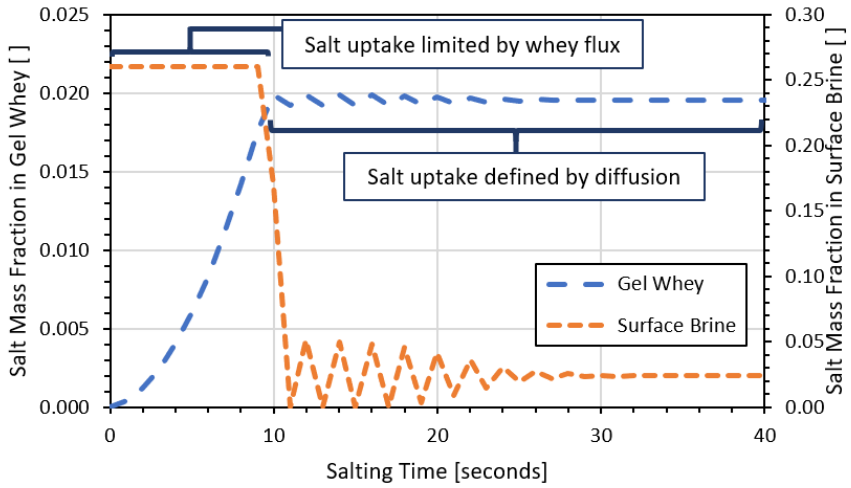

Figure 7-6: Simulated initial salt uptake behaviour and surface brine salt mass fraction depletion for a small (0.45 mL at onset of salting) pH 6.25 gel evenly coated with salt (2% of the gel mass at the onset of salting). The surface brine salt mass fraction is assessed using the y-axis on the right side of the figure, ranging from the equilibrium 0.023 value to the maximum salt solubility mass fraction in the surface whey of 0.26.

Unlike typical diffusion models that operate under conditions where there are large amounts of source brine surrounding the structure and extended periods of time for diffusion to slowly occur, the rapid transport of salt changes the concentration differential across the gel surface once all the surface salt has been dissolved. It is then prudent to evaluate Fickian diffusion in short time intervals, updating the "starting" salt concentration C_0 with the average salt mass fraction in the gel whey from the previous measurement and updating the surface brine concentration C_∞ to account for the changes from salt uptake and whey expulsion. Evaluating salt uptake and diffusion in short intervals allows for the rapid determination of the equilibrium, where the salt mass fraction of the surface brine and gel whey are equal.

The Fickian diffusion models presented in this section were evaluated in one second intervals. Other assumptions made during the development of the models include instant salt dissolution in expelled whey, instant and even application of dry salt over the entire gel surface, perfect mixing of salt in internal gel whey and surface brine, and no losses of whey or salt to the surrounding environment, whereby all salt and whey is either in the gel or on the gel surface. Figures 7-7 through 7-9 show the expected change in the gel mass, moisture mass fraction, and salt mass fraction in the whole gel for pH 6.25 gels of three different starting gel volumes and two different shapes treated with different salting regimes. The salting regimes apply the same salt mass (equal to 2% of the gel mass at the onset of salting) applied instantly at the onset of salting, in three equal ten-minute interval applications, or at a constant rate for thirty minutes, respectively.

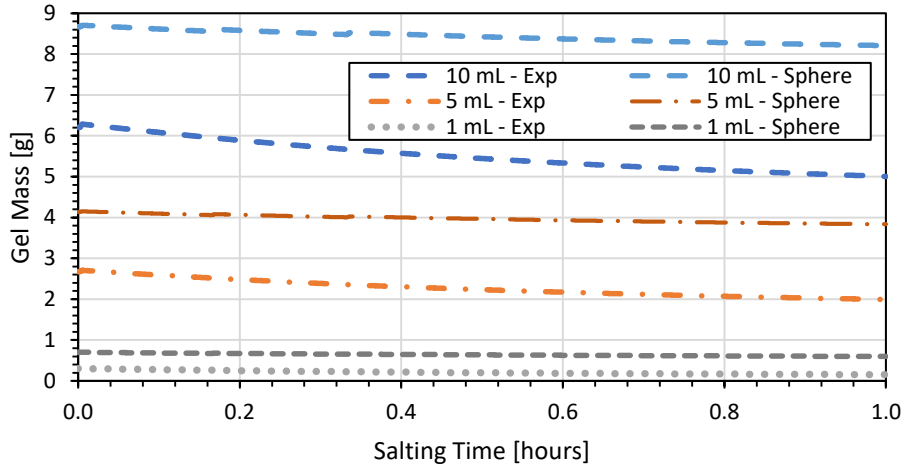

(a)

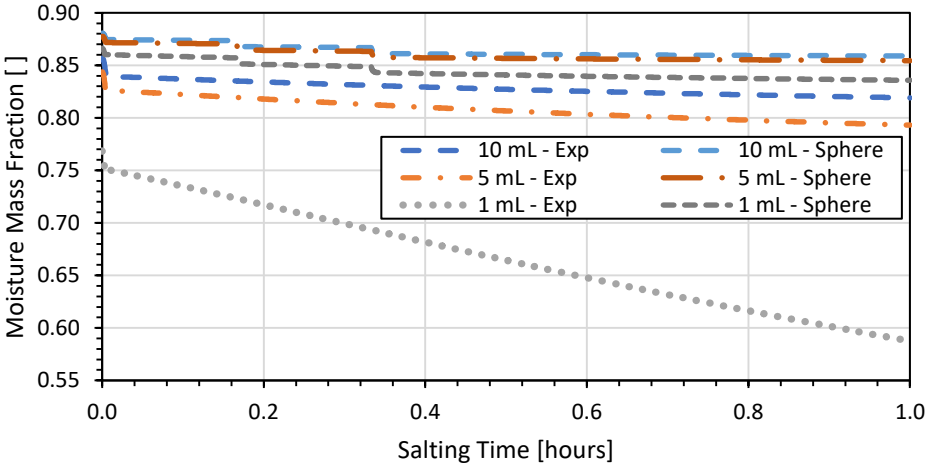

(b)

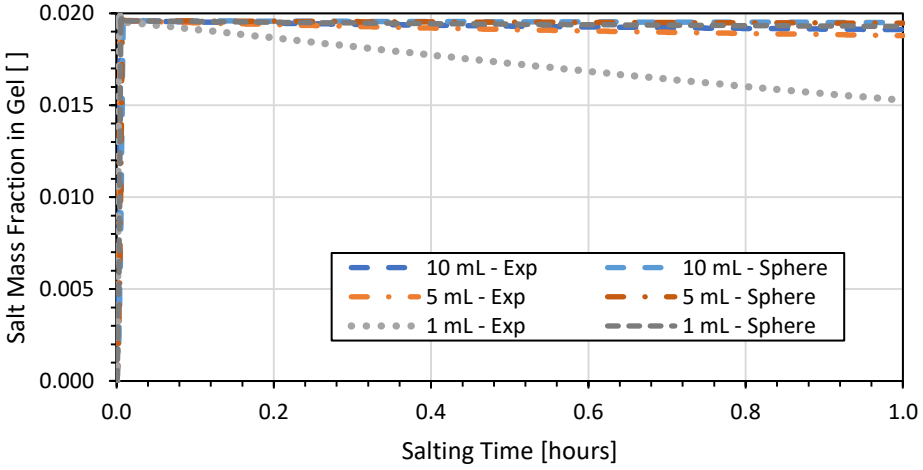

(c)

Figure 7-7: The simulated (a) gel mass, (b) moisture mass fraction, and (c) salt mass fraction in the whole gel for 10 mL, 5 mL, and 1 mL starting volume pH 6.25 gels in spherical and experimental shapes, after undergoing regular syneresis at 40 °C for two hours prior to salting. The salting treatment consists of uniform and instant coating of the gel surfaces with a salt mass equal to 2% of the gel mass at the onset of salting.

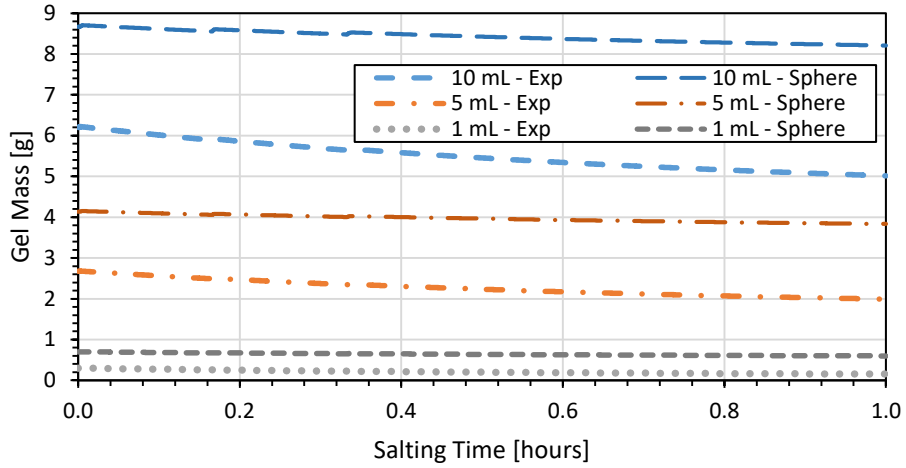

(a)

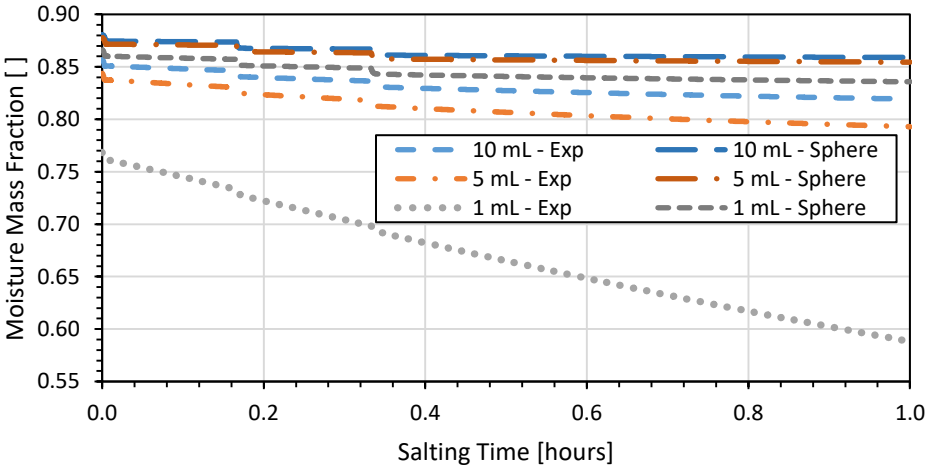

(b)

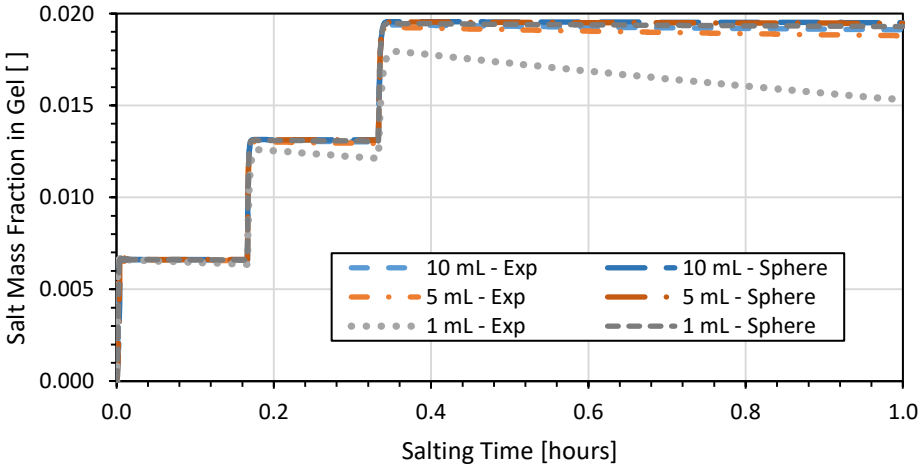

(c)

Figure 7-8: The simulated (a) gel mass, (b) moisture mass fraction, and (c) salt mass fraction in the whole gel for 10 mL, 5 mL, and 1 mL starting volume pH 6.25 gels in spherical and experimental shapes, after undergoing regular syneresis at 40 °C for two hours prior to salting. The salting application consisted of the addition of three equal masses of salt at 0, 10, and 20 minutes of salting time, totalling 2% of the gel mass at the onset of salting.

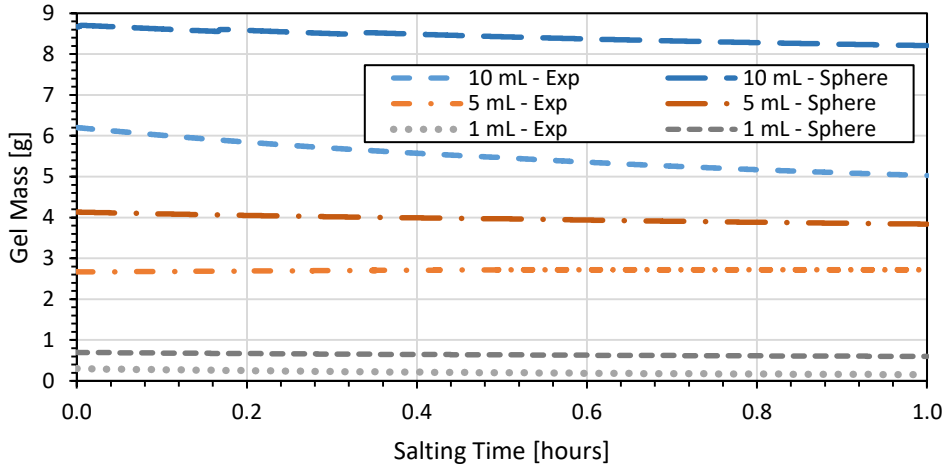

(a)

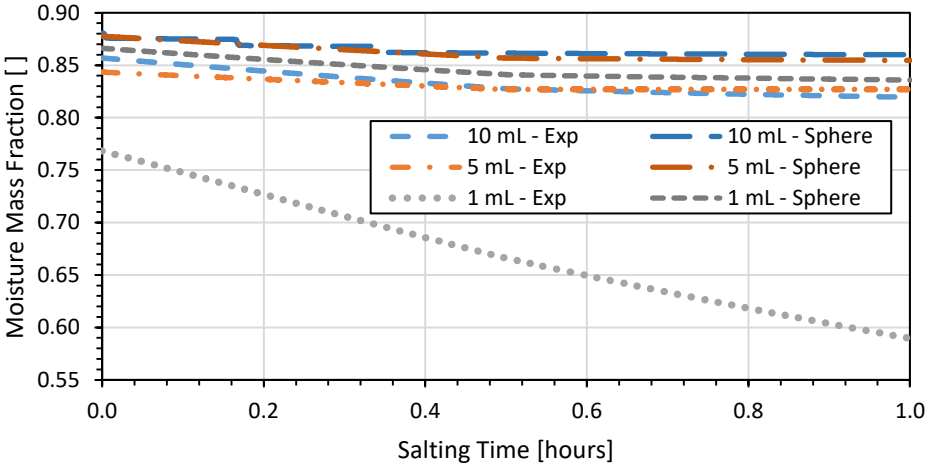

(b)

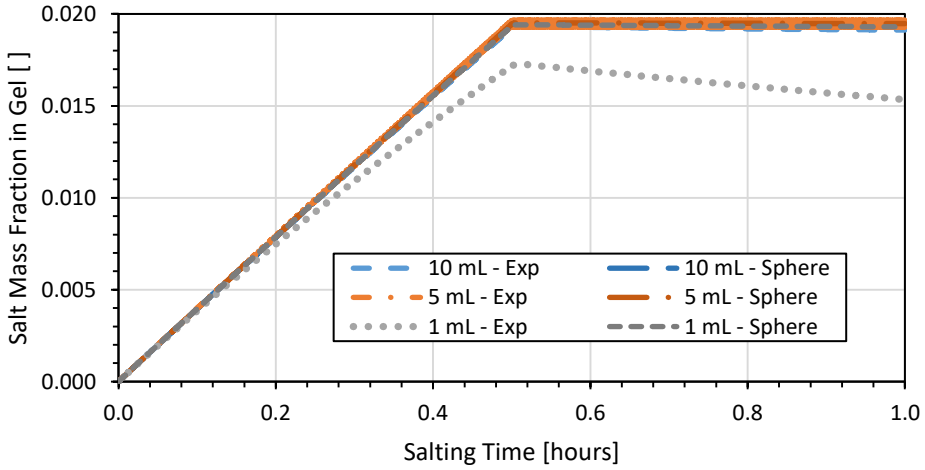

(c)

Figure 7-9: The simulated (a) gel mass, (b) moisture mass fraction, and (c) salt mass fraction in the whole gel for 10 mL, 5 mL, and 1 mL starting volume pH 6.25 gels in spherical and experimental shapes, after undergoing regular syneresis at 40 °C for two hours prior to salting. The salting treatment consists of a constant coating of the gel surfaces for the first thirty minutes of salting, totalling a mass equal to 2% of the gel mass at the onset of salting.

Figures 7-7 through 7-9 show that the larger, more spherical curds undergo the least amount of total mass change and reduction in moisture mass fraction, while achieving the same expected salt mass fraction equilibrium as the other gels, regardless of salting regime. Indeed, all the gels underwent minimal moisture mass and total mass loss due to the rapid reduction of the salt mass fraction differential between the surface brine and internal salted gel whey. The salt mass fraction in the total gel mass quickly achieved equilibrium in all cases before slowly starting to decrease after the conclusion of salt application, except in the case of the smallest experimental curd. Although the smallest experimentally shaped gel did achieve the same salt mass fraction in the gel whey as the other gels, it possessed less moisture than all the other gels (see Figure 7-4 (a)), thereby reducing the salt mass fraction in the total gel mass.

The primary point of interest from Figures 7-7 through 7-9 is that the gels achieved the equilibrium salt mass fraction in the gel whey extremely fast regardless of the salting regime used, gel shape, or gel size, provided no surface whey or salt was lost to the surroundings. However, both the application of salt all at once or in three equal applications did achieve slightly lower moisture mass fractions in the gel within a thirty-minute salt application time, particularly for the smaller experimentally shaped gels. This was due to the increased total whey expulsion from the large induced salt mass fraction differential after each salt application.

If the intended processing goal is to optimize both salt uptake and moisture loss, the best course of action would be to increase the amount of time the brine is concentrated at the surface, thereby promoting simultaneous fast salt uptake and whey expulsion. However, this practice may be particularly challenging to achieve if the desired equilibrium salt mass fraction in the gel is small and method of application is limited. If the goal is to optimize salt uptake by having salt uptake occur as quickly as possible, regardless of whey losses, the single application of salt would be appropriate as the target salt mass fraction is achieved within the first two minutes for all the gel sizes and shapes shown in Figure 7-7. Insight from Chapter 5 would suggest that most of the salt in the gel would be in the free gel whey fraction and would therefore be predisposed to expulsion during pressing. The next section applies the salt uptake and whey flux behaviours discussed in this section to theoretical curd bed systems.

7.3 Application of Syneresis Models to Theoretical Curd Beds

The previous section described the expected whey expulsion and salt uptake behaviours for individual renneted milk gels with starting cut volumes of one, five, and ten millilitres with either a spherical shape or a long, cylindrical experimental shape described by the models in previous chapters. While modelling the changing individual gels provides insight to the effect of different initial gel cutting or salting regimes on salt uptake and moisture losses, actual cheesemaking creates curd beds with a variety of starting curd sizes and shapes. It is therefore more appropriate to evaluate the expected average whole curd bed moisture loss and salt uptake behaviour, rather than single curds.

This section seeks to apply the results shown in section 7.2.4 to simple curd beds consisting of three different starting gel sizes (10, 5, and 1 mL), with the same long, cylindrical experimental shape previously described. Three different curd beds, totalling one cubic meter of renneted milk gel (1033 kg) at the onset of syneresis have been established to evaluate the effect of different gel sizes on the salt uptake and moisture loss of an entire bed of curds. Table 7-1 details the three curd beds and their breakdown by curd number and volume of the entire curd bed.

Table 7-1: Theoretical curd beds evaluated under the different pH treatment, curd shape, and salting regimes. Curd volume distribution are assessed at the onset of syneresis for a standard 1 m^3 of milk converted into curd.

Curd Bed Treatments	1 mL	5 mL	10 mL	Total
Standard Curd Bed	1.00E+05 Curds (10% volume)	1.60E+05 Curds (80% volume)	1.00E+04 Curds (10% volume)	2.70E+05 Curds (1 m^3 curd bed)
Small Curd Bed	2.00E+05 Curds (20% volume)	1.50E+05 Curds (75% volume)	5.00E+03 Curds (5% volume)	3.55E+05 Curds (1 m^3 curd bed)
Large Curd Bed	5.00E+04 Curds (5% volume)	1.50E+05 Curds (75% volume)	2.00E+04 Curds (20% volume)	2.20E+05 Curds (1 m^3 curd bed)

The standard curd bed listed in Table 7-1 was derived from an assessed curd size distribution of curds sampled from the salting belt of an industrial cheddar production line (figures showing the curd size distribution are detailed in section 7.6). The first step to evaluating the changing moisture and total mass of the curd beds is to evaluate the expected whey expulsion behaviour under regular syneresis conditions. Figure 7-10 shows the expected curd bed mass and moisture mass fraction reduction of the entire curd bed for each curd bed type listed in Table 7-1 for pH 6.25, 5.75, and 5.25 gels using the previously described whey expulsion models with Equation 7-3.

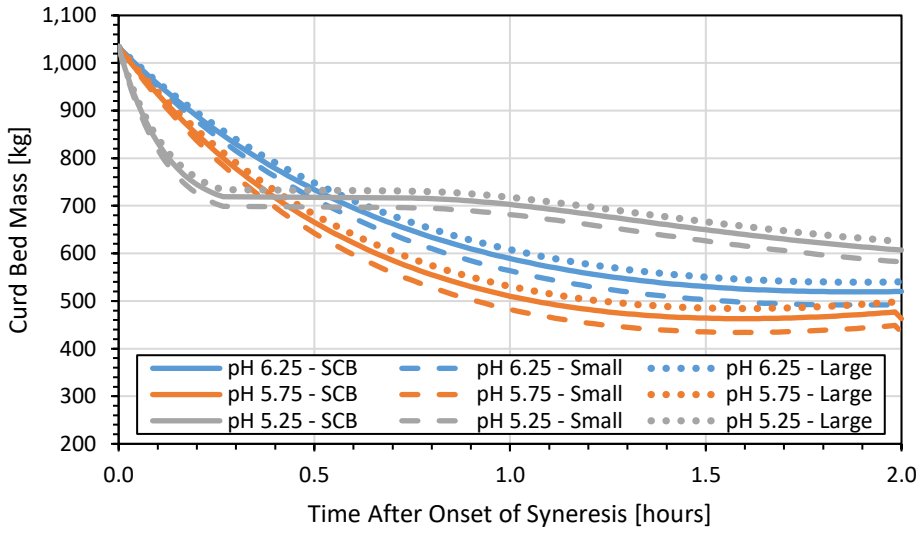

(a)

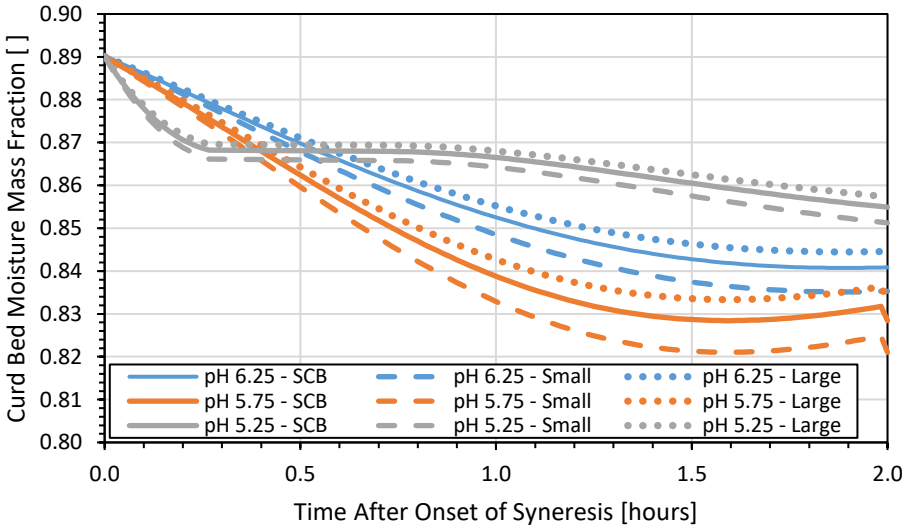

(b)

Figure 7-10: Simulated expected curd bed (a) mass and (b) moisture mass fraction of a starting total curd mass of 1033 kg (1 m^3) as a function of syneresis time using Equation 7-3 for pH 6.25, 5.75, and 5.25 renneted skim milk gels at 40 °C.

Figure 7-10 shows that the gel pH is expected to have the most significant effect on the total whey expulsion and moisture mass fraction. This is reasonable, given the insight from Chapter 3 concerning whey expulsion behaviour for individual gels with different pH values. Curd beds with a higher fraction of large starting curds are also expected to undergo less overall whey mass loss and maintain a larger moisture mass fraction, following the findings from section 7.2.3. The following sections apply the findings from section 7.2.4 to the different curd beds described in Table 7-1, under different salting regimes.

7.3.1 Single Salt Application

Application of all the salt in one, initial application is the simplest method for achieving dry salting. Figures 7-11 through 7-13 show the changing curd bed mass, moisture mass fraction, and salt mass fraction for the different curd bed treatments of experimentally shaped curds with pH values of 6.25, 5.75, and 5.25, respectfully treated with one application of dry salt at the onset of salting.

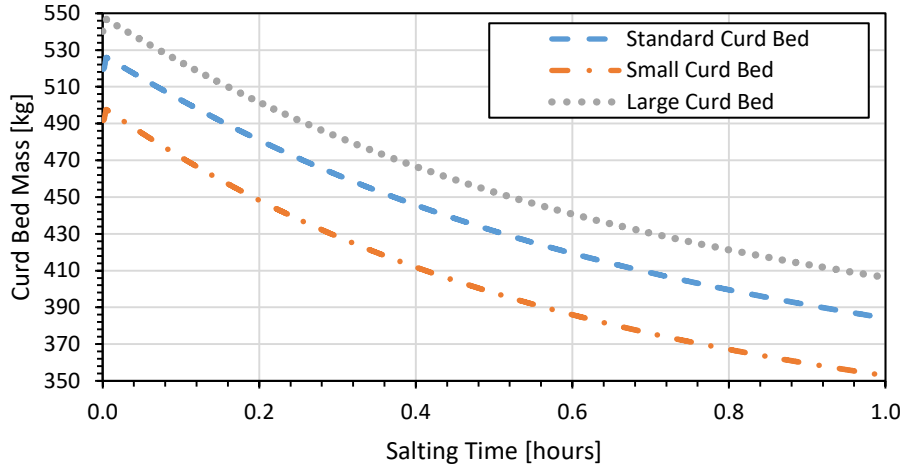

(a)

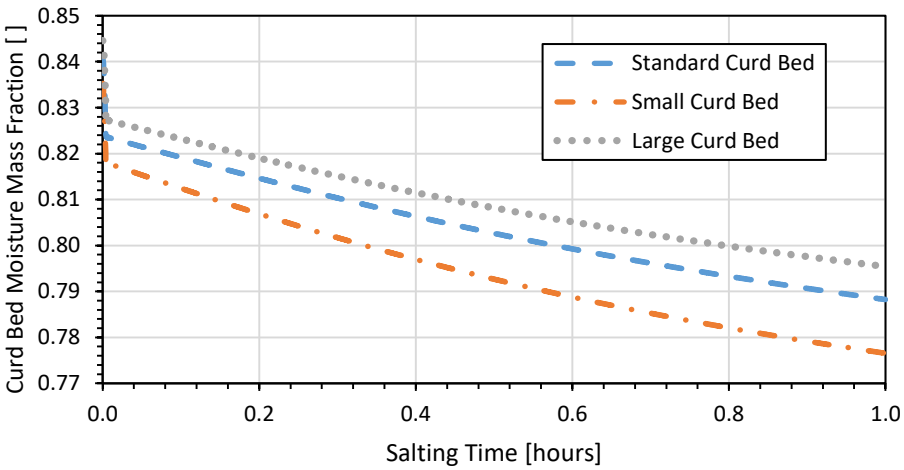

(b)

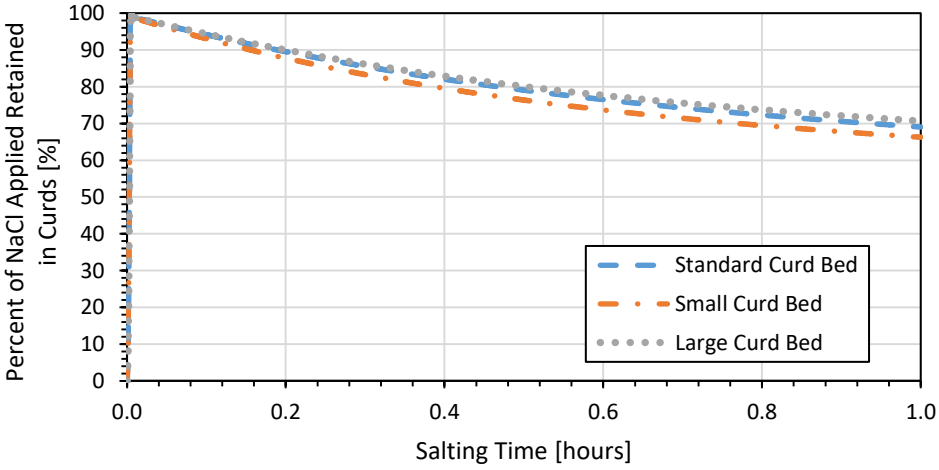

(c)

Figure 7-11: Simulated standard curd bed, small curd bed, and large curd bed of experimental shaped curds, pH 6.25 gels (a) curd bed mass, (b) moisture mass fraction, and (c) percent of applied retained in curd bed with respect to time after the onset of syneresis or salting time for single application of salt after two hours of regular syneresis.

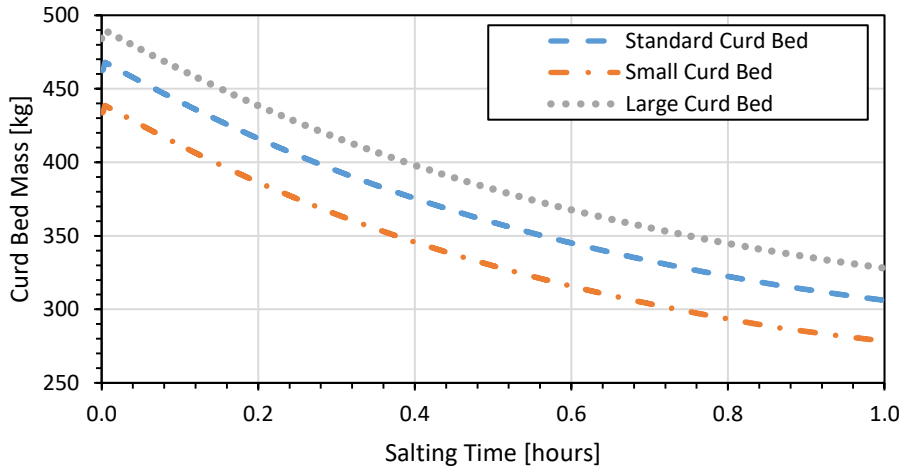

(a)

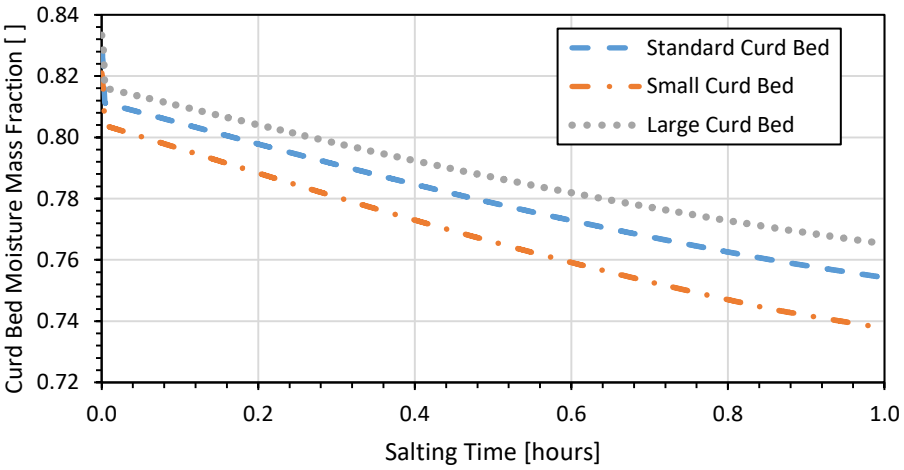

(b)

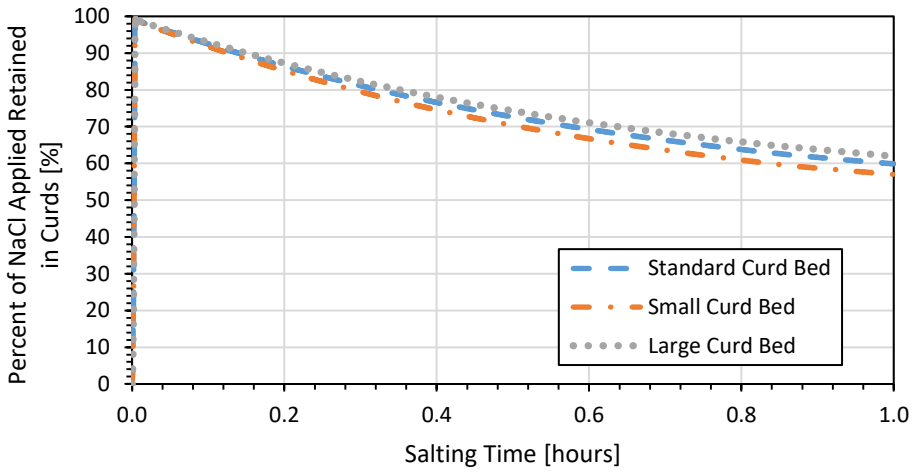

(c)

Figure 7-12: Simulated standard curd bed, small curd bed, and large curd bed of experimental shaped curds, pH 5.75 gels (a) curd bed mass, (b) moisture mass fraction, and (c) percent of applied retained in curd bed with respect to time after the onset of syneresis or salting time for single application of salt after two hours of regular syneresis.

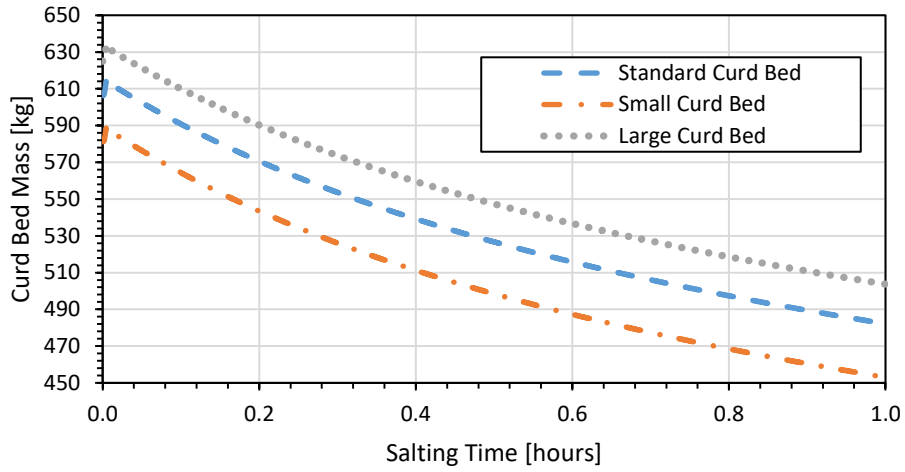

(a)

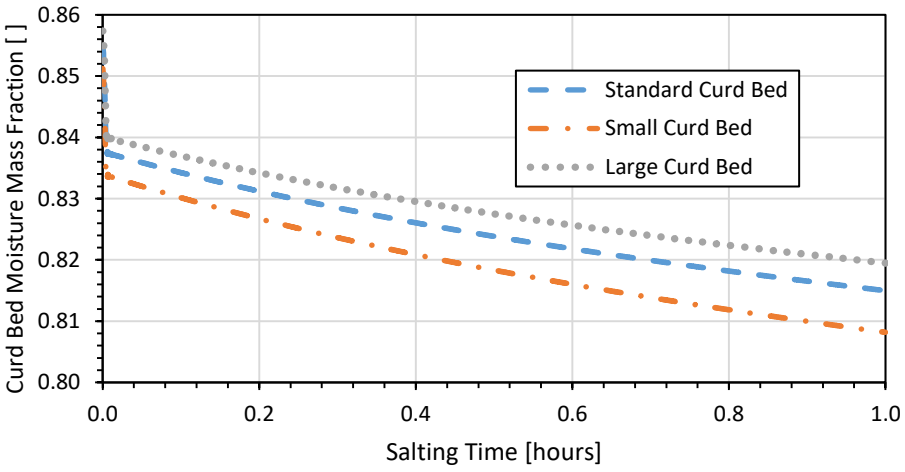

(b)

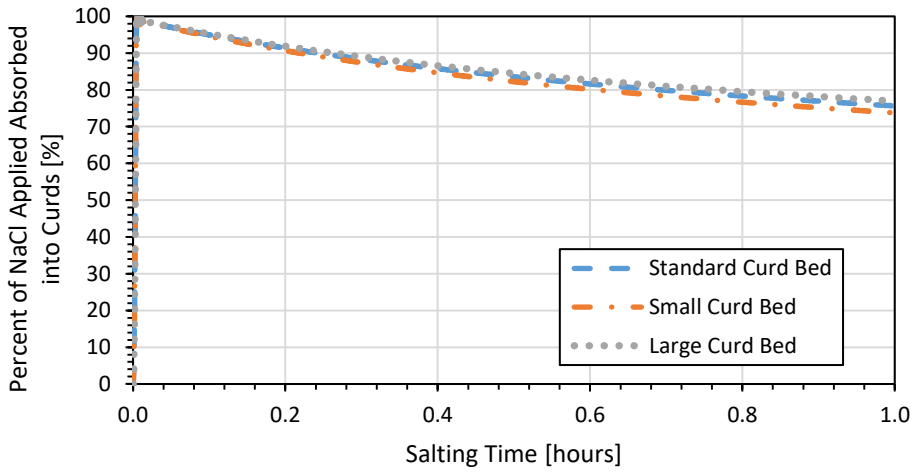

(c)

Figure 7-13: Simulated standard curd bed, small curd bed, and large curd bed of experimental shaped curds, pH 5.25 gels (a) curd bed mass, (b) moisture mass fraction, and (c) percent of applied retained in curd bed with respect to time after the onset of syneresis or salting time for single application of salt after two hours of regular syneresis.

Application of all the salt at the onset of the salting period leads to a rapid uptake of the salt, followed by the slow loss of the salt from the gel due to continued syneresis behaviour and pursuit of salt concentration equilibrium between the internal gel moisture and the surface brine. The moisture mass fraction was found to be higher for any curd beds with higher concentrations of large gels. This is unsurprising as the larger gels would have larger moisture masses that would require more time to expel for the given whey flux limits.

The whey expulsion for the curd beds with more small curds was also expected to affect the retention of salt within the gels. Longer "resting" times to allow the salt to be transported into the gel, may lead to some salt losses as the longer salting time allows for the gel moisture and surface brine to approach equilibrium. The next subsection addresses the expected salt retention and whey expulsion performance for gels treated with the same total mass of salt but deposited on the gel surface in three even applications.

7.3.2 Triplicate Salt Application

Figures 7-14 through 7-16 show the changing curd bed mass, moisture mass fraction, and salt mass fraction for the different curd bed treatments of experimentally shaped curds with pH values of 6.25, 5.75, and 5.25, respectfully treated with three even applications of salt in ten-minute intervals.

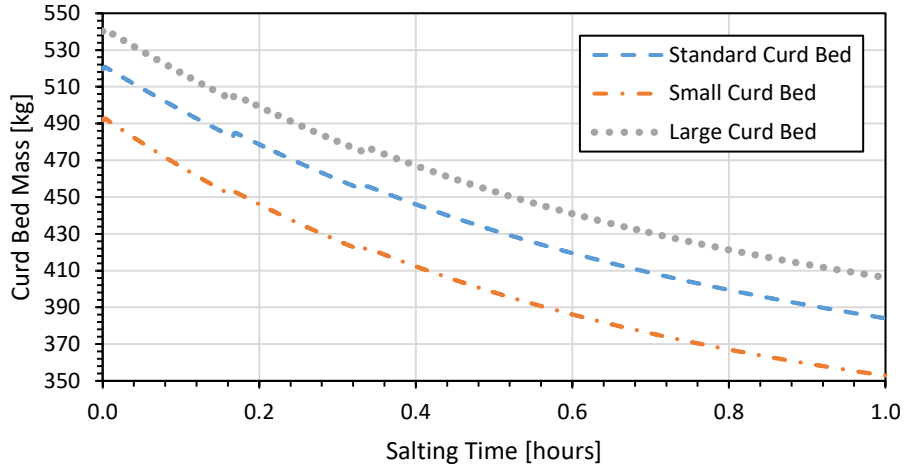

(a)

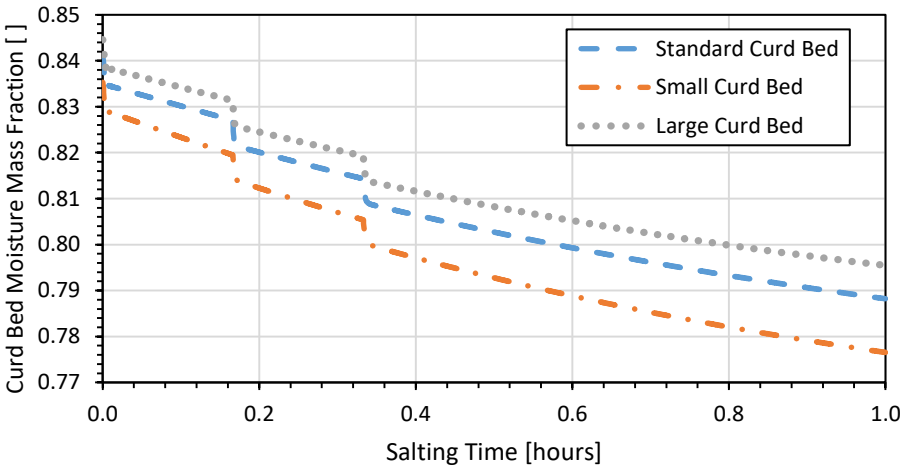

(b)

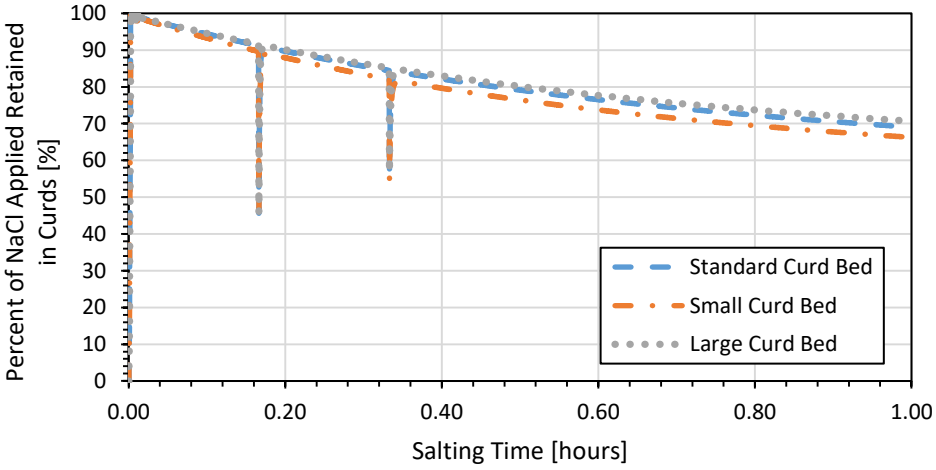

(c)

Figure 7-14: Simulated standard curd bed, small curd bed, and large curd bed of experimental shaped curds, pH 6.25 gels (a) curd bed mass, (b) moisture mass fraction, and (c) percent of applied retained in curd bed with respect to salting time for triplicate equal application of salt to the gel surfaces at 0, 10, and 20 minutes of salting time.

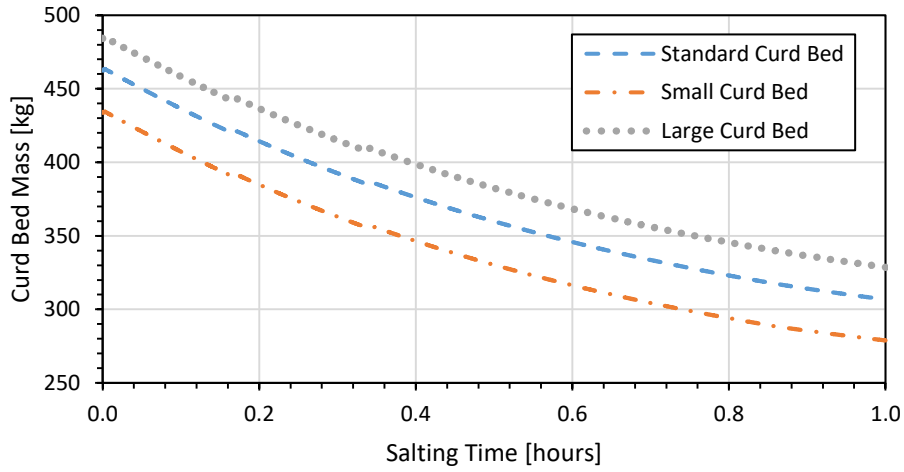

(a)

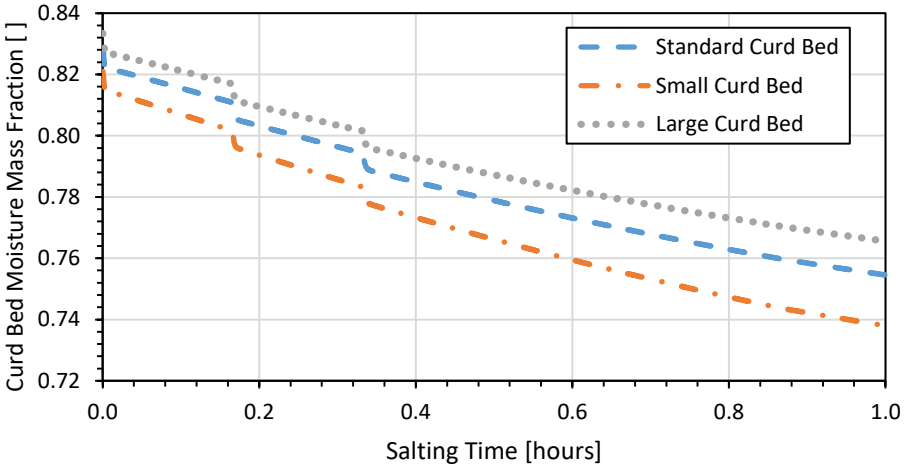

(b)

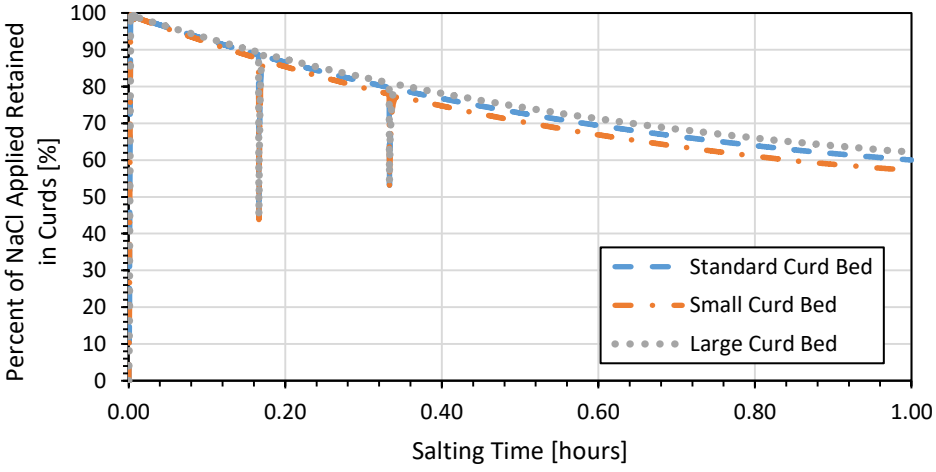

(c)

Figure 7-15: Simulated standard curd bed, small curd bed, and large curd bed of experimental shaped curds, pH 5.75 gels (a) curd bed mass, (b) moisture mass fraction, and (c) percent of applied retained in curd bed with respect to salting time for triplicate equal application of salt to the gel surfaces at 0, 10, and 20 minutes of salting time.

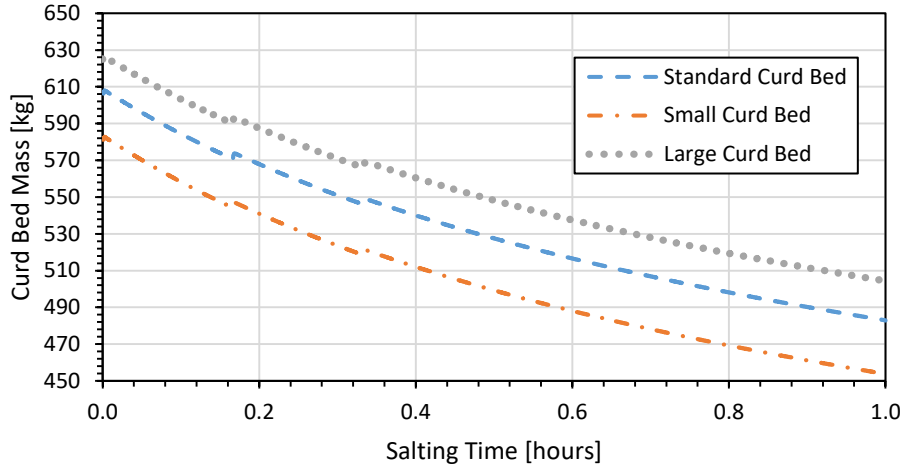

(a)

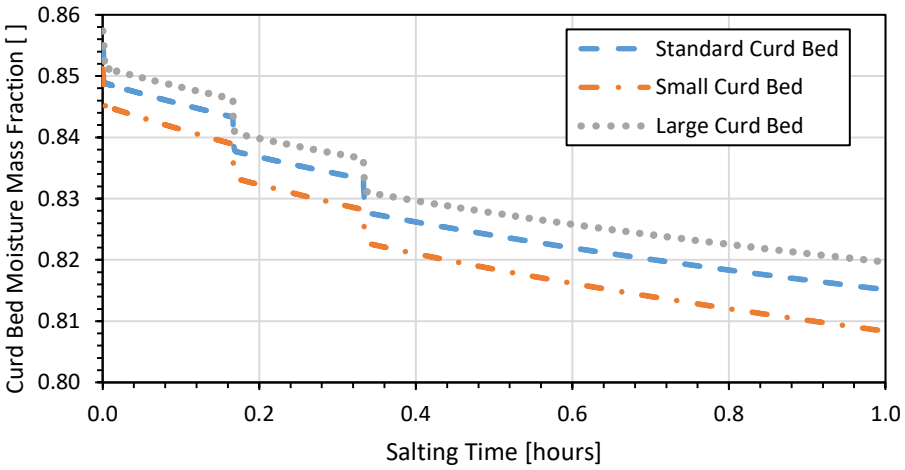

(b)

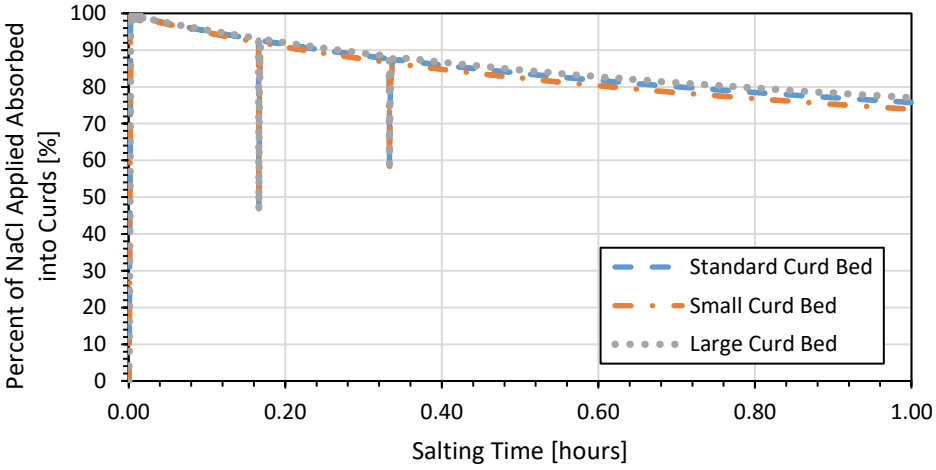

(c)

Figure 7-16: Simulated standard curd bed, small curd bed, and large curd bed of experimental shaped curds, pH 5.25 gels (a) curd bed mass, (b) moisture mass fraction, and (c) percent of applied retained in curd bed with respect to salting time for triplicate equal application of salt to the gel surfaces at 0, 10, and 20 minutes of salting time.

Application of the salt in three equal applications leads to a rapid uptake of the salt, followed by the slow loss of the salt from the gel due to continued whey expulsion in pursuit of salt concentration equilibrium between the internal gel moisture and the surface brine. The moisture mass fraction was found to be higher for any curd beds with higher concentrations of large gels. Given that salt uptake is achieved extremely quickly after each salt application, there is little need for additional resting time for the gels to continue salt uptake after the final application of salt, especially as some of that salt is likely to be lost in the continued, slow whey expulsion of the gels. However, the inclusion of additional resting time may allow for salt to slowly interact more with the proteinaceous structure of the gel, becoming less available for expulsion via pressing. The next subsection addresses the expected salt retention and whey expulsion performance for gels treated with the same total mass of salt but deposited on the gel surface continuously for thirty minutes in an even application.

7.3.3 Continuous Salt Application

Figures 7-17 through 7-19 show the changing curd bed mass, moisture mass fraction, and salt mass fraction for the different curd bed treatments of experimentally shaped curds with pH values of 6.25, 5.75, and 5.25, respectfully treated with a constant application of salt for thirty minutes.

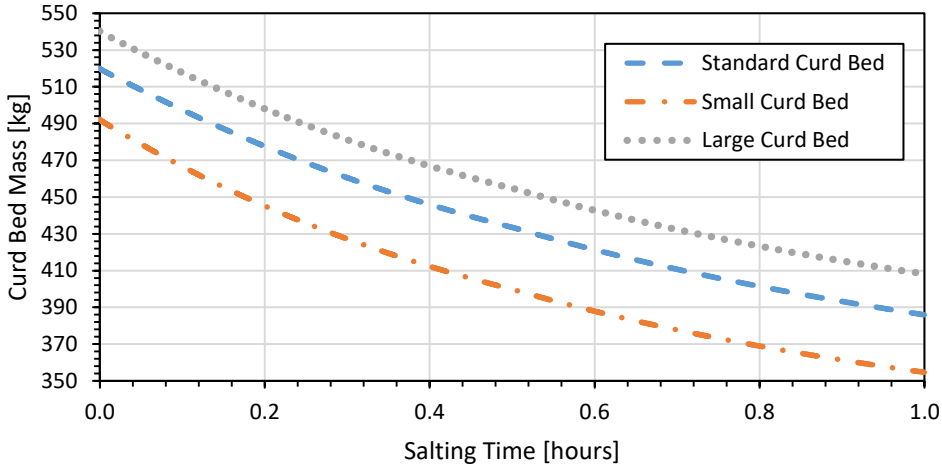

(a)

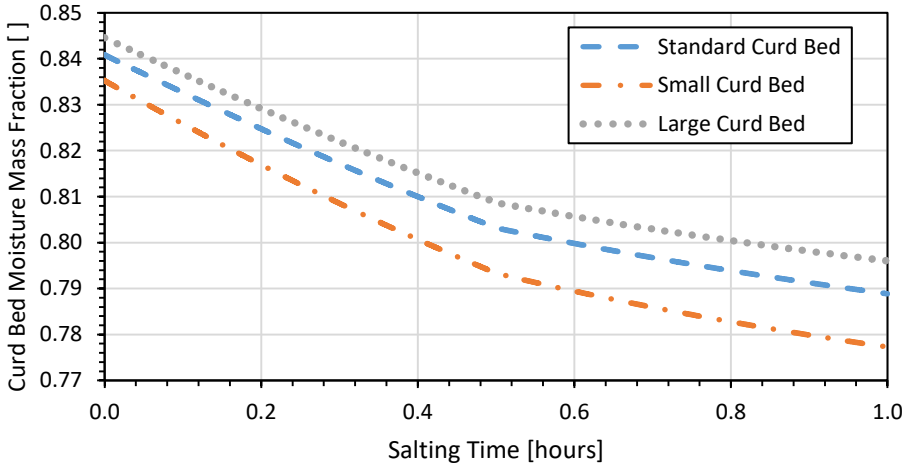

(b)

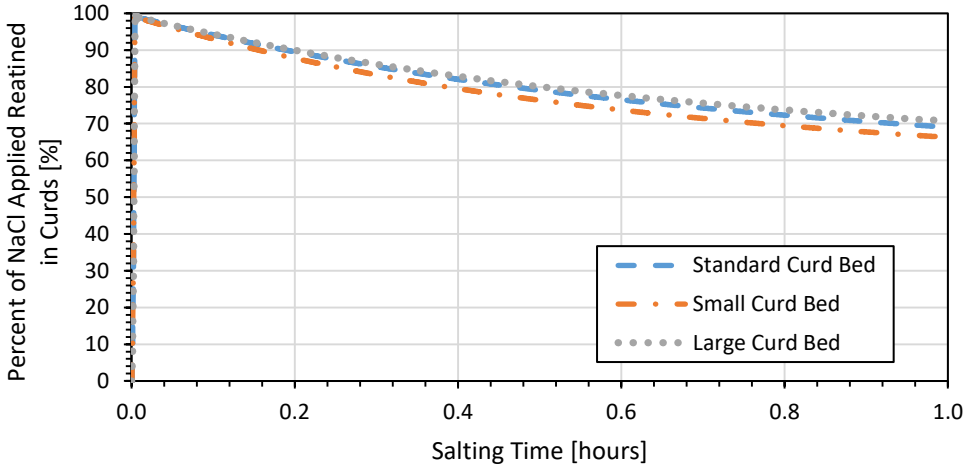

(c)

Figure 7-17: Simulated standard curd bed, small curd bed, and large curd bed of experimental shaped curds, pH 6.25 gels (a) curd bed mass, (b) moisture mass fraction, and (c) percent of applied retained in curd bed with respect to salting time for constant equal application of salt to the gel surfaces for the first 30 minutes of salting time.

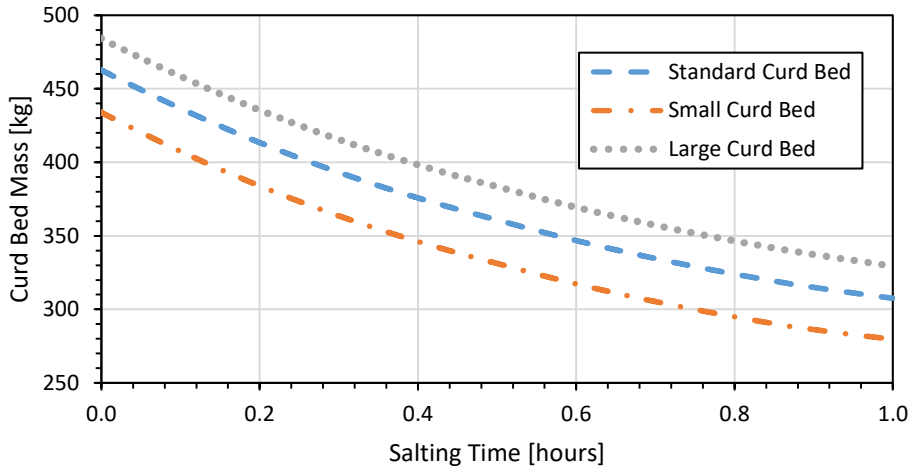

(a)

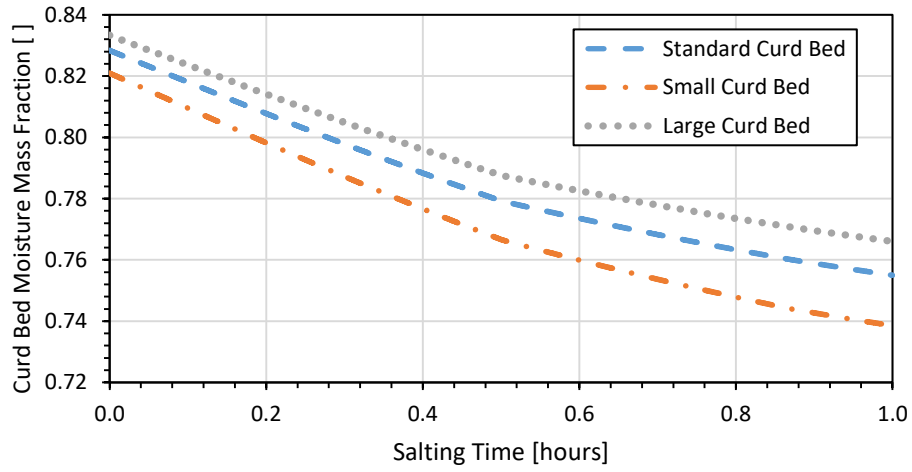

(b)

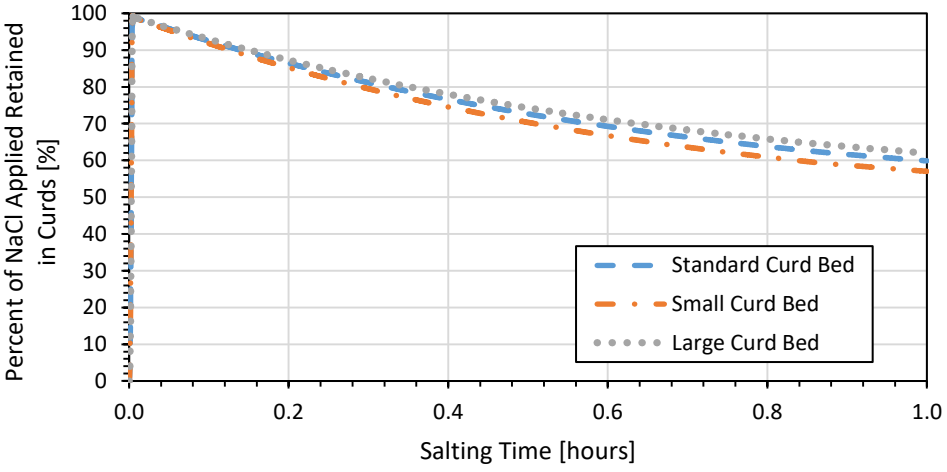

(c)

Figure 7-18: Simulated standard curd bed, small curd bed, and large curd bed of experimental shaped curds, pH 5.75 gels (a) curd bed mass, (b) moisture mass fraction, and (c) percent of applied retained in curd bed with respect to salting time for constant equal application of salt to the gel surfaces for the first 30 minutes of salting time.

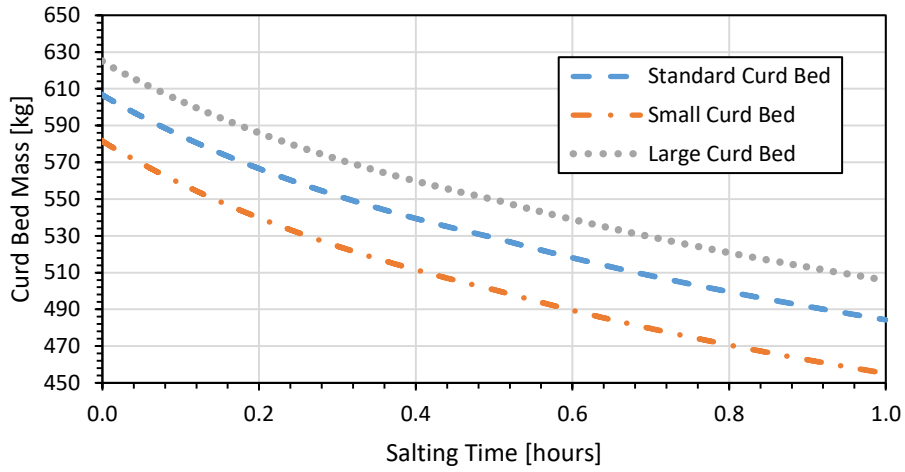

(a)

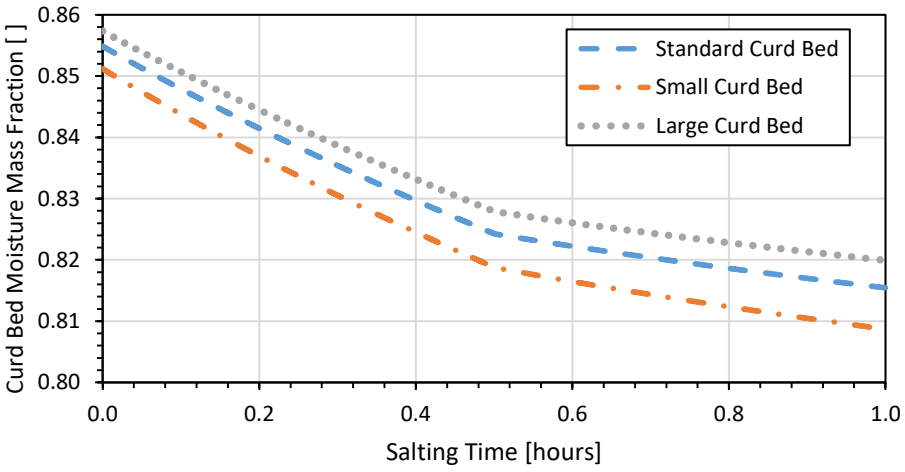

(b)

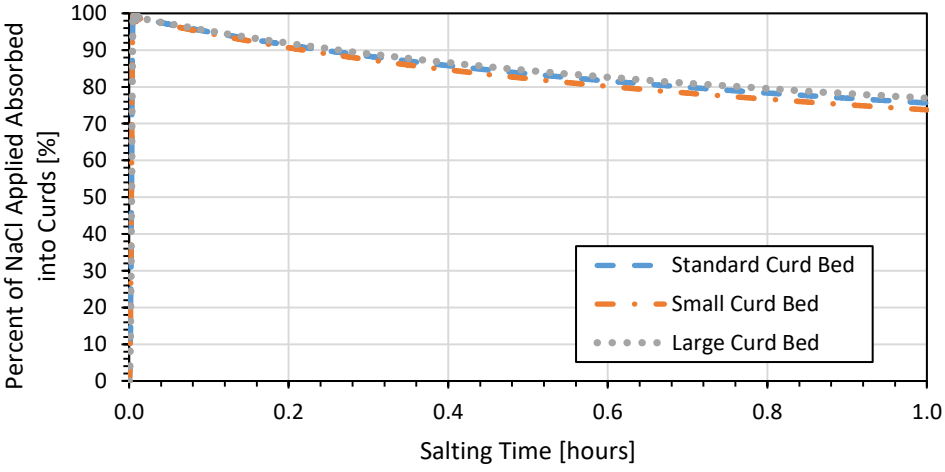

(c)

Figure 7-19: Simulated standard curd bed, small curd bed, and large curd bed of experimental shaped curds, pH 5.25 gels (a) curd bed mass, (b) moisture mass fraction, and (c) percent of applied retained in curd bed with respect to salting time for constant equal application of salt to the gel surfaces for the first 30 minutes of salting time.

Application of the salt at a constant rate for thirty minutes leads to a rapid uptake of the salt, followed by the slow loss of the salt from the gel due to continued whey expulsion in pursuit of salt concentration equilibrium between the internal gel moisture and the surface brine and the achievement of favourable thermodynamic equilibrium with the gel whey and protein structure. The moisture mass fraction was found to be higher for any curd beds with higher concentrations of large gels, as shown in the other salting regimes.

7.3.4 Model Findings and Limitations

The model results presented in the three previous subsections demonstrated the effect of curd pH, size, and approximate shape on the whey expulsion and salt uptake behaviour. If the gels are assumed to be evenly coated with the appropriate salt mass for their mass (2% of the gel mass at the onset of salting) with no expected whey or salt losses from the surface, there are minimal differences between the curd beds tested with the different salting regimes at the same gel pH. Ultimately, the gel pH predicts the whey mass and salt uptake behaviour, with minor adjustments for the curd size distribution. If the goal is to achieve a low final mass with lower moisture mass fraction, a curd bed of small pH 5.75 gels is the best choice. However, if optimization of salt retention (at least on the salting belt) is desired the best choice would be a curd bed of large pH 5.25 gels. Retention would be further improved by treating the curd bed with a single initial application of salt and enough rest time for the salt to move from the free gel whey fraction to the whey fraction associated with the proteinaceous gel structure, to prevent unnecessary losses during pressing.

It is important to note that the curd beds presented in the previous three sections were assumed to have evenly allocated the appropriate salt mass over the surface of each gel, with no losses occurring. The appropriate salt mass application of 2% of the gel mass over each curd is unrealistic under the best salting application techniques. This means that even if the proper salt mass for the entire curd bed is correct, it would be easy for more salt to be applied to the smaller gels than the larger gels due to the surface area to volume ratio. For example, 520 kilograms of pH 6.25 gels in the standard curd bed distribution would have been expected to be treated with 10.4 kilograms of salt, with an average salt coating of 2.06×10^{-5} g mm^{-2} over each gel. That application of salt per surface area would be insufficient for the 5 mL and 10 mL gels which would require 2.82×10^{-5} g mm^{-2} and 2.13×10^{-5} g mm^{-2}, respectively. It would also be nearly twice as much as required for the 1 mL gel of 1.02×10^{-5} g mm^{-2}. Applying a perfectly even amount of salt of 2.06×10^{-5} g mm^{-2} over all the gel

surface area in one application would yield the salt uptake behaviour in each gel size shown in Figure 7-20.

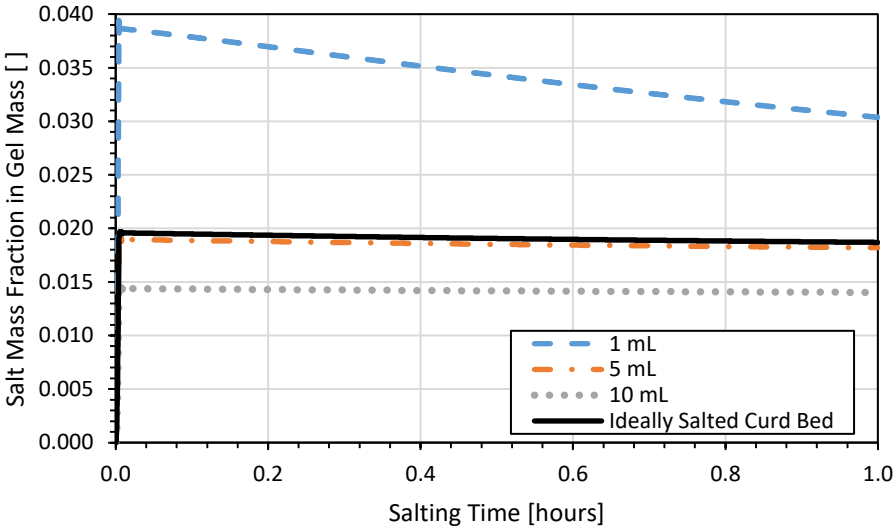

Figure 7-20: Simulated salt mass fraction in each pH 6.25 gel by size assuming even coating of 2.06 x 10^{-5} g mm^{-2}, compared to the ideally salted bed salt mass fraction discussed in section 7.3.1. Smaller gels achieve higher salt mass fractions due to the increased mass of salt per surface area compared to the larger gels.

Results from Figure 7-20 would suggest that even if the correct salt mass is applied to an entire curd bed, the likelihood of over-salting the smallest gels and under-salting the largest gels poses risks to controlling the salt distribution throughout the entire bed of curds, affecting the final product. The most prudent approach to mitigating the effects of unequal salt application would be to make the gel beds as uniform as possible and create salting and mixing regimes to prevent over or under-salting gels. Maintaining uniform curd sizes would also serve to control moisture losses and create a more uniform curd bed for producing more consistent products. The next section compares the model findings from this and the previous sections to curds sampled from the salting belt of an industrial cheddar production line.

7.4 Experimental Design

An experiment was designed to evaluate the curd size distribution, salt uptake, and moisture mass fraction of cheddar curds taken from the end of an industrial salting belt.

7.4.1 Curd Bed Sampling and Sieving Separation

A cross-section of the curd bed (approximately six inches deep and one foot wide) was collected from the beginning, midway, and end of the salting belt (approximately three minutes, fifteen minutes, and thirty minutes on the salting belt, respectively) before the curds

would be transferred to a “tower” system for final pressing into moulds and removal of any residual free whey or salt. Samples were quickly sieved into different size classes using a W.S. Tyler Ro-Tap® RX-29 sieve shaker (Massachusetts, USA) for one minute with sieve sizes of 0.5 inches (12.70 mm), 0.375 inches (9.53 mm), 0.25 inches (6.35 mm), 0.125 inches (2.35 mm), and fines (<2.35 mm). The sieved curds were weighed and reserved for additional analyses. The mass fraction of the total curd mass on each sieve was recorded to estimate the total contribution of the curd sizes on each sieve to the total curd size distribution. Replicate samples were collected on the same belt producing the same cheddar recipe on three different production days to evaluate the average curd bed properties at each sampling point along the salting belt.

7.4.2 Image Acquisition for Curd Size Distribution Analysis

The whole curd sample from each sieve (or a representative, random sample of the sieved curds) were assembled on a matte, black paper for imaging. Curds were arranged to limit the touching between individual curds. A standard ruler was placed adjacent to the curds to provide a calibration length for reference. A Logitech® C920 Pro HD Webcam (Lausanne, Switzerland) was arranged directly one foot above the curds to standardize the image capture procedure. The camera was autofocused and captured an image for each sieved sample. The images were reserved for analysis with ImageJ® software.

7.4.3 Moisture Content Evaluation

Sieved curd samples were used to evaluate salt uptake and moisture content after completion of the image capture, to limit any undue drying or fusing of the curds. Furthermore, the curds had active culture and would therefore continue to undergo some chemical-physical changes. Approximately ten to twenty grams of randomized curds were shredded using an Oster blender in five short pulses. Two to three-gram samples of the shredded curds were placed in each of three pre-weighed weighing dishes and weighed. The rest of the shredded curds were reserved for salt content assessment. The samples went into an oven to evaporate the free moisture for twenty-four hours at 38 ± 2 °C. Samples were weighed after oven drying and used to determine the moisture content of the curd samples prior to drying. Results from the replicates were used to calculate an average moisture content of the sieved curd samples.

7.4.4 Salt Content Evaluation

Approximately half a gram of well mixed, shredded curd was added to a container for digestion and weighed. Ten millilitres of 65% nitric acid was added and the slurry was

digested with an Anton Paar Multiwave GO Digester (Graz, Austria) using the standard heating curve. Digested samples were diluted with deionized water to a total volume of forty millilitres before undergoing assessment with ICP-MS. Results for the sodium mineral content were reported as parts-per-million of the curd sample mass, before conversion to salt content using the ratio of sodium chloride molar mass to sodium molar mass.

7.5 Image Analysis Techniques

Images of the curd samples from each sieve were assessed using ImageJ® by first establishing the calibration length using the ruler in the image to convert pixel lengths to inches. The image was then cropped to remove non-curd entities from the image, converted into 8-bit grayscale, automatically thresholded to convert the image to binary with a black background with white curds. The image was inverted to make the curds black and the background white, before undergoing assessment of each curd particle using the "Analyze Particles" function of ImageJ®. Results were produced detailing the location, area, perimeter, bounding square dimensions, and other properties for each curd identified. The results were used to calculate the equivalent circular diameter of each curd from the imaged area, using the same approach shown in Equation 6-11, where the square root of the area multiplied by four over pi is equivalent to the equivalent diameter. The equivalent circular diameter was used as a simple estimate for the curd volume, assuming a spherical shape. The curd sizes were compiled from the ImageJ® results for each sieved sample to determine the curd size distribution on each sieve. The curd weights on each sieve were assumed to be proportional to the gel volumes and were used to calculate the curd size distribution for the whole sample collected.

7.6 Experimental Results and Discussion

Curd size distribution results showed that the overall curd size distribution remained relatively uniform at all three sampling locations along the salting belt, indicating that little change was occurring in the curd sizes as they proceeded along the belt. This is unsurprising as the gels had previously expelled most of the free whey in earlier stages of processing. Figure 7-21 shows the curd size distribution by spherical volume and curd count at all three sampling locations.

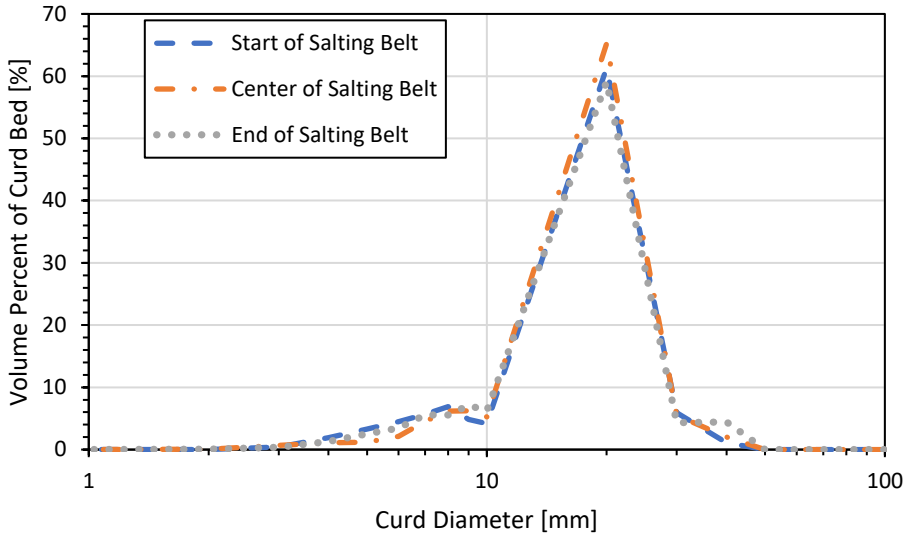

(a)

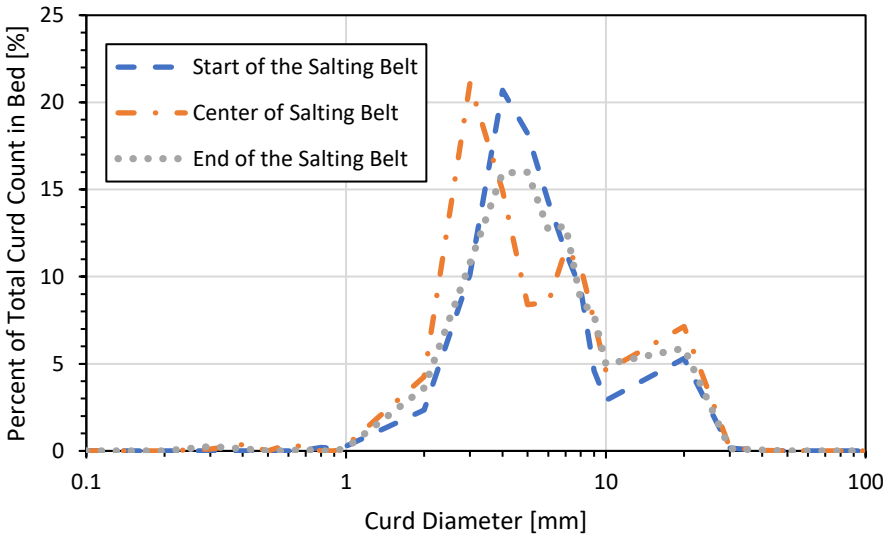

(b)

Figure 7-21: Curd size distribution by (a) calculated spherical volume and (b) curd count for curd samples taken from three locations on the salting belt, approximately equivalent to sampling within the first minute of salting, fifteen minutes of salting, and thirty minutes of salting.

Although the curd size distribution showed minimal variation between salting locations as assessed by the spherical curd volume, assessment of the curd size distribution using the curd count showed that a fraction of the gels appeared to become slightly larger as they proceeded along the belt. This is likely due to the agglomeration of some smaller curds and premature knitting occurring before the gels reach the end of the belt. Figure 7-21 shows the overall curd size distribution calculated from the mass fraction of the total curd mass collected on each sieve. Figure 7-22 provides the salt and moisture content of the curd samples from each of the sieves.

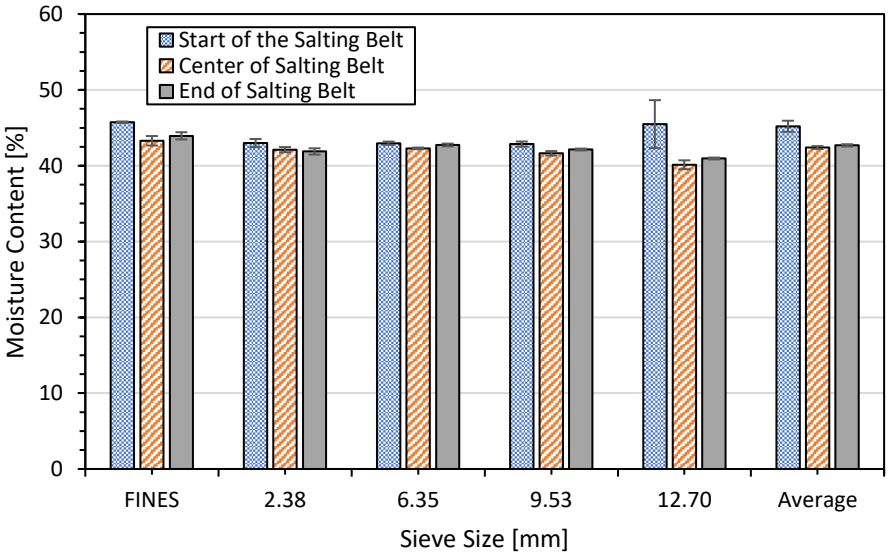

(a)

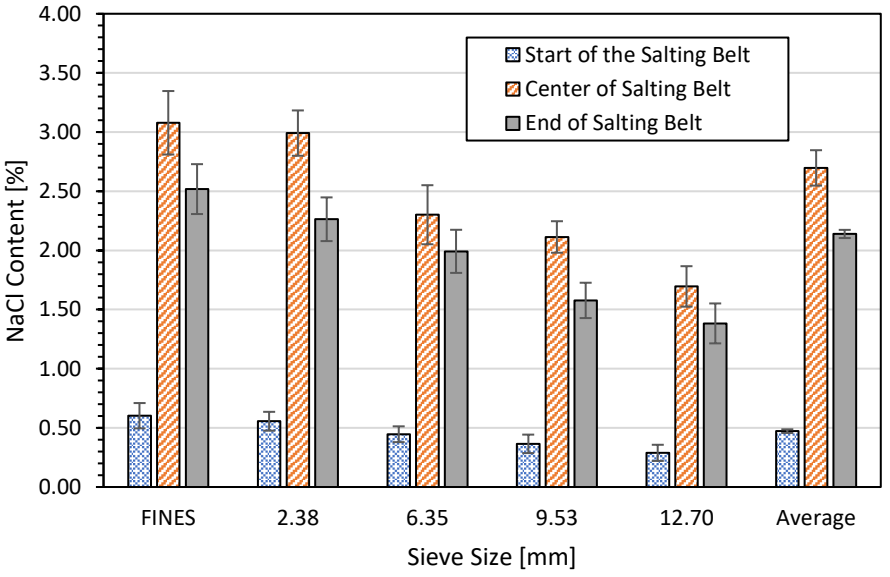

(b)

Figure 7-22: The (a) moisture content and (b) salt content and of curd samples each of the sieve-separated samples collected at the beginning, centre, and end of the salting belt. The mass average salt content and moisture content for the whole sample at each location is also included. Error bars represent the standard error for each measurement.

Results from Figure 7-22 show minimal variation in moisture content between curd samples on each sieve, with only the larger curds on the 12.7 mm sieve showing the expected larger moisture content in the samples selected from the beginning of the belt. The curd samples gradually decrease in moisture content as they proceed along the belt, in general. However, the lack of variation in moisture content may be due in part the presence of surface moisture affecting the moisture content measurement. The models presented in section 7.3 also predict larger moisture mass fractions during the salting step than what was reported in Figure 7-22.

This is primarily due to the nature of the syneresis models that were derived under brining conditions, where gravitational and external pressing affects on whey expulsion (detailed in section 6.1.2) were not contributing to the whey expulsion behaviour. Future work that includes the role of gravitational and external pressing should be conducted to improve the syneresis models presented in this thesis.

The salt content increases significantly midway along the salting belt compared to the beginning of the salting belt, before decreasing slightly in the final sample. This may be due to the location of the salting apparatus on the belt and the degree of mixing before the end of the belt. Interestingly, the salt content increased with a decrease in the curd sizes, as defined by the sieve size. This finding suggests that more salt may have been distributed on the smaller curds than the larger curds for their size, lending credibility to the proposed salting risks discussed in section 7.3.4, when the same salt mass is applied per curd surface area, regardless of curd size.

7.7 Conclusions

This chapter modelled the moisture mass fraction and salt mass fraction changes in differently sized and shaped gels of pH 6.25, 5.75, and 5.25. It also showed the effect of different salting regimens on the anticipated salt uptake and whey expulsion of curd beds with different curd size distributions. The model findings showed that gel pH and curd size demonstrate larger effects on the overall curd bed mass losses and moisture content, and that different salting regimes do not affect the total salt uptake in the gels if all the salt and whey are located within the gel or at the gel surface. However, the models presented in section 7.3.4 were limited in that it was assumed that the appropriate salt mass would be evenly coated on each curd surface.

Appropriate coating of salt is difficult to achieve during cheesemaking and it would be far more likely to have equal coatings over all cheese curds regardless of size. This would create a predicament where larger gels are coated with insufficient salt and smaller gels achieve salt masses exceeding the intended application. The equal coating of salt over all curds would result in considerable variation in the salt mass distribution throughout the curd bed, creating more inconsistent final cheese products.

Results of the models were then compared to curd samples collected from three different locations along the salting belt of an industrial cheddar production line. Findings from the salting belt indicated that smaller curds separated onto smaller sieves yielded higher salt

concentrations than larger gels, lending validity to the risks discussed in section 7.3.4. While there were several assumptions and limitations to the models presented in this chapter, this chapter successfully applied the salt uptake and whey expulsion findings from brining experiments to describe salt uptake in dry salting conditions.

Chapter 8 Research Conclusions and Future Work

8.1 Research Findings

Controlling salt uptake and moisture transport in fresh cheese curds is vital to the production of safe, functional, and delicious cheese products. This thesis has successfully developed new methods for evaluating and modelling salt uptake and syneresis in renneted skim milk gels as curd analogues using image analysis techniques. It has also investigated the effect of gel pH, induced osmotic pressure differentials, and the role of salt in whey expulsion and salt uptake behaviour, with care taken to describe salt uptake simultaneously with osmotic pressure induced whey expulsion.

Osmotic pressure differential induced whey expulsion models have been used to estimate internal pressure gradients driving syneresis, while both osmotic pressure differential induced syneresis models and diffusion models and have been applied to predicting salt uptake and whey losses during dry salting cheese curds. Salt uptake and whey expulsion models applied to dry salting conditions were compared to curd samples collected at three different locations along the salting belt of an industrial cheddar production line. Comparisons between model findings and curd properties showed that the curds likely undergo equal or near-equal salt application overall all curd surfaces, regardless of the curd size. This creates significant variation in the total salt uptake of curds, creating routes for inconsistency in the salt distribution within final cheese products. This does not consider any diffusion after the cheese has been pressed, where there is an opportunity for salt to diffuse through the cheese block.

8.2 Future Work Recommendations

The work presented in this thesis is a vital step towards an improved, mechanistically derived understanding of the processes governing the production of cheese products. Future work should seek to expand upon the existing mathematical models to account for the kinetic effects of changing temperatures and pH values throughout the syneresis and salting processes. Efforts should also be made to confirm the role of dairy fats or the presence of other protein components in the salt uptake and whey expulsion models developed to mechanistically describe salt uptake and whey expulsion behaviour. Furthermore, assessing the salt adsorption behaviour observed in Chapter 5 would provide insight to the molecular relationships between para-casein networks and salts. This thesis has provided an important step to better understanding the mechanisms driving salt uptake and whey expulsion and will

hopefully provide a starting point for assessing other dynamic processes occurring during the production of cheese and other dairy products.

Chapter 9 References

Aguilera, J. (2005). Why food microstructure? *Journal of Food Engineering, 67*(1–2), 3-11. doi:http://dx.doi.org/10.1016/j.jfoodeng.2004.05.050

Alsvik, I., & Hagg, M. (2013). Pressure Retarded Osmosis and Forward Osmosis Membranes: Materials and Methods. *Polymers, 5*(1), 303-327. doi:10.3390/polym5010303

Anderson, J., & Malone, D. (1974). Mechanism of Osmotic Flow in Porous Membranes. *Biophysical Journal, 14*(12), 957-982.

Arboatti, A., Olivares, M., Sabbag, N., Costa, S., Zorrilla, S., & Sihufe, G. (2014). The influence of sodium chloride reduction on physicochemical, biochemical, rheological and sensory characteristics of Mozzarella cheese. *Dairy Science & Technology, 94*(4), 373-386. doi:10.1007/s13594-014-0169-2

Baldwin, A., & Wiles, P. (1996). Dry salting of cheese. 2. Variability. *Food and Bioproducts Processing, 74*(C3), 133-139.

Baroni, A., Menezes, M., Ardell, E., & Ribeiro, E. (2003). Modeling of Prato cheese salting: fickian and neutral network approaches. In J. Welti-Chanes, J. Velez-Ruiz, & G. Barbosa-Canovas (Eds.), *Transport Phenomena in Food Processing* (pp. 192-212). Boca Raton, USA: CRC Press.

Bear, J. (2013). *Dynamics of fluids in porous media*: Courier Corporation.

Beghin, J. (2006). Evolving dairy markets in Asia: Recent findings and implications. *Food Policy, 31*(3), 195-200. doi:http://dx.doi.org/10.1016/j.foodpol.2006.03.001

Bellagha, S., Sahli, A., Farhat, A., Kechaou, N., & Glenza, A. (2007). Studies on salting and drying of sardine (Sardinella aurita): Experimental kinetics and modeling. *Journal of Food Engineering, 78*(3), 947-952. doi:10.1016/j.jfoodeng.2005.12.008

Bellwood, P. (2005). *First Farmers: The Origins of Agricultural Societies*. Oxford, UK: Blackwell Publishing.

Bennett, R., & Johnston, K. (2004). General Aspects of Cheese Technology. In P. Fox, P. McSweeney, T. Cogan, & T. Guinee (Eds.), *Cheese: Chemistry, Physics and Microbiology* (Third Edition ed., pp. 23-50). London, UK: Elesevier Academic Press.

Bhalla, G., & Deen, W. (2007). Effects of molecular shape on osmotic reflection coefficients. *Journal of Membrane Science, 306*(1-2), 116-124. doi:10.1016/j.memsci.2007.08.025

Bird, R. (2004). Five decades of transport phenomena. *AIChE Journal, 50*(2), 273-287. doi:10.1002/aic.10026

Bird, R., & Klingenberg, D. (2013). Multicomponent diffusion—A brief review. *Advances in Water Resources, 62, Part B*, 238-242. doi:http://dx.doi.org/10.1016/j.advwatres.2013.05.010

Bird, R., Stewart, W., & Lightfoot, E. (2007). *Transport Phenomena* (Revised Second Edition ed.). New York: Wiley.

Boisard, L., Andriot, I., Arnould, C., Achilleos, C., Salles, C., & Guichard, E. (2013). Structure and composition of model cheeses influence sodium NMR mobility, kinetics of sodium release and sodium partition coefficients. *Food Chemistry, 136*(2), 1070-1077. doi:10.1016/j.foodchem.2012.09.035

Bona, E., Borsato, D., Silva, R., & Silva, L. (2005). Multicomponent diffusion during simultaneous brining of Prato Brazilian cheese. [Difusao multicomponente durante a salga mista de queijo Prato.]. *Ciencia E Tecnologia De Alimentos, 25*(2), 394-400. doi:10.1590/s0101-20612005000200036

Bona, E., dos Santos Ferreira da Silva, R., Borsato, D., Monken e Silva, L., & de Souza Fidelis, D. (2010). Multicomponent diffusion during Prato cheese ripening:

mathematical modeling using the finite element method. *Ciencia E Tecnologia De Alimentos, 30*(4), 955-963. doi:10.1590/s0101-20612010000400018
Borsato, D., Moreira, I., dos Santos Ferreira da Silva, R., Bona, E., Nobrega, M., Roberto Pina, M., & Moreira, M. (2010). Simulation of the multicomponent diffusion during the osmotic dehydration of apple: determination of the diffusion coefficients by the simplex method. *Semina-Ciencias Agrarias, 31*(2), 391-403.
Boudhrioua, N., Djendoubi, N., Bellagha, S., & Kechaou, N. (2009). Study of moisture and salt transfers during salting of sardine fillets. *Journal of Food Engineering, 94*(1), 83-89. doi:10.1016/j.jfoodeng.2009.03.005
Breene, W., Price, W., & Ernstrom, C. (1964). Changes in Composition of Cheddar Curd during Manufacture as a Guide to Cheese Making by Direct Acidification. *Journal of Dairy Science, 47*(8), 840-&.
Caplice, E., & Fitzgerald, G. (1999). Food fermentations: role of microorganisms in food production and preservation. *International Journal of Food Microbiology, 50*(1-2), 131-149. doi:10.1016/s0168-1605(99)00082-3
Casales, M., Capaccioni, M., & Yeannes, M. (2009). Obtainment of equilibrium times and diffusion coefficients of acid and salt to design the marinating process of Engraulis anchoita fillets. *Ciencia E Tecnologia De Alimentos, 29*(4), 933-937.
Cath, T., Childress, A., & Elimelech, M. (2006). Forward osmosis: Principles, applications, and recent developments. *Journal of Membrane Science, 281*(1–2), 70-87. doi:http://dx.doi.org/10.1016/j.memsci.2006.05.048
Chevanan, N., & Muthukumarappan, K. (2007). Effect of calcium and phosphorus, residual lactose, and salt-to-moisture ratio on the melting characteristics and hardness of cheddar cheese during ripening. *Journal of Food Science, 72*(4), E168-E176. doi:10.1111/j.1750-3841.2007.00330.x
Choi, J., Horne, D., Johnson, M., & Lucey, J. (2008). Effects of the concentration of insoluble calcium phosphate associated with casein micelles on the functionality of directly acidified cheese. *Journal of Dairy Science, 91*(2), 513-522. doi:10.3168/jds.2007-0454
Choi, J., Horne, D., & Lucey, J. (2015). Effect of insoluble calcium concentration on endogenous syneresis rate in rennet-coagulated bovine milk. *Journal of Dairy Science, 98*(9), 5955-5966. doi:10.3168/jds.2015-9527
Cooper, C., Corredig, M., & Alexander, M. (2010). Investigation of the Colloidal Interactions at Play in Combined Acidification and Rennet of Different Heat-Treated Milks. *Journal of Agricultural and Food Chemistry, 58*(8), 4915-4922. doi:10.1021/jf100372b
Crank, J. (1975). *The Mathematics of Diffusion*. Oxford, UK: Oxford University Press.
CRC Handbook of Chemistry and Physics (2005). (D. Lide Ed. 86th ed.). Boca Raton, FL: CRC Press.
Creamer, L. (1985). Water-Absorption by Renneted Casein Micelles. *Milchwissenschaft-Milk Science International, 40*(10), 589-591.
Dalgleish, D. (2009). Coagulation of renneted bovine casein micelles: dependence on temperature, calcium ion concentration and ionic strength. *Journal of Dairy Research, 50*(3), 331-340. doi:10.1017/S0022029900023165
Daviau, C., Pierre, A., Famelart, M., Goudedranche, H., Jacob, D., Garnier, M., & Maubois, J. (2000). Residual amount of water in a draining curd of Camembert cheese and physicochemical characteristics of the drained curd as modified by the pH at renneting, the casein concentration and the ionic strength of milk. *Lait, 80*(6), 555-571.

Dejmek, P., & Walstra, P. (2004). The Syneresis of Rennet-coagulated Curd. In F. Fox, P. McSweeney, T. Cogan, & T. Guinee (Eds.), *Cheese: Chemistry, Physics and Microbiology* (Third Edition ed., pp. 71-103). London, UK: Elesevier Academic Press.

Dictionary, O. E. (1909). *"salary, n."*: Oxford University Press.

Dimos, A., Urbach, G., & Miller, A. (1996). Changes in flavour and volatiles of full-fat and reduced-fat Cheddar cheeses during maturation. *International Dairy Journal, 6*(10), 981-995. doi:10.1016/s0958-6946(97)84214-8

Dong, F. (2006). The outlook for Asian dairy markets: The role of demographics, income, and prices. *Food Policy, 31*(3), 260-271. doi:http://dx.doi.org/10.1016/j.foodpol.2006.02.007

Doulia, D., Tzia, K., & Gekas, V. (2000). A knowledge base for the apparent mass diffusion coefficient (D-EFF) of foods. *International Journal of Food Properties, 3*(1), 1-14.

Duplessis, J., & Masliyah, J. (1991). Flow through Isotropic Granular Porous-Media. *Transport in Porous Media, 6*(3), 207-221. doi:10.1007/bf00208950

El-Bakry, M., & Sheehan, J. (2014). Analysing cheese microstructure: A review of recent developments. *Journal of Food Engineering, 125*, 84-96. doi:10.1016/j.jfoodeng.2013.10.030

Emam-Djomeh, Z., Djelveh, G., & Gros, J. B. (2001). Osmotic dehydration of foods in a multicomponent solution Part I. Lowering of solute uptake in agar gels: Diffusion considerations. *Lebensmittel-Wissenschaft Und-Technologie-Food Science and Technology, 34*(5), 312-318. doi:10.1006/fstl.2001.0776

Euston, S., Piska, N., Wium, H., & Qvist, K. (2002). Controlling the structure and rheological properties of model cheese systems. *Australian Journal of Dairy Technology, 57*(2), 145-152.

Everett, D., & Auty, M. (2008). Cheese structure and current methods of analysis. *International Dairy Journal, 18*(7), 759-773. doi:10.1016/j.idairyj.2008.03.012

Everett, D., & Auty, M. (2017). Cheese Microstructure. In P. McSweeney, P. Fox, P. Cotter, & D. Everett (Eds.), *Cheese: Chemistry, Physics and Microbiology* (Fourth Edition ed., pp. 547-569). San Diego, California: Elsevier Science.

Fagan, C., Castillo, M., Payne, F., O'Donnell, C., Leedy, M., & O'Callaghan, D. (2007). Novel online sensor technology for continuous monitoring of milk coagulation and whey separation in cheesernaking. *Journal of Agricultural and Food Chemistry, 55*(22), 8836-8844. doi:10.1021/jf070807b

Fagan, C., O'Callaghan, D., Mateo, M., & Dejmek, P. (2017). The Syneresis of Rennet-Coagulated Curd. In P. McSweeney, P. Fox, P. Cotter, & D. Everett (Eds.), *Cheese: Chemistry, Physics and Microbiology* (Fourth Edition ed., pp. 145-177). San Diego, California: Elsevier Science.

FAO. (2016). Cheese (all types) *FAOSTAT*. Paris, France.

Fenoul, F., Le Denmat, M., Hamdi, F., Cuvelier, G., & Michon, C. (2008). Technical note: Confocal scanning laser microscopy and quantitative image analysis: Application to cream cheese microstructure investigation. *Journal of Dairy Science, 91*(4), 1325-1333. doi:10.3168/jds.2007-0531

Fick, A. (1995). On Liquid Diffusion (Reprinted from the London, Edinburgh, and Dublin Philosophical Magazine and Journal of Science, Vol 10, pg 30, 1855). *Journal of Membrane Science, 100*(1), 33-38. doi:10.1016/0376-7388(94)00230-v

Floury, J., Camier, B., Rousseau, F., Lopez, C., Tissier, J., & Famelart, M. (2009). Reducing salt level in food: Part 1. Factors affecting the manufacture of model cheese systems and their structure-texture relationships. *Lwt-Food Science and Technology, 42*(10), 1611-1620. doi:10.1016/j.lwt.2009.05.026

Floury, J., Jeanson, S., Aly, S., & Lortal, S. (2010). Determination of the diffusion coefficients of small solutes in cheese: A review. *Dairy Science & Technology, 90*(5), 477-508. doi:10.1051/dst/2010011

Floury, J., Madec, M., Waharte, F., Jeanson, S., & Lortal, S. (2012). First assessment of diffusion coefficients in model cheese by fluorescence recovery after photobleaching (FRAP). *Food Chemistry, 133*(2), 551-556. doi:10.1016/j.foodchem.2012.01.030

Floury, J., Rouaud, O., Le Poullennec, M., & Famelart, M. (2009). Reducing salt level in food: Part 2. Modelling salt diffusion in model cheese systems with regards to their composition. *Lwt-Food Science and Technology, 42*(10), 1621-1628. doi:10.1016/j.lwt.2009.06.002

Foegeding, E., & Drake, M. (2007). Invited review: Sensory and mechanical properties of cheese texture. *Journal of Dairy Science, 90*(4), 1611-1624. doi:10.3168/jds.2006-703

Fox, P., Guinee, T., Cogan, T., & McSweeney, P. (2000a). Cheese Rheology and Texture *Fundamentals of Cheese Science* (pp. 305-340). Gaithersburg, Maryland: Aspen Publishers, Inc.

Fox, P., Guinee, T., Cogan, T., & McSweeney, P. (2000b). Cheese: Historical Aspects *Fundamentals of Cheese Science* (pp. 1-9). Gaithersburg, Maryland: Aspen Publishers, Inc.

Fox, P., Guinee, T., Cogan, T., & McSweeney, P. (2000c). Overview of Cheese Manufacture *Fundamentals of Cheese Science* (pp. 10-18). Gaithersburg, Maryland.

Fox, P., Guinee, T., Cogan, T., & McSweeney, P. (2000d). Salting of Cheese Curd *Fundamentals of Cheese Science* (pp. 153-168). Gaithersburg, Maryland: Aspen Publishers, Inc.

Fox, P., Guinee, T., Cogan, T., & McSweeney, P. (2000e). Whey and Whey Products *Fundamentals of Cheese Science* (pp. 514-522). Gaithersburg, Maryland: Aspen Publishers, Inc.

Fox, P., & McSweeney, P. (2004). Cheese: An Overview. In P. Fox, P. McSweeney, T. Cogan, & T. Guinee (Eds.), *Cheese: Chemistry, Physics and Microbiology* (Third Edition ed., pp. 1-18). London, UK: Elesevier Academic Press.

Fucà, N., McMahon, D., Caccamo, M., Tuminello, L., La Terra, S., Manenti, M., & Licitra, G. (2012). Effect of brine composition and brining temperature on cheese physical properties in Ragusano cheese. *Journal of Dairy Science, 95*(1), 460-470. doi:http://dx.doi.org/10.3168/jds.2011-4438

Gal, S., & Bankay, D. (1971). Hydration of Sodium Chloride Bound by Casein at Medium Water Activities. *Journal of Food Science, 36*(5), 800-&.

Garcia-Castello, E., McCutcheon, J., & Elimelech, M. (2009). Performance evaluation of sucrose concentration using forward osmosis. *Journal of Membrane Science, 338*(1–2), 61-66. doi:http://dx.doi.org/10.1016/j.memsci.2009.04.011

Gencer, G., & Turhan, M. (1988). Modelling of Salt Transfer During Brining of Feta Cheese and Determination of Diffusion-Coefficient. *Journal of Food Protection, 51*(10), 826-826.

Gerla, P., & Rubiolo, A. (2003). A model for determination of multicomponent diffusion coefficients in foods. *Journal of Food Engineering, 56*(4), 401-410. doi:10.1016/s0260-8774(02)00213-3

Geurts, T. (1978). Some factors which affect the moisture content of cheese before salting. *Netherlands Milk and Dairy Journal, 32*, 112-124.

Geurts, T., & Oortwijn, H. (1975). Transport Phenomena in Butter, in Relation to its Structure. *Netherlands Milk and Dairy Journal, 29*(2-3), 253-262.

Geurts, T., Walstra, P., & Mulder, H. (1974). Transport of salt and water during the salting of cheese. 1. Analysis of the processes involved. *Netherlands Milk and Dairy Journal, 28*, 102-129.
Geurts, T., Walstra, P., & Mulder, H. (1980). Transport of Salt and Water during Salting of Cheese 2. Quantities of Salt Taken up and of Moisture Lost. *Netherlands Milk and Dairy Journal, 34*(4), 229-254.
Giroux, H., Bouchard, C., & Britten, M. (2014). Combined effect of renneting pH, cooking temperature, and dry salting on the contraction kinetics of rennet-induced milk gels. *International Dairy Journal, 35*(1), 70-74. doi:10.1016/j.idairyj.2013.10.016
Gomes, A., Vieira, M., & Malcata, F. (1998). Survival of probiotic microbial strains in a cheese matrix during ripening: Simulation of rates of salt diffusion and microorganism survival. *Journal of Food Engineering, 36*(3), 281-301. doi:10.1016/s0260-8774(98)00062-4
Greenfield, H. (2010). The Secondary Products Revolution: the past, the present and the future. *World Archaeology, 42*(1), 29-54. doi:10.1080/00438240903429722
Gros, J., & Ruegg, M. (1987). Determination of the apparent diffusion coefficient of sodium chloride in model foods and cheese. In R. Jowitt (Ed.), *Physical Properties of Foods* (Vol. Volume 2, pp. 71-108). London, UK: Elesevier Applied Science.
Grundelius, A., Lodaite, K., Ostergren, K., Paulsson, M., & Dejmek, P. (2000). Syneresis of submerged single curd grains and curd rheology. *International Dairy Journal, 10*(7), 489-496.
Guinee, T. (2004). Salting and the role of salt in cheese. *International Journal of Dairy Technology, 57*(2-3), 99-109. doi:10.1111/j.1471-0307.2004.00145.x
Guinee, T. (2007). Salt in Cheese. In P. McSweeney (Ed.), *Cheese Problems Solved* (pp. 80-99). Boca Raton, Florida: CRC Press.
Guinee, T., & Fox, P. (1986). Influence of Cheese Geometry on the Movement of Sodium-chloride and Water during Ripening. *Irish Journal of Food Science and Technology, 10*(2), 97-118.
Guinee, T., & Fox, P. (2017). Salt in Cheese: Physical, Chemical and Biological Aspects. In P. McSweeney, P. Fox, P. Cotter, & D. Everett (Eds.), *Cheese: Chemistry, Physics and Microbiology* (Fourth Edition ed., pp. 317-375). San Diego, California: Elsevier Science.
Guinee, T. P., & Fox, P. F. (2004). Salt in Cheese: Physical, Chemical, and Biological Aspects. In P. F. Fox, P. L. H. McSweeney, T. M. Cogan, & T. P. Guinee (Eds.), *Cheese Chemistry, Physics and Microbiology* (Third Edition ed., Vol. Volume 1 General Aspects). London, UK: Elesevier Academic Press.
Haerifar, M., & Azizian, S. (2012). Fractal-Like Adsorption Kinetics at the Solid/Solution Interface. *Journal of Physical Chemistry C, 116*(24), 13111-13119. doi:10.1021/jp301261h
Halmos, A., Pollard, A., Sherkat, F., & Seuret, M. (2003). Natural cheddar cheese texture variation as a result of milk seasonality. *Journal of Texture Studies, 34*(1), 21-40. doi:10.1111/j.1745-4603.2003.tb01053.x
Hardy, J. (1976). *Etude de la diffusion du sel dans les fromages à pâte molle de type camembert. Comparaison du salage à sec et du salage en saumure.* (PhD Thesis), Université Nancy 1, France.
Hardy, J., & Steinberg, M. (1984). Interaction Between Sodium-Chloride and Paracasein as Determined by Water Sorption. *Journal of Food Science, 49*(1), 127-&. doi:10.1111/j.1365-2621.1984.tb13688.x
Henneberry, S., Wilkinson, M., Kilcawley, K., Kelly, P., & Guinee, T. (2015). Interactive effects of salt and fat reduction on composition, rheology and functional properties of

mozzarella-style cheese. *Dairy Science & Technology, 95*(5), 613-638. doi:10.1007/s13594-015-0231-8
Higman, B. (2012). Preservation and Processing *How Food Made History* (pp. 103-124): Blackwell Publishing, Ltd.
Hinrichs, R., Bulca, S., & Kulozik, U. (2007). Water mobility during renneting and acid coagulation of casein solutions: a differentiated low-resolution nuclear magnetic resonance analysis. *International Journal of Dairy Technology, 60*(1), 37-43. doi:10.1111/j.1471-0307.2007.00290.x
Horne, D. (2002). Casein structure, self-assembly and gelation. *Current Opinion in Colloid & Interface Science, 7*(5-6), 456-461. doi:10.1016/s1359-0294(02)00082-1
Horne, D., & Banks, J. (2004). Rennet-induced Coagulation of Milk. In P. Fox, P. McSweeney, T. Cogan, & T. Guinee (Eds.), *Cheese: Chemistry, Physics, and Microbiology* (Third Edition ed., pp. 47-70). London, UK: Elsevier Academic Press.
Horne, D., & Lucey, J. (2017). Rennet-Induced Coagulation of Milk. In P. McSweeney, P. Fox, P. Cotter, & D. Everett (Eds.), *Cheese: Chemistry, Physics and Microbiology* (Fourth Edition ed., pp. 115-143). San Diego, California: Elsevier Science.
Horne, D. S., & Banks, J. M. (2004). Rennet-induced Coagulation of Milk. In P. F. Fox, P. L. H. McSweeney, T. M. Cogan, & T. P. Guinee (Eds.), *Cheese Chemistry, Physics and Microbiology* (Third Edition ed.). London, UK: Elesevier Academic Press.
Johnson, M., & Law, B. (1999). The origins, development and basic operations of cheesemaking technology. In B. A. Law (Ed.), *Technology of Cheesemaking* (pp. 1-32). Sheffield, UK: Sheffield Academic Press.
Kapur, V., Charkoudian, J., & Anderson, J. (1997). Transport of proteins through gel-filled porous membranes. *Journal of Membrane Science, 131*(1-2), 143-153. doi:10.1016/s0376-7388(97)00037-9
Kiil, F. (2003). Kinetic model of osmosis through semipermeable and solute-permeable membranes. *Acta Physiologica Scandinavica, 177*(2), 107-117. doi:10.1046/j.1365-201X.2003.01062.x
Kindstedt, P. (2012). *Cheese and Culture: A History of Cheese and Its Place in Western Civilization*. White River Junction, VT: Chelsea Green Publishing.
Lauverjat, C., Deleris, I., Trelea, I., Salles, C., & Souchon, I. (2009). Salt and Aroma Compound Release in Model Cheeses in Relation to Their Mobility. *Journal of Agricultural and Food Chemistry, 57*(21), 9878-9887. doi:10.1021/jf901446w
Law, B. (2001). Cheddar cheese production. In A. Y. Tamine & B. A. Law (Eds.), *Mechanisation and Automation in Dairy Technology* (pp. 204-224). Sheffield, UK: Sheffield Academic Press.
Lawrence, R., & Gilles, J. (1969). The formation of bitterness in cheese: a critical evaluation. *New Zealand Journal of Dairy Science and Technology, 4*, 89-196.
Liu, Y., & Shen, L. (2008). From Langmuir Kinetics to First- and Second-Order Rate Equations for Adsorption. *Langmuir, 24*(20), 11625-11630. doi:10.1021/la801839b
Lodaite, K., Ostergren, K., Paulsson, M., & Dejmek, P. (2000). One-dimensional syneresis of rennet-induced gels. *International Dairy Journal, 10*(12), 829-834. doi:10.1016/s0958-6946(01)00027-9
Logan, A., Day, L., Pin, A., Auldist, M., Leis, A., Puvanenthiran, A., & Augustin, M. (2014). Interactive Effects of Milk Fat Globule and Casein Micelle Size on the Renneting Properties of Milk. *Food and Bioprocess Technology, 7*(11), 3175-3185. doi:10.1007/s11947-014-1362-2
Lu, Y., & McMahon, D. (2015). Effects of sodium chloride salting and substitution with potassium chloride on whey expulsion of Cheddar cheese. *Journal of Dairy Science, 98*(1), 78-88. doi:10.3168/jds.2014-8600

Lucey, J. (2002). Formation and physical properties of milk protein gels. *Journal of Dairy Science, 85*(2), 281-294.
Lucey, J., Johnson, M., & Horne, D. (2003). Invited review: Perspectives on the basis of the rheology and texture properties of cheese. *Journal of Dairy Science, 86*(9), 2725-2743. doi:10.3168/jds.S0022-0302(03)73869-7
Lucey, J., Tamehana, M., Singh, H., & Munro, P. (1998). A comparison of the formation, rheological properties and microstructure of acid skim milk gels made with a bacterial culture or glucono-δ-lactone. *Food Research International, 31*(2), 147-155. doi:http://dx.doi.org/10.1016/S0963-9969(98)00075-1
Lucey, J., Tamehana, M., Singh, H., & Munro, P. (2000). Rheological properties of milk gels formed by a combination of rennet and glucono-delta-lactone. *Journal of Dairy Research, 67*(3), 415-427. doi:10.1017/s0022029900004246
Lucey, J., Tamehana, M., Singh, H., & Munro, P. (2001). Effect of heat treatment on the physical properties of milk gels made with both rennet and acid. *International Dairy Journal, 11*(4-7), 559-565. doi:10.1016/s0958-6946(01)00081-4
Lucey, J., van Vliet, T., Grolle, K., Geurts, T., & Walstra, P. (1997a). Properties of acid casein gels made by acidification with glucono-δ-lactone. 1. Rheological properties. *International Dairy Journal, 7*(6–7), 381-388. doi:http://dx.doi.org/10.1016/S0958-6946(97)00027-7
Lucey, J., van Vliet, T., Grolle, K., Geurts, T., & Walstra, P. (1997b). Properties of acid casein gels made by acidification with glucono-δ-lactone. 2. Syneresis, permeability and microstructural properties. *International Dairy Journal, 7*(6–7), 389-397. doi:http://dx.doi.org/10.1016/S0958-6946(97)00028-9
Luna, J., & Bressan, J. (1986). Mass-Transfer during Brining of Cuartirolo Argentino Cheese. *Journal of Food Science, 51*(3), 829-831. doi:10.1111/j.1365-2621.1986.tb13942.x
Luna, J., & Bressan, J. (1987). Mass-Transfer during Ripening of Cuartirolo Argentino Cheese. *Journal of Food Science, 52*(2), 308-311. doi:10.1111/j.1365-2621.1987.tb06600.x
Luo, J., Pan, T., Guo, H., & Ren, F. (2013). Effect of calcium in brine on salt diffusion and water distribution of Mozzarella cheese during brining. *Journal of Dairy Science, 96*(2), 824-831. doi:10.3168/jds.2012-5888
Luo, Y., & Roux, B. (2010). Simulation of Osmotic Pressure in Concentrated Aqueous Salt Solutions. *Journal of Physical Chemistry Letters, 1*(1), 183-189. doi:10.1021/jz900079w
Marczewski, A. (2010). Analysis of Kinetic Langmuir Model. Part I: Integrated Kinetic Langmuir Equation (IKL): A New Complete Analytical Solution of the Langmuir Rate Equation. *Langmuir, 26*(19), 15229-15238. doi:10.1021/la1010049
Mateo, M., O'Callaghan, D., Gowen, A., & O'Donnell, C. (2010). Evaluation of a vat wall-mounted image capture system using image processing techniques to monitor curd moisture during syneresis with temperature treatments. *Journal of Food Engineering, 99*(3), 257-262. doi:10.1016/j.jfoodeng.2010.02.019
Mateo, M., O'Callaghan, D., Everard, C., Castillo, M., Payne, F., & O'Donnell, C. (2009). Validation of a curd-syneresis sensor over a range of milk composition and process parameters. *Journal of Dairy Science, 92*(11), 5386-5395. doi:http://dx.doi.org/10.3168/jds.2009-2363
Mavroudis, N., Gekas, V., & Sjöholm, I. (1998). Osmotic dehydration of apples. Shrinkage phenomena and the significance of initial structure on mass transfer rates. *Journal of Food Engineering, 38*(1), 101-123. doi:http://dx.doi.org/10.1016/S0260-8774(98)00090-9

McCarthy, C., Wilkinson, M., Kelly, P., & Guinee, T. (2016). Effect of salt and fat reduction on proteolysis, rheology and cooking properties of Cheddar cheese. *International Dairy Journal, 56*, 74-86. doi:10.1016/j.idairyj.2016.01.001

McMahon, D., Paulson, B., & Oberg, C. (2005). Influence of calcium, pH, and moisture on protein matrix structure and functionality in direct-acidified nonfat Mozzarella cheese. *Journal of Dairy Science, 88*(11), 3754-3763.

McSweeney, P. (2004). Biochemistry of Cheese ripening: Introduction and Overview. In P. Fox, P. McSweeney, T. Cogan, & T. Guinee (Eds.), *Cheese: Chemistry, Physics and Microbiology* (Third Edition ed., pp. 347-360). London, UK: Elesevier Academic Press.

McSweeney, P. (2007). Syneresis. In P. McSweeney (Ed.), *Cheese Problems Solved* (pp. 72-79). Boca Raton, Florida: CRC Press.

McSweeney, P., Ottogalli, G., & Fox, P. (2004). Diversity of cheese varieties: An overview. In P. Fox, P. McSweeney, T. Cogan, & T. Guinee (Eds.), *Cheese: Chemistry, Physics and Microbiology* (pp. 1-23). London, UK: Elesevier Academic Press.

Melilli, C., Barbano, D., Licitra, G., Portelli, G., Di Rosa, G., & Carpino, S. (2003). Influence of the temperature of salt brine on salt uptake by Ragusano cheese. *Journal of Dairy Science, 86*(9), 2799-2812. doi:10.3168/jds.S0022-0302(03)73877-6

Melilli, C., Carcò, D., Barbano, D., Tumino, G., Carpino, S., & Licitra, G. (2005). Composition, Microstructure, and Surface Barrier Layer Development During Brine Salting. *Journal of Dairy Science, 88*(7), 2329-2340. doi:http://dx.doi.org/10.3168/jds.S0022-0302(05)72911-8

Mellema, M., Heesakkers, J., van Opheusden, J., & van Vliet, T. (2000). Structure and Scaling Behavior of Aging Rennet-Induced Casein Gels Examined by Confocal Microscopy and Permeametry. *Langmuir, 16*(17), 6847-6854. doi:10.1021/la000135i

Milk and Milk Products Price and Trade Update. (2015). Retrieved from Paris, France:

Moller, K., Rattray, F., Hoier, E., & Ardo, Y. (2012). Manufacture and biochemical characteristics during ripening of Cheddar cheese with variable NaCl and equal moisture content. *Dairy Science & Technology, 92*(5), 515-540. doi:10.1007/s13594-012-0076-3

Moreira, R., & Sereno, A. (2003). Evaluation of mass transfer coefficients and volumetric shrinkage during osmotic dehydration of apple using sucrose solutions in static and non-static conditions. *Journal of Food Engineering, 57*(1), 25-31. doi:10.1016/s0260-8774(02)00217-0

Morris, H., Guinee, T., & Fox, P. (1985). Salt Diffusion in Cheddar Cheese. *Journal of Dairy Science, 68*(8), 1851-1858. doi:10.3168/jds.S0022-0302(85)81041-9

O'Callaghan, D., & Guinee, T. (2004). Rheology and Texture of Cheese. In P. Fox, P. McSweeney, T. Cogan, & T. Guinee (Eds.), *Cheese: Chemistry, Physics and Microbiology* (Third Edition ed., pp. 511-540). London, UK: Elesevier Academic Press.

Ochoa-Martinez, C., Ramaswamy, H., & Ayala-Aponte, A. (2007). A comparison of some mathematical models used for the prediction of mass transfer kinetics in osmotic dehydration of fruits. *Drying Technology, 25*(10), 1613-1620. doi:10.1080/07373930701590665

OECD-FAO Agricultural Outlook 2015. (2015). Retrieved from Paris, France:

Ong, L., Dagastine, R., Kentish, S., & Gras, S. (2011). Microstructure of milk gel and cheese curd observed using cryo scanning electron microscopy and confocal microscopy. *Lwt-Food Science and Technology, 44*(5), 1291-1302. doi:10.1016/j.lwt.2010.12.026

Ong, L., Dagastine, R., Kentish, S., & Gras, S. (2012). The effect of pH at renneting on the microstructure, composition and texture of Cheddar cheese. *Food Research International, 48*(1), 119-130. doi:10.1016/j.foodres.2012.02.020

Ong, L., Lawrence, R., Gilles, J., Creamer, L., Crow, V., Heap, H., . . . Gras, S. (2004). Cheddar cheese and related dry-salted cheese varieties. In P. Fox, P. McSweeney, T. Cogan, & T. Guinee (Eds.), *Cheese: Chemistry, Physics and Microbiology* (Third Edition ed., pp. 71-102). London, UK: Elesevier Academic Press.

Pajonk, A., Saurel, R., & Andrieu, J. (2003). Experimental study and modeling of effective NaCl diffusion coefficients values during Emmental cheese brining. *Journal of Food Engineering, 60*(3), 307-313. doi:10.1016/s0260-8774(03)00052-9

Parente, E., & Cogan, T. (2004). Starter Cultures: General Aspects. In P. Fox, P. McSweeney, T. Cogan, & T. Guinee (Eds.), *Cheese: Chemistry, Physics and Microbiology* (Third Edition ed., pp. 123-147). London, UK: Elesevier Academic Press.

Parsegian, V., Rand, R., Fuller, N., & Rau, D. (1986). Osmotic-stress for the Direct Measurement of Intermolecular Forces. *Methods in Enzymology, 127*, 400-416.

Payne, M., & Morison, K. (1999). A multi-component approach to salt and water diffusion in cheese. *International Dairy Journal, 9*(12), 887-894. doi:10.1016/s0958-6946(99)00157-0

Peri, C., Lucisano, M., & Donati, E. (1985). Studies on Coagulation of Milk Ultrafiltration Retentates 2. Kinetics of Whey Syneresis. *Milchwissenschaft-Milk Science International, 40*(11), 650-652.

Phelan, J., Renaud, J., & Fox, P. (1993). Some non-European cheese varieties. In P. Fox (Ed.), *Cheese: Chemistry, Physics and Microbiology* (Second Edition ed., pp. 421-465). London, UK: Chapman & Hall.

Prasad, N., & Alvarez, V. (1999). Effect of salt and chymosin on the physico-chemical properties of feta cheese during ripening. *Journal of Dairy Science, 82*(6), 1061-1067.

Reid, D., & Fennema, O. (2008). Water and Ice. In S. Damodaran, K. Parkin, & O. Fennema (Eds.), *Food Chemistry* (Fourth Edition ed., pp. 18-82). New York: Marcel Dekker.

Rodriguez, A., Rodriguez, M., & Mascheroni, R. (2015). Characteristic Process Variables during the Osmotic Dehydration of Stone Fruits: Experimental Values and Correlations between Components Content. *Journal of Food Process Engineering, 38*(5), 415-425. doi:10.1111/jfpe.12171

Roos, Y. (1997). Water activity in milk products. In P. Fox (Ed.), *Advanced Dairy Chemistry, Vol. 3, Lactose, Water, Salts and Vitamins* (pp. 303-346). London, UK: Chapman & Hall.

Salque, M., Bogucki, P., Pyzel, J., Sobkowiak-Tabaka, I., Grygiel, R., Szmyt, M., & Evershed, R. (2013). Earliest evidence for cheese making in the sixth millennium BC in northern Europe. *Nature, 493*(7433), 522-525. doi:10.1038/nature11698

Sanchez, E., Simal, S., Femenia, A., Benedito, J., & Rossello, C. (1999). Influence of ultrasound on mass transport during cheese brining. *European Food Research and Technology, 209*(3-4), 215-219. doi:10.1007/s002170050483

Sanchez, E., Simal, S., Femenia, A., & Rossello, C. (2000). Effect of acoustic brining on the transport of sodium chloride and water in Mahon cheese. *European Food Research and Technology, 212*(1), 39-43. doi:10.1007/s002170000181

Sandine, W., & Elliker, P. (1970). Microbially Induced Flavors and Fermented Foods - Flavor in Fermented Dairy Products. *Journal of Agricultural and Food Chemistry, 18*(4), 557-&. doi:10.1021/jf60170a601

Santapaola, J., Maldonado, S., & Medina, J. (2013). NaCl diffusion kinetics in dry salting of goat cheese. *Journal of Food Engineering, 118*(2), 172-177. doi:10.1016/j.jfoodeng.2013.03.028

Sereno, A., Moreira, R., & Martinez, E. (2001). Mass transfer coefficients during osmotic dehydration of apple in single and combined aqueous solutions of sugar and salt. *Journal of Food Engineering, 47*(1), 43-49. doi:http://dx.doi.org/10.1016/S0260-8774(00)00098-4

Shang, W., Tu, C., & Wang, X. (2009). Theoretical calculation of reflection coefficients of single salt solutions through charged porous membranes. *Desalination, 236*(1-3), 306-315. doi:10.1016/j.desal.2007.10.081

Silva, J., Peixoto, P., Lortal, S., & Floury, J. (2013). Transport phenomena in a model cheese: The influence of the charge and shape of solutes on diffusion. *Journal of Dairy Science, 96*(10), 6186-6198. doi:10.3168/jds.2013-6552

Simal, S., Sanchez, E., Bon, J., Femenia, A., & Rossello, C. (2001). Water and salt diffusion during cheese ripening: effect of the external and internal resistances to mass transfer. *Journal of Food Engineering, 48*(3), 269-275. doi:10.1016/s0260-8774(00)00169-2

Sobukola, O., & Olatunde, S. (2011). Effect of salting techniques on salt uptake and drying kinetics of African catfish (Clarias gariepinus). *Food and Bioproducts Processing, 89*(C3), 170-177. doi:10.1016/j.fbp.2010.06.002

Song, Y. (2009). A 2D NMR method to characterize granular structure of dairy products. *Progress in Nuclear Magnetic Resonance Spectroscopy, 55*(4), 324-334. doi:10.1016/j.pnmrs.2009.07.001

St-Gelais, D., Lessard, J., Champagne, C., & Vuillemard, J. (2009). Production of fresh Cheddar cheese curds with controlled postacidification and enhanced flavor. *Journal of Dairy Science, 92*(5), 1856-1863. doi:10.3168/jds.2008-1761

Sutherland, B. (1974). Control of Salt Absorption and Whey Drainage in Cheddar Cheese Manufacture. *Australian Journal of Dairy Technology, 29*(2), 86-93.

Tellier, C., Mariette, F., Guillement, J., & Marchal, P. (1993). Evolution of Water Proton Nuclear Magnetic-Relaxation during Milk Coagulation and Syneresis - Structural Implications. *Journal of Agricultural and Food Chemistry, 41*(12), 2259-2266. doi:10.1021/jf00036a007

Tijskens, E., & De Baerdemaeker, J. (2004). Mathematical modelling of syneresis of cheese curd. *Mathematics and Computers in Simulation, 65*(1-2), 165-175. doi:10.1016/j.matcom.2003.09.016

Timkin, V., & Lazarev, V. (2015). Determination of the osmotic pressure of multicomponent solutions in the food industry. *Petroleum Chemistry, 55*(4), 301-307. doi:10.1134/s0965544114090011

Turhan, M. (1996). Modelling of salt transfer in white cheese during short initial brining. *Netherlands Milk and Dairy Journal, 50*(4), 541-550.

Turhan, M., & Gunasekaran, S. (1999). Analysis of moisture transfer in White cheese during brining. *Milchwissenschaft-Milk Science International, 54*(8), 446-450.

Turhan, M., & Kaletunc, G. (1992). Modeling of Salt Diffusion in White Cheese During Long-Term Brining. *Journal of Food Science, 57*(5), 1082-1085. doi:10.1111/j.1365-2621.1992.tb11269.x

Turner, K., & Thomas, T. (1980). Lactose Fermentation in Cheddar Cheese and the Effect of Salt. *New Zealand Journal of Dairy Science and Technology, 15*(3), 265-276.

van den Bijgaart, H. (1988). *Syneresis of rennet-induced milk gels as influenced by cheesemaking parameters.* (PhD), Wageningen University, Wageningen, Netherlands.

van den Bijgaart, H. (1989). Syneresis of Rennet-Induced Milk Gels as Influenced by Cheese-making Parameters. *Netherlands Milk and Dairy Journal, 43*(1), 92-94.

van Dijk, H. (1982). *Syneresis of Curd.* (PhD), Wageningen University, Wageningen, Netherlands.
van Dijk, H., & Walstra, P. (1986). Syneresis of curd. 2. One-dimensional syneresis of rennet curd in constant conditions. *Netherlands Milk and Dairy Journal, 40*, 3-30.
van Dijk, H., Walstra, P., & Geurts, T. (1979). Preliminary note on syneresis pressure in rennet curd. *Netherlands Milk and Dairy Journal, 33*(1), 60-61.
van Vliet, T., Lakemond, C., & Visschers, R. (2004). Rheology and structure of milk protein gels. *Current Opinion in Colloid & Interface Science, 9*(5), 298-304. doi:10.1016/j.cocis.2004.09.002
van Vliet, T., & Walstra, P. (1994). Water in Casein Gels; How to Get it Out or Keep it In. In P. Fito, A. Mulet, & B. McKenna (Eds.), *Water in Foods* (pp. 75-88). Amsterdam: Pergamon.
Vedamuthu, E. (1979). Microbiologically induced desirable flavors in the fermented foods of the West. *Developments in Industrial Microbiology, 20*, 187-202.
Vogt, S., Smith, J., Seymour, J., Carr, A., Golding, M., & Codd, S. (2015). Assessment of the changes in the structure and component mobility of Mozzarella and Cheddar cheese during heating. *Journal of Food Engineering, 150*, 35-43. doi:http://dx.doi.org/10.1016/j.jfoodeng.2014.10.026
Walstra, P., & van Dijk, H. (1983). Gel Formation and Syneresis. *Netherlands Milk and Dairy Journal, 37*(1-2), 92-93.
Walstra, P., van Dijk, H., & Geurts, T. (1985). The Syneresis of Curd 1. General - Considerations and Literature Review. *Netherlands Milk and Dairy Journal, 39*(4), 209-246.
Welti-Chanes, J., Mujica-Paz, H., Valdez-Fragoso, A., & Leon-Cruz, R. (2003). Fundamentals of Mass Transport. In J. Welti-Chanes, J. F. Velez-Ruiz, & G. V. Barbosa-Canovas (Eds.), *Transport Phenomena in Food Processing* (pp. 11-65). Boca Raton, USA: CRC Press.
Welty, J., Wicks, C., Wilson, R., & Rorrer, G. (2008). Differential Equations of Mass Transfer *Fundamentals of Momentum, Heat, and Mass Transfer* (Fifth Edition ed., pp. 433-451). Hoboken, N. J.: Wiley & Sons, Inc.
Wiles, P., & Baldwin, A. (1996). Dry salting of cheese. 1. Diffusion. *Food and Bioproducts Processing, 74*(C3), 127-132.
Yanniotis, S., & Anifantakis, E. (1983). Diffusion of salt in dry-salted Feta cheese. In R. Jowitt, F. Escher, B. Hallström, H. F. T. Meffert, W. E. L. Spiess, & G. Vos (Eds.), *Physical Properties of Foods, Applied Sciences*. London, UK: Applied Science Publishers.
Ye, A., Anema, S., & Singh, H. (2007). Behaviour of homogenized fat globules during the spray drying of whole milk. *International Dairy Journal, 17*(4), 374-382. doi:10.1016/j.idairyj.2006.04.007
Yousef, M., Datta, R., & Rodgers, V. (1998). Understanding nonidealities of the osmotic pressure of concentrated bovine serum albumin. *Journal of Colloid and Interface Science, 207*(2), 273-282. doi:10.1006/jcis.1998.5789
Zorrilla, S., & Rubiolo, A. (1994a). Fynbo Cheese NaCl and KCl Changes During Ripening. *Journal of Food Science, 59*(5), 972-&. doi:10.1111/j.1365-2621.1994.tb08170.x
Zorrilla, S., & Rubiolo, A. (1994b). A Model for Using the Diffusion Cell in the Determination of Multicomponent Diffusion-Coefficients in Gels or Foods. *Chemical Engineering Science, 49*(13), 2123-2128. doi:10.1016/0009-2509(94)e0006-c

Chapter 10 Nomenclature

Symbol	Definition	Units
A	Image Area	m^2
A_{CS}	Cross-sectional area of the porous medium	m^2
A_{Disk}	Outer edge surface area of the local disk	mm^2
$A_{Disk\text{-}Peak}$	Surface area of the local disk at a peak	mm^2
$A_{p,i}$	Cross-sectional area of an individual pore i	m^2
A_{SA}	Best fit gel surface area at equilibrium	mm^2
$A_{SA,osm}$	Best fit gel surface area at equilibrium during osmotic induced syneresis	mm^2
A_{s0}	Best fit Carman-specific surface	m^{-1}
A_W	Best fit accumulated whey volume at equilibrium	mL
$A_{W,osm}$	Best fit accumulated whey volume at equilibrium during osmotic induced syneresis	mL
A_ε	Best fit gel porosity at equilibrium	-
a_i	Activity of species i	-
B_{SA}	Gel surface area amplitude for long term dominating rate constant	mm^2
$B_{SA,osm}$	Gel surface area amplitude for long term dominating rate constant during osmotic induced syneresis	mm^2
B_{s0}	Carman-specific surface amplitude for long term dominating rate constant	m^{-1}
B_W	Accumulated whey volume amplitude for long term dominating rate constant	mL
$B_{W,osm}$	Accumulated whey volume amplitude for long term dominating rate constant during osmotic induced syneresis	mL
B_ε	Porosity amplitude for the long-term dominating rate constant	-
C_A, C_B	Concentrations in compartments A and B	kg m^{-3}
C_{avg}	Average concentration	kg m^{-3}
C_i, C_j	Concentration of solute i and j	kg m^{-3}
C_s	Concentration of solute at the curd interface or surface	kg m^{-3}
C_{SA}	Gel surface area amplitude for short term dominating rate constant	mm^2
$C_{SA,osm}$	Gel surface area amplitude for short term dominating rate constant during osmotic induced syneresis	mm^2
C_{s0}	Carman-specific surface amplitude for short term dominating rate constant	m^{-1}
C_W	Accumulated whey volume amplitude for short term dominating rate constant	mL
$C_{W,osm}$	Accumulated whey volume amplitude for short term dominating rate constant during osmotic induced syneresis	mL
C_ε	Porosity amplitude for the short-term dominating rate constant	-
C_0	Initial Concentration of solute i at the start of diffusion time	kg m^{-3}
$C_{0,brine}$	Initial concentration in the brine at the onset of adsorption	kg m^{-3}
C_∞	Concentration within structure in equilibrium with surrounding brining conditions	kg m^{-3}

c	Kozeny pore shape factor	-
c_i	Molar concentration of species *i*	mol m^{-3}
c_{Tot}	Total mass concentration of all the components in the system	kg m^{-3}
D_{eff}	Effective diffusion coefficient	m^2 s^{-1}
D_{Disk}	Diameter of the local disk	mm
$D_{equiv\text{-}circ}$	Equivalent circular pore diameter	µm
D_i	Ideal mass diffusion coefficient of solute *i*	m^2 s^{-1}
D_{ii}	Independent main diffusion coefficients of solute *i*	m^2 s^{-1}
D_{ij}	Independent cross diffusion coefficients of solutes *i* and *j*	m^2 s^{-1}
D_{ij}^{SM}	Binary Stefan-Maxwell diffusion coefficient between components *i* and *j*	m^2 s^{-1}
DM	Dry Matter content	g kg^{-1}
d	Diameter of circular pipe	m
F_0	Fourier number	-
Fat	Fat content	g kg^{-1}
G	Gibbs free energy	J
H_{disk}	One-pixel length height of the local disk	mm
i_j	Number of ions produced per dissolved solute	mol mol^{-1}
J_{fluid}	Volumetric fluid flux	m^3 m^{-2} s^{-1}
J_i	Mass flux rate for solute *i*	kg m^{-2} s^{-1}
J_0, J_1	First-order Bessel functions	-
J_W	Volumetric whey flux	m^3 m^{-2} s^{-1}
$J_{W,p}$	Volumetric whey flux through porous regions	m^3 m^{-2} s^{-1}
K	Hydraulic transport coefficient	m^2 Pa^{-1} s^{-1}
K_{Gel}	Shape factor for the experimental gels	-
K_{Shape}	Shape factor	-
k	Rate Constant	s^{-1}
k_1, k_2	Rate constants for the pseudo first-order and pseudo second-order kinetic adsorption models, respectively	s^{-1}
$k'_{1,0}$	Kinetic rate coefficient for the fractal-like integrated kinetic Langmuir Equation	$s^{-\alpha}$
L	Length of the matrix diffusion occurs through	m
L_{min}	Minimum distance for contiguous transport along a tortuous path	m
L_s	Straight line length for flow	m
M_{FF}	Mass of gel free fluid fraction	kg
$M_{gel,tosm=0}$	Mass of the gel at the onset of exposure to the osmotic pressure differential	kg
M_{Gel}	Mass of the gel	kg
$M_{NaCl,P}$	Mass salt in pellet fraction	kg
$M_{NaCk,S}$	Mass of salt adsorbed to pellet solids	kg
$M_{non\text{-}NaCl\ whey,,PF}$	Mass of salt-free whey in the pellet fraction	kg
$M_{non\text{-}whey,DS}$	Mass of the non-whey dairy solids in the gel	kg
M_{osm}	Osmolarity	osmoles m^{-3}
$MF_{NaCl\text{-}whey}$	Mass fraction salt in NaCl-whey solution	-
$MF_{NaCl,PF}$	Mass fraction salt in pellet fluid	-
MMF	Moisture mass fraction of the gel	-
$MMF_{gel,tosm=0}$	Moisture mass fraction of the gel at the onset of exposure to the osmotic pressure differential	-

MMF_{milk}	Moisture mass fraction of the starting milk gel before the onset of syneresis	-
MMF_{osm}	Moisture mass fraction of the gel during osmotically induced syneresis	-
MMF_{whey}	Moisture mass fraction of the whey expelled	-
n_j	Number of moles of solute *j* dissolved in solution per solution volume	mol m^3
n_A	Number of cylindrical pores per unit area	Pores m^{-2}
n_t	Total number observations	-
P	Pressure across cheese curd driving syneresis	Pa
p	Proportionality factor for the salt and water flux behaviour	-
p_g	Pressure from the gravitational effects on the curd structure driving syneresis	Pa
p_i	Perimeter of single pore *i*	m
p_n	Number of parameters tested	-
p_p	Pressure driving syneresis due to external pressure applied to curd structure	Pa
p_s	Endogenous pressure driving syneresis	Pa
p_{Total}	Total pressure driving syneresis	Pa
$p_{SA,1}$	Gel surface area long term dominating rate constant	s^{-1}
$p_{SA,2}$	Gel surface area short term dominating rate constant	s^{-1}
$p_{SAosm,1}$	Gel surface area long term dominating rate constant during osmotic induced syneresis	s^{-1}
$p_{SAosm,2}$	Gel surface area short term dominating rate constant during osmotic induced syneresis	s^{-1}
$p_{s0,1}$	Carman-specific surface long term dominating rate constant	s^{-1}
$p_{s0,2}$	Carman-specific surface short term dominating rate constant	s^{-1}
p_{total}	Total pressure driving syneresis	Pa
$p_{W,1}$	Accumulated whey volume long term dominating rate constant	s^{-1}
$p_{W,2}$	Accumulated whey volume short term dominating rate constant	s^{-1}
$p_{Wosm,1}$	Accumulated whey volume long term dominating rate constant during osmotic induced syneresis	s^{-1}
$p_{Wosm,2}$	Accumulated whey volume short term dominating rate constant during osmotic induced syneresis	s^{-1}
$p_{1,\varepsilon}$	Porosity long term dominating rate constant	s^{-1}
$p_{2,\varepsilon}$	Porosity short term dominating rate constant	s^{-1}
Q	Volumetric flow through a single cylindrical pore	m^3 s^{-1}
$Q_{total\ pores}$	Volumetric flow through multiple cylindrical pores	m^3 s^{-1}
q	Mass adsorbed per mass of adsorbent	-
q_e	Mass adsorbed per mass of adsorbent at equilibrium	-
R	Ideal Gas Constant	m^3 Pa K^{-1} mol^{-1}
R_{Total}	Mass of water per mass of casein in the curd	g H_2O g^{-1} casein
R_1, R_2	Linear constants	g H_2O g^{-1} casein
R_3	Mass of water per mass of casein in the curd at equilibrium	g H_2O g^{-1} casein
$RMSE$	Root mean squared error	mL or mm^2
r	Average gel radius	m
r_{max}	Maximum radius	m
r^2	Coefficient of determination	-

S	Cross-sectional area of the matrix where diffusion occurs	m^2
S_x	Mass of salt per 100 grams of solids-not-salt at a location x distance from the brined surface of the cheese	g 100 g^{-1}
SA_{Gel}	Surface area of the gel	mm^2
SA_{Shape}	Surface area of a three-dimensional shape that undergoes uniform contraction	mm^2
SSE	Sum of the squared errors	mL^2 or mm^4
SST	Total sum of squares	mL^2 or mm^4
s	Specific surface	m^{-1}
s_0	Carman-specific surface	m^{-1}
T	Temperature	K
$T_{°C}$	Temperature	°C
t	Time	s
t_D	Solute diffusion time	s
t_{osm}	Osmotic pressure differential exposure time	s
t_{RegSyn}	Total time of regular, bulk syneresis	s
V	Curd volume	mL
V_A	Volume of liquid that is the source of diffusing solute	m^3
V_{Disk}	Volume of local disk	mm^3
V_{inf}	Curd volume at infinite time	mL
V_{Gel}	Volume of gel	mL
$V_{Gel,i}$	Volume of gel at measurement i	mL
$V_{Gel,t=0}$	Volume of the gel before the onset of the syneresis	mL
V_{Shape}	Volume of three-dimensional shape that undergoes uniform contraction	mm^3
V_w	Accumulated whey volume	mL
$V_{W,i}$	Accumulated whey volume at measurement i	mL
V_0	Initial curd volume	mL
v	Net velocity of fluid flowing out of a porous media	
v_i	Velocity relative to stationary coordinates of component i	m s^{-1}
W_x	Mass of water per 100 grams of solids-not-salt at a location x distance from the brined surface of the cheese	g 100 g^{-1}
x	Distance from the surface	m
x_i, x_j	Molar fraction of components i and j	-
∇x_j	Concentration gradient of a single solute j over the system length	kg m^{-4}
y_i	Data value of observation i	mL or mm^2
$\bar{y}$	Average value of all data	mL or mm^2
$\hat{y}_i$	Predicted value of observation i using the model	mL or mm^2

Greek Symbols

Symbol	Definition	Units
α	Fractional time index	-
β_m	Roots of the first order Bessel function	-
ε	Porosity of the matrix	-
κ	Intrinsic permeability	m^2
μ	Dynamic viscosity of the whey	Pa s
μ_i	Molar chemical potential gradient of component i	J mol^{-1}

μ_i^0	Standard chemical potential under prescribed temperature and pressure conditions	J mol^{-1}
Π	Osmotic pressure	Pa
ρ	Density of cheese matrix	kg m^{-3}
ρ_{fluid}	Density of fluid	kg m^{-3}
ρ_{milk}	Density of milk	kg m^{-3}
$\rho_{NaCl\text{-}whey}$	Density of NaCl-whey solution	kg m^{-3}
ρ_{whey}	Density of whey	kg m^{-3}
τ_D	Diffusive tortuosity of pores in the matrix	-
τ_h	Hydraulic tortuosity of porous matrix	-
τ_1, τ_2	Relaxation constants	s
φ_j	Osmotic coefficient which accounts for the non-ideal solute *j* behaviour	-
$\nabla \omega_i$	Gradient of mass fraction of species *i* with respect to a diffusion distance	m^{-1}

Chapter 11 Appendices

Appendix A – MATLAB® Code to Evaluate Gel Volume and Surface Area

```
%% Assess Gel Images and Evaluate for Volume and Surface Area

% The purpose of this code is to process gel images from their raw state to binary, and then evaluate the whole gel for average surface area and volume values.  This is done by establishing the coordinates of the perimeter and measuring the distance between perimeter pixels at the same vertical coordinate to calculate the surface area and volume of a local disk comprising the gel, and then repeat the process until all coordinates are assessed.

contents = dir('*.JPG'); % Read in all the photos
A_Matrix = [0, 0, 0, 0, 0, 0, 0, 0, 0, 0, 0];
row = 0;
col = 0;
csvwrite('Export_Test.csv', A_Matrix, row, col);

Length = 0.5*(656.7800+654.7332); % Average calibration from two known 20 mm measurements
level = 0.85; % Level for thresholding

xmin = 1650;
ymin = 500;
width = 3500 - xmin;
height = 2400 - ymin;

rect = [xmin ymin width height]; % Crop the image to these dimensions

for i = 1:numel(contents) % Read in photos in a file
    filename = contents(i).name;
    RawPhoto = imread(contents(i).name);
    imshow(RawPhoto);
    I1 = rgb2gray(RawPhoto); % Convert to gray scale
    imshow(I1);

    I2 = imcrop(I1,rect); % Crop the image
    imshow(I2);

    % Complement Image, Fill in holes, and Threshold
    Icomp = imcomplement(I2);% Imcomplements the image, switching the black and white pixels
    Ifilled = imfill(Icomp,'holes');% Fills holes (where a hole is defined as a set of background pixels that cannot be reached by filling in the background from the edge of the image)
    Ihisteq = histeq(Ifilled);
    Icomp2 = imcomplement(Ihisteq);
    Ifilled2 = imfill(Icomp2,'holes'); % Fills holes (where a hole is defined as a set of background pixels that cannot be reached by filling in the background from the edge of the image)
    Ithresh = im2bw(Ifilled2, level); % Converts the image to black and white using a threshold level value between 0 and 1, between black and white, respectively.  This value needs to be very large to only capture the truely porous regions.

    figure
    imshow(Ithresh);
    title('Thresholded Image');
    % Selection for morphological element

    se = strel('disk', 15); % Creates a flat,disk-shaped structural element with a 15 pixel radius
    Iopenned = imopen(Ithresh, se); % Performs morphological opening on the thresholded image with the structuring element, consisting of an erosion followed by a dilation

    figure
    imshowpair(Iopenned, Ithresh);
```

```
    Iopenned2 = bwareaopen(Iopenned, 100000);

    figure
    imshow(Iopenned2);

    % Extract Features and Summarize Results
    [labeled,numObjects] = bwlabel(Iopenned2,8); % Labels each pore
    boundaries = bwboundaries(Iopenned2);
    stats = regionprops(labeled,'Area', 'Perimeter','MajorAxisLength', 'MinorAxisLength',
'Centroid','BoundingBox', 'Orientation'); % Determines the pore properties for each pore
    area = [stats.Area]; % Area for each pore in pixels^2
    perimeter = [stats.Perimeter]; % Perimeter of each pore in pixels
    majoraxislength = [stats.MajorAxisLength]; % Major axis of fitted ellipse in pixels
    minoraxislength = [stats.MinorAxisLength]; % Minor axis of fitted ellipse in pixels
    centroid = [stats.Centroid]; % Centroid of each pore (pixel x and y locations)
    boundingbox = [stats.BoundingBox];
    orientation = [stats.Orientation];

    milimetersperpixel =  20/Length; % Number of mm in the pixel length from the calibration ruler

    % Convert all the properties from pixels to microns and into column form
    Area = (milimetersperpixel^2)*vec2mat(area,1);
    Majoraxis = milimetersperpixel*vec2mat(majoraxislength,1);
    Minoraxis = milimetersperpixel*vec2mat(minoraxislength,1);
    Perimeter = milimetersperpixel*vec2mat(perimeter,1);
    Centroid = milimetersperpixel*vec2mat(centroid,2);
    CentroidX = Centroid(:,1);
    CentroidY = Centroid(:,2);
    BoundingBox = milimetersperpixel*vec2mat(boundingbox,4); % Bounding box dimensions
    BBWidth = BoundingBox(:,3);
    BBHeight = BoundingBox(:,4);
    Orientation = vec2mat(orientation,1);
    AdjustedWidth =  BBWidth*sin(abs(Orientation*pi()/180));
    AdjustedHeight = BBHeight/sin(abs(Orientation*pi()/180));

    imshow(Iopenned2); % Open the black-white image
    hold (imgca,'on');
    plot(imgca,centroid(:,1),centroid(:,2),'b*'); % Plot a blue star on the image at the location of the centroid on
the particle
    rectangle('Position', boundingbox, 'LineWidth', 4, 'EdgeColor', 'r'); % Plots the Bounding Box around the
particle
    hold (imgca,'off');

    [Y] = bwboundaries(Iopenned2);

    % Determine the distance between the gel perimeter boundaries and the centroid of the image
    [Boundary] = Y{:,1};
    PerimeterX = Boundary(:,2);
    PerimeterY = Boundary(:,1);
    CorrectedBoundary = [PerimeterX, PerimeterY];

    XDistFromCentroid = milimetersperpixel*abs(CorrectedBoundary(:,1)- centroid(:,1));
    YDistFromCentroid = milimetersperpixel*abs(CorrectedBoundary(:,2)- centroid(:,2));
    DistFromCentroid = sqrt(((XDistFromCentroid(:,1)).^2)+(YDistFromCentroid(:,1)).^2);

    % Measuring Distances between the pixels at the perimeter with the same y-value

    [Y] = bwboundaries(Iopenned2);
    [Boundary] = Y{:,1};
```

```
        SortedBoundary = sortrows(Boundary);
    [imax,jmax] = size(Boundary);

    DiskDiameters = cell(imax,1);
    DiskVolumes = cell(imax,1);
    DiskEdgeAreas = cell(imax,1);
    TopDiameters = cell(imax,1);
    TopAreas = cell(imax,1);
    BottomDiameters = cell(imax,1);
    BottomAreas = cell(imax,1);
    DiskDiameters{1,1} = 0;

    DiskDiameters{1,1} = 0;
    DiskVolumes{1,1} = 0;
    DiskEdgeAreas{1,1} = 0;
    TopDiameters{1,1} = 0;
    BottomDiameters{1,1} = 0;

    TotalDiskVol = 0;
    TotalDiskSideArea = 0;
    TotalTopArea = 0;
    TotalBottomArea = 0;
    TotalSurfaceArea = 0;
    DiskEdgeArea = 0;

    for i=2:imax
       if SortedBoundary(i,1) == SortedBoundary(i-1,1)
          DiskDist = (SortedBoundary(i,2) - SortedBoundary(i-1,2)); % Distance between two boundaries at the
same y coordinate
       else
          DiskDist = 0;
       end

       CorrDiskDist = milimetersperpixel * DiskDist; % Distance is converted to mm fronm pixels
       DiskDiameters{i,1} = CorrDiskDist;
       DiskVolume = ((pi()/4)*(CorrDiskDist)^2)*milimetersperpixel; % Local disk volume is calculated
       DiskVolumes{i,1} = DiskVolume;

       if DiskDiameters{i,1} > 0

          if DiskDiameters{i,1} > 0.02 * AdjustedWidth % If the disk diameters are larger than 2% of the adjusted
width of the gel, the outer edge of the disk is used to calculate surface area
             DiskEdgeArea = pi()*CorrDiskDist*milimetersperpixel;
             DiskEdgeAreas{i,1} = DiskEdgeArea;
             TopDiameters{i,1} = 0;
             BottomDiameters{i,1} = 0;
             TopAreas{i,1} = 0;

          else
               DiskEdgeAreas{i,1} = 0;
                  if i < 0.5*imax
                     TopDiameters{i,1} = DiskDiameters{i,1};
                     TopArea = 0.25*pi()*CorrDiskDist^2; % Surface area for a disk located at the top of the gel
                     TopAreas{i,1} = TopArea;
                     TotalTopArea = TotalTopArea + TopAreas{i,1};
                     BottomDiameters{i,1} = 0;
                     BottomArea = 0;
                     BottomAreas{i,1} = BottomArea;
                  else
                     TopDiameters{i,1} = 0;
```

```
                    TopArea = 0;
                    TopAreas{i,1} = TopArea;
                    BottomDiameters{i,1} = DiskDiameters{i,1};
                    BottomArea = 0.25*pi()*CorrDiskDist^2; % Surface area for a disk located at the bottom of
the gel
                    BottomAreas{i,1} = BottomArea;
                    TotalBottomArea = TotalBottomArea + BottomAreas{i,1};
                end
            end
            else
            DiskEdgeAreas{i,1} = 0;
            TopDiameters{i,1} = 0;
            BottomDiameters{i,1} = 0;
            end

    TotalDiskVol = TotalDiskVol + DiskVolume; % Total volume of the gel mm^3
    TotalDiskSideArea = TotalDiskSideArea + DiskEdgeArea; % Total disk side surface area of gel mm^2
    end

    FinalVol = TotalDiskVol*0.001; % Converts mm^3 to mL, final gel volume
    TotalSurfaceArea = TotalDiskSideArea + TotalTopArea + TotalBottomArea; % Final gel surface area

    A_Matrix = [Area, Perimeter, AdjustedWidth, AdjustedHeight, Majoraxis, Minoraxis, Orientation, FinalVol,
TotalSurfaceArea, TotalTopArea, TotalBottomArea];
    dlmwrite('Export_Test.csv', A_Matrix, 'delimiter', ',', '-append');

end
```

Appendix B – MATLAB® Code to Fit Biexponential Models to Accumulated Whey Volume or Gel Surface Area

```
%% Biexponential Modelling of Contracting Gel Surface Area or Accumulated Whey Volume

% This code determines the best fit for both nonlinear exponential and linear constants by first establishing a
'dummy' linear constant and through which to optimize and determine the best fit for the nonlinear exponential
values first using the \ option, before then solving for the linear variable values.  Both concepts use lsqnonlin to
solve for the values that lead to the global SSE minimum.  The original code that this code was adapted from
may be found at https://au.mathworks.com/help/optim/ug/nonlinear-data-fitting-example.html

filename = 'READIN.csv'; % Reads in the data file
M = dlmread(filename); % Reads file data into a matrix
t = M(:,1); % Syneresis time(seconds)is reported in the first column
Y = M(:,2); % Gel surface area [mm^2] or gel volume [mL] is reported in the second column

Yeq = 0; % Establishes a equilibrium Y value of 0
Yeqtot = 0; % Establishes a total Y value of 0
icount = 0; % Establishes a count for the number of values assessed as equilibrium values at 0
LocalYeq = 0; % Establishes the value of the minimum Y value as 0

%The following loop is used to determine the average equilibrium Y at 48 hours of syneresis, which represents
the equilibrium case
for i=1:length(t)
   if t(i,1)>(3600*24)
      LocalYeq=Y(i,1);
      icount=icount + 1;
   else
       LocalYeq=0;
   end
   Yeqtot = Yeqtot + LocalYeq;
end

Yeq = Yeqtot/icount; % Yeq is the average equilibrium value of Y

Yadj = Y-Yeq; % Adjusts Y to subtract Yeq value, so that Yadj = B*exp(-p1*t)+C*exp(-p2*t)

type fitvector

lam=2; % There are two nonlinear variables to fit
xdata = t;
ydata = Yadj; % The ydata uses the adjusted Y values to fit the nonlinear variables first
yEst = fitvector(lam,xdata,ydata);

A = zeros(length(xdata),length(lam));  % build A matrix
for j = 1:length(lam)
  A(:,j) = exp(-lam(j)*xdata);
end
c = A\ydata; % solve A*c = y for linear parameters c (c is the dummy variable)
yEst = A*c; % return the estimated response based on c
% Solve the problem using lsqcurvefit, starting from a two-dimensional initial point lam(1), lam(2):

x1start = [0.00001 0.00005]; % Initial guesses for the nonlinear exponential variables
F1 = @(x,t) fitvector(x,t,Yadj);

[x1,resnorm2,~,exitflag2,output2] = lsqcurvefit(F1,x1start,t,Yadj); % lsqcurvefit uses the initial x1start guesses,
time data, and Yadj data to fit the exponential variables.  The fitted values are reported in x1.
```

```
F2 = @(x,t) x(1)+x(2)*exp(-x1(1,1)*t)+x(3)*exp(-x1(1,2)*t); % Fitting for the whole model, including the constant

x2start = [Yeq 1000 2000]; % Initial guesses for the linear variables and the constant

[x2,resnorm,~,exitflag,output] = lsqcurvefit(F2,x2start,t,Y); % lsqcurvefit to solve for the linear variables and the constant

Time = 3600*[0 0.1 0.2 0.3 0.4 0.5 0.6 0.7 0.8 0.9 1.0 1.1 1.2 1.3 1.4 1.5 1.6 1.7 1.8 1.9 2.0 5 10 24 48]; % Sample time points to plot model
yfitplot = x2(1,1)+(x2(1,2)*exp(-x1(1,1).*Time)+x2(1,3)*exp(-x1(1,2).*Time)); %Plot of the fitted model
FirstExp = x2(1,2)*exp(-x1(1,1).*Time); % Plotting first exponential (slow)
SecondExp = x2(1,3)*exp(-x1(1,2).*Time); % Plotting second exponential (fast)
Ymean = mean(Y); % Average of all V or SA data

figure

plot(t,Y,'ko')
hold on
plot(Time,yfitplot,'k')
plot(Time,FirstExp,'g-')
plot(Time,SecondExp,'r-')
legend('Data points','Fitted Model','First Exponential','Second Exponential')

sse = sum((Y-(x2(1,1)+x2(1,2)*exp(-x1(1,1)*t)+x2(1,3)*exp(-x1(1,2)*t))).^2); % SSE for the entire fitted model
mse = sse/(length(Y)-4-1); % MSE for the entire fitted model
rmse = sqrt(mse); % RMSE for the entire fitted model - it represents the average distance between the data points and the model at the same time point
sst = sum((Y-Ymean).^2); % Sum of the total squares for the surface area data
rsq = 1 - sse/sst; % Coefficient of determination for the model

Q = [sse sst mse rmse rsq];
Val = [x2(1,1) x2(1,2) x2(1,3) x1(1,1) x1(1,2)];
Stats = array2table(Q,'VariableNames',{'sse','sst','mse','rmse','rsq'});
FittedVariables = array2table(Val,'VariableNames',{'A','B','C','p1','p2'});
```

Appendix C – Standard Curves of PEG and NaCl in Whey Solutions

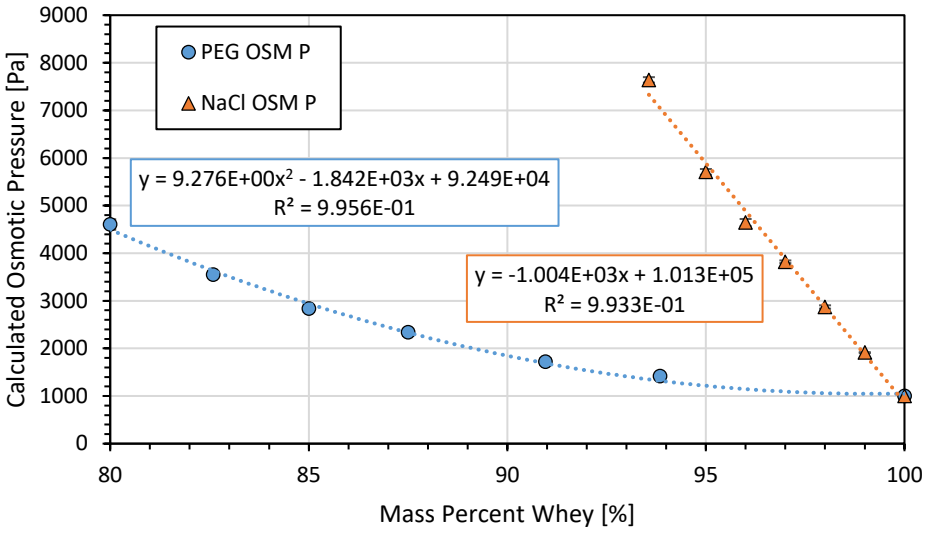

Figure C - 1

Figure 11-1: Osmotic pressure curves for pH 6.25 NaCl-whey and PEG-whey solutions

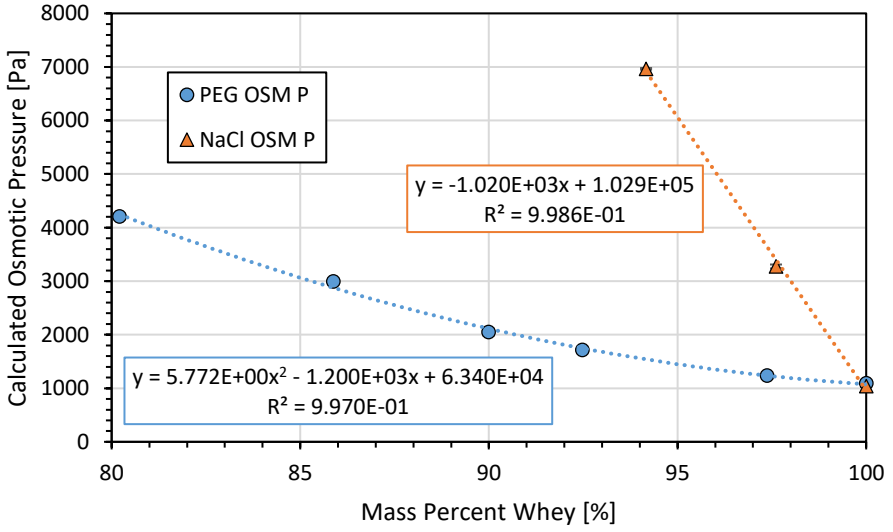

Figure 11-2: Osmotic pressure curves for pH 5.75 NaCl-whey and PEG-whey solutions

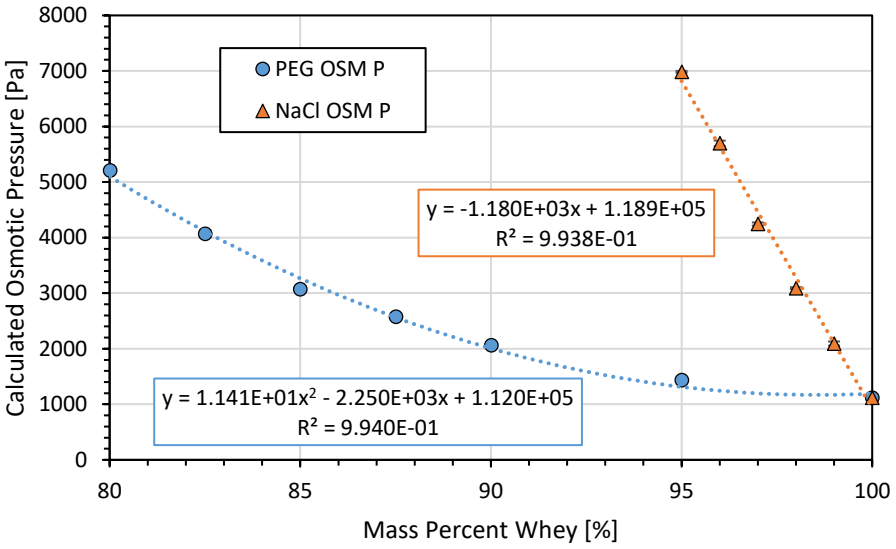

Figure 11-3: Osmotic pressure curves for pH 5.25 NaCl-whey and PEG-whey solutions

Appendix D – MATLAB® Code to Determine Best-Fit Effective Diffusion Coefficient for Salt Uptake into Gel Fluid

```
%% Nonlinear Regression, for Fitting Average Salt Uptake and Determining Best-fit Deff

filename = 'READIN.csv';
M = dlmread(filename);
t = M(:,1); % Time data
Cavg = M(:,2); % Average salt mass fraction in gel fluid data

Ci = 0; % Initial salt concentration in gel fluid
DeffOverR2 = 0; % Ratio of Deff over the average radius of the gel squared
Cinf = 0; % Average salt concentration in gel fluid after infinite time
CAVERAGE = mean(Cavg); % Average of all concentration values

Beta1 = 2.4048; % Roots of the first order Bessel function
Beta2 = 5.5201;
Beta3 = 8.6537;
Beta4 = 11.7919;
Beta5 = 14.9309;
Beta6 = 18.0711;

funC =@(x,t)x(2)+(Ci-x(2))*(((4/(Beta1^2))*exp(-(Beta1^2)*x(1)*t))+ ((4/(Beta2^2))*exp(-
(Beta2^2)*x(1)*t))+((4/(Beta3^2))*exp(-(Beta3^2) *x(1)*t))+((4/(Beta4^2))*exp(-(Beta4^2)*
x(1)*t))+((4/(Beta5^2))*exp(-(Beta5^2)*x(1)*t))+((4/(Beta6^2))*exp(-(Beta6^2)*x(1)*t))); % Function to fit
the average salt uptake data with the effective diffusion coefficient

xstart = [0.00001, 0.025]; % Starting guess for DeffoverR^2 and Cinf

[x,resnorm,residual,exitflag,output] = lsqcurvefit(funC,xstart,t,Cavg); % Fitting using least squares method with
lsqcurvefit
DeffOverR2 = x(1);
Cinf = x(2);

sse = sum((Cavg-(Cinf+(Ci-Cinf)*(((4/(Beta1^2))*exp(-(Beta1^2)* DeffOverR2*t))+((4/(Beta2^2))*exp(-
(Beta2^2)*DeffOverR2*t))+ ((4/(Beta3^2))*exp(-(Beta3^2)*DeffOverR2*t))+((4/(Beta4^2))*exp(-
(Beta4^2)*DeffOverR2*t))+((4/(Beta5^2))*exp(-(Beta5^2)*DeffOverR2*t)) +((4/(Beta6^2))*exp(-
(Beta6^2)*DeffOverR2*t))))).^2); % Sum of square errors
sst = sum((Cavg-CAVERAGE).^2); % Sum of total squares
mse = sse/(length(Cavg)-2-1); % Mean square error
rmse = sqrt(mse); % Root mean square error
rsq = [(1-sse/sst)]; % Coefficient of determination

Cavgfitplot = Cinf+(Ci-Cinf)*(((4/(Beta1^2))*exp((Beta1^2)*DeffOverR2*t))+ ((4/(Beta2^2))*exp(-
(Beta2^2)*DeffOverR2*t))+((4/(Beta3^2))*exp(-(Beta3^2)* DeffOverR2*t))+((4/(Beta4^2))*exp(-
(Beta4^2)*DeffOverR2*t))+((4/(Beta5^2))* exp(-
(Beta5^2)*DeffOverR2*t))+((4/(Beta6^2))*exp((Beta6^2)*DeffOverR2*t)));
figure
plot(t,Cavg,'ro')
title('Compared Data Points')
hold on
plot(t,Cavgfitplot,'k')
Q = [sse sst mse rmse rsq];
Val = [x(1,1) x(1,2)];
Stats = array2table(Q,'VariableNames',{'sse','sst','mse','rmse','rsq'});
FittedVariables = array2table(Val,'VariableNames',{'DeffOverR2','Cinf'});
```

Appendix E – MATLAB® Code to Model Fractal Integrated Kinetic Langmuir Equation

```
%% Best Fit Modelling of Salt Adsorption with Fractal IKL Model

% This code determines the best fit for the constants in the fractal IKL model to describe salt adsorption
behaviour in gels undergoing brining.

filename = 'READIN.csv'; % Reads in the data file
M = dlmread(filename); % Reads file data into a matrix
t = M(:,1); % Syneresis time(seconds)is reported in the first column
Y = M(:,2); % Ratio of adsorbed NaCl to mass of dairy solids adsorbing NaCl
Ceq = 0.19797914; % Mass fraction NaCl in the surrounding brine at equilibrium
C0 = 0.2; % Starting salt mass fraction in brine surrounding the gel
qm = 0.185438; % Maximum mass of NaCl possible to adsorb per mass of dairy solids adsorbing NaCl
qe = 0.136909; % Mass of NaCl adsorbed per mass of dairy solids adsorbing at equilibrium
feq = (1-Ceq/C0)*(qe/qm);

fun = @(x,t)(((qe-qe*exp(-x(1)*t.^x(2)))./(1-(feq*exp(-x(1)*t.^x(2))))); % Function fitting the adsorption data
with the fractal IKL model
xstart = [0.0584 0.1]; % Initial gues for k'1,0 and alpha, respectively

[x,resnorm,residual,exitflag,output] = lsqcurvefit(fun,xstart,t,Y); % Fit the curve

Time = 3600*[0 0.1 0.2 0.3 0.4 0.5 0.6 0.7 0.8 0.9 1.0 1.1 1.2 1.3 1.4 1.5 1.6 1.7 1.8 1.9 2.0 5 10 24];
yfitplotnum = (qe-qe*exp(-x(1,1)*Time.^x(1,2)));
yfitplotdenom = (1-(feq)*exp(-x(1,1)*Time.^x(1,2)));
yfitplot = yfitplotnum./yfitplotdenom; % Plot for the fitted curve
Ymean = mean(Y);

figure

plot(t,Y,'ko')
hold on
plot(Time,yfitplot,'k')
legend('Data points','Fitted Model')

sse = sum((Y-(qe-qe*exp(-x(1,1)*t.^x(1,2)))./(1-(feq)*exp(-x(1,1)*t.^x(1,2)))).^2);
mse = sse/(length(Y)-2-1);
rmse = sqrt(mse);

sst = sum((Y-Ymean).^2);
rsq = 1 - sse/sst;

Q = [sse sst mse rmse rsq];
Val = [x(1,1) x(1,2)];
Stats = array2table(Q,'VariableNames',{'sse','sst','mse','rmse','rsq'});
FittedVariables = array2table(Val,'VariableNames',{'k10prime','alpha'});
```

Appendix F – MATLAB® Code for Assessing Internal Porous Gel Properties and Example Work

```
%% Evaluation of Internal Porous Gel Properties
% The purpose of this code is to process SEM images for analysis of the porous regions of freeze dried curds.
% This code crops the image of the image of interest, undergoes incomplementing, equalizing of pixels, and
% filling holes, and smooths the final black and white image to remove any extraneous pixels.  The standardized
% image is then assessed using the regionprops function to assess the area and perimeter (in addition to other
% values) for each pore.  These values are converted into micron-based units and then reported in a table for
% analysis.  A final figure of the porous region of interest is made to include different colour-based outlines to
% provide a visual distinction between pores of different areas.

% Reading in the image and cropping it
I = imread('24hours_004.tif');

I1 = imcrop(I, [0 0 2050 1770]);

% Improving Image Contrast
figure
imhist(I1); %Histogram of the pixel intensity in the original image
I2 = histeq(I1); %Transformation of the image using histogram equalization

figure
imshow(I2);
title('Histogram Equalized Image');

% Complement Image, Fill in holes, and Threshold (multiple times)
Icomp = imcomplement(I2); %Imcomplements the image, switching the black and white pixels
Ifilled = imfill(Icomp,'holes'); %Fills holes (where a hole is defined as a set of background pixels that cannot be
reached by filling in the background from the edge of the image)
Ihisteq = histeq(Ifilled);
Icomp2 = imcomplement(Ihisteq);
Icomp3 = imcomplement(Icomp2);
Ifilled2 = imfill(Icomp3,'holes');

level = 0.845; %Level for thresholding
Ithresh = im2bw(Ifilled2, level); %Converts the image to black and white using a threshold level value between
0 (black) and 1 (white).  This value needs to be very large to only capture the truly porous regions.
figure
imshow(Ithresh);
title('Thresholded Image');

% Selection for morphological elements
se = strel('disk', 2); %Creates a flat,disk-shaped structural element with a 2 pixel radius
Iopenned = imopen(Ithresh, se); %Performs morphological opening on the thresholded image with the
structuring element, consisting of an erosion followed by a dilation
figure
imshowpair(Iopenned, Ithresh);
figure
imshow(Iopenned);

% Extract Features and Summarize Results in pixel units
[labeled,numObjects] = bwlabel(Iopenned,8); %Labels each pore
stats = regionprops(labeled,'Eccentricity', 'Area', 'Perimeter','MajorAxisLength', 'MinorAxisLength', 'Solidity',
'Centroid','EquivDiameter'); %Determines the pore properties for each pore
area = [stats.Area]; %Area for each pore in pixels^2
eccentricity = [stats.Eccentricity]; %Eccentricity of each pore [ ]
perimeter = [stats.Perimeter]; %Perimeter of each pore in pixels
majoraxislength = [stats.MajorAxisLength]; %Major axis of fitted ellipse
```

```
minoraxislength = [stats.MinorAxisLength]; %Minor axis of fitted ellipse
centroid = [stats.Centroid]; %Centroid of each pore (x and y locations)
equivdiameter = [stats.EquivDiameter]; %Equiv circular diameter

%Convert all the properties from pixels to microns and into column form
micronsperpixel = 50/822.6667; %Scale of 50 microns per 822.6667 pixels
Area = (micronsperpixel^2)*vec2mat(area,1);
Majoraxis = micronsperpixel*vec2mat(majoraxislength,1);
Minoraxis = micronsperpixel*vec2mat(minoraxislength,1);
Perimeter = micronsperpixel*vec2mat(perimeter,1);
Equivdiameter = micronsperpixel*vec2mat(equivdiameter,1);
Eccentricities = vec2mat(eccentricity,1);
Centroid = micronsperpixel*vec2mat(centroid,2);
CentroidX = Centroid(:,1);
CentroidY = Centroid(:,2);

%Create a table with relevant pores properties
S = table(Area, Majoraxis, Minoraxis, Perimeter, Equivdiameter, Eccentricities, Centroid);

% Finding, outlining, and labeling pores in figure
[B, L, N, A] = bwboundaries(Iopenned);
figure;
imshow(Iopenned);
hold on;
colors=['b' 'g' 'r' 'c' 'm' 'y'];

for k=1:length(B)
   boundary = B{k};
   CurrentArea = Area(k);
   if CurrentArea >  25
      cidx = 1; %Largest pores (>55 square microns) are in blue
   elseif CurrentArea > 20
      cidx = 2; %Second largest pores are in green
   elseif CurrentArea > 15
      cidx = 3; %Third largest pores are in red
   elseif CurrentArea > 10
      cidx = 4; %Fourth largest pores are in cyan
   elseif CurrentArea > 5
      cidx = 5; %Fifth largest pores are in magenta
   else
      cidx = 6; %Smallest Pores in Yellow
   end
   plot(boundary(:,2), boundary(:,1),colors(cidx),'LineWidth',1);

   % Randomize text position for better visibility
   rndRow = ceil(length(boundary)/(mod(rand*k,7)+1));
   col = boundary(rndRow,2); row = boundary(rndRow,1);
   h = text(col+1, row-1, num2str(L(row,col)));
   set(h,'Color',colors(cidx),'FontSize',2,'FontWeight', 'normal');
end
```

Example Analysis of Porous Properties

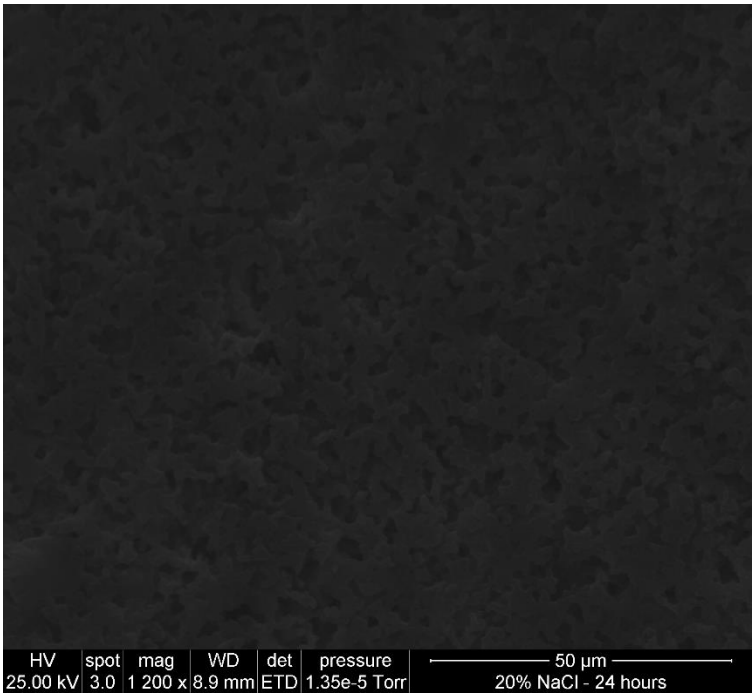

Figure 11-4: SEM Image from pH 5.75 - 20% NaCl-whey treatment at 24 hours of brining, pre-processing and analysis. The image is extremely dark to allow for improved pre-processing, whereby the pixel histogram is reallocated to provide greatest contrasts between porous and non-porous regions.

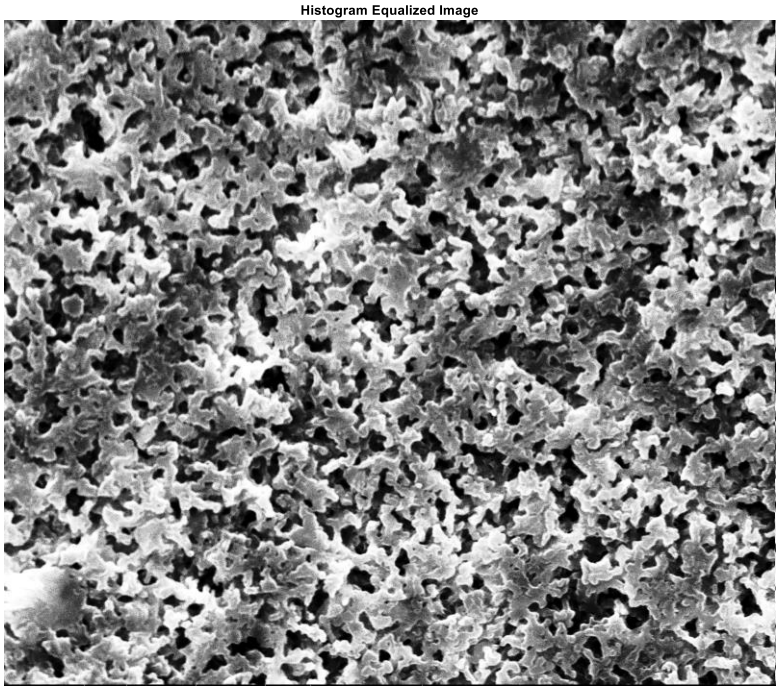

Figure 11-5: Cropped and histogram equalized image of Figure A. Porous areas appear as darkened regions.

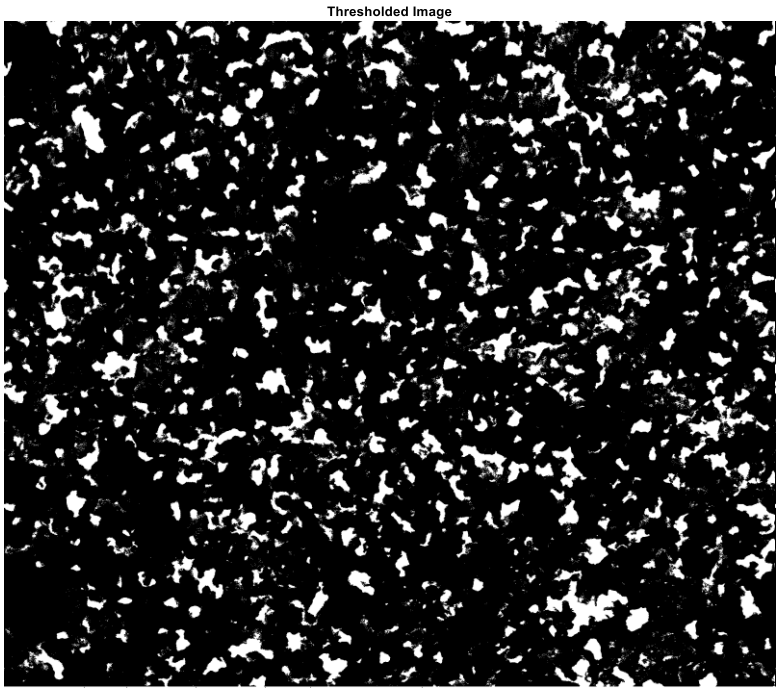

Figure 11-6: Thresholded image which converts pixels with light values larger than the threshold value (the non-pores) to black and any space with a light value less than the threshold value to white, making a binary image that is the inverse to the previous image.

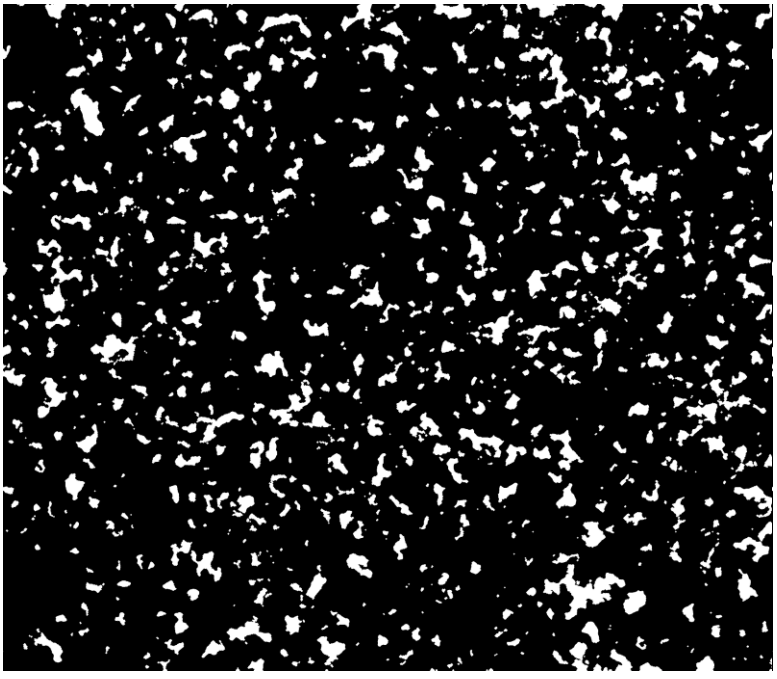

Figure 11-7: Binary image assessed for two-pixel structural elements identified and removed to prevent undue addition of noise to the data. This is the image that is assessed for the porous properties.

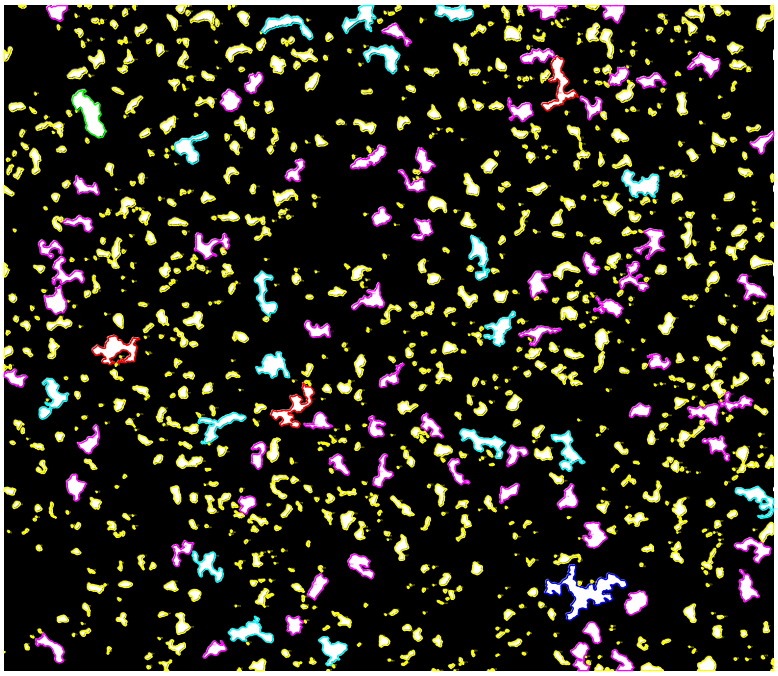

Figure 11-8: Final processed image with different colours outlining pores of different area ranges. This image provides a direct visual method of assessing the range and approximate number of pores with different area ranges.